Volume 10, No. 5

March, 1962

BS - file

THE SOVIET JOURNAL OF

ATOMIC ENERGY

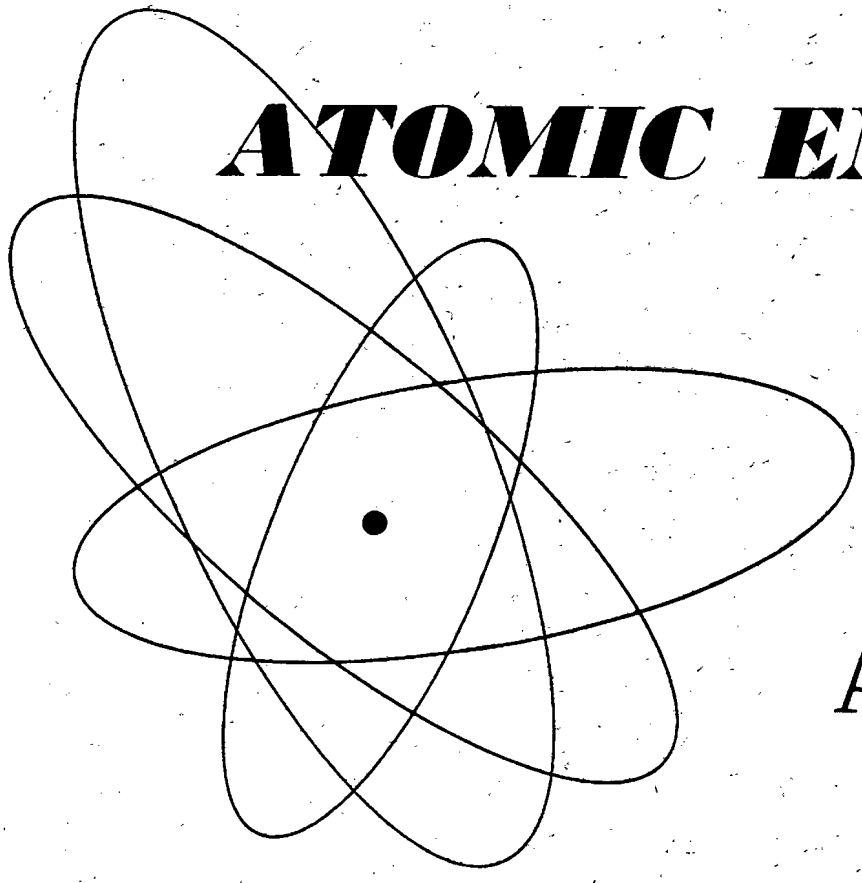

Атомная энергия

TRANSLATED FROM RUSSIAN

CONSULTANTS BUREAU

THE SOVIET JOURNAL OF

ATOMIC ENERGY

A translation of ATOMNAYA ÉNERGIYA, a publication of the Academy of Sciences of the USSR

(Russian original dated May, 1961)

Vol. 10, No. 5 March, 1962

CONTENTS

Annual subscription $75.00
Single issue 20.00
Single article 12.50

CONTENTS (continued)

NOTE. The Table of Contents lists all material that appears in Atomnaya Énergiya. Those items that originated in the English language are not included in the translation and are shown enclosed in brackets. Whenever possible, the English-language source containing the omitted reports will be given.

Consultants Bureau Enterprises, Inc.

GLORY TO THE SOVIET SCIENTISTS, BUILDERS, ENGINEERS, TECHNICIANS, AND WORKERS – THE CONQUERORS OF SPACE!

TO ALL THE SCIENTISTS, ENGINEERS, TECHNICIANS, AND WORKERS, TO ALL THE COLLECTIVES AND ORGANIZATIONS WHICH TOOK PART IN THE SUCCESSFUL PERFORMANCE OF THE FIRST MANNED SPACE FLIGHT IN THE WORLD IN THE SATELLITE SHIP "VOSTOK"

TO THE FIRST SOVIET SPACE MAN, COMRADE YURII ALEKSEEVICH GAGARIN

On the frontispiece of this issue of the Russian text there appears an article commemorating the orbital flight of Yurii Gagarin. Since the article does not deal with either details of nuclear research or even its historical development, it has been omitted from the translation.

YURII ALEKSEEVICH GAGARIN

A FAST-NEUTRON PULSE REACTOR

G.E. Blokhin, D.I. Blokhintsev, Yu.A. Blyumkina, I.I. Bondarenko, B.N. Deryagin, A.S. Zaimovskii, V.P. Zinov'ev, O.D. Kazachkovskii, Kim Khen Bon, N.V. Krasnoyarov, A.I. Leipunskii, V.A. Malykh, P.M. Nazarov, S.K. Nikolaev, V.Ya. Stavisskii, F.I. Ukraintsev, I.M. Frank, F.L. Shapiro, Yu.S. Yazvitskii

Translated from Atomnaya Énergiya, Vol. 10, No. 5,
pp. 437-446, May, 1961
Original article submitted October 12, 1960

In June, 1960, criticality was reached on the fast-neutron pulse reactor constructed at the United Institute of Nuclear Studies.

The fast-neutron pulse reactor is designed to work under periodic pulse conditions at a mean power output of about 1 kw. The power pulses are developed from the multiplication of prompt neutrons during an interval in which the reactor is in a supercritical state. The half-width of the power pulses is 36 microseconds, and the pulse repetition frequency may be varied between the limits 8–80 pulses/sec.

Introduction

The fast-neutron pulse reactor (IBR) is a pulsed neutron source intended for experiments in physics and especially for time-of-flight experiments. It is designed essentially to work under periodic pulse conditions, but it can be used to get powerful single pulses.

The power pulses in the reactor are developed by a rapid change in its reactivity, in which the reactor reaches prompt supercriticality for a short time periodically. In these instants of time, there is a substantial buildup in power. The rest of the time, the reactor is subcritical.

The total number of fissions in each pulse (the pulse energy) is determined by the "background" (the intensity of the auxiliary neutron source) preceding the pulse and the amount of prompt supercriticality. At sufficiently high mean powers, the background is provided by the delayed neutrons, born in all the preceding pulses.

At some value of the mean reactivity of the system (and thus of the peak reactivity), an equilibrium operating level is reached, which corresponds to a constant mean power output. Here the formation of delayed neutron sources during each pulse is exactly equal to the decay of sources between pulses, and the average intensity of the background stays constant.

The way in which the mean power output of the IBR reactor varies with time is, in principle, the same as for an ordinary reactor. If the reactivity of the system differs only slightly from the equilibrium value, the mean power changes slowly. If the excess reactivity is increased, the rate of rise or fall of the power is increased. The behavior of the reactor in this respect is described by the ordinary kinetic equations of a nonpulsed reactor. The only peculiarity in the behavior of the IBR reactor is that the effective fraction of delayed neutrons is very small. Under the nominal operating conditions, it is $\sim 10^{-4}$, i.e., almost a hundred times less than for an ordinary stationary reactor using uranium fuel. This fact, naturally, places stringent requirements on the operating precision of the control system units. The theory of the IBR reactor is given in [1].

Basic Constructional Elements of the IBR Reactor

A general view and the constructional layout of the IBR reactor are shown in Figs. 1 and 2.

The active zone of the IBR reactor has fixed and movable parts. The periodic change in the reactivity of the system is produced by the shifting of the movable parts which consist of two U-235 inserts fastened to two rotating discs

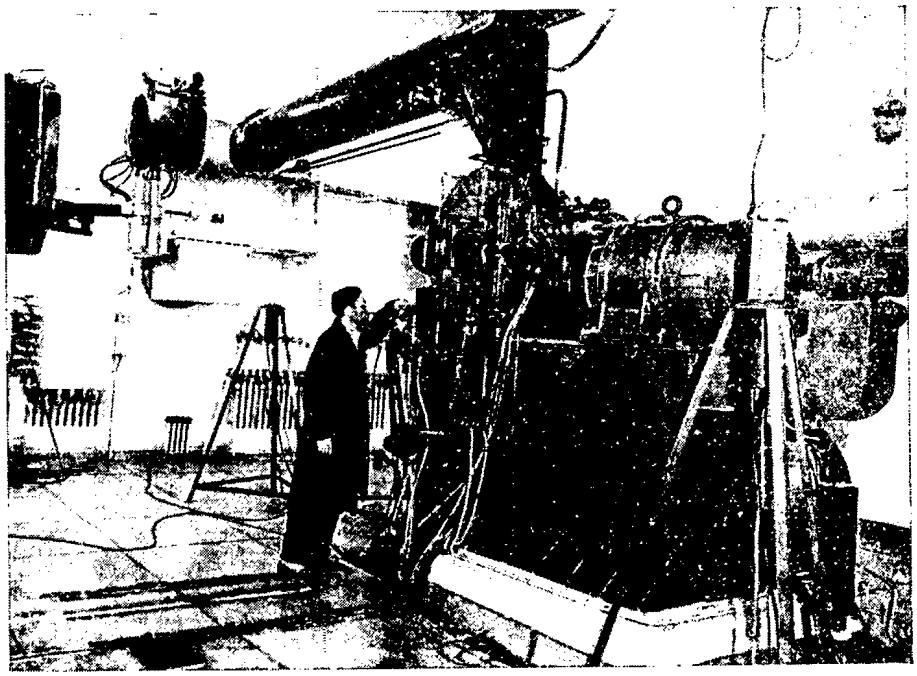

Fig. 1. General view of the IBR reactor.

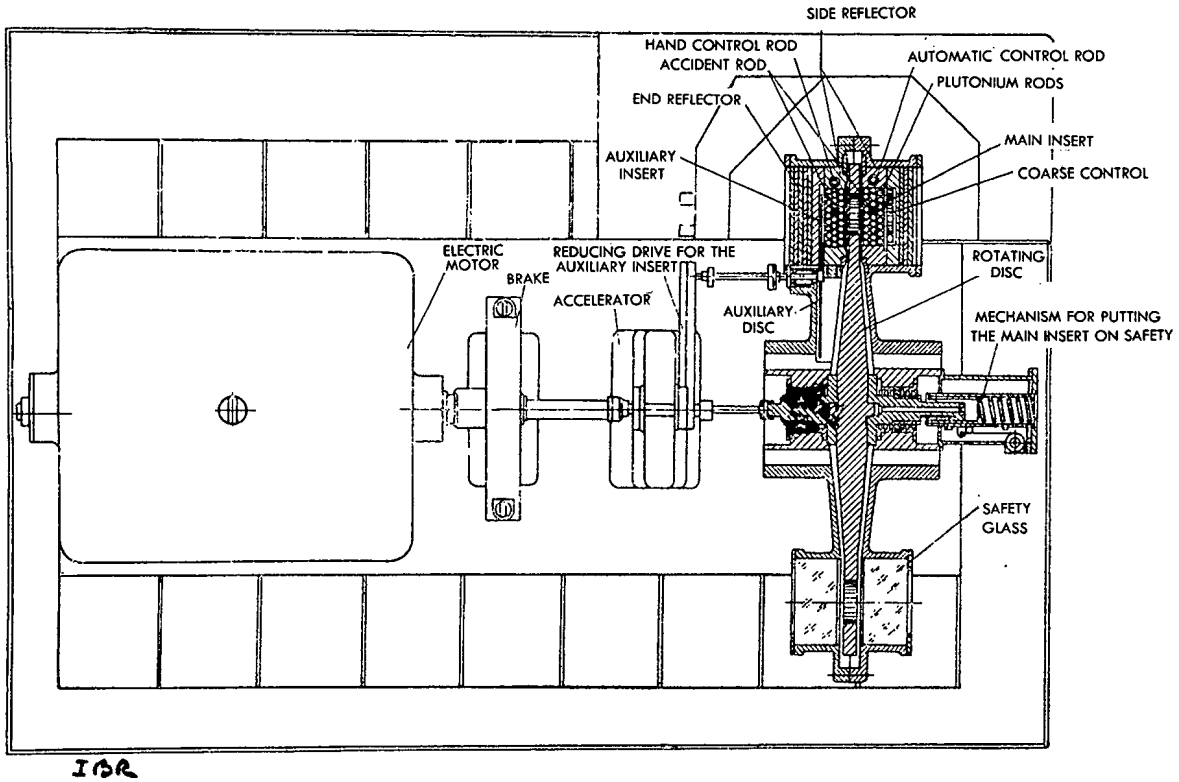

Figure 24

Fig. 2. Constructional layout ~~of the IBR reactor~~ IBR. 1) Rotating disc; 2) auxiliary disc; 3) main insert; 4) plutonium rods; 5) accident rod; 6) coarse control; 7) automatic control rod; 8) hand control rod; 9) side reflector; 10) end reflector; 11) safety glass; 12) mechanism for putting the main insert on safety; 13) accelerator; 14) reducing drive for the auxiliary insert; 15) brake; 16) electric motor; 17) auxiliary insert.

(see Fig. 2). The main insert is pressed into a disc 1100 mm in diameter and can be moved with a rotational velocity up to 276 meters per second (at 6,000 revolutions per minute) going through the active zone. The auxiliary insert is pressed into a small disc and moves on the edge of the active zone. It serves to change the frequency of the impulses without changing their form and may be rotated at different frequencies relative to the frequency of the principal disc. The reactor becomes supercritical and the power pulses are developed only in case the main and auxiliary inserts coincide simultaneously with the fixed part of the active zone. The maximum change in reactivity in moving the main insert amounts to 7.4%; on moving the auxiliary insert it amounts to 0.4%. The fixed part of the active zone consists of plutonium rods with a stainless steel cladding. Each rod is provided with a conical end piece which holds it in the upper or lower supporting lattice of the active zone. Fastening the rods on only one side ensures a negative temperature coefficient of reactivity (because of the bending of the rods on heating in the nonuniform neutron field) and thus improves the safe operating conditions of the reactor. The safety and control system of the IBR reactor provides the reactivity change required at startup, in working, and at shutdown of the reactor (including shutdown from accident) as well as control of the power level under all operating conditions and automatic hold-down of the power level when working at power outputs greater than 1 watt. Startup of the reactor is accomplished by means of the coarse control (see Fig. 2), which is a movable part of the reflector. By means of a servomechanism the coarse control can be moved in such a way as to produce reactivity changes at a rate from 13.10^{-5} to 1.3×10^{-5} sec $^{-1}$. The hand control, which is a 20-mm diameter rod, is likewise part of the reflector. The automatic control (likewise a rod) is connected to its own servomechanism. The accident shutdown mechanism consists of two plutonium rods in the fixed zone (AC-1 and AC-2) supported by electromagnets. At the appearance of the accident signal, the rods, moved by springs and their own weight, drop out of the active zone with an acceleration of 20 g.

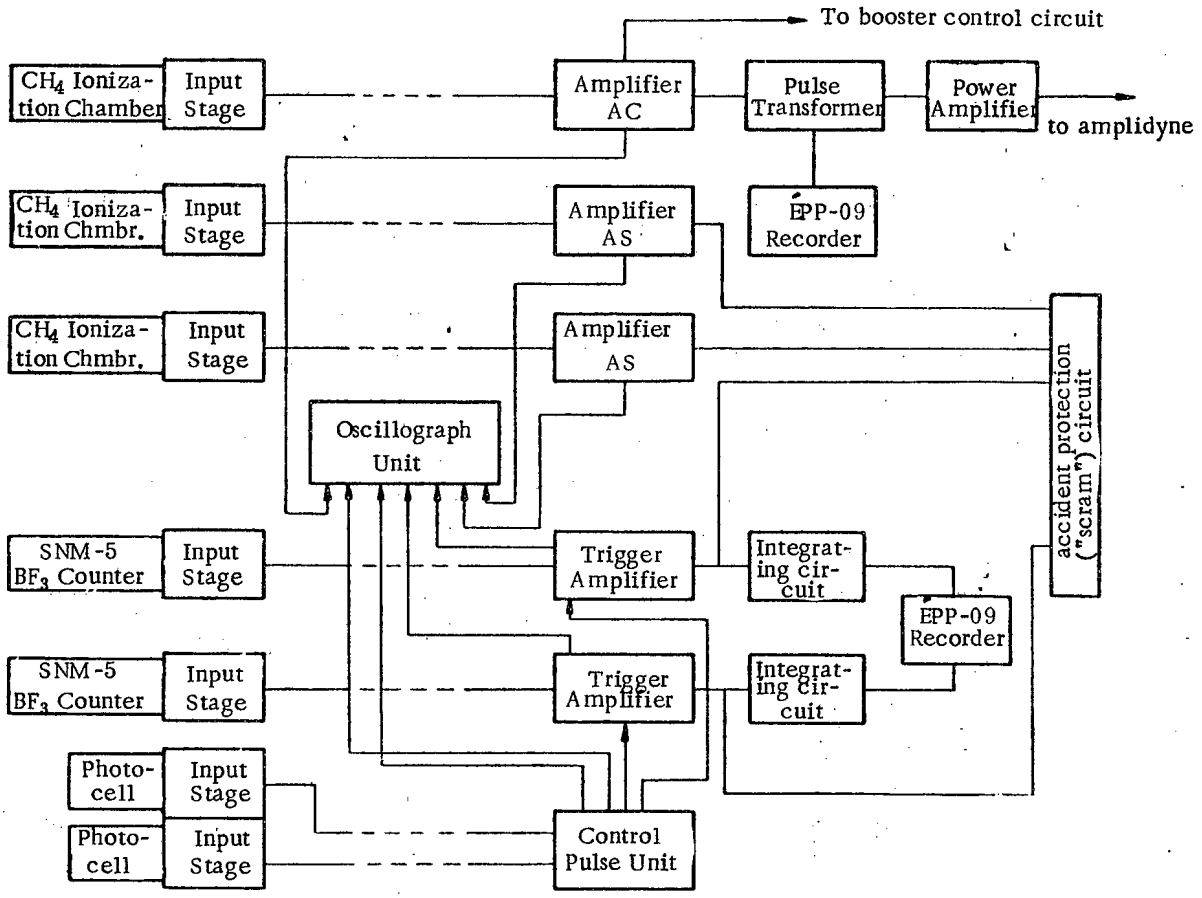

Fig. 3. Block diagram of electronic equipment.

The various parts of the control system give the following reactivity changes: AC-1 and AC-2, 1.1% (each); the coarse control, 2.4%; the hand control, 0.1%; and the automatic control, 0.036%.

The reactor is provided with a special mechanism intended to produce powerful single pulses (reactivity booster).

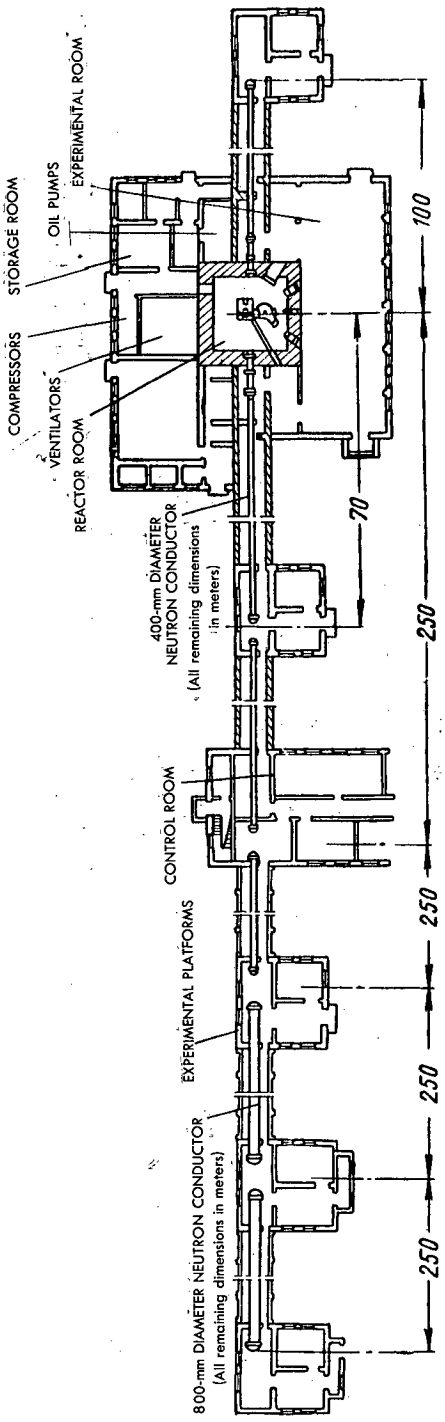

Fig. 4. Plan of IBR reactor facility: 1) reactor room; 2) control room; 3) experimental room; 4) oil pumps; 5) ventilators; 6) compressors; 7) storage room; 8) experimental platforms; 9) 800-mm diameter neutron conductor; 10) 400-mm diameter neutron conductor (all remaining dimensions in meters).

The safety and control system uses two groups of indicators – starting indicators and working indicators. The starting indicators are proportional BF_3 counters in paraffin. At low powers (very subcritical) the amplified pulses from the counters of about 0.5-microsecond duration are fed to scaling circuits and rate counters. A time-gate system is used, synchronized with the rotation of the main disc by means of a photocell. This scheme insures neutron counting only at the time that the main insert is passing through the fixed zone. At higher powers the pulses from the proportional counters are integrated and the resulting pulses, with the duration of about 600 microseconds, the amplitude of which is proportional to the energy of the power pulse, are measured by means of the integrating circuits and are observed on an oscillograph. At powers above 1 watt, an electronic pulse apparatus is used, the indicators of which are pulse current ionization chambers filled with methane. The pulse of ionization current in the chamber produced by neutrons and γ rays is amplified and fed to the trigger circuit of the accident control (two independent channels) and to the input of the pulse transformer.

The accident control system shuts down the reactor if the amplitude of one of the power pulses exceeds a given value. The voltage at the output transformers is proportional to the amplitude of the power pulse. It is fed to an automatic control circuit of the usual type (comparison circuit, power amplifier, amplidyne and servomechanism). A block diagram of the electronic circuits of the safety and control system is given in Fig. 3 (where the amplifier AC is the amplifier for the automatic control and the amplifier AS is the amplifier for the automatic safety).

The rotation of the main and auxiliary discs is accomplished by means of a powerful setup with a maximum output of 100 kw. The setup includes an accelerator with electric drive as invented by Leonardo (three-machine assembly). A control system is provided for starting and stopping the machine and maintaining a constant rotational speed with an accuracy of about 2% over the range 2000 to 6000 revolutions per minute.

To cool the air which is heated by friction in the main disc housing, the air is circulated through a system of water-cooling pipes and is passed into the reactor room. The fixed part of the active zone is cooled with atmospheric air circulated by a compressor. The air flow is about 60 m^3/hr.

The IBR reactor is located in the center of a room with dimensions 10× 10× 7 meters (Fig. 4). The concrete walls of the room give complete protection from radiation. The reactor is provided with a considerable number of special apparatus setups which would make it possible to carry out a wide range of neutron experiments. The basic experimental setup is the main neutron conductor with a length of 1000 meters.

The main neutron conductor is a metallic pipe with a diameter of 400 mm in the first section and 800 mm in the second section. A vacuum of the order 0.1 mm Hg is maintained in the pipe. The neutron conductor is provided with a chain of intermediate platforms which make it possible to set up experimental apparatus at distances of 70, 250, 500, 750 and 1000 m from the reactor. Along with the main neutron conductor there is an auxiliary neutron con-

ductor 100 m long. Directly adjoining the reactor room (see Fig. 4) is an experimental room. Four neutron beams of diameters up to 800 mm may be led into it. Neutron beams may also be led into an upper experimental room which is located over the reactor room.

Startup and Physical Tests on the IBR Reactor

The first step of the physical tests on the IBR reactor was carried out on builtup assemblies with an immobile or slowly moving main insert. Otherwise the builtup assemblies completely simulated the active zone of the reactor. The basic purpose of the builtup assemblies was to determine the critical loading, measure the efficiency of the control circuit and to study the fundamental characteristics which determine the length of the pulse, namely, the main useful lifetime of the neutrons in the reactor (τ) and the parameter which gives the rate of change of reactivity when the main insert is going through the fixed zone (α). Actually the half-width of the power pulse from the IBR reactor (Θ) can be expressed at equilibrium (see [1]) by the formula

$$\Theta = K\left(\frac{\tau}{\alpha}\right)^{1/3} v^{-2/3}. \tag{1}$$

Here $\underline{v}$ is the rate of motion of the main insert, K is a coefficient which is only slightly dependent on τ, α, $\underline{v}$ and the pulse energy; α is a parameter of the parabola which gives the approximate relationship between the reactivity ϵ and the motion of the main insert in the region of the maximum multiplication factor;

$$\varepsilon = \varepsilon_m - \alpha x^2, \tag{2}$$

where ϵ_m is the reactivity at the maximum multiplication factor of the system (where for prompt neutrons $\epsilon_m > 0$); $\underline{x}$ is the displacement of the main insert.

The determination of the critical loading and the measurement of the efficiency of the control units were carried out in usual fashion (see, for example, [2]). Rossi's method [3], was used to measure τ. α was measured by noting the change in reactivity of the system when the main insert is moved slowly through the fixed zone. The experiments were made in the subcritical state (the maximum multiplication in the intensity of a constant neutron source was about 1000). A number of different layouts in the fixed part of the active zone were studied. With the optimum layout chosen, the values of α and τ were $\alpha = 0.7 \cdot 10^{-3}$ cm^{-2}, $\tau = 1.2 \cdot 10^{-8}$ seconds.

While we were testing the builtup assemblies, we also measured the temperature coefficient of reactivity for uniform heating of the active zone. The value of the coefficient was -0.8×10^{-5}/°C.

After assembling the active zone of the IBR and completing the studies on the immobile reactor, further experiments were made on the nominal rate of motion of the main insert (230 m per second; 5000 revolutions per minute). In these experiments we used a Ra-α-Be source placed in the active zone. The more the power was raised, the greater was the effect of the delayed neutrons, the intensity of which at a power of about 0.1 watt was comparable with the intensity of neutrons from the Ra-α-Be source.

The multiplication factor of the IBR reactor as a function of time with the control elements withdrawn is given in Fig. 5. As the reactor is started up the maximum multiplication factor (K_{max}) increases and the reactivity curve approaches the level K = 1. Here the system goes through the following regions:

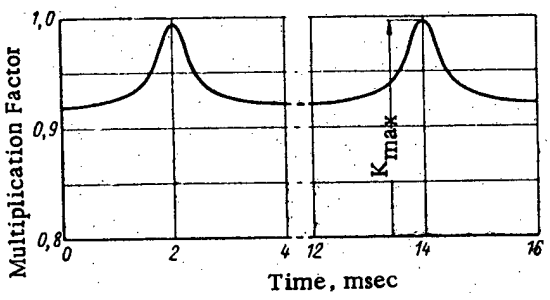

Fig. 5. Multiplication factor as a function of time (83 pulses per sec.)

1. The quasi-stationary region (very subcritical for prompt neutrons, $K_{max} < 1$). In this region the neutron flux in the reactor is able to "follow" the changes in reactivity of the system (excluding, of course, the delayed neutrons). Therefore the multiplication in the intensity of the auxiliary neutron source is given for any moment of time by

$$Y = \frac{1}{|\varepsilon|}. \tag{3}$$

The half-width of the power pulse (Θ) as a function of the reactivity ($-\epsilon_m$) at the moment the movable and fixed parts of the active zone coincide may be expressed by the equation

$$\Theta = 2\sqrt{\frac{|\varepsilon_m|}{\alpha v^2}}. \tag{4}$$

2. The region near prompt criticality. Here the maximum multiplication is already considerably less than that given by Eq. (3). Along with this, even the form of the pulse differs from the quasi-stationary one. The pulse begins to be delayed relative to the moment which corresponds to the maximum value of the multiplication factor.

3. Pulse subcriticality region. In this region the system is for a short time supercritical with prompt neutrons, but this supercriticality is not sufficient for equilibrium operation of the reactor (the maximum value of the positive supercriticality ϵ_m is less than the equilibrium value). In this region the pulse energy may be expressed by (see [1])

$$\left.\begin{aligned} E &= \frac{S}{\nu} K(\varepsilon_m); \\ K(\varepsilon_m) &= \frac{2{,}5}{v\sqrt{\alpha\varepsilon_m}} \exp\frac{1{,}33\varepsilon_m^{3/2}}{v\tau\alpha^{1/2}}, \end{aligned}\right\} \tag{5}$$

where ν is the mean number of secondary neutrons from fission and S is the intensity of the auxiliary neutron source.

The behavior of the mean reactor power with time in this region is similar to the behavior of the power of the usual subcritical reactor, i.e., the rapid introduction of some amount of positive or negative reactivity causes a jump in the mean power and then a slow change in power to a value which corresponds to the new value of reactivity.

4. Region of Pulse Criticality. The reactor is in an equilibrium state and the behavior with time of its mean power level is not different from the behavior of the mean power of an ordinary critical reactor in which the effective fraction of delayed neutrons has been reduced. The kinetic behavior of the IBR reactor at equilibrium is described by the equations

$$\left.\begin{aligned} W(t) &= \frac{\Sigma C_i(t)\lambda_i}{\nu} K(\varepsilon_m) n; \\ \frac{dC_i(t)}{dt} &= -\lambda_i C_i(t) + W(t)\beta\nu. \end{aligned}\right\} \tag{6}$$

Here W(t) is the mean reactor power, $C_i(t)$ is the concentration of delayed neutron sources belonging to the ith group. β is the yield of delayed neutrons belonging to the ith group and $\Sigma\beta_i = \beta$. The condition for equilibrium operation of the reactor is given by the following expression:

$$K(\varepsilon_m) n\beta = 1. \tag{7}$$

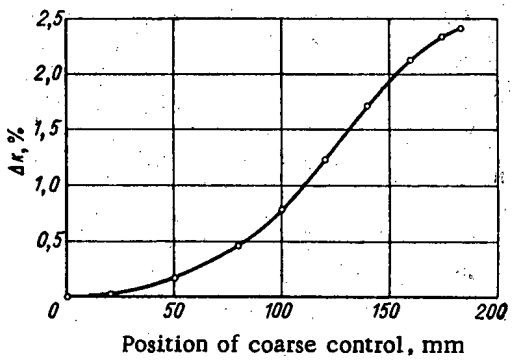

Fig. 6. Reactivity as a function of the position of the coarse control.

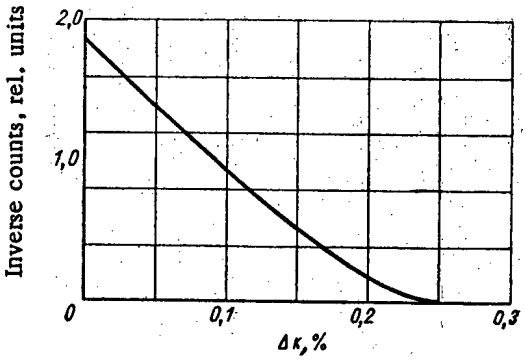

Fig. 7. Extrapolation curve for pulse criticality.

While the reactor was going from the quasi-stationary region to the region of impulse criticality, we studied the form of the power pulses and recorded the growth in the mean reactor power. In order to observe the form of the

pulses we used a scintillation counter with a phosphor consisting of ZnS on Plexiglas. The pulses from this detector were fed to the input of a 1024-channel time analyser which was triggered by the photocell to synchronize with the rotation of the main disc.

The monitoring of the mean power was accomplised by fission chambers containing layers of U-235. Two chambers located at different distances from the reactor made it possible to cover a range of mean powers from 10 milliwatts to 500 watts. In addition, to measure the mean power in the range 50-200 watts we used a fission chamber with a known quantity of U-235.

The degree of criticality in the course of raising the reactor power level was determined by extrapolation, in which we used the curve of reactivity as a function of position of the coarse control (Fig. 6). Extrapolation was done from "the multiplication of the pulse" given by the time analyzer as the ratio of the maximum counting rate of the neutron detector to the counting rate between pulses (the multiplication of the background between pulses with the main insert withdrawn from the reactor was measured to sufficient accuracy in experiments with the main insert stationary).

The extrapolation curve (Fig. 7) shows a straight portion directed toward the region of prompt criticality ($\epsilon_m = 0$). This portion corresponds to the quasi-stationary region [Eq. (3)]. Near prompt criticality the curve begins to depart from linearity and subsequently extrapolation is no longer made from the multiplication in the pulse, but from the counting rate at the peak, including the increase in the background from delayed neutrons.

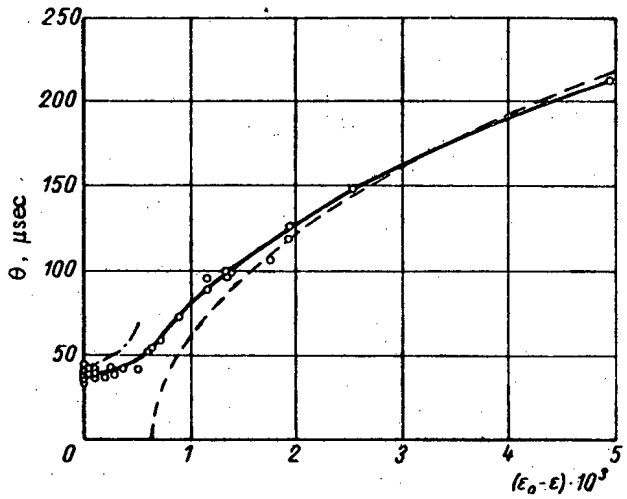

Fig. 8. Pulse half-width, Θ, as a function of reactivity. Reactivity reading from equilibrium supercriticality: – – – – quasistationary case, – · – · – Eq. (1).

The quasi-stationary region and the transition to prompt and pulse criticality are easily followed also in the curve of Fig. 8, which gives the half-width of the pulse as a function of the reactivity. Here the dotted curves are the half-widths as a function of reactivity for the quasi-stationary case (Eq. 4) and for Eq. (1). The characteristic pulse forms for different values of reactivity are given in Figs. 9-11. The half-width of the pulse at equilibrium was 36 microseconds. Thus the peak power of the reactor operating at 90 pulses per second reaches 360 kw.

It should be emphasized that the statistical character of the neutron multiplication has more effect on the operation of a pulse reaction than on the operation of ordinary stationary reactors. This arises especially at small mean powers from the relatively small number of primary fission events which determine the development of the pulse. This causes considerable fluctuation in the energy and consequently in the amplitude of the pulses.

It can be shown that the expression for the mean square

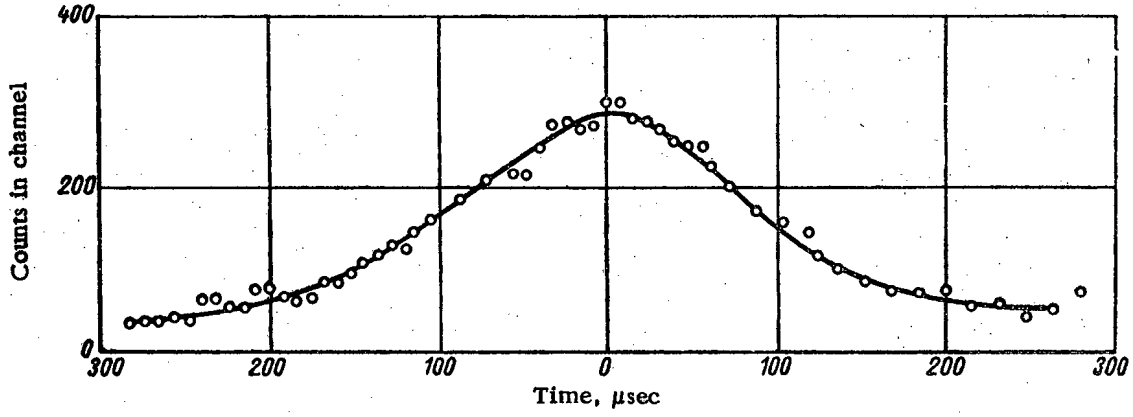

Fig. 9. Form of power pulse for $\epsilon_m = -5 \cdot 10^{-3}$.

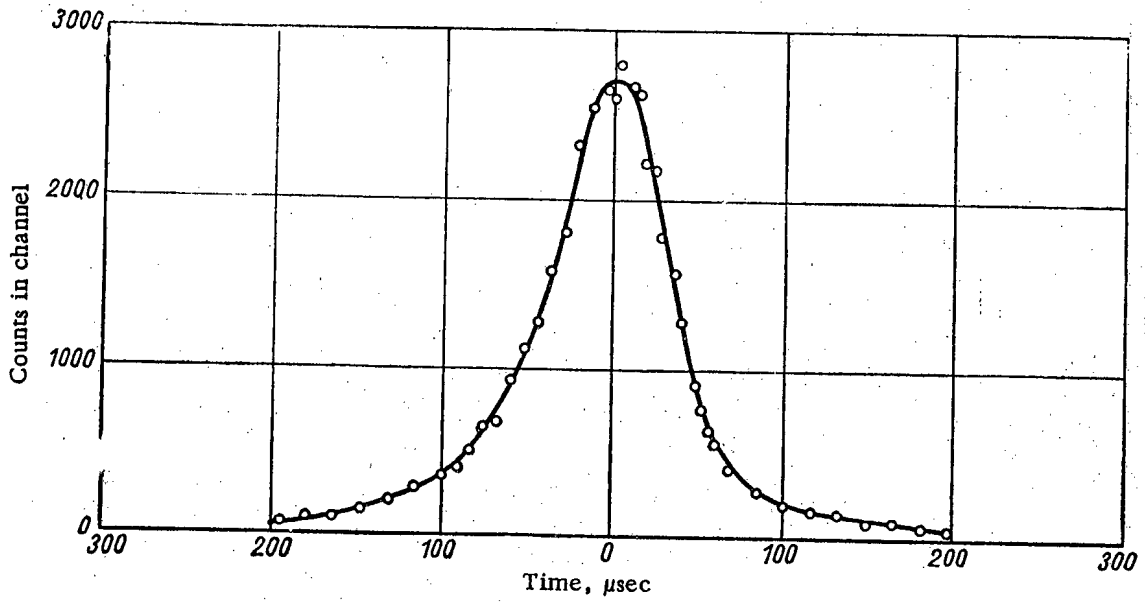

Fig. 10. Form of power pulse for $\epsilon_m = -0.4 \cdot 10^{-3}$.

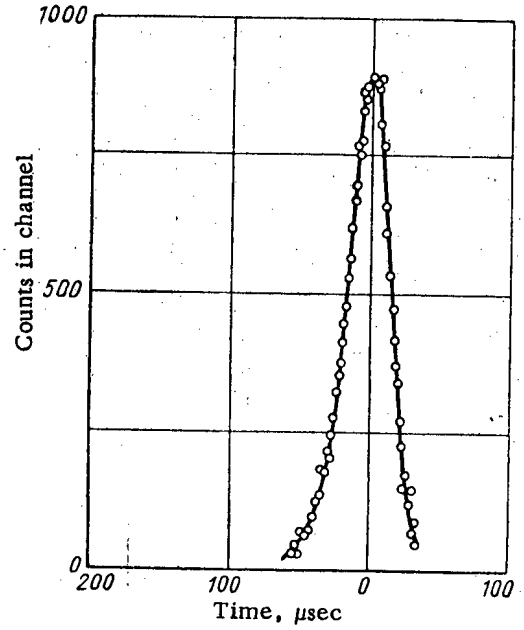

Fig. 11. Form of the power pulse at equilibrium (pulse criticality, $\epsilon_0 \simeq 0.6 \cdot 10^{-3}$).

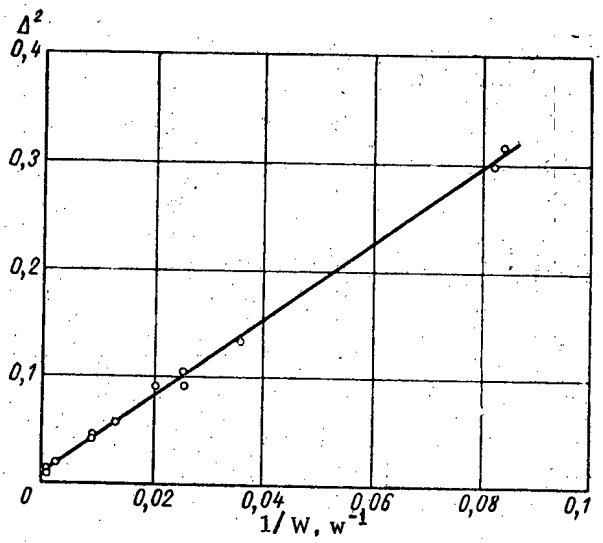

Fig. 12. Relative half-width of the pulse amplitude distribution as a function of power.

spread in amplitude of the pulses from the IBR reactor has the following form:

$$\frac{\sigma(I)}{\bar{I}} = \sqrt{\frac{\nu\Delta^2}{2S\tau}}. \tag{8}$$

Here I is the amplitude of the pulse and Δ^2 is the dispersion in the multiplication factor for a single fission event. Since the probability of emitting a definite number of neutrons on fission is relatively well described by the Poisson distribution, we can for an approximate estimate of the fluctuation take Δ^2 about equal to one. Then for equilibrium operation of the IBR reactor we obtain

$$\frac{\sigma(I)}{\bar{I}} = \frac{1}{\sqrt{2W\beta\tau}}. \tag{9}$$

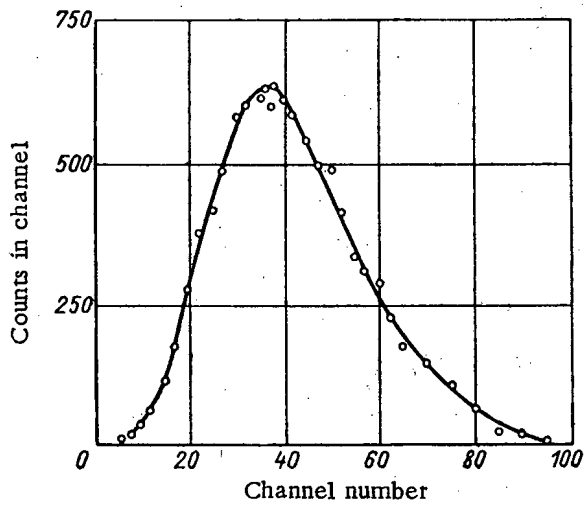

Fig. 13. Pulse amplitude distribution at a power of 4 watts.

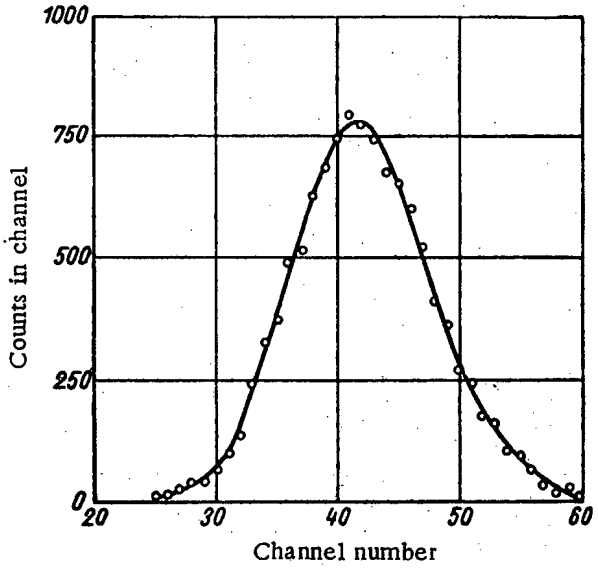

Fig. 14. Pulse amplitude distribution at a power of 40 watts.

Here W is the mean power output (the number of fissions per second) and β is the effective fraction of delayed neutrons.

The fluctuations in the amplitude of the power pulses were investigated by means of an amplitude analyzer which received the impulses from the methane ionization chamber. The amplitude distribution was measured at different mean power outputs. Figure 12 shows the square of the dispersion as a function of the mean power. Figures 13-15 show the distribution and amplitude of the pulses at mean powers of 4, 40 and 1200 w respectively. It is interesting to see that the values of mean reactor power obtained from these distributions by means of Eq. (9) were in good agreement with the results of the measurements of mean power by two other methods, namely from a calibrated neutron source and from a fission chamber with a known quantity of U-235.

At the present time experiments have been started on the IBR reactor to measure the total cross sections and the cross sections for scattering, capture and fission using the time-of-flight method. The physics experiments are also being continued in the direction of raising the mean power and reducing the pulse length.

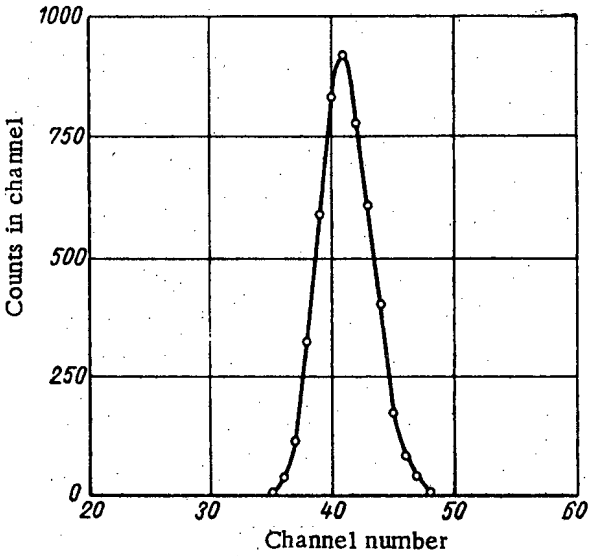

Fig. 15. Pulse amplitude distribution at a power of 1200 watts.

LITERATURE CITED

1. I.I. Bondarenko and Yu.Ya. Stavisskii, Atomnaya Énergiya 7, No. 5, 417 (1959).
2. A.I. Leipunskii et al., Atomnaya Énergiya 5, No. 3, 277 (1958).
3. J. Orndoff, Nucl. Sci. and Engng 2, No. 4, 450 (1957).

All abbreviations of periodicals in the above bibliography are letter-by-letter transliterations of the abbreviations as given in the original Russian journal. *Some or all of this periodical literature may well be available in English translation.* A complete list of the cover-to-cover English translations appears at the back of this issue.

BEHAVIOR OF GRAPHITE IN NUCLEAR REACTOR STACKS

V.I. Klimenkov

Translated from Atomnaya Énergiya, Vol.10, No. 5,
pp. 447-460, May, 1961
Original article submitted July 14, 1960

The results of a study of radiation effects in graphite and the influence of those effects on the design of graphite stacks for nuclear reactors are discussed in this article. Several of the manifestations of these effects may lead to serious complications in reactor performance. Measures used to avert such complications are considered. A unified approach to the physical nature of the radiation effects in graphite is suggested for a broad range of elevated temperatures. The problem of preventing oxidation of graphite is approached in the light of the high temperatures prevailing in the graphite stacks of reactors of recent design.

Introduction

The use of graphite as a moderator for neutrons and as a structural material in nuclear reactors is explainable in terms of its excellent nuclear properties and its availability. As experimental data on graphite and its behavior have progressively accumulated, it has become increasingly clear that the properties of graphite experience pronounced modification upon exposure to in-pile nuclear radiation. The effect of these changes is of sufficient importance to warrant their being taken into account in reactor design and performance studies.

From the practical standpoint, the most important radiation effects observed in graphite, predicted in general terms by Wigner (hence the term "Wigner effects," which is sometimes used) at the very dawn of reactor technology, are the dimensional instability of graphite components, the storing of latent energy (Wigner energy), and lowering of thermal conductivity. These effects have been studied for low-temperature reactors, and the results of the research were published in 1955. Nevertheless, the incomplete nature of the available information and the failure to take due account of the laws operating in the storage and release of latent energy in graphite led in 1957 to a major accident at the reactor No. 1 of the Windscale plutonium plant in Britain. The aftermath of this accident was the focusing of serious attention on the part of researchers upon this problem of stored energy and its effects. In the meanwhile, much data has been accumulated on radiation effects in graphite with increased irradiation dosage in low-temperature reactors, and manifestations of radiation damage in the structure of reactor graphite stackings have been subjected to study.

In view of the fact that radiation effects in graphite show a marked dependence on graphite temperature during exposure to radiation and that such effects are not conspicuous at elevated temperatures, the problem of using graphite at high temperatures in reactors, utilizing its unique properties as a high-temperature refractory, has gained in interest. However, we then encounter the question of accounting for the effects of irradiation on the properties of graphite in a high-temperature environment, as well as the question of graphite oxidation.

Effects of Prolonged Irradiation on Graphite

Until 1955, radiation effects in graphite had been studied in an integral flux of thermal neutrons of approximately $(4\text{-}7) \cdot 10^{20}$ neutrons/cm^2 [1-4]. As a result of these studies, it became known that the higher the temperature of the graphite under irradiation, the slower the rate of change of the properties of the irradiated graphite and the more rapidly a point of saturation and tapering off in the change of properties would be encountered. The saturation sets in as a result of competing processes of imperfections caused by the irradiation and the disappearance of such imperfections through annealing action. Upon saturation, the rate of anneal of the imperfections is roughly equal to the rate at which the imperfections appear. For these competing rates to reach equilibrium at an irradiation temperature of about 30°C, a dosage larger than that attained in the investigations cited would be required.

Investigations were later carried out at an irradiation dose $nvt = 2.34 \cdot 10^{21}$ neutrons/cm^2 [5]. This large dose was sufficient to attain a near-saturation state, even for irradiation at 30°C (Fig. 1).

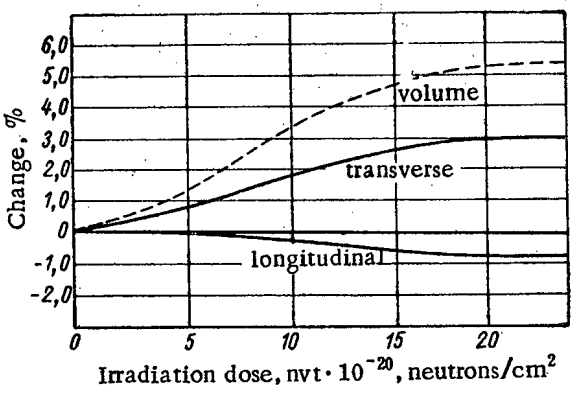

Fig. 1. Change in length and volume of one of the conventional grades of CSF reactor graphite at an irradiation temperature of 30°C.

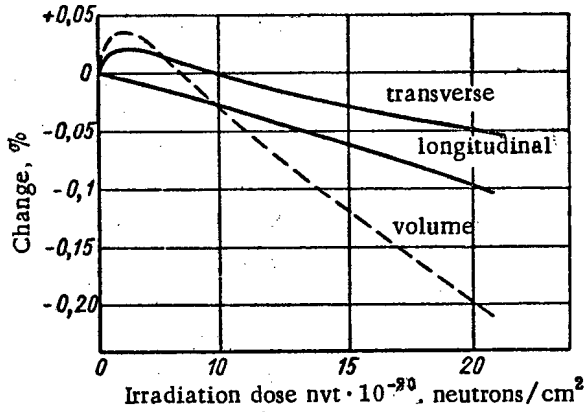

Fig. 2. Change in length and volume of CSF graphite at irradiation temperature 400-500°C.

In Fig. 1 (see also Fig. 2), the terms "longitudinal" and "transverse" characterize the directions in which the specimens were cut, either parallel or perpendicular to the axis of extrusion of the graphite block. The anisotropy evident in the properties of graphite is related to the pronounced anisotropy of the crystal and to the texture formed by the eccentricity of the coke particles from which the graphite is fabricated. In planar or elongated particles of coke, the graphite sheets are orientated parallel to the axis of the particles. During the extrusion process, the long axes of the particles are orientated predominantly parallel to the direction of extrusion, so that the graphite sheets of the crystallites turn out to be parallel to the axis of extrusion in graphite components. As the distance between those sheets increases, the crystallite expands in the direction perpendicular to the graphite sheets. The sheets are bonded together by weak Van der Waals forces, and may therefore be shifted appreciable distances when atoms or groups of atoms become intercalated between them. The crystallite contracts in the direction aligned with the graphite sheets, since the atoms held together by covalent bonding in the sheet layers are drawn together along the contour of the sheet when vacancies occur, thus diminishing the mean interatomic spacing.

As a result of these peculiar features, graphite expands much more readily in the direction perpendicular to the extrusion axis. In CSF graphite, which has a higher degree of preferential orientation, longitudinal specimens even evidence some contraction. However, this contraction is considerably less than the expansion observed in perpendicular specimens, since an increase in the volume of the graphite is observed on the whole, attaining 5.5% upon saturation,

It is interesting to note that the interplanar spacing (along the c_0 axis of the crystal) increases by 16%, while the volume of a unit cell of the crystal lattice increased to a degree far exceeding the bulk swelling of graphite. This effect of lack of correspondence between swelling of graphite on the microscopic and on the macroscopic level was known even earlier; it has now been proved that a 50% difference occurs upon saturation. Nightingale et al. [5] and earlier authors [2, 3] have accounted for this effect by the view that the density of conventional reactor-grade graphites, including CSF graphite, is only about 75% that of the crystal, and that an appreciable free volume permitting the crystals to expand without a general increase in volume exists within the graphite. However, a set of new facts on dimensional instability of graphite at elevated temperatures [5] favor a somewhat different and unique interpretation of the mechanism responsible for those effects, as well as new effects.

Radiation Effects in Graphite at Elevated Temperatures

Data characterizing the behavior of graphite at elevated temperatures were previously restricted to a temperature of 250°C. As the development of nuclear power engineering progressed, attention was called to the need to investigate the temperature range from 500 to 1000°C.

Figure 2 shows the effect of pile irradiation at high temperatures (400-500°C) on the dimensional characteristics of CSF graphite [5]. As is evident, a contraction of transverse specimens occurs, rather than the expansion observed at 30°C. Longitudinal specimens which diminish in length at 30°C also suffer contraction at higher temperatures, even more so than do transverse specimens, but still to a lesser extent than the contraction observed at 30°C. Bidirectional contraction in response to the highest doses of irradiation investigated (nvt = $1.7 \cdot 10^{21}$ neutrons/cm^2) follows an almost linear pattern, but this contraction is far inferior in magnitude to the expansion recorded in low-temperature irradiation. The over-all volume decrease in graphite constitutes several tenths of a percent.

It is common knowledge that the development of graphitic structure in graphitization of carbon materials is determined by the graphitization temperature, with the degree of graphitization varying as the temperature. In [5] it is shown that the material with the less-developed graphitic structure contracts to a considerably greater degree. One would naturally assume contraction to proceed predominantly as a result of the further development of the graphite structure, which might occur in response to a higher temperature, and possibly in response to neutron bombardment. However, the increase in the crystal lattice parameter c_0 and the apparent decrease in crystallite size, observed at high temperatures as well as in low-temperature irradiation (at 30°C), testify to an accumulation of the radiation-induced imperfections and to a disordering of the structure. Thermal cycling tests under laboratory conditions failed to indicate any changes in the dimensions of CSF graphite [5]. Contraction is therefore a consequence of in-pile irradiation.

The change in properties of graphite at irradiation temperatures 400-500°C is insignificant, but nevertheless perceptible. The decrease in thermal conductivity shows a clearly pronounced tendency to saturation occurring at an irradiation dose of about $1.2 \cdot 10^{21}$ neutrons/cm^2. At an irradiation temperature of 400°C, thermal conductivity drops by about four times. The variation in thermal conductivity recorded at 500°C is somewhat less. Latent energy is stored up to some extent and is completely released at moderate annealing temperatures up to 1000°C.

Nightingale et al. [5] offer no information on changes in other properties of graphite, but do report data on changes in its properties for irradiation temperatures up to 1050°C. An increase in the parameter c_0 and a reduction in crystallite size are reported. Graphite experiences a disarrangement in its crystalline structure even at 1050°C, as we see. On the whole, graphite shows a contraction which even up to 750°C is not much greater than that observed at 500°C, although the degree of contraction shows an increase at higher temperatures (975 and 1050°C). No further data are needed to support the conclusion deduced.

The Mechanism Underlying Radiation Effects in Graphite and Radiation-Stable Graphite

According to the views of Nightingale and associates [5], contraction of graphite in high-temperature irradiation occurs as a consequence of more efficient packing of the crystals. When fast neutrons are scattered on the carbon atoms in graphite, an appreciable quantity of energy is imparted to the carbon atoms, so that a large number of atoms in localized volumes of the crystallite acquire the energy of activation for diffusion. Crystallites joined by edges and corners in the process of development of the graphitic structure during graphitization may come asunder through radiation-induced diffusion. Stresses "frozen in" during the graphitization process may be relieved in that manner. The increase in density of the graphite, expressed in a reduction of specimen dimensions. may follow as a result. However, this hypothesis fails in its present form to account for the specifics of high-temperature effects observed in graphite exposure. Available facts indicate that both processes, i.e.,swelling of the graphite as a result of increased volume occupied by the unit cell of the crystal lattice, and contraction of the graphite as a result of closer packing of crystallites, occur simultaneously over a broad range of graphite irradiation temperatures and are superposed upon one another. The definitive effect associated with dimensional instability is the difference in these two opposing and competing phenomena, which also differ in the way they depend on temperature.

Swelling depends strongly on temperature: At low irradiation temperatures (30°C), swelling is intense, but falls off in response to comparatively moderate temperature rises (to 150-200°C irradiation temperature). The effect associated with contraction is considerably less in amplitude, and is a sensitive function of temperature only when the temperature reaches very high levels (beyond 1000°C), whereupon it steps up slightly in amplitude. As a result, the swelling effect predominates in low-temperature irradiation. However, macroscopic swelling is less than the increase in volume occupied by the unit cell of the crystal lattice because of contraction of the graphite, which was viewed earlier only in terms of a masking of part of the microscopic swelling by porosity. In Fig. 2., the anomaly in the initial behavior of the curve of variation in dimensions of transverse specimens at irradiation temperatures 400-500°C apparently indicates some moderate degree of swelling which might counteract the contraction predominating under the given irradiation conditions. As we see, these two competing phenomena are associated with structural elements of different orders of magnitude. Swelling of the graphite is a result of a deep-lying effect of atomic scale, taking place inside the crystallite and consisting essentially of the disordering effect of irradiation upon graphite. Swelling is manifested with particular sharpness in a single crystal almost entirely free of imperfections. In a polycrystal, the effect depends on the initial state of the crystal lattice and will decrease as the degree of orderedness of the lattice decreases.

In contrast to swelling, contraction takes place on the scale of the polycrystal and is the result of a rearrangement of bonds between crystallites. It depends on the initial state of the bonding, which may be different depending

on the heat-treatment conditions of the material or depending upon graphitization conditions. High temperatures relieve stresses, so that contraction is insignificant in graphite subjected to intense graphitization. It should be completely absent in a single crystal.

In view of the presence of two such oppositely directed effects responsible for dimensional instability in graphite, the problem of producing a graphite stable to radiation is greatly complicated. It was reported [5] that carbon materials with a less developed graphitic structure and obtained at a somewhat lower graphitization temperature were employed in reactor design for those cases where large graphite swelling was inadmissible. However, those materials contracted to a large extent at elevated temperatures. To avert contraction, it was necessary to resort to the countermeasure of extreme graphitization. The only way out of the dilemma is apparently to make use of both types of graphite in reactor stacks.

Manifestation of Radiation Effects in Reactor Stacks

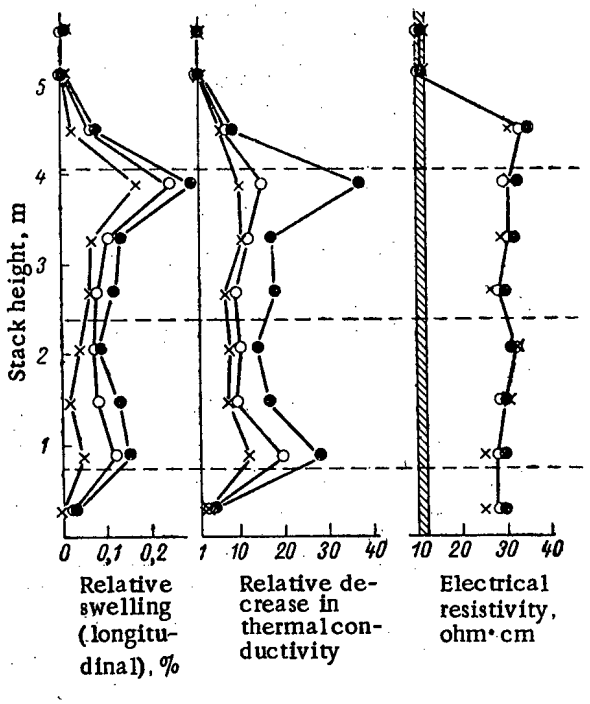

Fig. 3. Change in properties of irradiated graphite along height of stack, in layers: ● close to channel; O moderately removed; × furthest removed (about 8 cm). The horizontal dashed lines denote the boundaries and center of the core.

Radiation effects in the structure of graphite stacking, including dimensional instability effects, become manifest in a complicated manner depending on the space distribution of neutron flux and graphite temperature, as well as on the design of the particular reactor. Because of the marked temperature dependence of radiation effects [1, 2], zones of maximum storage of radiation-induced defects become delineated in the reactor stack, situated in stack regions where graphite temperature is at a minimum. Another characteristic dependence of the storage of radiation effects on neutron energy [1] leads to a nonuniform accumulation of radiation defects in the bulk of the graphite, in a cross section of the lattice cell. The greatest accumulation of radiation-induced imperfections is observed to take place in those layers of graphite which are closer to the source of radiation (to the uranium), i.e., at spots where the neutron spectrum is harder.

These patterns observed in the distribution of radiation-induced imperfections in a stack have been reported by Brokhovich et al. [6], who described research on radiation effects in graphite at the IR reactor. This research was conducted in the course of a dismantling of the reactor stack as the reactor was being disassembled after four years of service at an average power output of 50 Mw. The integral thermal neutron flux at the center of the reactor core was $4.5 \cdot 10^{21}$ neutrons/cm^2. The peak temperature of the graphite at the core center reached 400-500 °C.

The distribution of changes in the properties and dimensions of graphite along the height of the reactor stack are shown in Figures 3 and 4 [5]. The greatest changes in properties are noted in the upper core, with slightly less imposing changes seen in the lower core. A characteristic saddle point appears in the curves of variation of graphite properties vs. stack height at the center of the core.

In correspondence with the cases of close and distant exposure of graphite described in [1], the degree of swelling and the changes in thermal conductivity in the graphite bulk at about 8 cm along the direction leading from the cell axis to its periphery drops to about half. However, this decrease need not be interpreted exclusively as a result of a change in the neutron spectrum over the cell cross section, since a certain contribution is also made by the change in graphite temperature. Electrical resistivity and the mechanical properties of the graphite vary almost uniformly over the cell cross section.

Radiation-induced imperfections in the structure of the reactor stack cause swelling of the graphite, which in turn leads to a change in the dimensions of the graphite blocks. The maximum increase in the width and height of blocks placed in the peripheral zone of the IR reactor stack was 2 mm. The dimensions of blocks found in the central portion of the stack remained unchanged.

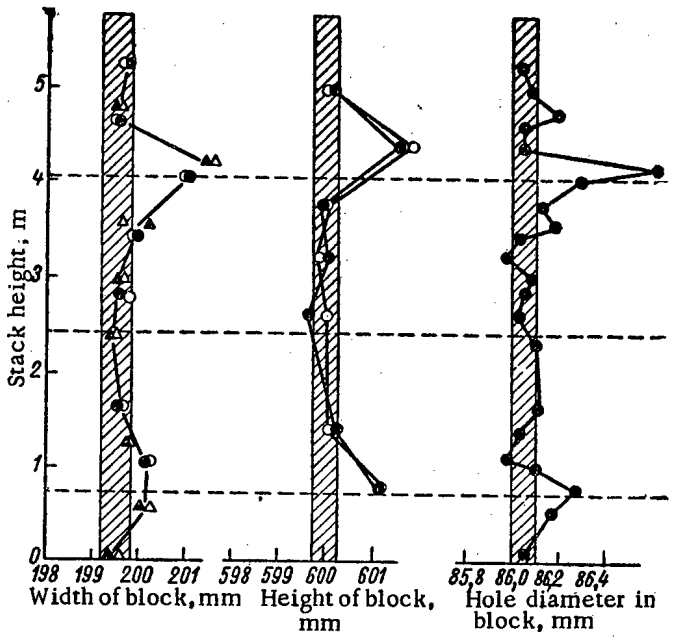

Fig. 4. Change in dimensions of graphite blocks along the height of the IR reactor stack. The horizontal dashed lines indicate the boundaries and center of the core. Symbols indicate different measurements at various graphite block edges.

Data on radiation damage in the graphite of the reactor built in the First Atomic Power Station (USSR) have been reported by Dollezhal' et al. [7], from whom we learn that the high temperature of the in-pile graphite (700-800°C) acted as a hindrance to any large-scale changes in graphite dimensions (as was indeed expected and taken into account in the design of the First Power Station reactor, based on extrapolations of empirical data on graphite behavior available at the time [8, 9]), while the temperature performance of the stack graphite was such that lower-temperature zones were absent in the stack.

Powell and associates [10] have described radiation damage in the graphite stack of the Brookhaven BNL research reactor (USA). The graphite in this reactor stack exhibited a fairly low peak temperature (about 250°C), favoring a net increase in radiation damages. This is aggravated by the fact that the coolant air is admitted to the center of the reactor stack, with the result that the graphite temperature reaches a minimum at the center of the stack, where neutron flux is at its peak. Under those conditions, the zone of maximum storage of radiation damage is the central portion of the stack, where the rate of accumulation of radiation effects is very high because of the high flux values.

When work was begun on construction of the BNL reactor (in 1947), information of radiation damage was still quite meager, but nevertheless the anisotropy of the swelling phenomenon was clearly indicated [10]. Measures were therefore taken during construction of the reactor to alleviate some of the expected difficulties attributed to expansion of the graphite and provisions were made for monitoring the dimensions of the entire stack. Results of a measurement of stack expansion are given in Fig. 5. It is clearly evident that the expansion is maximal at the center of the reactor near the air gap (18 mm in height and 22 mm in width).

The nonuniform deformation and the warping of reactor channels associated with it, as well as the generation of mechanical stresses in the graphite may, in a case where the reactor stack has a complicated configuration, result in the failure of graphite components, involving a hazard of jamming and wedging of fuel elements, control rods, or scram rods. A serious accident may be the end result. For that reason, the graphite used in the BNL reactor, as well as in other reactors where radiation effects are fraught with such serious consequences, is periodically annealed, in order to at least partially remove radiation defects accumulated in the stack. The increase observed in the height of the BNL reactor stack is plotted in Fig. 6 against irradiation dose and effect of annealing on the graphite.

Annealing of Radiation Damage

The principle of annealing [1-4] consists in the fact that the structure and properties of graphite, which undergo

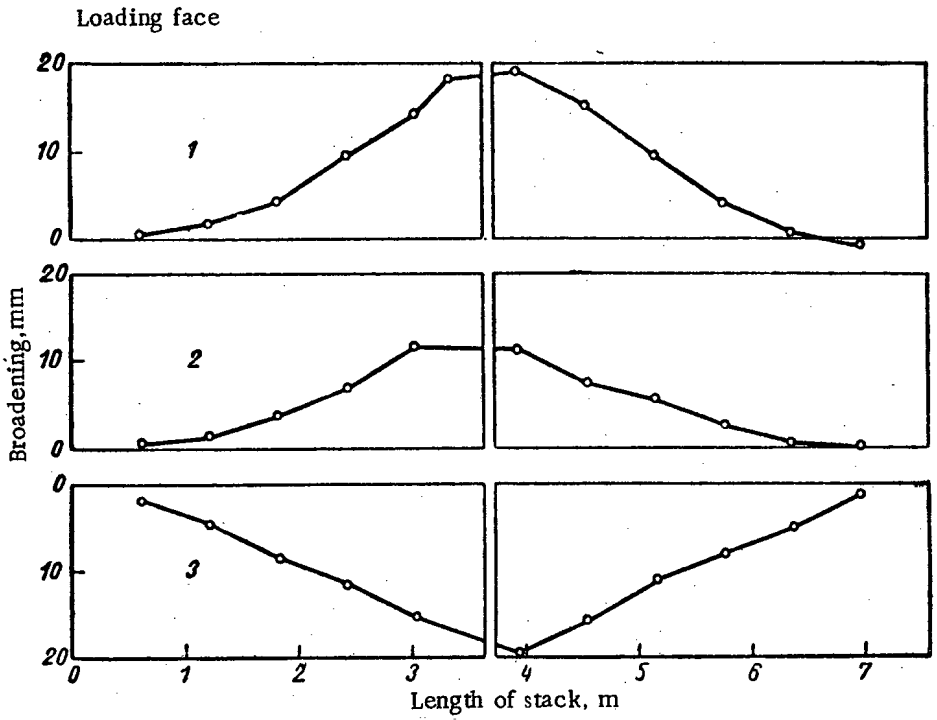

Fig. 5. Broadening of BNL reactor stack: 1) in height; 2, 3) in breadth.

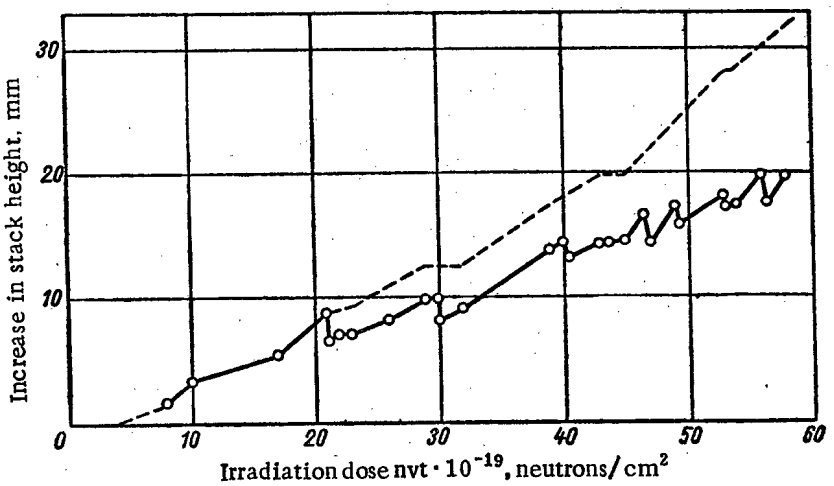

Fig. 6. Dose dependence of stack height in BNL reactor. Jogs in the graph indicate anneals. The dashed line interprets assumed increase without annealing.

changes induced by irradiation, recover their initial state when the graphite is heated to above the irradiation temperature. The potential energy stored by the graphite is thereupon released. Annealing of defects begins at a temperature somewhat higher than the irradiation temperature, and continues to temperature levels ranging 2000-3000°C.

An earlier contribution [2] barely mentioned nuclear annealing, i.e., radiation annealing. More detailed data may be found in [5]. The effect of thermal and radiation anneals on the crystal lattice parameters of graphite was shown. Radiation annealing is related to an intense local increase in temperature in the crystal lattice of graphite bombarded by fast particles, the result being that defects whose quantity is determined by the equilibrium state at the mean temperature of the graphite are retained in the lattice.

Annealing of radiation-induced defects in graphite is achieved through controlled heating of the stack to temperatures higher than operating temperatures, most of the heating being carried out by nuclear means, i.e., the heat released in the course of reactor operation is used for the heating, while the rise in graphite temperature is achieved by

varying the cooling conditions in the stack. Annealing thus proceeds in the presence of neutron flux, but it is nevertheless not properly considered radiation annealing as such. Annealing is usually carried out when the reactor is at a fairly low power level, and consequently at low neutron flux, and annealing time is of insignificant duration. Radiation annealing requires a large integral flux.

The first experimental anneals carried out in the BNL reactor took place, according to [10], during a change in the direction and magnitude of the stream of coolant air when the reactor was operating at a power level 1-2 Mw (the reactor power is rated at 26 Mw). The first anneal was performed in 1953 after two and a half years of operation, when the thermal neutron integral flux at the center of the active section was $1.7 \cdot 10^{20}$ neutrons/cm^2. This annealing operation is carried out periodically at an integral neutron flux of about $4 \cdot 10^{10}$ neutrons/cm^2 at the center, corresponding roughly to a four-month reactor period, or to a total power production of about 75,000 megawatt-hours.

When a stack is being annealed, provisions must be made for removing, under equilibrium conditions, not only the energy generated by the fission chain reaction, which is the heat source, but also the stored energy of the graphite, which is released during annealing, and may bring about a significant increase in the temperature of the graphite in case the rate of heat removal is inadequate. Because of this, reliability in the methods used to monitor and control the temperature of the graphite and fuel elements is a prime requisite when annealing is being carried out.

An unforeseen release of latent energy occurred while the No. 1 reactor at Windscale was shut down in 1952 [11]. No serious accident resulted at the time, and the incident served rather as a stimulus to further research on a subsequently successful method of pile annealing and release of stored energy. Only in the course of the eighth scheduled annealing of the No. 1 reactor stack in 1957 did a serious accident ensue, because of a number of errors committed.

The thermocouple wells for sensing the temperature of the pile graphite and uranium had been positioned in regions of peak operating temperatures, rather than in the region where maximum release of stored energy was to be expected [11-14].

In early 1958, a large-scale experiment on pile stack annealing was undertaken on the British BEPO reactor (British Experimental Pile, zero power, at Harwell) in order to study safe annealing conditions [15]. In contrast to heating operations on the BNL reactor stacking and that of the Windscale No. 1 pile, the BEPO reactor stacking was heated by means of a stream of hot air fed into the stacking through the normal course of the coolant stream. During the annealing, the reactor was operated at 10-kw power, allowing for reliable monitoring of fuel-element failure. The rated power of the reactor is 4-6 Mw, exit air temperature reaching 80°C.

Some attention should be directed to the careful preparations behind this experiment. Thermocouples (389) for recording pile graphite and uranium temperatures were positioned in a complex pattern throughout the stack. Before the anneal was started, a study was made of the distribution of stored energy in the graphite throughout the stack, and some estimates were made, on the basis of those findings, to aid in arriving at annealing conditions such that the upper temperature limit for the graphite would not be too high. This estimate was complicated by the fact that annealing of the graphite by pile heating has already been resorted to in 1954, after the BEPO pile had produced 160,000-Mw·hr power. During the annealing operation the reactor was operated at 0.5-Mw power with coolant air shut off for approximately 7 hours. The graphite temperature at the core center was raised to 120°C; the release of stored energy which then commenced raised the temperature to 325°C. As a result, only the central part of the stack was annealed. Despite this troublesome complication, theoretical data were excellently confirmed in practice during the second anneal in 1958, when the reactor had produced another 170,000-Mw·hr power.

The results of the annealing experiment demonstrated that there is a possibility of safe annealing of the stack and also a danger of self-sustained energy release which, initiated at a single point, may spread to most of the stacking.

Release of Stored Energy

The processes of energy storage during irradiation and release of the stored energy during annealing, with the energy amounting to possibly 500 cal/g, are subjected to the general laws governing the behavior of radiation effects. However, the process of release of stored energy features a peculiar trait of major importance. At an anneal temperature of about 200°C, an energy release peak occurs in a narrow temperature interval where the rate of energy release* appreciably exceeds the specific heat of the graphite. Although a large portion of the total energy is still re-

* The term "rate of energy release" is here understood to mean the quantity $\frac{\partial Q}{\partial T}$, where Q is the amount of energy released, and T is the temperature.

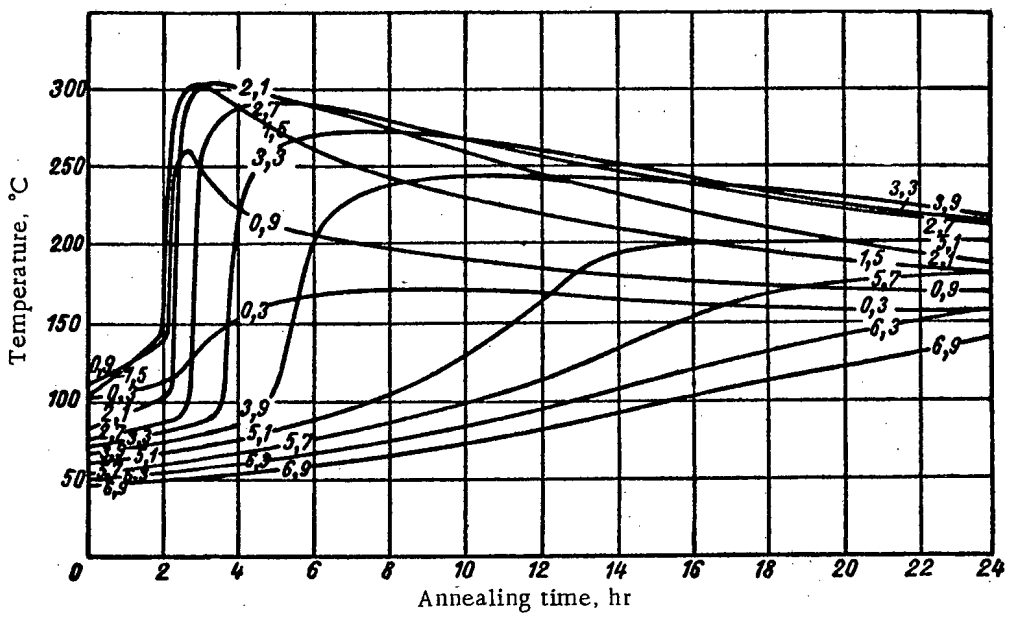

Fig. 7. Typical graph of graphite temperature vs. anneal time at various points along the length of the channel. Figures on curves indicate the distance (in meters) from the face of the stack to which air is being fed.

tained over the remaining portion of the temperature interval, it is released at a lesser rate. Accordingly, should the graphite be heated to the temperature at which the rate of energy release will become greater than the specific heat, a rapid and almost instantaneous spontaneous evolution of heat on the part of the graphite will take place, to a temperature which will be determined in each concrete case by the heat-removal conditions and the nature of the change in the rate of energy release as a function of the graphite exposure conditions. An illustration of this rapid heating up of the graphite is the discontinuity in temperature observed during the anneal of the BEPO reactor stack (Fig. 7).

If the graphite has a temperature close to 200°C under irradiation, release of stored energy will proceed smoothly without abrupt transitions, and an effective "apparent" specific heat will be lower than the normal value during the heating of the irradiated graphite. Consequently, any reactor transient during which the moderator becomes heated will yield a slightly larger temperature excursion than in the case of unirradiated graphite. However, when heat removal is efficient, this excursion will be transitory and insignificant. Danger arises only when the rate of heat removal drops. This danger is particularly prevalent in air-cooled reactors, because of the low operating temperature of the graphite in those cases. Release of stored energy [11] may begin as the stacking becomes heated to higher than operating temperature, as for example during a reactor shutdown, when air blowers and ventilating gear are shut off, and the stacking heats up on being irradiated by the core materials.

In water-cooled reactors, this danger of spontaneous heating up of the stack may arise when water is dumped from the reactor, which is sometimes a necessary operation during shutdown.

In order to evaluate safety conditions for a reactor, information must be available on the amount of energy stored in various parts of the stack and on the initial temperature of energy release as a function of exposure temperature. The solution of these problems is the primary task of stored-energy studies, such as those made prior to the experiment on energy release in the BEPO reactor [15]. The amount of energy stored and the conditions under which it is released were determined by sampling graphite specimens from various points in the reactor stack. The specimens were cut from the stack, off the surface of the graphite channels, by means of a trepanning instrument. Preliminary steps were taken to ensure against the specimen heating up while it was being cut from the stack. Special calorimeters for specific heat determinations were used to measure the stored energy in specimens.

In Fig. 8, we have data on the distribution of stored energy radially through the core, at various distances along the length of the BEPO pile. Breaks in the curves are boundaries of the region [15] in which release of stored energy took place during the first anneal (1954). Figure 9 presents a typical curve of the distribution of stored energy along the length of a fuel channel situated in a peripheral section of the core, where the radial coefficient of the neutron flux is approximately 0.5. The channel was not annealed at a single point. The fall-off in stored energy down the

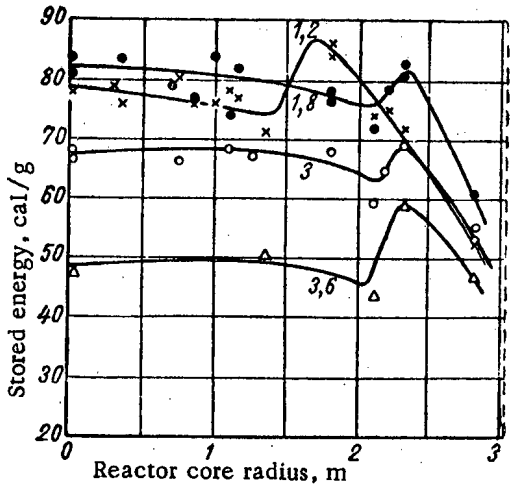

Fig. 8. Distribution of stored energy in graphite radially through the stack, at various distances along the length of the stack. Figures on the curves indicate distance (in meters) from the air-inlet face of the stack.

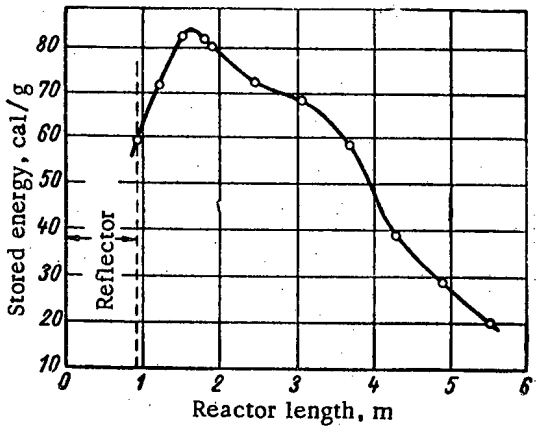

Fig. 9. Distribution of stored energy in graphite along the length of a fuel channel in the stack.

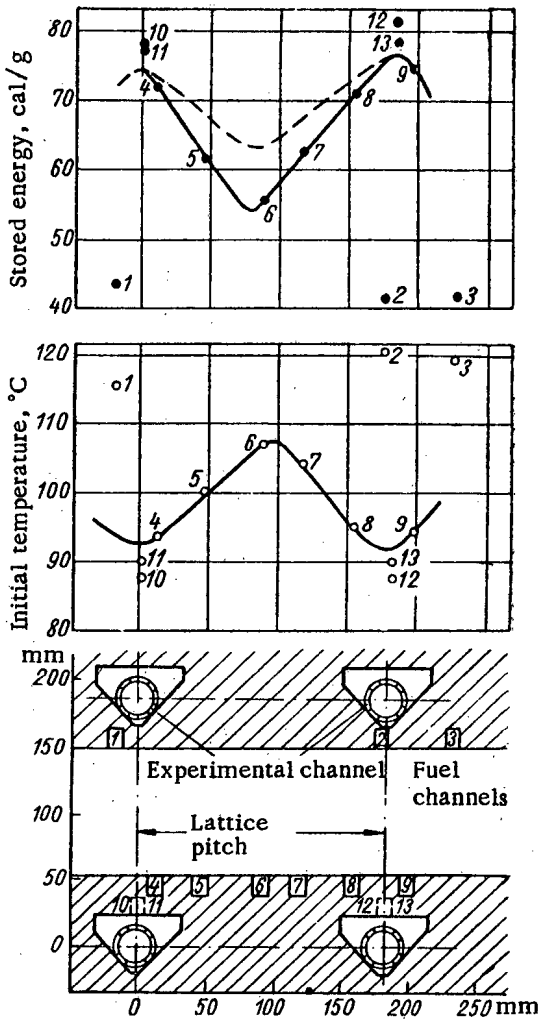

Fig. 10. Distribution of stored energy and temperature of onset of energy release inside graphite bulk, at extremes of lattice pitch. The dashed line is the expected stored-energy distribution affected solely by the spectrum of neutrons with the effect of operating temperature inoperative. Figures designate the number of measurement points. The arrangement of these points is seen in the lower diagram.

length of the channel is associated with a rise in graphite temperature. An abrupt fall-off in the reflector is ascribed to the reduced fast-neutron flux. Figure 10 shows the distribution of stored energy in the graphite according to the distance from fuel channels. The slope of this distribution is greatly affected by the graphite temperature distribution, characterized by the initial temperature seen in Fig. 10. It is clear that the total fall-off in stored energy at the point of the lattice furthest removed from the fuel channels is about 30%.

The data reported by Dickson et al. [15] aid in plotting an isoenergy contour diagram of stored energy for the BEPO reactor stack, which appears in Fig. 11 with reference to the graphite on the surface of the fuel-element channels. The region of maximum buildup of stored energy is obviously situated not far from the core-reflector boundary. If we remember that the fall-off in stored energy is around 30% according to the data plotted in Fig. 10, the maximum stored energy will amount to roughly 90 cal/g at the surface of the fuel channels and roughly 60 cal/g in the bulk of the graphite remote from the fuel channel.

As follows from the annealing process in the stack (cf. Fig. 7), peak graphite temperatures (about 300°C) were reached in the region of maximum buildup of stored energy as the energy was released. By comparing the rate of re-

lease of stored energy to the specific heat of the graphite, which averages at 0.3 cal/g · deg, the conclusion can be drawn that a temperature rise due to release of stored energy must proceed to about 250°C, under adiabatic conditions. If we bear in mind that energy release sets in at a graphite temperature of 90°C, the peak temperature for adiabatic conditions will be 340°C. The agreement between the observed and the adiabatic temperatures upon annealing indicates that the conditions governing the release of stored energy are close to adiabatic, despite the existing removal of heat from graphite at its peak temperature because of thermal conductivity and air flow. This fact bears evidence that a spontaneous and uncontrolled release of stored energy may lead to grief even when the region where a large amount of stored energy is accumulated may encompass only an insignificant fraction of the stack. It is precisely at that spot that an abrupt heating up of the graphite, capable of bringing about a meltdown of the aluminum jacketing of the fuel elements upon release of stored energy, occurs.

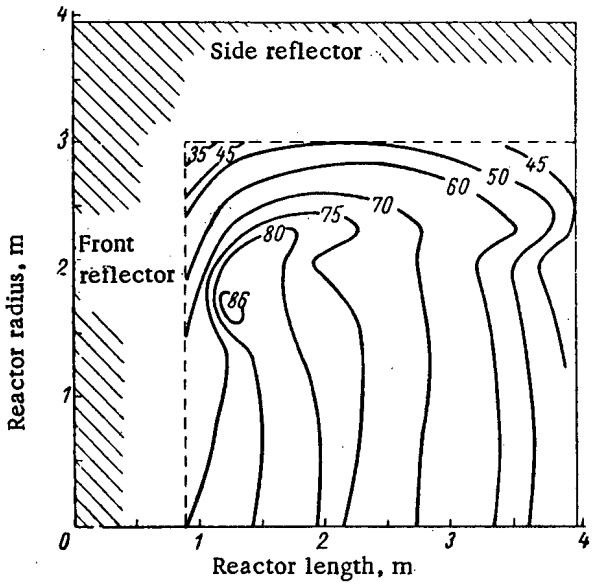

Fig. 11. Contour diagram of stored energy (figures indicate quantity of stored energy, in cal/g) in a longitudinal cross section through the stack (only part of the cross section is shown).

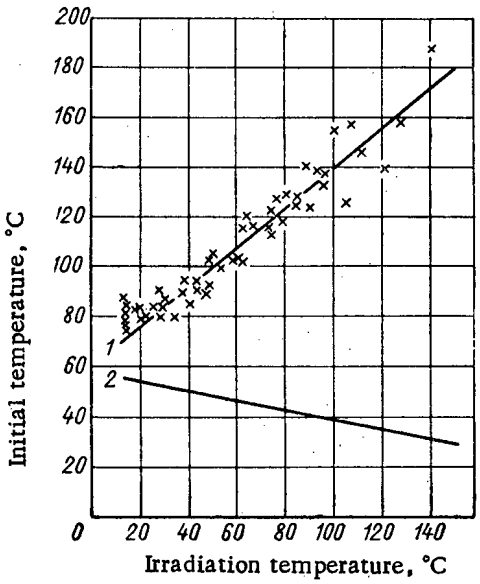

Fig. 12. Dependence of initial temperature of release of stored energy on irradiation temperature of graphite (curve 1) and difference between those temperatures (curve 2).

The relationship between the temperature corresponding to onset of stored-energy release and the graphite exposure temperature, as well as the difference between those two temperatures at various reactor operating temperatures, is illustrated in Fig. 12. Inspection of the graph shows that the difference referred to does not exceed 55°C at any point and drops to 25°C as the irradiation temperature rises to 160°C. This difference, if we go into its physical significance, is apparently related to the vibrational spectrum in the crystal lattice of graphite at a given mean graphite temperature and in the presence of local thermal spikes induced by radiation, and is also related to the activation energy of lattice distortions, on which the accumulation of stored energy depends. This difference is in practice responsible for the temperature margin of safety which wards off the danger of a sudden release of stored energy.

In a reactor with elevated graphite temperature, no danger of a buildup of low-temperature stored energy exists. However, the high-temperature contribution to the energy may turn out to be appreciable over large integral flux ranges, so much so that a total release of the stored energy may result in self-sustained heating to high temperatures, e.g., to 1500°C when, as may be assumed, a second peak appears in the rate of energy release, although playing no large role. Safety is achieved in the case where the mean specific capacity of the graphite over the entire temperature interval exceeds the mean rate of release of the entire stored energy, which can easily be computed if the total stored energy is known. This method for estimating safety [16] may have some practical application, since the total stored energy may be determined by the technique of combustion in terms of the excess of heat of combustion of the irradiated graphite [2, 3].

In dual-purpose reactors of the Calder-Hall type using carbon dioxide gas coolant, an additional recycling gas annealing loop is used to feed gas from the reactor exit at 340°C to the inlet gas duct instead of a heat-exchange medium, despite the high operating temperature of graphite in such reactors.

Accumulation of stored energy, a change in thermal conductivity, and swelling of graphite in Calder-Hall type reactors are monitored by testing samples irradiated in the stack, with exact controls on temperature and neutron flux. This test shows that the state of the stacking following two years of continuous operation is perfectly safe, and that annealing is probably unnecessary for at least a two-year period [17].

Oxidation of Pile Graphite

One important drawback in graphite is its ease of oxidizability at elevated temperatures. At moderate temperatures, graphite interacts more weakly with oxygen than do many metals, but since graphitic oxides are volatile no protective oxide film has a chance to form on the surface. The high porosity of graphite encourages penetration of oxygen into the bulk phase of the graphite, promoting the oxidation of large areas. The rate of oxidation, which is modest at low temperatures, displays a sharp exponential rise with temperature according to the law $e^{-E/kT}$ [17].

The oxidation reaction in air is exothermic. Self-sustaining combustion of graphite in a reactor channel sets in at temperatures 830-930°C [10]. In a Calder-Hall type reactor, the heat of oxidation remains negligible right up to 400°C temperature, but increases to 5 kw per channel when the temperature rises to 500°C, and then shoots up rapidly [17]. This behavior of the oxidation process entails a potential danger of rapid combustion breaking out in the graphite stack. However, in reactors with the graphite bathed in air streams, the temperature remains much lower than the level which would be specified by that consideration alone. Some other limitation associated with long-term oxidation apparently operates here, resulting in heavy losses of material and crumbling and disintegration of the graphite with a resulting breakdown of the stack, e.g., at the surface of the fuel channels. It is a well-known fact that the graphite temperature in air-cooled reactors remains at a level of 200-300°C, e.g., in the BNL reactor or the Oak Ridge X-10 reactor (USA), where the temperature of the graphite is 135°C [18].

If burnup conditions require high stack temperatures, the graphite must be protected against environmental oxygen. In gas-cooled reactors, provisions for this are made by using carbon dioxide instead of air and the stack is enveloped in a hermetically sealed enclosure, e.g., in reactors of the Calder-Hall type, and in the G-2 and G-3 reactors.

However, graphite also oxidizes in a carbon dioxide environment at high temperatures, reducing carbon dioxide to the monoxide. But this reaction is endothermic and, as noted by Brown et al. [17], entails no danger of rapid combustion, in contrast to the oxidation reaction in air, because graphite acts as a "heat sink" when its temperature rises. Nevertheless, graphite losses may prove dangerous for a stack, and this has prompted studies of graphite oxidation in carbon dioxide gas [19]. As these studies have shown, an equilibrium content of carbon dioxide and carbon monoxide becomes established in a gas recycling system, and graphite losses under normal reactor operating conditions are insubstantial. When the gas loop is damaged, the gas being pumped through the stack may become entrained by air; under these conditions further operation of the reactor is inadmissible in view of the increased rate of interaction between air and graphite over the temperature range 400-500°C [20].

As examples of reactors concerned with these problems, we cite the reactor of the First Atomic Power Station or the IR reactor, where it is evident that protection of pile graphite in water-cooled reactors may also be carried out by means of a gas. Dollezhal' and co-workers [7] have reported that the stack in the reactor of the First Atomic Power Station was filled with technical-grade nitrogen, which was first purified of oxygen to 0.1–0.2 vol.%. There was practically no combustion of graphite at operating temperatures up to 800°C. The nitrogen was also used to cool the IR stack [6]. Ignition of the graphite was reported only in the regions of the stack near cells in which failure of uranium fuel elements occurred. A nitrogen protective atmosphere will also be provided for graphite [22] in the reactors of the I.V. Kurchatov nuclear power station at Belyi Yar [21].

SUMMARY

It is evident that radiation effects in graphite lead to extremely serious conditions in the stacks of reactors operated at fairly low moderator temperatures (~200°C). Anneals of the stacks are resorted to because of the danger of core materials undergoing combustion and meltdown. In reactors where high graphite temperatures (400-500°C) prevail, radiation effects become manifested to a lesser extent, and then only in the outer regions of the stack where the graphite temperature is lower. And again only in the case where there are no regions of reduced graphite temperature in the reactor, low-temperature damages are minimized.

However, radiation effects in graphite are not solely due to low-temperature damages. At high temperatures (i.e., 400°C and higher), graphite undergoes shrinkage which tends to counteract the low-temperature swelling effect.

This radiation effect combines with the low-temperature swelling effect to compound operating problems. The graphite in the outer regions of the stack where the temperature is lower may expand at the same time that the graphite at the center of the core is contracting. If the size of the dimensional changes taking place in the pile graphite is known, operating difficulties may be overcome by an appropriate redesign of the graphite stack. Moreover, different grades of graphite may be employed in the various regions of the reactor, to take advantage of dimensional stability at particular temperature ranges.

Protection of graphite from high-temperature oxidation may be successfully engineered by a judicious choice of nonoxidative gas medium for the reactor stack.

In conclusion, the author would like to take this opportunity to express his gratitude to B.M. Dolishnyuk and to A.G. Lanin for their critical comments of the manuscript, and to L.Ya. Stolchneva for her excellent work on the accompanying illustrations.

LITERATURE CITED

1. V.I. Klimenkov and Yu.N. Aleksenko. Session of the USSR Academy of Sciences on the peaceful uses of atomic energy (panel of the Division on Physical and Mathematical Sciences). Moscow, publ. by USSR Academy of Sciences, 1955. Available in English translation, CB.
2. Woods et al. Geneva 1955 Conference on the peaceful uses of atomic energy, p. 746.
3. Kinchin. Geneva 1955 Conference on the peaceful uses of atomic energy, p. 442.
4. Hennig and Howe. Geneva 1955 Conference on the peaceful uses of atomic energy, p. 754.
5. Nightingale et al. Second Geneva conference on the peaceful uses of atomic energy. 1958, p. 614.
6. B.V. Brokhovich et al. Geneva 1958 Conference on the peaceful uses of atomic energy, p. 2297.
7. N.A. Dollezhal' et al. Geneva 1958 Conference on the peaceful uses of atomic energy, pp. 2139, 2183.
8. D.I. Blokhintsev and N. A. Nikolaev. Geneva 1955 Conference on the peaceful uses of atomic energy, p. 615.
9. D.I. Blokhintsev, N.A. Dollezhal' and A.K. Krasin. Atomnaya energiya, No. 1, 10 (1956).
10. R. Powell et al. Geneva 1958 Conference on the peaceful uses of atomic energy, p. 462.
11. Nucleonics, 15, December, 43 (1957).
12. N. Stewart and R. Crooks. Nature, 182, No. 4636, 627 (1958).
13. A. Chamberlain and H. Dunster, Nature, 182, No. 4636, 629 (1958). Atomnaya énergiya 6, No. 1, 97 (1959).
14. Nucl. Engng, 2/207, 453 (1957).
15. G. Dickson et al. Geneva 1958 Conference on the peaceful uses of atomic energy, p. 1805.
16. P. Grant, J. Nucl. Engng. 4, No. 35, 69 (1959).
17. G. Brown et al. Geneva 1958 Conference on the peaceful uses of atomic energy, p. 267.
18. Ramsey, Cahill. Geneva 1955 Conference on the peaceful uses of atomic energy, p. 486.
19. A. Anderson et al. Geneva 1958 Conference on the peaceful uses of atomic energy, p. 303.
20. F. Farmer et al. Geneva 1958 Conference on the peaceful uses of atomic energy, p. 2331.
21. V.S. Emel'yanov. Geneva 1958 Conference on the peaceful uses of atomic energy, pp. 2023, 2054, 2055, 2415.
22. N.A. Dollezhal' et al. Geneva 1958 Conference on the peaceful uses of atomic energy, pp. 2139, 2183.

All abbreviations of periodicals in the above bibliography are letter-by-letter transliterations of the abbreviations as given in the original Russian journal. ***Some or all of this periodical literature may well be available in English translation.*** **A complete list of the cover-to-cover English translations appears at the back of this issue.**

AN IRON-CURRENT MAGNETIC CHANNEL FOR THE EXIT AND INJECTION OF CHARGED PARTICLES

A.A. Arzumanov, N.I. Venikov, E.S. Mironov and L.M. Nemenov

Translated from Atomnaya Énergiya, Vol. 10, No. 5,
pp. 461-468, May, 1961
Original article submitted August 18, 1960.

The possibility has been shown of developing a magnetic channel which introduces practically no distortions into the main magnetic field. The magnetic channel is intended for the exit and injection of charged particles. A method is given for calculating the magnetic channels and the results of calculation and experiment are compared.

Introduction

It is a well-known fact that an iron tube is a magnetic screen. This screen can serve as a channel for the exit and injection of charged particles. However, the introduction of an iron screen into a magnetic field sharply distorts the shape of the field, which in many cases is not permissible.

A theoretical and experimental study was made of iron and current magnetic channels, resulting in the middle of 1958 in the development of an "iron-current" magnetic channel which introduced practically no distortions into an external magnetic field.

All experiments were carried out on a magnet with 500-mm diameter pole pieces and a 180-mm gap. The field meter was a 2.0-mm diameter coil of height 1.5 mm, connected to a ballistic galvanometer. A special device (coordinator) made it possible to adjust the coil with an accuracy of up to 0.3 mm. The stability of the current in the magnet windings was 0.3%. The error in measuring the field did not exceed 5 oe.

1. Iron Screen in Magnetic Field

If an infinitely long cylindrical screen is placed in a homogeneous magnetic field with induction B_0 so that its axis is perpendicular to the lines of force (Fig. 1), then the expression for the components of the magnetic induction in Cartesian coordinates outside the screen will have the form

$$B_y = B_0\left[1 - \frac{R_2^2 - R_1^2}{\frac{k+1}{k-1} - \frac{R_1^2}{R_2^2}\frac{k-1}{k+1}}\frac{x^2-y^2}{(x^2+y^2)^2}\right]; \tag{1a}$$

$$B_x = 2B_0\frac{R_2^2 - R_1^2}{\frac{k+1}{k-1} - \frac{R_1^2}{R_2^2}\frac{k-1}{k+1}}\frac{xy}{(x^2+y^2)^2}; \tag{1b}$$

at the walls of the screen

$$B_y = 2B_0\frac{1}{\frac{k+1}{k-1} - \frac{R_1^2}{R_2^2}\frac{k-1}{k+1}} \times \left[\frac{k}{k-1} + \frac{k}{k+1}R_1^2\frac{x^2-y^2}{(x^2+y^2)^2}\right]; \tag{2a}$$

$$B_x = -4B_0\frac{\frac{k}{k+1}}{\frac{k+1}{k-1} - \frac{R_1^2}{R_2^2}\frac{k-1}{k+1}}\frac{R_1^2 xy}{(x^2+y^2)^2}; \tag{2b}$$

inside the screen

$$B_y = B_0 \frac{4k}{(k+1)^2 - \frac{R_1^2}{R_2^2}(k-1)^2}; \tag{3a}$$

$$B_x = 0, \tag{3b}$$

where $k = \frac{\mu}{\mu_0}$ is the ratio of the magnetic permeabilities of the material of the screen and the space outside it; R_1 is the internal radius of the screens; R_2 is the external radius of the screen.

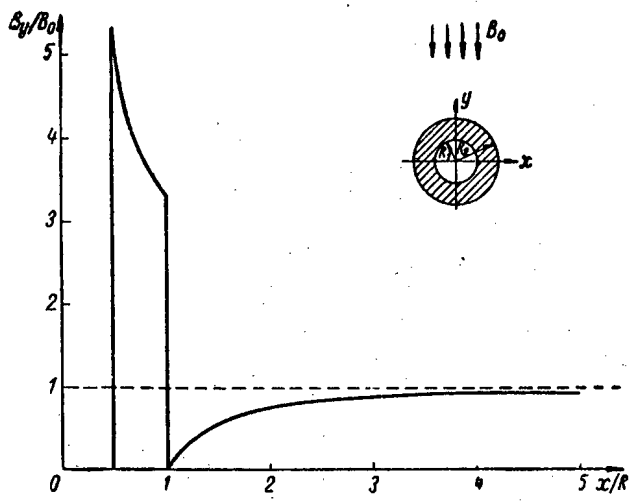

Fig. 1. Distribution of magnetic induction in the plane y = 0 for an infinitely long cylindrical screen with $\mu \to \infty$. The axis of the screen is perpendicular to the lines of force.

From the formulas given, for $k \to \infty$ the following can be clearly seen:

1) The external magnetic field does not penetrate inside the screen.

2) The dimensions of the hole in the screen do not affect the degree of distortion of the external field.

3) In the iron of the screen the difference in the vertical components of induction at the internal and external walls is independent of the thickness of the wall and is equal to $2B_0$.

4) For a continuous cylinder the induction in the wall is constant and equal to $2B_0$.

Figure 1 shows a curve for the distribution of magnetic induction for a cylindrical screen when $\frac{R_1}{R_2} = 0.5$ and $k \to \infty$.

2. Current Channel

If surface currents pass along an infinitely long circular cylinder with a density changing according to the law

$$j = \frac{I}{2R}\cos\theta, \tag{4}$$

where I is the total current; R is the radius of the cylinder; θ is an angle measured from the axis x, then inside the cylinder

$$B_y = 0{,}1\mu_0\pi\frac{I}{R}; \quad B_x = 0; \tag{5}$$

outside the cylinder

$$B_y = 0{,}1\mu_0\pi IR\frac{y^2 - x^2}{(x^2+y^2)^2};$$

$$B_x = 0{,}1\mu_0\pi IR\frac{2xy}{(x^2+y^2)^2}. \tag{6}$$

It can be seen from formulas (5) and (6) that the field inside the cylinder is constant and in the external region it falls according to a quadratic law.

Since the formation of a purely "cosine" distribution of the current density involves certain difficulties, a magnetic field was considered which was created by a finite number of wires, placed on the surface of the cylinder according to the cosine law (the same current passes along all conductors). In the plane y = 0 the total field from all terms in this case is

$$B_y = 0{,}2i\mu_0 \sum_n \frac{x - p_n}{l_n^2 + (x-p_n)^2}, \tag{7}$$

where i is the current in the conductor; p_n and l_n are the horizontal and vertical coordinates of the conductor.

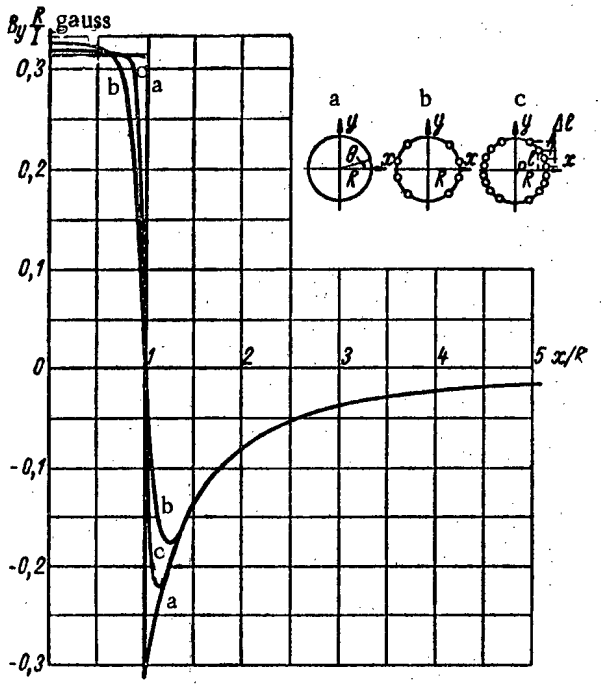

Fig. 2. Magnetic field in the plane y = 0 for a current channel with a cosine distribution of the current density: a) change in current density according to the law $j = \frac{I_0}{2R}\cos\theta$; b) winding consists of eight conductors ($i = \frac{I_0}{4}$); c) winding consists of 16 conductors ($i = \frac{I_0}{8}$).

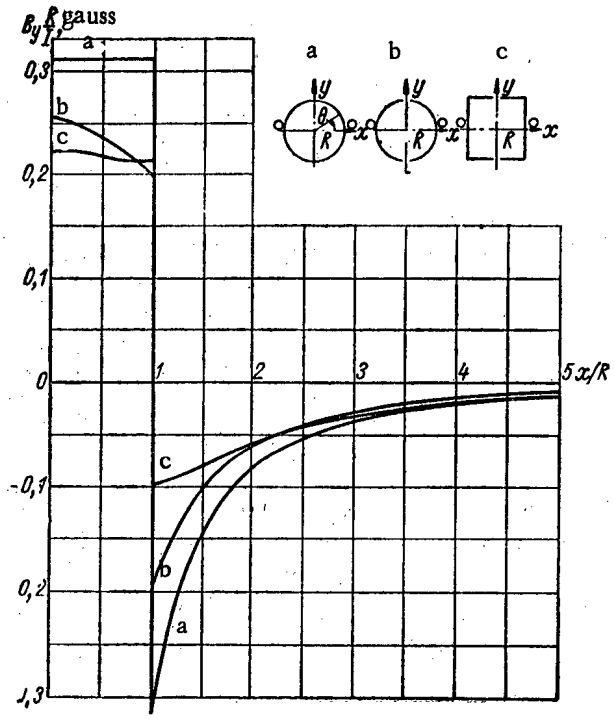

Fig. 3. Distribution of magnetic field in the plane y = 0 for various current channels: a) $j = \frac{I_0}{2R}\cos\theta$; b) $j = \frac{I_0}{\pi R}$; c) $j = \frac{I_0}{4R}$.

Figure 2 shows the dependence of the field induction on the distance to the axis of the channel in relative units. For all three cases given, the sum of the currents of all conductors is the same.

As can be seen from Fig. 2, if the winding consists of sixteen conductors, in the region with radius $x < 0.8R$ the field is practically constant.

It is interesting to consider a field of conductors placed along the surface of a cylinder with a constant density. In this case

$$B_y = \frac{-0,2I\mu_0}{\theta_2-\theta_1}\left[\frac{1}{2}\frac{y}{x^2+y^2}\ln\frac{x^2+y^2+R^2-2R(x\cos\theta_2+y\sin\theta_2)}{x^2+y^2+R^2-2R(x\cos\theta_1+y\sin\theta_1)}\right.$$
$$\left.+\frac{x}{x^2+y^2}\arctan\frac{(x^2+y^2)\sin(\theta_2-\theta_1)+xR(\sin\theta_1-\sin\theta_2)+yR(\cos\theta_2-\cos\theta_1)}{(x^2+y^2)\cos(\theta_2-\theta_1)-xR(\cos\theta_2+\cos\theta_1)-yR(\sin\theta_2+\sin\theta_1)+R^2}\right]; \quad (8)$$

$$B_x = \frac{0,2I\mu_0}{\theta_2-\theta_1}\left[\frac{1}{2}\frac{x}{x^2+y^2}\ln\frac{x^2+y^2+R^2-2R(x\cos\theta_2+y\sin\theta_2)}{x^2+y^2+R^2-2R(x\cos\theta_1+y\sin\theta_1)}\right.$$
$$\left.+\frac{y}{x^2+y^2}\arctan\frac{(x^2+y^2)\sin(\theta_1-\theta_2)+xR(\sin\theta_2-\sin\theta_1)+yR(\cos\theta_1-\cos\theta_2)}{(x^2+y^2)\cos(\theta_1-\theta_2)-xR(\cos\theta_1+\cos\theta_2)-yR(\sin\theta_1+\sin\theta_2)+R^2}\right], \quad (9)$$

where θ_1 and θ_2 are the azimuthal boundaries of the current-conducting layer; R is the radius of the cylinder.

This distribution of the vertical component of the magnetic field induction in the middle plane for the case $\theta_2 = 90°$ and $\theta_1 = -90°$ is shown in Fig. 3 (curve b).

Also of practical interest is the field of a rectangular-cross-section current channel. This field is conveniently represented as the sum of the fields of flat thin busbars placed on the surface of the channel.

The field of a thin busbar of height 2a, the coordinates of whose center are m and n, has the form

$$B_y = \frac{0,1\mu_0 I}{a}\left(\arctan\frac{y-n+a}{x-m} - \arctan\frac{y-n-a}{x-m}\right). \quad (10)$$

For a thin horizontal busbar of width 2b with center coordinates p and l, the field has the form

$$B_y = \frac{0,1I\mu_0}{b}\ln\sqrt{\frac{(y-l)^2+(x-p+b)^2}{(y-l)^2+(x-p-b)^2}}. \quad (11)$$

The graph of the function B_y (x, 0) for a current channel of square cross section is given in Fig. 3 (curve c).

3. Method of Calculation and Experimental Study of Iron Screens

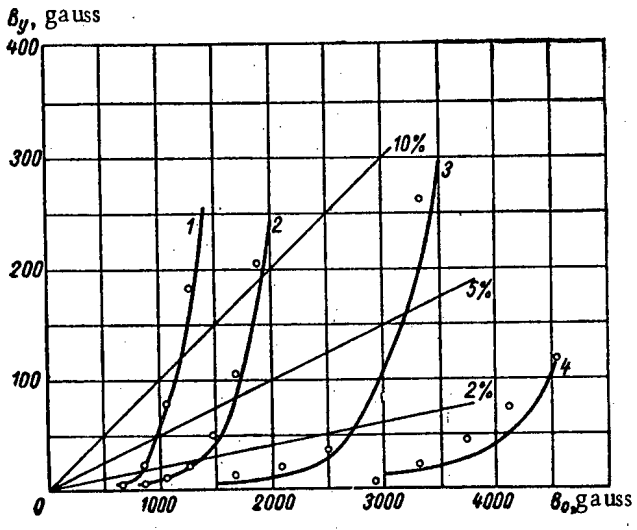

Fig. 4. Dependence of induction of the magnetic field within the screens on the induction of the external field (—— - calculation; O — experiment). The values of R_2 and R_1 are as follows, mm: 1) R_2 = 16; R_1 = 14; 2) R_2 = 13; R_1 = 10.5; 3) R_2 = 16; R_1 = 10.5; 4) R_2 = 16; R_1 = 7.5.

The intensity inside the screens placed in a transverse magnetic field can be calculated on the basis of results given in section 1. The mean value of induction is conveniently taken as the induction in the wall:

$$(B_y \text{ m.w.})_{y=0} = \frac{1}{R_2-R_1}\int_{R_1}^{R_2}[B_y(x)]_{y=0}\,dx \quad (12)$$

or, after integration,

$$(B_y \text{ m.w.})_{y=0} = \frac{2B_0}{1-\frac{R_1}{R_2}+\frac{1}{k}\left(1+\frac{R_1}{R_2}\right)}. \quad (13)$$

Using this expression and the relationships $\mu = f(B)$ we determine μ.

B_{in} can be determined from the found value of the magnetic permeability, using expression (3a). The results of the calculation are presented in Table 4.

A study was made of several cylindrical screens in a homogeneous magnetic field with induction B_0, perpendicular to the axes of the screens. The length of the screen was not less than eight external diameters. Figure 4 shows the dependence of the field inside the screens on B_0 for various values of R_1/R_2. The auxiliary straight lines passing through the origin of the coordinates correspond to an internal field intensity equal to 2, 5, and 10% of B_0.

Figure 5 shows graphs characterizing the distortions of the external field due to the introduction of an iron screen into it. B_y was measured in the plane x = 0 (upper curve) and in the plane y = 0 (lower curve).

Figures 6a and 6b give the distribution of magnetic field in a region at the end of the screen. The axis z coincides with the axis of the screen. The value z = 0 corresponds to the edge of the screen. It can be seen that the distortions of the field at the end of the screen are increased and the magnetic field within the screen rapidly falls, so that at a distance R_1 from the edge there is only 2-3% of B_0.

Also of interest are the screening properties of cylindrical screens placed along the lines of force of the magnetic field. An accurate calculation of the field for this case is very complex; however it is possible to find approximately the value of induction in the wall of the cylinder, considering it as an ellipsoid of rotation. A half of the height of the cylinder is taken as equal to the large semiaxis of the ellipsoid and the radius of the cylinder is taken as the small semiaxis of the ellipsoid.

The magnetic induction within a continuous cylinder is

$$B = \varkappa a B_0, \quad (14)$$

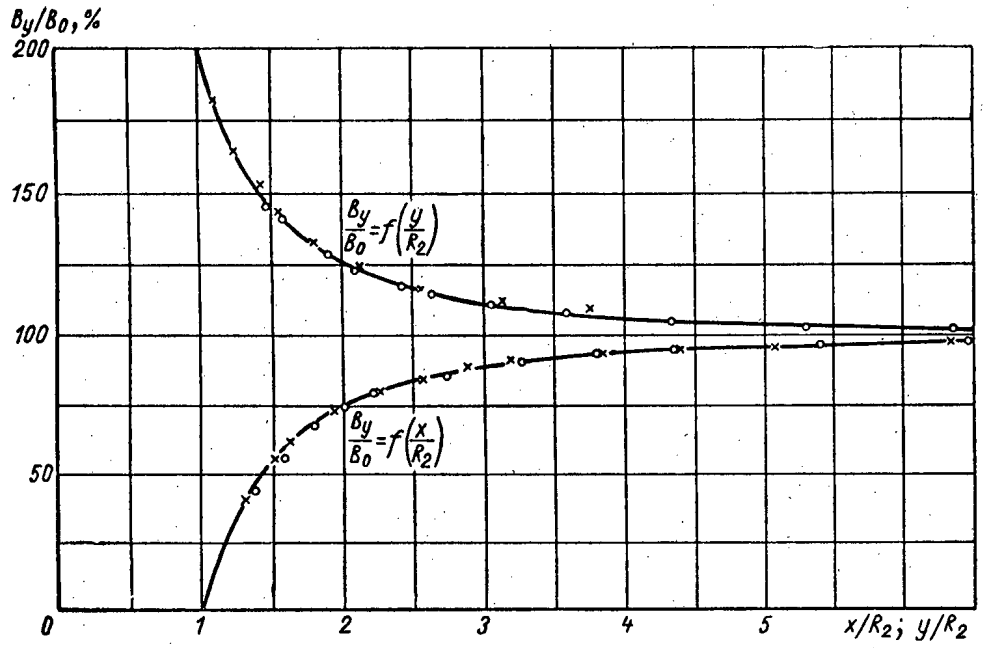

Fig. 5. Distortion of homogeneous field by a screen orientated perpendicular to the lines of force (B_0 = 850 gauss): ——— – calculation; × – experiment (R_2 = 16 mm, R_1 = 10.5 mm); O – experiment (R_2 = 9.5 mm, R_1 = 7.5 mm).

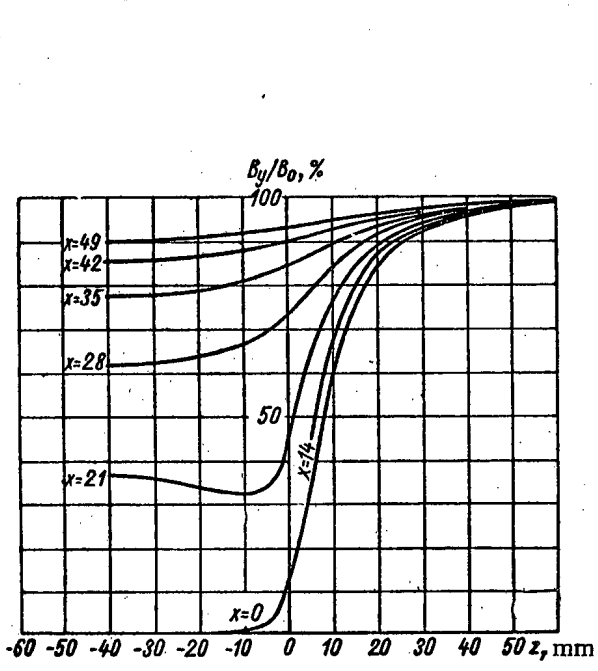

a

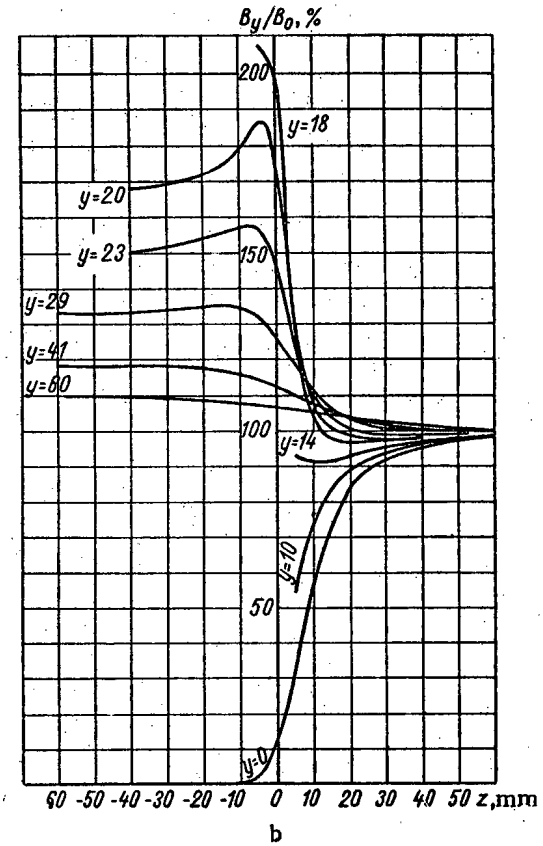

b

Fig. 6. Distribution of magnetic field at the end of the screen when it is placed in a homogeneous field perpendicular to the lines of force (R_2 = 16 mm; R_1 = 7.5 mm; B_0 = 2500 gauss): a) in the plane y = 0; b) in the plane x = 0.

where $\varkappa$ is a coefficient taking into account the difference between the cylinder and the ellipsoid ($\varkappa$ = 1.25-1.28); the coefficient of strengthening of the field in the ellipsoid is

$$a = \frac{\lambda^2 - 1}{\frac{\lambda}{\sqrt{\lambda^2 - 1}} \ln(\lambda + \sqrt{\lambda^2 - 1}) - 1}, \qquad (15)$$

where λ is the ratio of the larger semiaxis of the ellipsoid to the smaller.

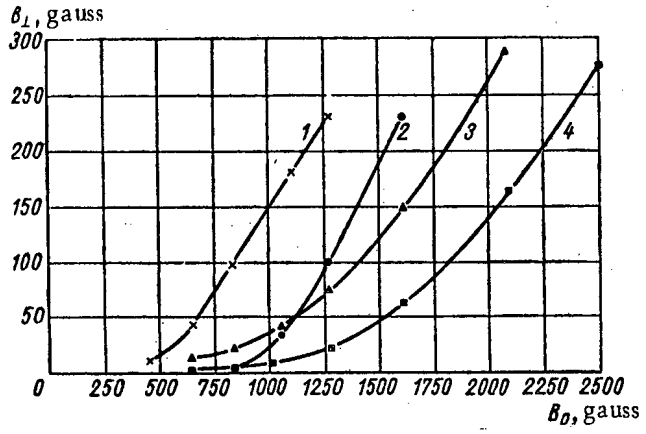

Fig. 7. Dependence of the transverse component of induction of the magnetic field within the screens on B_0 (the screens are placed in a homogeneous field at an angle of 75° to the lines of force). The values of R_2, R_1, l are as follows, mm: 1) R_2 = 13; R_1 = 10.5; l = 200; 2) R_2 = 13; R_1 = 10.5; l = 100; 3) R_2 = 13; R_1 = 7.5; l = 200; 4) R_2 = 16; R_1 = 7.5; l = 200.

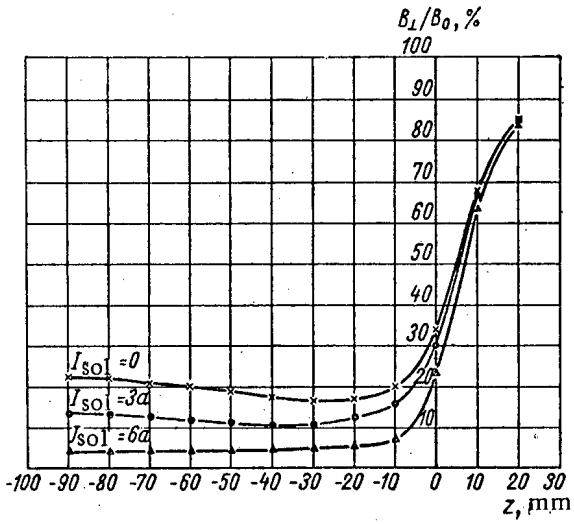

Fig. 8. Magnetic field within an iron screen placed in a homogeneous magnetic field at an angle of 75° to the lines of force. The cylinder is connected to a compensation solenoid winding (R_2 = 13 mm; R_1 = 10.5 mm; L = 200 mm; $\frac{W}{L}$ = 52 cm^{-1}; B_0 = 1600 gauss).

When calculating the induction in the wall of the screen it can be assumed that the absence of material within the screen leads to an additional increase in the magnetic induction in the wall in the ratio $\sim\frac{R_2^2}{R_2^2 - R_1^2}$ (in the absence of saturation of the walls).

On the basis of the above it is possible to approximately calculate a screen placed at an arbitrary angle to the lines of force of the magnetic field. As a first approximation in the calculation determinations are made of the longitudinal and transverse (perpendicular to the axis of the screen) components of induction with the condition $\mu \gg \mu_0$. The found components are added together geometrically. Then, as in the transverse position of the channel, the field intensity inside the screen is found.

Figure 7 shows several experimental curves representing the dependence of the component induction of the magnetic field $B_\perp$ within the screen on B_0. The screens are placed at an angle of 75° to the lines of force of the field. As can be seen from a comparison of Fig. 7 with Fig. 4, the slope of the screen considerably increases the penetration of the field through the walls. This phenomenon can be explained in the following way. With an inclined position of the screen a component of the external field appears, directed along the axis of the screen. Even if this component is small, the screen is readily saturated when the length of the screen is much greater than its diameter. The action of the longitudinal component of the field can be weakened or be removed completely, creating, by means of a solenoid placed on the screen, a magnetic field directed against the longitudinal component of the external field $B_\parallel$.

A fine solenoid winding was wound on the tested screen with number of turns per unit length w = 52 cm^{-1}. The transverse component of the residual magnetic field was measured as a function of the current in the solenoid. The results of the measurements are given in Fig. 8.

4. Iron-Current Magnetic Channel

As was shown, a fault of both the current and the iron channels is the fact that they introduce distortions into the external magnetic field. Combining these channels, it is possible to exclude the distortions. For the case of saturated iron this problem was considered by G.I. Gudker in 1950. In the present work the case of unsaturated iron is considered.

We will assume that the cylindrical current channel with cosine distribution of the current is placed in an external homogeneous field B_0. The value of the current in the winding is chosen so that the vertical component of the field created by the current within the channel is equal to $B_y = -\frac{1}{2} B_0$. Outside the channel the same component will have the form

$$B_y = \frac{1}{2} B_0 \frac{x^2 - y^2}{(x^2+y^2)^2} R^2. \qquad (16)$$

If an iron cylinder of the same radius is now placed within the current channel, then the vertical component of the external field created by the iron cylinder when $\mu \to \infty$ will be equal to

$$B_y = -B^* \frac{x^2 - y^2}{(x^2+y^2)^2} R^2, \qquad (17)$$

where B^* is the induction of the field which contains the iron cylinder, equal to $\frac{1}{2} B_0$.

Therefore, the values of B_y caused by the current and iron are equal in value and opposite in sign over the whole space, which means the absence of distortions. A similar compensation of distortions also takes place for B_x.

As already mentioned, when $\mu \gg \mu_0$ the presence of a hole in the cylinder has practically no effect on the shape of the external field. Consequently, the iron screen along whose surface a longitudinal current passes with density $j = j_0 \cos\theta$ is a system introducing practically no distortions into the external magnetic field.

Figure 9 shows curves characterizing the distortions of the external homogeneous field created by an iron cylindrical screen with a cosine winding with different currents in it. It can be seen from the figure that with a current of ~1030 a there will be practically no distortions of the external field.

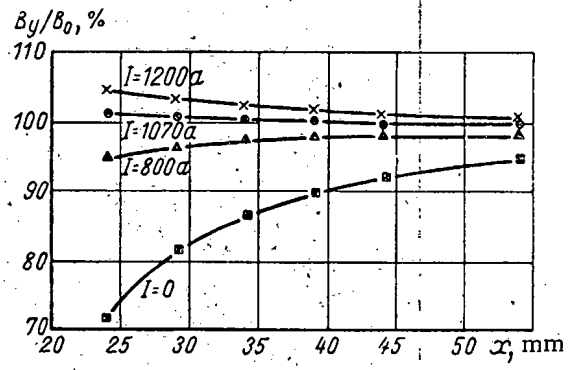

Fig. 9. Distribution of external field in the plane y = 0 for an iron screen placed in a homogeneous field perpendicular to the lines of force. On the cylinder there is a cosine-type winding.

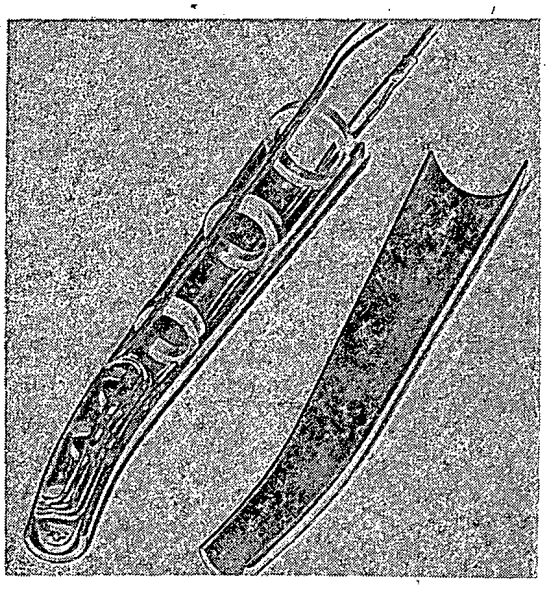

Fig. 10. Inside view of the iron-current channel.

In the more general case of an inclined position of the channel, two windings are required to compensate distortions of the field. The cosine winding which has just been considered forms the first winding. The second winding can be a solenoid, as mentioned in section 3. The compensation of the field distortions caused by longitudinal magnetization is the same as the compensation of the transverse distortions, i.e., a current in the solenoid is established so that the induction of the field created by the current is equal to a half of the longitudinal component of induction of the external field.

The calculations were used as the basis of an iron-current channel for B_0 = 2,000 gauss, causing rotation of charged particles in the magnetic field through an angle of 20° and movement of the particles outside the magnetic field at an angle of 90° to the lines of force. The channel is a tapered iron tube with the smaller aperture measuring 22 mm and the larger aperture measuring 50 mm and wall thickness 3 mm. Its length is ~360 mm. At the section of length

110 mm the tube is bent. The radius of curvature is 370 mm. To provide rotation of the charged particles within the tube, at the curved section there is a winding consisting of 16 wires arranged according to the cosine law. The induction of the rotating field was 550 gauss, the current in the winding being 150 a.

To compensate the distortions of the transverse component of the external field another winding of 16 wires was placed on the iron screen, arranged according to the cosine law (current in the conductor 685 a).

The distortions caused by the longitudinal component of the field at the bent part of the channel are compensated by the solenoid winding which consists of 11 turns placed at the top of the cosine winding. The current in the winding is 310 a. All the windings are cooled with water. The arrangement of the channel and the position of the windings are shown in Figs. 10 and 11.

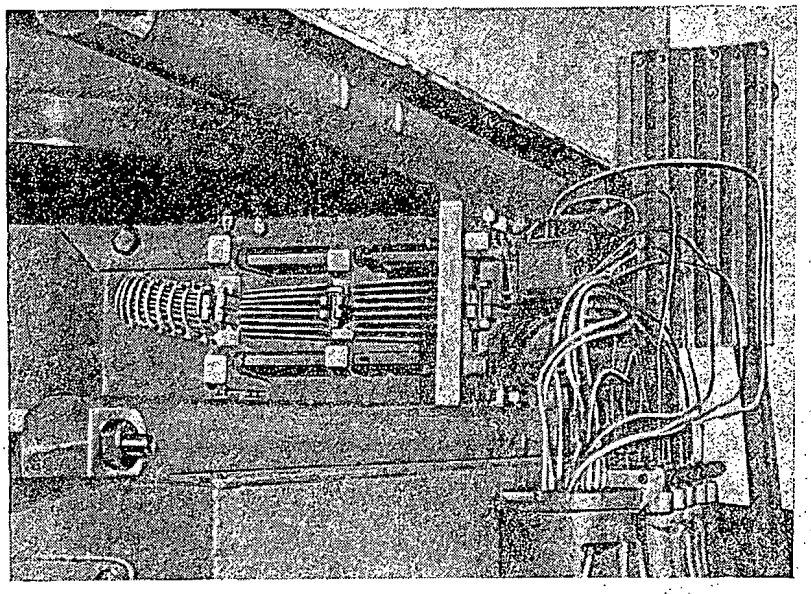

Fig. 11. Iron-current channel on the test bench.

An experimental study of the iron-current channel led to the following conclusions:

1. The external magnetic field does not penetrate into the channel.
2. The distortions of the external field were reduced on an average 20- to 30-fold compared with the distortions caused by the iron channel without compensation windings, and were mostly reduced to a few tenths of a percent. Only at isolated points in the immediate vicinity of the channel were the distortions ~3%.
3. The heterogeneity of the internal rotating field across the channel does not exceed 5%.

In conclusion the authors would like to thank L.F. Kondrashov for his work in designing the iron-current channel.

A STUDY OF ACCELERATING SYSTEMS OPERATING WITH WAVES SIMILAR TO H*

P.M. Zeidlits and V.A. Yamnitskii

Translated from Atomnaya Énergiya, Vol. 10, No. 5,
pp. 469-477, May, 1961
Original article submitted June 27, 1960

In the period 1947-1957 linear accelerating systems using vibrations similar to H-waves, in view of the impossibility of their accurate calculation and the necessity for prolonged experimental selection, were rejected without good reasons. Our systematic measurements have shown the considerable advantage of volume resonators operating with waves of this type over the widely used resonators working with the E_{010} wave.

Linear accelerating systems using waves similar to H can be used up to particle speeds equal to C without changing their basic structure, which is impossible with the E_{010} wave.

The mentioned system can be used widely to accelerate ions since it gives long waves in small equipment and a reduction in the required high-frequency power is shown particularly strongly at low particle speeds.

Introduction

As well as the thoroughly developed resonance linear accelerators for ions using the E_{010} wave, in the period 1931-1958 various authors have described the following linear accelerating systems:

1) a linear accelerator on loops with concentrated parameters [1];
2) a chain of toroidal or coaxial resonators;
3) waveguides, loaded with a dielectric;
4) spiral waveguide [2-6];
5) waveguides with a spiral groove [7];
6) chain of connected endovibrators, working on a running wave [8];
7) "restricted tube" – a waveguide with a system of quarter-wave antenna-vibrators [9];
8) a "snake" or spiral of a waveguide on a transverse-electric wave [10];
9) "interfinger" system using vibrations of the type H_{111} [9];
10) system of chasers, also working on the mode H_{111} (private communication of Potier, 1958).

Most of these accelerating systems are of little interest due to the impossibility of arranging the focussing devices (restricting tube) or due to the necessity for extremely high high-frequency powers (spiral waveguide, chain of endovibrators, "snake," circuits with concentrated parameters, etc.).

More promising in this respect are the last two types of accelerators, using vibrations of the type H_{111}.

A reduction in the high-frequency power is extremely important, since the cost of the sources of high-frequency supply and the constructional work forms the main part of the cost of a modern linear resonance accelerator.

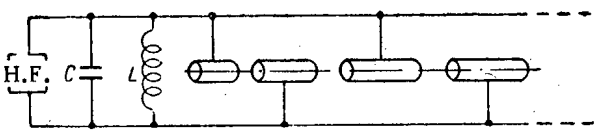

Fig. 1. Accelerator on a circuit with concentrated parameters.

One of the simplest methods for reducing the high-frequency power is to make a particle pass through the same accelerating voltage repeatedly. This possibility was used in the very first linear accelerators [1], where the drift tubes were fastened alternately on busbars connected with the capacitor plates of the oscillatory circuit (Fig. 1).

* The main results were reported at the conference of the Physicotechnical Institute, Academy of Sciences, UkrSSR in November, 1959.

If the particle passes successively through n gaps with a voltage U on each of them, then the total accelerating voltage V is

$$V = nU.$$

Let R_{rs} be the "radiotechnical" shunt resistance of the circuit, i.e.,a value determined by the voltage on the capacitor plates of the oscillatory circuit:

$$R_{rs} = \frac{U^2}{2P}$$

(P is the power loss in the circuit). Let R_{as} be the "accelerating" shunt resistance of the accelerating system, determined by the total accelerating voltage:

$$R_{as} = \frac{V^2}{2P}.$$

It is obvious that

$$R_{as} = R_{rs}n^2.$$

Expressing n by the length of the accelerator l and the mean period of the structure $\beta_m\lambda/2$ (since the acceleration occurs in each half-period of thehigh-frequency voltage), we obtain

$$R_{as} = R_{rs}\left(\frac{l}{\frac{\beta_m\lambda}{2}}\right)^2. \quad (1)$$

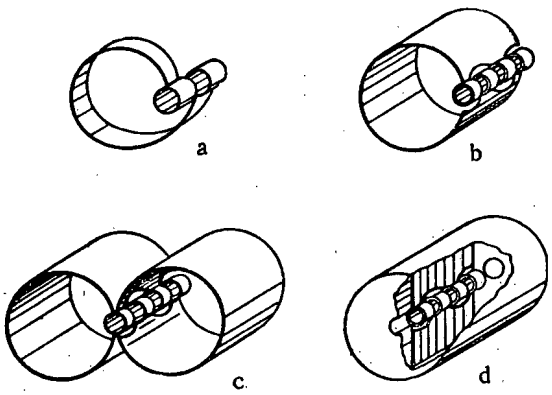

Fig. 2. Evolution from a simple circuit to an endovibrator.

Yet another value is frequently used, also called a shunt resistance, but related to unit length of the accelerator and expressed in meg/m. We will call it R_{se} – the shunt equivalent resistance –since it is numerically equal to the shunt resistance of that equivalent circuit in which, when the same power is fed into it, a voltage is developed equal to the accelerating voltage, acting on unit length of the accelerator in question. Then

$$R_{se} = \frac{R_{as}}{l}. \quad (2)$$

Substituting in formulas (1) and (2) the value R_{rs}, expressed by the parameters of the oscillatory circuit, we obtain

$$R_{se} = kf^{1/2}C_0^{-3/2}\beta^{-2}, \quad (3)$$

where C_0 is the capacity of the capacitor per unit length of the accelerator; f is the working frequency of the circuit. A similar result was obtained by Potier (private communication, 1958) for special forms of endovibrators (using a wave similar to H_{111}).

Formulas (1) and (2) apply both to circuits with concentrated parameters and to some forms of endovibrators, which can be considered as screened circuits (Fig. 2).

Since the choice of the working frequency f is limited by a number of conditions, the only way of increasing the shunt resistance is to decrease the capacity C_0, i.e.,the concentration of the electric field (other conditions being equal) exclusively in the region of the working gap, where it is essential,and to remove it in all other regions, where it is useless. This can be achieved by using a periodic structure of a special type.

If a field is set up similar to H and the structure of an endovibrator is used, as in Fig. 2d, then with the same diameter of the endovibrator we obtain a wavelength which is three to five times greater than with the mode E_{010}. The shunt resistance will also be very high, since a particle repeatedly passes the same accelerating voltage, as in accelerators using circuits with concentrated parameters, and the electric field is concentrated exclusively in the region of the accelerating gap.

Therefore, a resonator using a wave similar to H has the advantages of a simple circuit and an endovibrator, opening up considerable possibilities for reducing the high-frequency powers. An accurate calculation of the loaded endovibrators is very complex. For special cases (for example, loading a waveguide with discs) there are good numerical methods of calculation [11, 12]. More complex structures are much more difficult to study theoretically. In a general form for a resonator loaded with slit antennas and having a wavelength greater than the critical value, the problem was solved by A.I. Akhiezer and G.Ya. Lyubarskii [8]. However, for practical use these calculations are not very suitable.

Waveguides with a load of this type, as shown in Fig. 2d, can be calculated by numerical and graphical methods which are extremely laborious and complex.

Method of Measurements

The measurements (Fig. 3) were carried out mainly by the perturbing-body method [13].

On the introduction of a metal sphere into the endovibrator the change in the resonance frequency of the latter is

$$\frac{\Delta f}{f_0} = \frac{3}{2}\left(\frac{4}{3}\pi r^3\right)\frac{E^2 - \frac{1}{2}H^2}{\int\limits_V E^2\,dV}, \qquad (4)$$

where Δf is the change in resonance frequencies; f_0 is the resonance frequency of the endovibrator; r is the radius of the sphere; E and H are the undisturbed fields at the point where the sphere is introduced; V is the volume of the endovibrator.

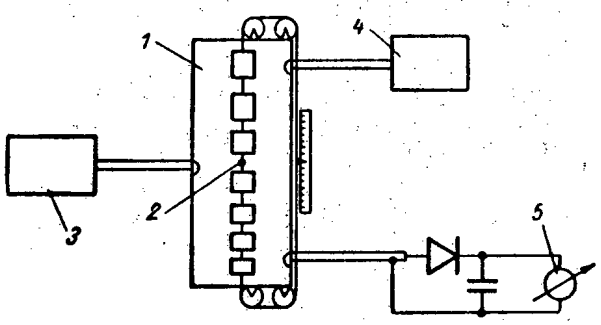

Fig. 3. Diagram of apparatus for determining the shunt resistances: 1) endovibrator; 2) sphere on caprone thread of diameter 0.2; 3) high-frequency generator GSS-12; 4) VVT-D ondometer; 5) 0.1-100 μa microammeter.

For a dielectric sphere

$$\frac{\Delta f}{f_0} = \left(\frac{4}{3}\pi r^3\right)\frac{1}{\int\limits_V E^2\,dV}\left(\frac{\varepsilon-1}{\varepsilon+2}E^2 + \frac{\mu-1}{\mu+2}H^2\right). \qquad (5)$$

Polystyrene is usually used as the dielectric (μ = 1).

Therefore, by measuring the changes in frequency with an ondometer when the copper and polystyrene spheres are placed at a certain point of the resonator, it is possible to measure both the magnetic and electric fields in relative units. If the direction of the field vector is unknown, then it is more convenient to use a perturbing body in the form of an ellipsoid (H = O):

$$\frac{\Delta f}{f_0} = \frac{3}{2}\left(\frac{4}{3}\pi L^3\right)\frac{E^2}{\int\limits_V E^2\,dV}F\left(\frac{l}{L}\right), \qquad (6)$$

where L, l are the large and small axes of the ellipsoid respectively; the relationship $F\left(\frac{l}{L}\right)$ was calculated and for $\frac{l}{L}$ = 0.1 with L parallel to E it is equal to 0.15 and for L perpendicular to E it is equal to 0.005.

The metal ellipsoid therefore determines not only the value but the direction of the electric field.

The perturbing-body method was also used to measure the field intensity along the axis of the accelerator:

$$E_z = f(z).$$

Using equation (4) and the expressions for R_{se}, the following result can readily be obtained:

$$\frac{R_{se}}{Q} = \frac{\left(\int\limits_0^l E_z\,dz\right)^2 \Delta f_0}{\pi r^3 E_0^2 f_0^2 l}. \qquad (7)$$

Here E_z is expressed in relative units such that $E_0 = 1$; Δf_0 is measured at the same point as E_0. The Q-factor was determined from the resonance curve.

When using this method for the measurements the error in the determination of the shunt resistance does not exceed ± 10% and is mainly due to the inaccuracy in determining the coordinates of the sphere due to the elasticity of the 0.2-mm diameter caprone thread on which it is suspended and the inaccuracy in determining the characteristics of the receiving indicator.

Results of Main Measurements

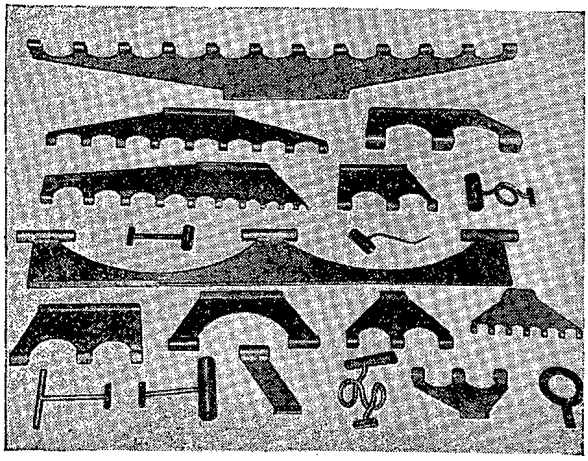

Fig. 4. Some types of drift tube suspensions.

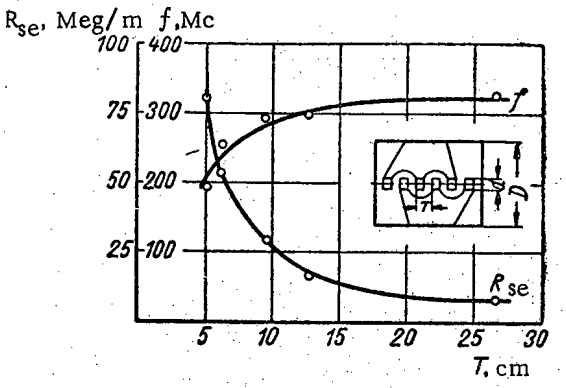

Fig. 5. Change in the parameters of the resonator for various periods of the structure (D = 300 mm; d = 30 mm).

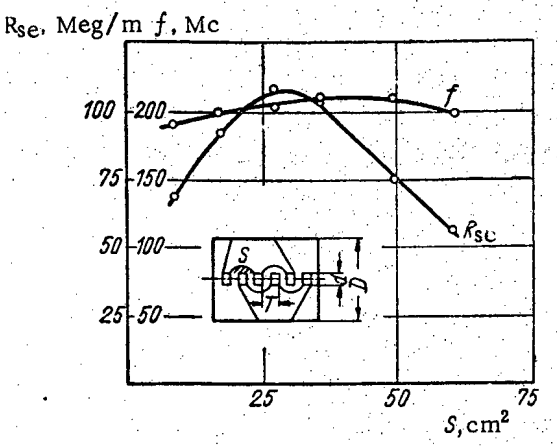

Fig. 6. Change in the parameters of the resonator for various recess areas (D = 300 mm; d = 30 mm; T = 46 mm).

Figure 4 shows photographs of certain types of structures studied in the present work.

If in a system of accelerators using the E_{010} wave the drift tubes are an insignificant load and do not change the general relationships for the mentioned mode of oscillations, then in a field of the type H_{11n} they can distort it so strongly that the parameters of the resonance circuit will be determined not so much by the dimensions of the endovibrator as by the type and dimensions of the structure of the drift tubes and their suspension, as is the case in a simple circuit.

Some measurements were made to find the regions of application of separate forms of resonators and to select the optimum relationships of the dimensions.

In Fig. 5 the curves characterize the change in the shunt resistance and frequency during change in the period of the structure, when the drift tubes are fastened onto chasers. With increase in the period the shunt resistance falls, since there is a reduction in the number of accelerating intervals per unit length, as follows from formula (1). For each period there is an optimal relationship between the dimensions of the chaser giving an optimal value of R_{se}. Figure 6 shows the dependence of R_{se} and f on the area of the recess S. For small areas of the recess the capacity between the drift tube and the chaser is still important [C_0 in formula (3)]; with large areas the surfaces are contracted for passage of the current, i.e., the losses increase. At some optimal area of the recess the shunt resistance has its best value.

A reduction in the angle of the strut, α (Fig. 7), spoils the shunt resistance due to reduction in the surface of the chaser and an increase in losses. With increase in α above 45° the value of R_{se} also falls due to a reduction in inductance.

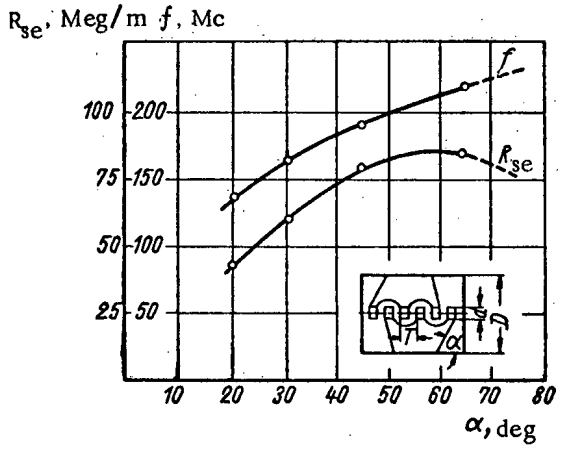

Fig. 7. Change in the parameters of the resonator for various strut angles of the chaser (D = 300 mm; d = 30 mm; T = 46 mm).

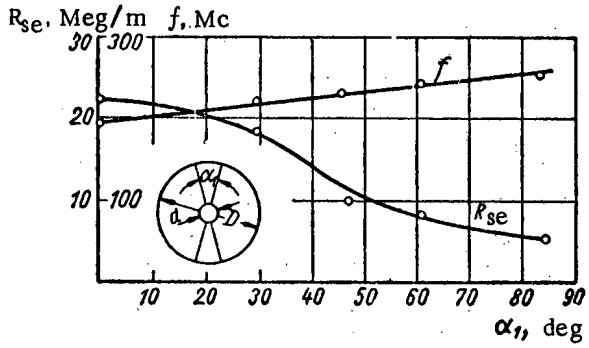

Fig. 8. Change in the parameters of the resonator for various transverse profiles of the chaser (D = 300 mm; d = 30 mm).

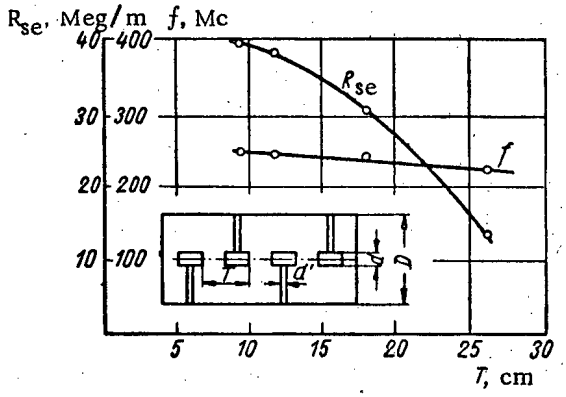

Fig. 9. Change in the parameters of the resonator with drift tubes on circular stems for different periods of structure (D = 300 mm; d = 30 mm; d' = 10 mm).

In the transverse cross section the best is a flat shape of chaser, giving the least frequency with small losses (Fig. 8).

As shown by experiment, the diameter of the drift tubes should be as small as possible (the requirement of field concentration).

A study was also made of the suspension of drift tubes on flat, round or separately shaped standing stems. Figures 9 and 10 show curves of R_{se} and f with change in the period of the accelerating structure. In the study of tubes on separately standing stems (the interfinger system [9]) it was found that the shunt resistance of such a system is not less than for the mode E_{010}, up to very high energies (but not to 10 Mev, as stated by Blewett [9]) and that this mode even exists at $\beta \approx 1$, whereas the mode E_{010} at $\beta \approx 0.35$ requires a fundamental rearrangement of the structure.

The parameters of the interfinger system depend to a large extent on the shape of the stems, as can be seen from the table.

Parameters of Interfinger System as a Function of the Shape of the Stems for D = 300 mm, d = 30 mm, T = 276 mm.

Type of stem	f, Mc	R_{se}, meg/m
Chaser	321	9.4
Flat stem measuring 60 × 3 mm	282	21.3
Flat stem measuring 30 × 3 mm	257	20.9
Round stem of 10-mm diameter	236	12.9
Stem of 1.5 turns of 50-mm diameter	166	24
Two round stems of 10-mm diameter	313	9.7

The dependence of the parameters on the mutual position of the suspensions is very small. Thus, with the suspensions placed on one side of the tube R_{se} = 12.5 meg/m and f = 242.0 Mc (for the same values of D, d, T); with the suspensions placed on the opposite sides of the tube R_{se} = 12.9 meg/m; f = 235.6 Mc.

These two facts indicate that the given type of oscillation is closer to the oscillations in a circuit with concentrated parameters than to the endovibrator waves. This is shown by the sharp increase in the shunt resistance on the replacement of a straight circular stem by a coil of 1.5 turns (see table).

When separately standing stems are used the diameter of the drift tubes is selected from the same considerations as in the case of suspensions of the chaser type.

To compare suspensions of the chaser type with suspensions in the form of separately standing stems it is essential to use the experimental curves of $R_{se} = f(\beta)$ (Fig. 11). As can be seen from these graphs, the chaser is economi-

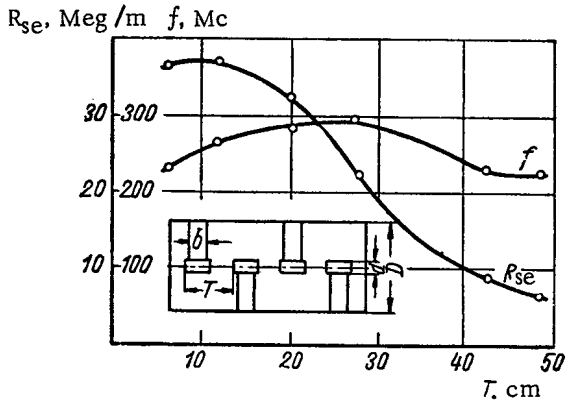

Fig. 10. Change in the parameters of the resonator with drift tubes on flat stems for various periods of the structure (D = 300 mm; d = 30 mm; b = 60 mm).

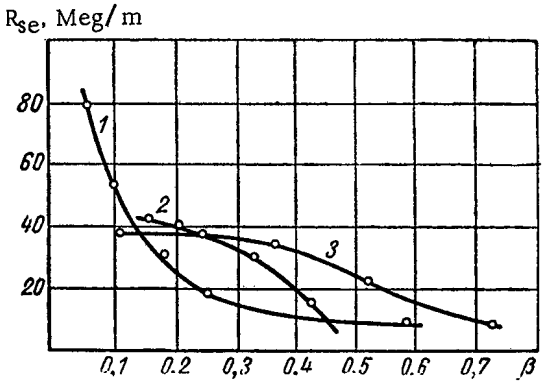

Fig. 11. Graphs for determining the ranges of application of various forms of suspensions (D = 300 mm; d = 30 mm): 1) drift tubes on the chaser; 2) drift tubes on round stems; 3) drift tubes on flat stems.

cal when $\beta < 0.15$. When $\beta > 0.15$ tubes should be placed on circular stems and when $\beta > 0.2$–0.25, on flat stems. On the whole with optimum relationships in the dimensions of these suspensions in the range $\beta = 0.015$–0.15 the value of R_{se} changes from 600-700 meg/m to 40-50 meg/m; when using separately standing stems the shunt resistance keeps a value of about 40 meg/m and only after reaching a value of $\beta = 0.35$ is there a further drop in R_{se} to 20-25 meg/m (when $\beta = 0.5$). On the average within the limits $\beta = 0.05$–0.35 the value of the shunt resistance is 45-50 meg/m.

Even with an increase in diameter of the drift tubes to the dimension needed for installing the focussing devices (60-70 mm) the shunt resistance in the limits of change $\beta = 0.05$-0.35 maintains an average value of about 35-40 meg/m.

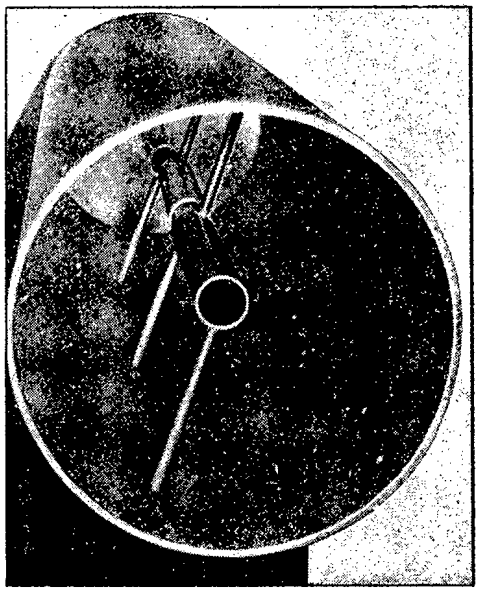

Fig. 12. System for $\beta \simeq 1$.

The system under consideration is suitable up to $\beta = 0.7$-0.8 and with two stems on each drift tube (Fig. 12) up to $\beta \simeq 1$ with a value of $R_{se} = 2$-3.5 meg/m. A system on a wave E_{010} has $R_{se} = 20$ meg/m up to $\beta = 0.35$ and at high speeds drastic rearrangement of the structure is needed, connected with the sharp deterioration in the value of the shunt resistance ($R_{se} = 1$-1.5 meg/m when $\beta = 0.55$).

Matching the Frequencies and Tuning the Field

The frequencies of different sections can be matched by changing the diameter of the drift tubes, the diameter of the waveguides, by changing the configuration of the chasers and stems in the axial and diametral planes, and by using shaped stems.

Changing the diameter of the waveguide at different sections is a complex technical problem; changing the diameter of the drift tubes is limited on one side by the diameter of the beam and on the other side by the drop in the shunt resistance and the coefficient of utilization of the field G.

By changing the shape of the tube suspensions it is possible to achieve a frequency trimming of up to 30%, which is quite sufficient for practical purposes. When trimming the frequency it is necessary to deviate from the optimum (from the point of view of a shunt resistance) configuration of the suspension but, since the optimums are weakly expressed in most cases, the reduction in R_{se} does not exceed 15%.

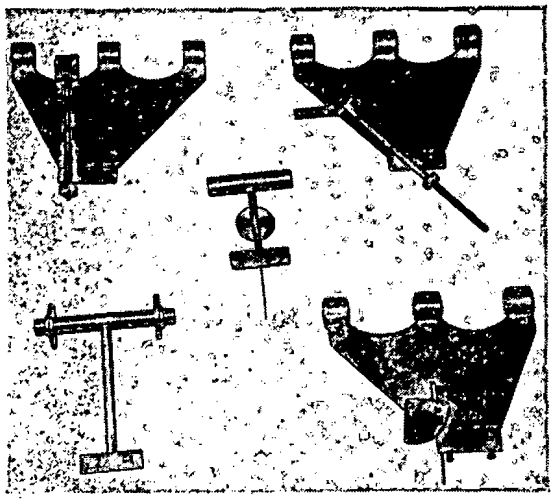

Fig. 13. Some types of trimming elements.

The fine trimming of the frequency, needed for balancing the field, is best achieved by special trimming elements. They can be introduced into both the electric and magnetic fields. In the first case the trimming element is the plate of a capacitor, the second plate of which is the drift tube; in the second case it is a flag intersecting the magnetic lines of force (Fig. 13).

If the chaser consists of 6-8 periods, one trimming element is sufficient since it changes the resonance frequency of the chaser without changing the distribution of field within its limits.

If the chaser is long, then the distribution of the field in it depends on the local heterogeneities, for example on the point of attachment of the trimming element (Fig. 14). The distribution of field in long chasers is affected by the configuration of the suspension (Fig. 15) in contrast to the distribution in short chasers, where it is practically impossible to change the field. This is due to the fact that in long systems the perturbing action of the structure heterogeneities is proportional to the square of the length of the system, as shown in a general form by Alvarez [14]. This means that the field can be adjusted uniformly even when there is a great difference in the accelerating gaps within the limits of one chaser. Each tube on separately standing stems must be fitted with a trimming element.

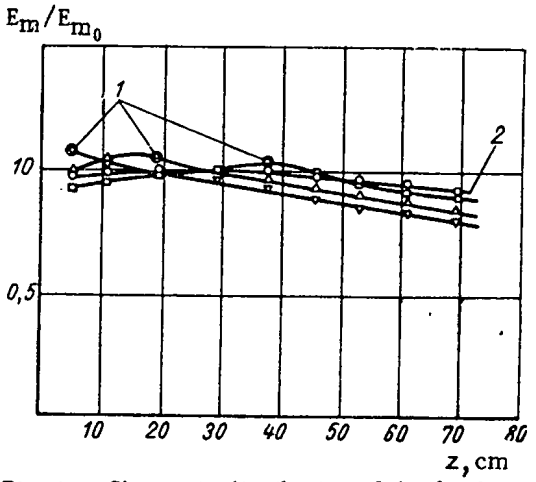

Fig. 14. Change in distribution of the field at the gaps as a function of the point of installation of the trimming element in a long chaser; D = 300 mm; d = 30 mm; T = 46 mm; E_m is the mean field intensity in the gap. E_{m0} is the mean field intensity in that gap where it is at a maximum; 1) point of installation of trimming elements; 2) field in chaser without trimming element.

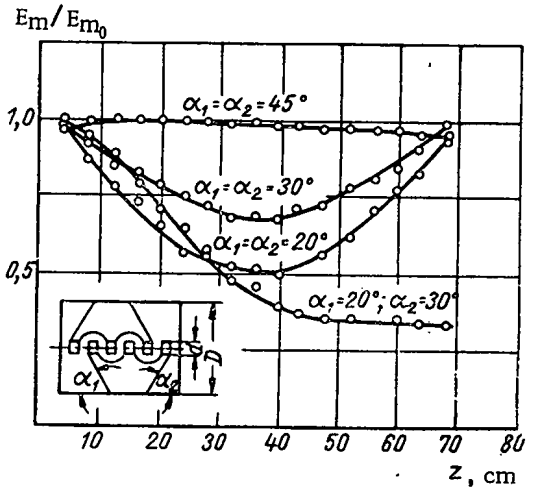

Fig. 15. Change in distribution of field at the gaps as a function of the configuration of a long chaser (D = 300 mm; d = 30 mm; T = 46 mm).

The field should be tuned starting from the condition E_{zm} = const. In fact, since the power is proportional to E^2_{zm} and the energy of the particle is proportional to E_{zm}, then it is apparent that their ratio is inversely proportional to the square of the coefficient of the shape of the field curve, which, according to the Cauchy-Bunyakovskii theorem, reaches a minimum value when $E_{zm} \rightarrow$ const. This tuning is readily attainable in accelerators using a wave type E_{010}, where it gives a magnetic field proportional to E_{zm} at the periphery. In an accelerator using a wave similar to H, the mentioned proportionality is not always observed and in some cases it is necessary to trim by the method of a perturbing body with subsequent integration of the field curve to obtain a mean value. Models of accelerating systems were studied to check the relationships on sections which were different in energy. Figure 16 shows a model of an accelerator at energies of 2-23 Mev for protons. The gaps change from 22 to 69 mm, the frequency is 240 Mc, R_{se} = 46 Meg/m. Figure 17 shows a model of an accelerator for protons at energies of 0.1-2.5 Mev. Here the gaps change from 5 to 30 mm, the frequency is 200 Mc, R_{se} = 140 Meg/m.

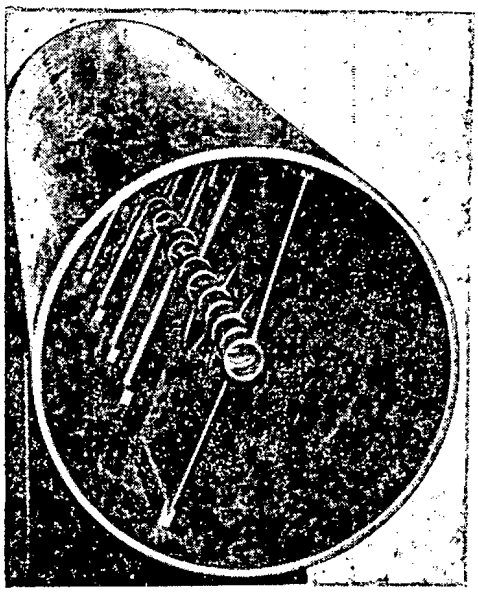

Fig. 16. Model of an accelerating system at proton energies of 2-23 Mev.

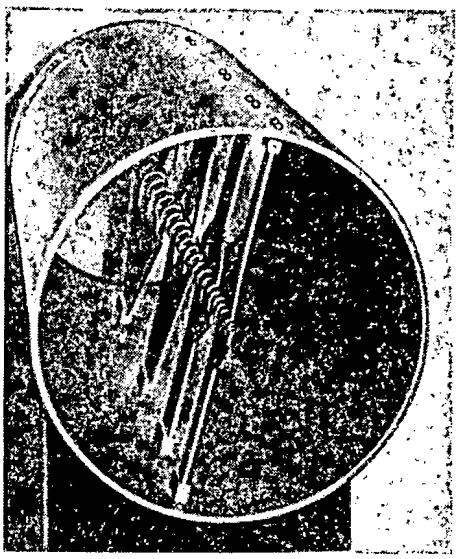

Fig. 17. Model of an accelerating system for proton energies of 0.1-2.5 Mev.

SUMMARY

The considered acceleration system with the condition of selecting optimum dimensions is suitable over all energy ranges except possibly for $\beta \simeq 1$, where it is inferior to accelerators with a running wave at oscillations of E_{010} at a frequency ~3,000 Mc (R_{se} = 30 meg/m). In all other cases this system gives a 2- to 3-fold or greater economy in the high-frequency power, the length of the accelerator is a half (since it uses a π-wave) and the reduction in vacuum volumes is not less than 20-fold.

The system can be used to accelerate ions for which, due to their low speeds, much greater wavelengths are needed than for electrons. It can have very low frequencies at high shunt resistances if a waveguide of increased diameter is used or a suspension of tubes of several turns. The advantages of resonators with a field similar to H in this case appear particularly clearly since at small values of β, characteristic for ions, a particle can pass repeatedly through the same accelerating voltage.

LITERATURE CITED

1. D. Sloan, Phys. Rev. 38, 2021 (1931).
2. A.K. Berezin et al, Zh. tekhn. fiz. 29, 808 (1959).
3. A.K. Berezin et al, Zh. tekhn. fiz. 29, 815 (1959).
4. Ya.B. Fainberg. Dissertation. Physicotechnical Institute, Academy of Sciences, Ukr.SSR, 1949.
5. L.N. Loshakov and B.B. Ol'derogge, Radiotekhnika 3, No. 2, 11 (1948).
6. S.Kh. Kogan, Dokl. AN SSSR 74, No. 3, 489 (1950).
7. D.I. Voskresenskii and R.A. Granovskaya, Izv. vyssh. uchebn. zavedenii. Radiotekhnika 2, No. 3 (1959).
8. A.I. Akhiezer and G.Ya. Lyubarskii, Zh. tekhn. fiz. 25, 1957 (1955).
9. J. Blewett, Symposium CERN, 1956.
10. E. Hudspath, Phys. Rev. 69, 761 (1946).
11. W. Hansen, Rev. Scient. Instrum. 19, 89 (1948).
12. V.V. Vladimirskii, Zh. tekhn. fiz. 17, 1269 (1947).
13. J. Slater, Appl. Phys. 23, 68 (1952).
14. L. Alvarez, Rev. Scient. Instrum. 26, 111 (1955).

THE SPACE-ENERGY DISTRIBUTION OF NEUTRONS IN A STRATUM CONTAINING A BORE HOLE

O. A. Barsukov and V. S. Avzyanov

Translated from Atomnaya Énergiya, Vol. 10, No. 5,
pp. 478-486, May, 1961
Original article submitted July 1, 1960

The article gives the theoretical and experimental results of an investigation of the space-energy distribution of neutrons in limestone pierced by a bore hole. In the calculation the differential equations describing the interaction of the neutrons with the medium were reduced to finite-difference equations. The results of the calculation are compared with experimental data.

The Theoretical Investigation of the Energy Distribution of Neutrons in Complex Media (Real Geometry)

Statement of the problem. In the solution of the problem of the distribution of neutrons in multilayer media, the best results can be obtained by numerical methods based on the use of high-speed computers. However, numerical methods of solving such a problem for a reactor (for example, the multigroup method developed by G. I. Marchuk [1]) are not applicable to the system of a stratum containing a bore hole. The reason for this is that in nuclear reactors we observe an established energy spectrum in almost the entire active section, and therefore the moderating process is described by linear partial differential equations. In the bore-hole-stratum system the energy spectrum of the neutrons near the bore hole (in the regions which interests us), according to our experimental data, is strongly dependent on the coordinates, and the equations accordingly become nonlinear (we are thinking of the group method). In other words, for a correct solution of the problem it is necessary to consider from the very beginning the strong mutual influence of the bore hole and the stratum, since the nonlinearity mentioned can be explained by precisely this interaction. Consequently, it is methodologically incorrect to consider such an interaction as a simple effect of the bore hole on the pure case (distribution in a homogeneous medium). From this viewpoint the statement of the problem in [2] and [3] can be considered correct.

The multigroup equations in the diffusion approximation, which describe the space-energy distribution of neutrons in the bore-hole-stratum system, reduce to the following systems of difference equations. For the one-dimensional case

$$\varphi_{k+1}^{j} - B_k^j \varphi_k^j + C_k^j \varphi_{k-1}^j = -F_k^j \ (j = 1, 2, \ldots m), \tag{1}$$

where B_k^j, C_k^j, and F_k^j are given positive numbers. For the two-dimensional case

$$\bar{\varphi}_{k+1}^{j} - \bar{B}_k^j \bar{\varphi}_k^j + \bar{C}_k^j \bar{\varphi}_{k-1}^j = -\bar{F}_k^j \ (j = 1, 2, \ldots m), \tag{2}$$

where $\bar{B}_k^j$, and $\bar{C}_k^j$ are matrices; $\bar{\varphi}_k^j$ and $\bar{F}_k^j$ are vectors; φ_k is the neutron flux for group j at the point k; j is the ordinal number of the energy group; k is the number of the nodal point of the subdivision.

Such a formulation of the equations allows us to standardize the process of solution of the problems, since the properties of the latter are based on the coefficients of the equations. For example, for a medium with a continuously changing rock composition this change is taken into account in calculating the coefficients at the nodes. It is also possible to solve the problem with a changing energy spectrum, using the appropriate averages of the sections over the energy spectra at the nodes.

The indicated system must be supplemented by boundary conditions. We shall mention two types of conditions: 1) the general boundary conditions of the problem, defined at the center of symmetry on the axis of the bore hole and

at infinity, where the flux must become zero; 2) conditions on the boundaries of the adjoining regions of the bore-hole-stratum system. The latter conditions are satisfied if we construct a difference scheme for the solution of problem (1).

The condition that the flux becomes zero at infinity is not applicable to the difference scheme, since for the solution of the difference equation by the factorization method we must restrict ourselves to a finite number of subdivision nodes. This condition must therefore be replaced by an approximate condition obtained from the following considerations: The neutron density values decrease monotonically starting from some effective radius R_{max}, defined for each energy group, and since the distributed neutron sources for the groups are defined by these same fluxes, the source density values also decrease. In view of this behavior of the functions, the following method for solving the problem can be suggested: At some distance greater than R_{max}, defined by the region of establishment of a constant energy spectrum, the solution of the problem is cut off; that is, it is assumed that at some point r_m the function φ_m becomes zero ($\varphi_m = 0$).

For the solution of the equation

$$\varphi_{k+1}^j - B_k^j \varphi_k^j + C_k^j \varphi_{k-1}^j = -F_k^j$$

the method of difference factorization is used, by means of which the equation is representable in the form of the system

$$\left.\begin{aligned} \beta_{k+1} &= \frac{C_{k+1}^j}{B_k^j - \beta_k^j}, \\ Z_{k+1}^j &= \beta_{k+1}^j (Z_k^j + F_k^j); \\ \varphi_k^j &= \frac{\beta_{k+1}^j \varphi_{k+1}^j + Z_{k+1}^j}{C_{k+1}^j}. \end{aligned}\right\} \qquad (3)$$

In computations with system (3) the round-off errors will not increase from node to node, that is, the computation will be stable. The use of such calculations in practice has shown that an error accidentally committed by the operator is rapidly damped out by the time the adjacent nodes are reached. This circumstance is exceptionally useful, since the error introduced by cutting off the solution at the point r_k is automatically excluded in the process of solution without any supplementary conditions. The further generalization of the theory is related to the nonlinear problem, for the solution of which the following iterative process is proposed:

1. Having specified the assumed energy spectra in some local regions of the system, defined by a subdivision network, we average the constants of the difference equations over this spectrum.

2. Solving the difference system, we obtain new energy distributions of neutrons in the local regions.

3. We perform a new averaging of constants over the resulting spectrum, and we again solve the difference system.

These operations are performed until we obtain a satisfactory agreement of energy spectra in the local regions of the system which are under consideration.

The iterative process of solving the problem is constructed by analogy with the physical process of establishment of the spectrum in the system, so that we may expect satisfactory convergence, since the spectrum in the real system is established fairly rapidly.

Analysis of the Resulting Solution We performed the numerical calculations for the neutron distribution in a two-group diffusion approximation. We considered a medium consisting of five layers in a cylindrical configuration (Fig. 1) (the real geometry of the reinforced bore hole). The energy spectrum of the neutrons was divided into two intervals, corresponding to the two groups of neutrons (fast and slow). The interval of the first group extended from the energy of the neutrons at the source to 3 ev, and the second from 3 ev to 0.03 ev. The point source of fast neutrons was located at the origin.

The results of the calculations for the five-layer medium (see Fig. 1) show that a characteristic property of the distribution of the neutrons of the slow group is the presence of maxima of density on the interface between the cement and the rock, as well as between the iron column and the water in the bore hole.

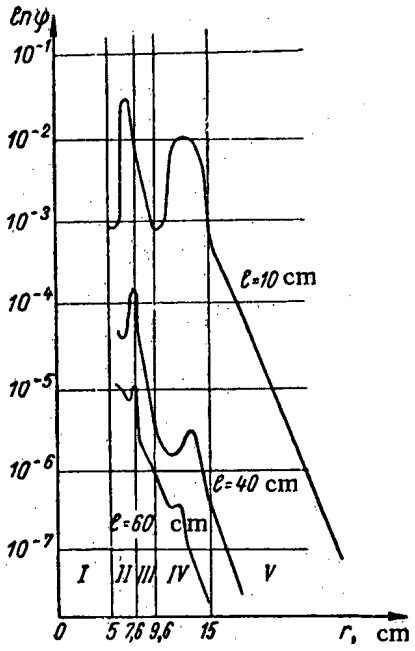

Fig. 1. Distribution of neutrons of the slow group in the bore-hole-stratum system (l is the length of the probe): I) air; II) water; III) iron; IV) cement; V) oil-bearing sandstone (porosity 20%).

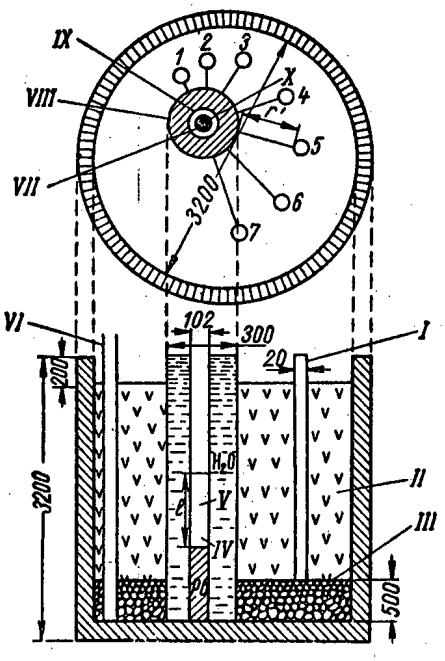

Fig. 3. Diagram of the stratum model. II) Limestone; VI) water supply pipe; VII) neutron apparatus [distance r in mm from the test hole (t.h.), to the boundary of the bore hole: 1) 47; 2) 100; 3)153; 4) 248; 5) 386; 6) 598; 7) 900].

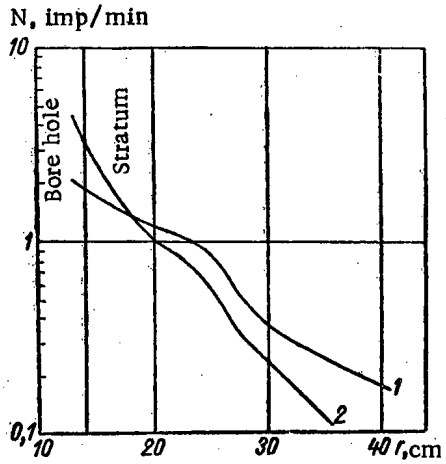

Fig. 2. Comparison of theoretically obtained radial distribution of neutrons of the fast group with experimental distribution for neutrons with energies of 15-50 ev. 1) experimental curve; 2) theoretical curve.

In addition, we calculated the distribution of neutrons in a model of the stratum on which we performed the experiments described below (we simulated an unreinforced bore hole filled with water, located in limestone with a minimum hydrogen content). A comparison was made for the fast group. It was assumed that the source was distributed along the axis of the bore hole. An analysis of this comparison (Fig.2) shows the following:

1. The slope of the curve obtained theoretically is greater than the slope of the experimental curve. This difference is related, to a considerable extent, with the small number of groups used in the calculation and the presence of a linearly distributed source.

2. The curves have a characteristic break point related to the boundary effect (r = 25 cm). A significant circumstance here is that the regions of influence of the boundary in the two cases (experiment and theory) coincide, regardless of the crude simplifications used.

Experimental Study of the Space-Energy Distribution of Neutrons

Description of the Investigation. For the experiments we used the method of resonance absorbers, making use of a set of europium (or erbium), rhodium (or indium) and silver detectors. The fundamental resonances of these absorbers allow the separation of neutrons with energies of 0.46 ev (Eu^{151}); 0.51 ev (Er^{170}); 1.26 ev (Rh^{103}); 1.46 ev (In^{155}); 5.23 ev (Ag^{109}); 15-50 ev (Ag^{107}).

The experiments were so conducted that the resulting data, upon being processed further, made it possible to give information of a quantitative nature. From this viewpoint it was necessary to satisfy two requirements: in the first place, to perform the measurements under "clean conditions," that is, on such a large model

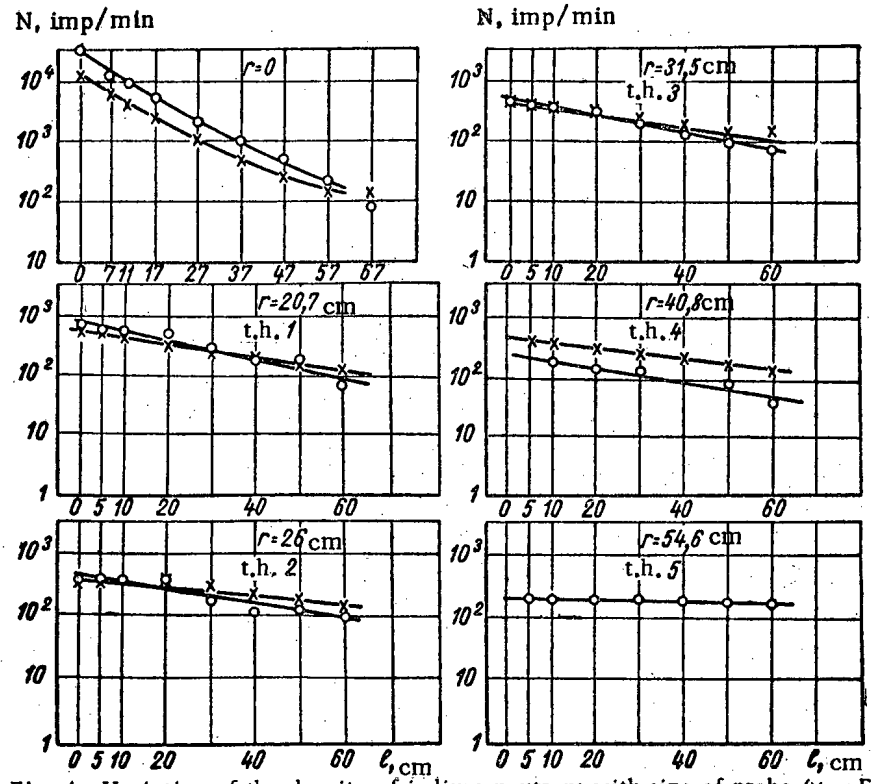

Fig. 4. Variation of the density of indium neutrons with size of probe (× – E_n = 0.003 ev; ○ – E_n = 1.44 ev).

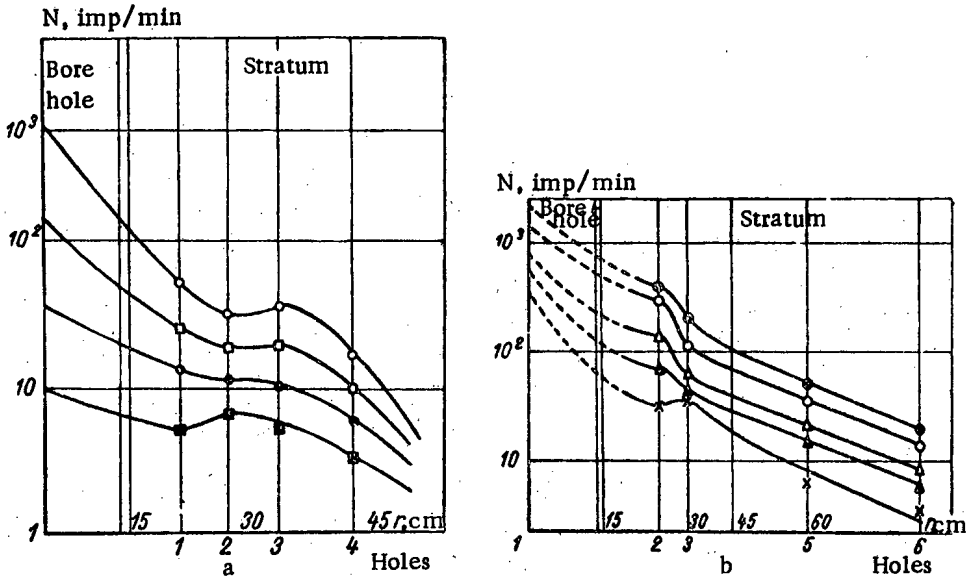

Fig. 5. Radial distribution of neutron density: a) for indium neutrons with E_n = 0.03 ev (○, □, ●, ■ – l, equal respectively to 2; 32; 42; 52 cm); b) for epithermal silver neutrons with E_n = 5-50 ev (●, ○, △, ▲, × – l equal respectively to 12; 27; 42; 52; 62 cm).

that the effect of its boundaries and of the neutron escape associated with it was negligibly small; in the second place, to consider and exclude numerous factors affecting the measuring process.

We shall consider these requirements in greater detail.

1. One of the chief faults of most measurements made up to the present time by various investigators for the purpose of obtaining quantitative information was the fact that the measurements were made on models whose dimensions

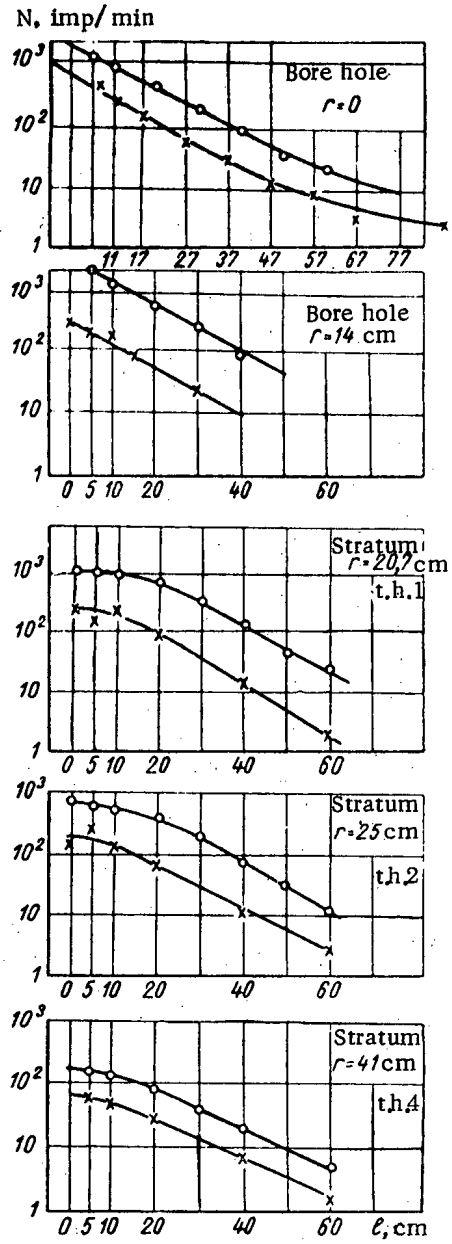

Fig. 6. Variation of density of rhodium neutrons with size of probe (○-E_n = 0.03 ev; × − E_n = 1.26 ev).

were too small. According to [4] the minimum radius of the cylindrical model must be equal to 280 cm (for a reinforced bore hole in a homogeneous medium). These data were considered in the construction of the model, a diagram of which is shown in Fig. 3. The model was located underground in a cylindrical pit. For the complete expulsion of air from the pores of the rock, water is introduced into the stratum at the bottom through a layer of gravel, III. Measurements were made in the bore hole and in the stratum. The model of the bore hole is a cylinder, VIII, of diameter 294 mm, filled with water (unreinforced bore hole). In the latter we placed a standard case of depth apparatus, IX, with an external diameter of 102 mm and a wall thickness of 10 mm. Inside the case was a metal pipe, X, of diameter 80 mm, in which were placed the sources, IV, and the detectors, V. In the stratum the measurements were made in test holes, I, consisting of aluminum pipes with an external diameter of 20 mm. In order to prevent interaction the test holes were located along a spiral (they are shown in Fig. 3 by the numbers 1-7).

2. In precise measurements with resonance absorbers we must take account of the following factors: 1) the effect of other resonances or intervals of absorption with large capture cross section (correction α); 2) distortion of the neutron field by the resonance detector (correction β); 3) absorption by cadmium of the epithermal neutrons (correction γ); 4) absorption of beta particles in the material of the detector (correction δ); 5) absorption of beta particles in the material of the window of the end-window counter (correction ϵ); 6) the geometry factor (correction ζ).

All measurement data were corrected by the combined correction factor $K = \alpha\beta\gamma\delta\epsilon\zeta$. In addition, we introduced a background correction and a correction for the disintegration of the polonium-beryllium source. All the end-window beta counters were calibrated with a single standard. In order to obtain a high statistical precision we used sources with strengths of up to 30 curies. The measurements were made four to six times on the average. The attached graphs show points corresponding to mean values. The statistical errors are so small that they cannot be shown on the graphs.

Distribution of Neutrons in the Limestone with Minimum Hydrogen Content (M = 0%). Measurements were made with indium and silver, which made it possible to separate neutrons with energies of 0.03, 1.44, and 5-50 ev.

Fig. 4 shows the curves of $\ln N = f(l)$ for resonance and thermal neutrons of indium (here N is the density of neutrons with a given energy; l is the length of the probe). It should be remarked that the readings decrease monotonically with increasing l, which indicates the extraordinarily slow process of neutron moderation. An inspection of these graphs by holes shows that in the central hole (the bore hole) and in the first test hole, located at a distance of r = 20 cm from the axis of symmetry of the bore hole, the spectrum is characterized by some excess in the densities of neutrons of the thermal group over the densities of the neutrons of the resonance group with energies of about 1 ev. As r increases further, the picture changes: The thermal neutrons become fewer and fewer, and in the last hole they are not recorded at all. It also interesting to note that the slope of the curves decreases with increasing r and in hole 5 the curve is almost parallel to the abscissa axis. Furthermore, in this case the results of measurements with and without a cadmium filter agreed.

Fig. 5a shows the distribution of the density of thermal neutrons along a radial section. It should be noted that the curves have a characteristic break point associated with holes 2 and 3 (r = 25 cm and r = 31.3 cm). The distribution curves of epithermal indium neutrons along a radial section show approximately the same behavior.

Fig. 5b shows the radial distribution of epithermal silver neutrons. In these curves, which decrease with increasing r more steeply than the corresponding curves for indium, we can also observe the characteristic break point associated with holes 2 and 3.

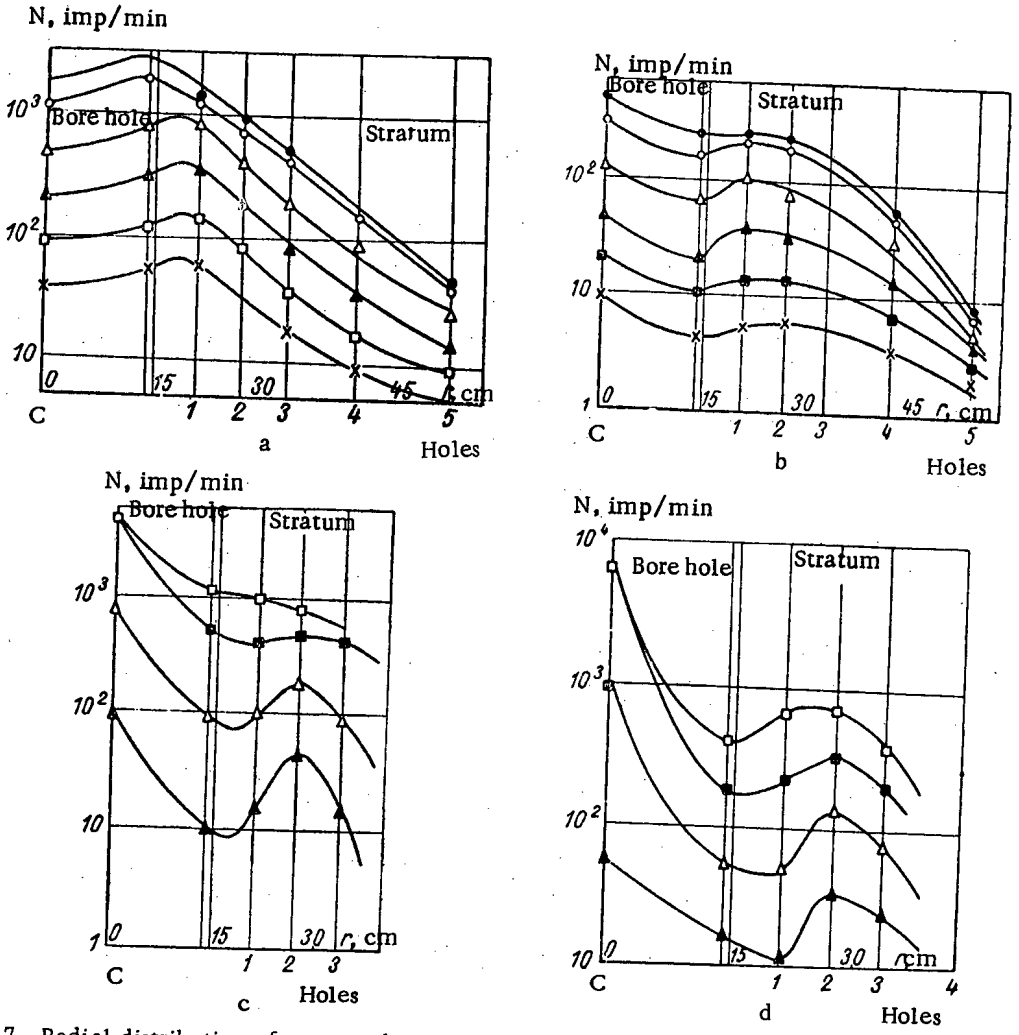

Fig. 7. Radial distribution of neutron density: a) for rhodium neutrons with an energy of 0.03 ev; b) for rhodium neutrons with an energy of 1.26 ev (in both cases ●, ○, △, ▲, ■, ×: l, equal respectively to 7, 12, 22, 32, 42, 52 cm); c) for silver neutrons with an energy of 5.1 ev; d) for silver neutrons with an energy of 15-50 ev (in both cases □, ■, △, ▲: l, equal respectively to 14, 22, 32, 42 cm.

Distribution of Neutrons in the Limestone with Maximum Hydrogen Content (m = 30%.) By means of rhodium, europium, and silver detectors we investigated the distribution of neutrons with energies of 0.03, 0.5, 1.26, and 15-50 ev.

Let us consider as an example the results of the measurements with rhodium detectors. The curves of $\ln N = f(l)$ for thermal and resonance neutrons with an energy of 1.26 ev in various holes is shown in Fig. 6. Near the bore hole (holes 1 and 2) the density of thermal neutrons considerably exceeds the density of neutrons with an energy of 1.26 ev. At large distances from the bore hole the curves are closer together, which indicates a relative decrease of the thermal component as compared with the epithermal. Figure 7 shows the family of curves of the type $\ln N = f(r)$ for neutrons with various energies. Inspection of these functions shows that with increased size of probe and increased neutron energy the characteristic bend of the curves near the boundary of the bore hole and the stratum increases sharply. On the basis of the material cited the interaction of the neutrons with the rock and the bore hole may be represented as follows: The fast neutrons emitted by the source are slowed down and are distributed in various regions of the stratum and the bore hole with a highly inhomogeneous energy distribution. Thus, if the distribution of neutrons with an energy of E_n = 0.03 ev in the bore hole and the stratum at distances up to about 10 cm from the wall of the bore hole is approximately homogeneous (see curves, Fig. 7a), the density of epithermal neutrons (E_n = 1-50 ev) decreases approximately by one order of magnitude upon passing from the center of the bore hole to the region located 3-5 cm beyond the indicated boundary (see Figs. 7b, c, and d). Here, a sort of "vacuum" of epithermal neutrons is created. Finally, beyond this region there is another region, where the density of epithermal neutrons increases sharply, with a maximum first observed for rhodium neutrons (E = 1.26 ev), and then for silver neutrons (E_n = 5 ev and E_n = 15-50 ev).

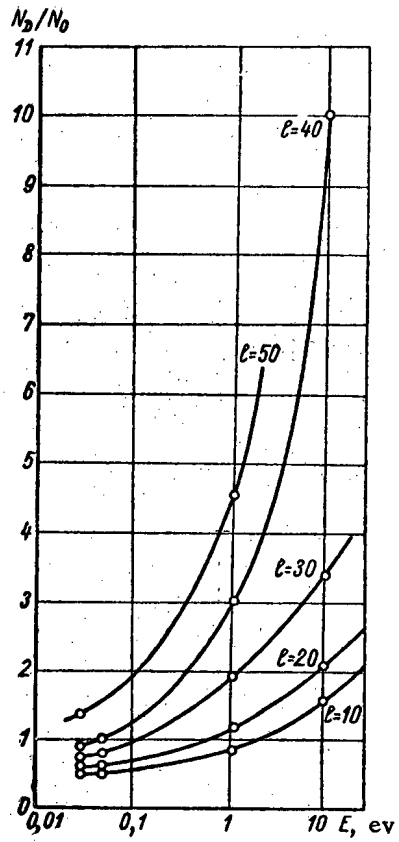

Fig. 8. Variation of the ratio $N_{D=30}/N_{D=0}$ with neutron energy for various probes.

Study of the Effect of the Bore Hole. The most important problem which must be solved in the development of any quantitative method is taking the effect of the bore hole into account. The results of the corresponding experiment (m equals 30%) are shown in Fig. 8, where the ordinate axis shows the ratio of neutron density N_D, determined at the center of the bore hole, to the neutron density N_0, measured in the absence of a bore hole in the stratum, and the abscissa axis shows neutron energy E_n. Inspection of the curves of Fig. 8 shows that this ratio increases with increasing neutron energy. Obviously, when the readings in the stratum and in the bore hole coincide, the ratio $N_D/N_0 = 1$. From these curves it can also be assumed that for l = 20 cm and l = 30 cm we can choose neutron fluxes with energies at which the readings of the instruments in the bore hole and the stratum will agree in absolute value. At the same time, the behavior of the curve at l = 50 cm clearly indicates that in this case it is impossible to obtain such an agreement between the readings.

Analysis of the results of the experiments described leads us to the conclusion, paradoxical at first glance, that as l increases, the effect of the bore hole must increase. However, this conclusion becomes clear on comparison with the results obtained earlier. Thus, studying the radial distribution of neutrons, we found that the bore hole is surrounded on the outside by a sort of "plasma" formed by the epithermal neutrons with a maximum near an energy of 5 ev. The density of this plasma is low for small distances from the source and increases sharply with an increase in l. At distances of more than 20 cm from the source the effect of the flux of neutrons which were slowed down in the bore hole is almost equal to zero (since the deceleration occurs in water). Therefore, for $l > 50$ cm the basic effect on the recorded readings will be caused by the epithermal neutrons migrating from the stratum into the bore hole. The role of the bore hole in this case is reduced to the role of a moderator of the plasma neutrons. In other words, the effect of the bore hole for these values of l increases sharply, since it becomes an "amplifier" of the effect. Therefore, the increase of the effect of the bore hole for large probes cannot be considered a negative phenomenon.

SUMMARY

From the investigations described in the present article the following conclusions may be drawn:

1. The suggested theoretical method for the solution of the problem of the distribution of neutrons in complex media, which consists of reducing to finite difference equations the differential equations describing the process of interaction of the neutrons with the medium, may be effectively used for a bore-hole-stratum system.

2. The solution obtained for a multilayer medium in a two-group approximation should be considered as an intermediate step in the development of the theory. Passing to the multigroup case will cause no difficulties of principle. The most essential fact is that a version acceptable in practice has been found for the rapid solution of the problem of the distribution of neutrons in the real geometry. We should also emphasize the flexibility of the method, which lies in the possibility of its further generalization by passing to the consideration of higher harmonics of the expansion (method of spherical harmonics).

3. The investigation of the space-energy distribution of neutrons by means of a model allowed us to determine a sharp inhomogeneity in the distribution of neutron fluxes of different energies in the bore hole and the stratum. In the rock along the bore hole we established the existence of a neutron plasma with an energy of 5-10 ev for probes measuring 25-50 cm. The density distribution of neutrons with an energy of 0.3-1 ev in the region around the bore hole apparently requires further refinement.

The inhomogeneous energy distribution of neutrons around the bore hole indicates that the effect of the bore hole leads to a sharp distortion of the neutron spectrum.

This leads to an extraordinarily important consequence for the theory. The fact is that for an estimate of the spectrum distortion in the multigroup approximation we must replace the constant coefficients in the equations showing

neutron distribution by variable coefficients, that is, change from the solution of linear differential equations to the solution of nonlinear equations of the same type.

4. The indicated property of the energy distribution of the neutrons allows us to draw a number of important conclusions. One of these states that it is impossible to eliminate the effect of the bore hole for large probes (that is, under conditions where the rocks differ greatly in hydrogen content)as a result of the increase of its active role, intensively decelerating the plasma neutrons. This leads to a methodologically important consequence, defining a method for taking the effect of the bore hole into account exactly. For this it is necessary to make complicated measurements in one of which the energy interval of the recorded neutrons and the probes is chosen in such a way that the readings in the stratum and the borehole begin to agree (in the region of weak plasma effect, that is, for small probes). It is useful to make a second measurement with very long probes, which assures a considerable degree of differentiation between the rocks.

LITERATURE CITED

1. G. I. Marchuk, Numerical Methods of Calculation For Nuclear Reactors [in Russian] (Moscow, Atomizdat, 1958).
2. A. E. Glauberman, I. I. Tal'yanskii, Atomnaya Energiya 3, No. 7, 23 (1957).
3. O. A. Barsukov et al., Radioactive Investigation of Oil and Gas Bore Holes [in Russian] (Moscow, State Fuel Engineering Press,1958), p. 225.
4. A. V. Zolotov, Proceedings of the All-Union Conference on the Application of Radioactive Radiation in Science and the National Economy (Moscow, State Fuel Engineering Press, 1958), p. 144.

AN AUTOMATIC CASCADE DEVICE FOR PRODUCING HIGHLY CONCENTRATED HEAVY NITROGEN ISOTOPE

I. G. Gverdtsiteli, Yu. V. Nikolaev, E. D. Oziashvili, K. G. Ordzhonikidze, G. N. Muskhelishvili, N. Sh. Kiladze, V. R. Mikirtumov, and Z. I. Bakhtadze

Translated from Atomnaya Énergiya, Vol. 10, No. 5, pp. 487-492, May, 1961
Original article submitted June 7, 1960

The present article describes an automatic device for producing N^{15} by using the method of exchange in the $NO-HNO_3$ system. In separating ~ 0.5 g of nitrogen per day, a N^{15} concentration of 99.8% was obtained by means of this device. The enrichment starts at the level of the natural N^{15} concentration, which is equal to 0.365%.

Introduction

Due to the fact that there are no radioactive nitrogen isotopes that would be suitable for use as labeled atoms, the heavy nitrogen isotope N^{15} is extensively used in physicochemical, agricultural, medical, and biological investigations. In the form of the $N^{15}H_3$ compound, this isotope is used in molecular electromagnetic radiation generators. The use of the $N^{15}H_3$ compound makes it possible to secure high-frequency stability due to the fact that this compound does not have a superfine structure. Thorium nitrates with a N^{15} base can be used in nuclear power engineering. The application of nitrates in homogeneous reactors offers promising possibilities because of their high solubility. The necessity of using nitrates with a N^{15} base is determined by the fact that natural nitrogen has a large thermal neutron capture cross section (1.8 b), while the capture cross section of N^{15} amounts to only $2 \cdot 10^{-5}$ b.

One of the main difficulties encountered in producing highly concentrated N^{15} is its low content in the natural mixture (0.365%). Therefore, in order to produce N^{15} in amounts worth considering, it is necessary to use highly efficient separation methods which would also be suitable from the point of view of energy. Perhaps the most effective of the known methods for concentrating N^{15} is the method of chemical exchange between NO and HNO_3, which has been proposed in 1955 [1]. The authors of papers [1] have constructed a cascade device consisting of two columns, by means of which a product with a N^{15} concentration of 99.8% was obtained. On the basis of this, we have developed and constructed an automated cascade device for the production of N^{15}. According to data available in the literature, an automated device with a theoretical output of 1 g of nitrogen per day with a N^{15} concentration of 99.37% has also been constructed at the National Laboratory at Oak Ridge, USA [2].

Method of Concentrating N^{15} by Using the Exchange in the $NO-HNO_3$ System

Water solutions of HNO_3 form with nitrogen oxides an equilibrium system which consists of a number of ionic and molecular compounds. The gaseous phase contains NO, NO_2, N_2O_3, N_2O_4, H_2O, HNO_3 and HNO_2. The liquid phase contains, besides HNO_3 and H_2O also NO, NO_2, N_2O_3, N_2O_4, HNO_2, H_3O^+, NO_3^-, and NO_2^-. The concentration of each component depends on temperature, pressure, and the concentration of acid.

The calculation of the separation factors in the exchange reactions which take place in such a system has been described in [3] on the basis of spectroscopic data. The values of the separation factors for the case of nitrogen exchange between the oxides of nitrogen and nitrate and nitrite ions are given below:

Exchange system	Separation factor
$NO—NO_3^-$	1,096
$NO_2—NO_3^-$	1,053
$NO—NO_2$	1,040
$NO—NO_2^-$	1,006
$NO_2—NO_2^-$	0,966

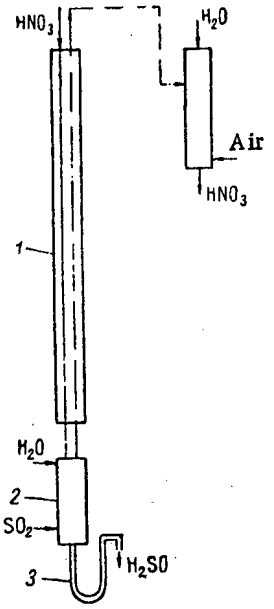

Fig. 1. Diagram of the device for concentrating N^{15} according to the method of exchange in the $NO-HNO_3$ system.

It is obvious from the adduced data that the maximum value of the separation factor was obtained for the $NO-NO_3^-$ system. The effective separation factor, which is defined as the ratio of N^{14}/N^{15} in the gaseous phase to N^{14}/N^{15} in the liquid phase, depends on the phase composition. The concentration of higher oxides increases with an increase in the acid concentration, and, therefore, the value α of the effective separation factor decreases. Thus, in 1.03 M solutions, $\alpha = 1.065$, while in 11.1 M solutions, $\alpha = 1.045$. Conversely, the exchange rate increases with an increase in the concentration of acid. The repetition of the primary effect, which is produced in a single process, can be realized in packed columns. The diagram of the device for concentrating N^{15} by using the method of exchange in the $NO-HNO_3$ system is shown in Fig. 1. HNO_3 enters the upper end of column 1. After passing through the column, the acid flows off into the reaction vessel 2, where it enters into reaction with sulfur dioxide SO_2:

$$3SO_2 + 2HNO_3 + 2H_2O = 3H_2SO_4 + 2NO.$$

The reaction between HNO_3 and SO_2 is exothermic. Because of this, heating and a partial decomposition of HNO_3 with the formation of NO_2 take place in the reaction zone. In order to reduce the partial pressure of NO_2 to a level approximately equal to the equilibrium pressure, the reation vessel is cooled by means of circulating water and, moreover, a certain amount of water (~ 25% of the acid flow) is supplied to the upper end of the reaction vessel. NO_2 dissolves in water:

$$3NO_2 + H_2O = 2HNO_3 + NO.$$

The mixture of nitrogen oxides that forms in the reaction vessel passes through the column in the direction opposite to that of HNO_3 and is brought out of its upper end. The N^{15} isotope is concentrated in HNO_3 and is transfered to the lower end of the column. The nitrogen oxides that come out of the upper end of the column are impoverished with respect to isotope N^{15}.

Sulfuric acid is brought out of the reaction vessel through trap 3 (see Fig. 1). For the purpose of HNO_3 regeneration, the nitrogen oxides that come out of the upper end of the column are oxidized by oxygen from the air so that NO_2 is formed and are then dissolved in water, whereby HNO_3 is formed:

$$4NO + 2H_2O + 3O_2 = 4HNO_3.$$

Thus, HNO_3 is practically completely regenerated, while SO_2 is transformed into H_2SO_4.

Cascade Device for Producing N^{15}

A cascade device consisting of two columns with different cross sections was constructed for producing highly concentrated N^{15} [4]. The profiled system has the following advantages:

1) The time necessary for attaining the equilibrium state in the cascade is reduced; this is especially important in the case of concentrating N^{15}, since, due to the low initial concentration value, the migration of N^{15} throughout the cascade is not sufficiently intensive, and, consequently, the equilibrium-establishment time is large.

2) N^{15} losses that are caused by the carrying away of nitrogen with H_2SO_4 from the reaction vessel are reduced.

3) The cascade volume is reduced. The latter is especially important if a large industrial device is to be constructed.

The cascade device is shown in Fig. 2. Items 3 and 6 represent the first and the second column of the cascade, respectively. The columns are located one above the other. Such a layout makes it possible to dispense with the use of transferring pumps, and it secures a reliable flow distribution between the columns.

HNO_3 is fed from tank 1 to the upper end of the first column through a regulating value, 4, and a flowmeter, 2. The acid flows down through the packing to the lower end of the column and enters the flow distributor, whence a portion of the enriched solution is conveyed through the regulating valve 5 and flowmeter 2 to the upper end of the second column for further enrichment, while the remaining portion flows into the reaction vessel through drain pipe 7.

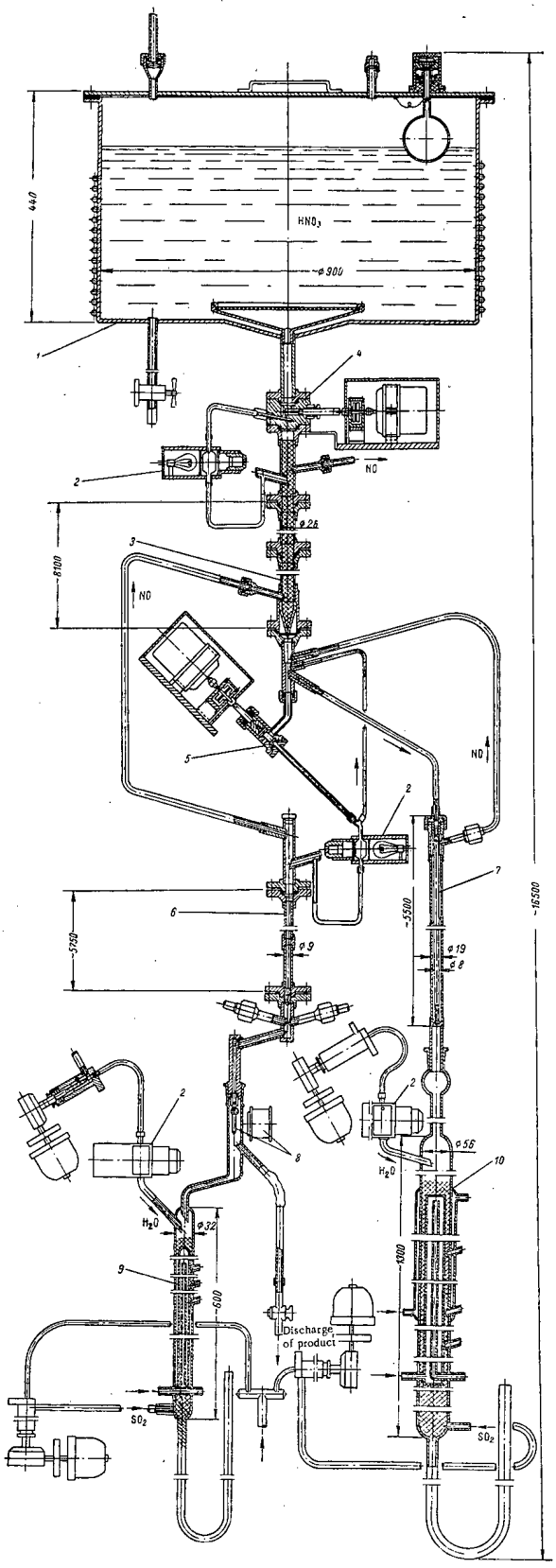

Fig. 2. Cascade device for concentrating N^{15}.

In the reaction vessel 10, HNO_3 enters into reaction with SO_2 that is supplied there. The mixture of nitrogen oxides which has formed as a result of the reaction is directed to column 3, where it initiates isotopic exchange with nitric acid that flows through the packing. From column 6, HNO_3 enters reaction vessel 9, which is similar to reaction vessel 10. From the reaction vessel the nitrogen oxides return to column 6, flowing through it in the direction opposite to the direction of HNO_3 flow, and are conveyed to the lower end of the first column. Nitrogen oxides that are impoverished with respect to N^{15} are brought out of the cascade. H_2SO_4 that has formed in the reaction vessels is drained through traps into tanks. HNO_3 which is enriched with N^{15} is taken out from the lower end of the second column by moving the electromagnetic drop tube 8 toward the drain pipe.

The columns, the regulating valve, and the cascade's connecting pipes are made of stainless steel 1Kh18N9T. Argon-arc welding as well as flange joints were used for connecting the pipes. The gaskets were made of teflon. Needle regulating valves with differential threads and a spring for adjusting the backlash were used for regulating the liquid flow. The valve stems were made airtight by means of teflon packing glands. Needle valves with bellows were used for regulating the gas flow.

The reaction vessels were made of quartz and were filled with packing in the shape of rings that were also made of quartz. The reaction zone length in the reaction vessel of the first column was ~ 15 cm, while the reaction zone length in the reaction vessel of the second column was ~ 3 cm. The first reaction-vessel length was 130 cm, and the second reaction-vessel length was 60 cm. The large reaction vessel was provided with external and internal cooling, and the small reaction vessel had only internal cooling.

Automatic Control System of the Cascade

The following arrangement was chosen for rendering the control of the device fully automatic: The acid flow and the water flow in the large and the small reaction vessels were stabilized; stabilization of the amount of the product (acid) separated was provided and the gas supply was regulated with respect to the position of the reaction zone in the reaction vessels. The control system comprises the following devices: automatic acid-and water-flow stabilizers, automatic gas-flow regulators for the large and the small reaction vessels, devices for stabilizing the assigned separation rate, a signaling unit which controls the operation of the automatic regulators and stabilizers, and an electrical supply unit which feeds the entire device.

The necessary accuracy and high reliability in continuous operation over long periods of time and the possibility of operation in an aggressive medium of acid vapors and under high-humidity conditions, constituted the requirements imposed on the automatic control system. The control system does not have any contact devices.

The automatic stabilizer constitutes a closed-loop system. From the data transmitter, the signals are fed to a comparing device, which determines the deviation from the assigned value and supplies a command to the servomechanism, where control is effected according to an assigned program.

The acid-and water-flow stabilizers of the first and second column are of the same design, and they differ only with respect to the intensities of the flows to be stabilized. They have the same layout and they can be interchanged.

Each of the liquid-flow stabilizers consists of the following basic units: a flow meter, a pulse regulator (with a phase-detecting converter at the input and an output power amplifier), and a servomechanism; the block diagram of the stabilizer is shown in Fig. 3.

The method of drop counting is used for measuring the discharge of small amounts of liquid in this device. The contactless drop-count data transmitter is based on photoresistors, which are enclosed in airtight glass bulbs. From the data transmitter, the pulses are fed to an electronic circuit, where they are shaped, and are then supplied to an integrating device. An indicating M-24 microammeter serves as the drop counter. For convenience, the passage of each drop is signaled by a neon-lamp flash.

The flow meter output signal is supplied to the input of the phase-detecting converter and is transformed into industrial-frequency ac voltage. In this, the voltage amplitude of the transformed signal is proportional to the deviation of the number of drops from the assigned number, while the deviation sign is determined by the phase. A magnetic modulator is used as the phase-detecting converter.

The signal from the output of the phase-detecting converter is fed to a pulse regulator and also the control and signaling unit. If the flow meter breaks down or if the liquid flow changes to a large extent, this signal disconnects the servomechanism from automatic control. The emergency signaling system is actuated if the flow value differs from the nominal value by more than 8%.

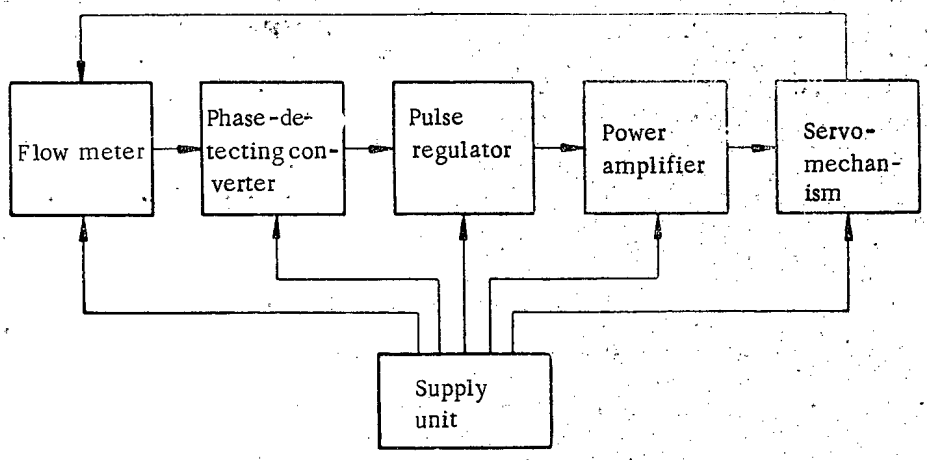

Fig. 3. Block diagram of the liquid-flow stabilizer.

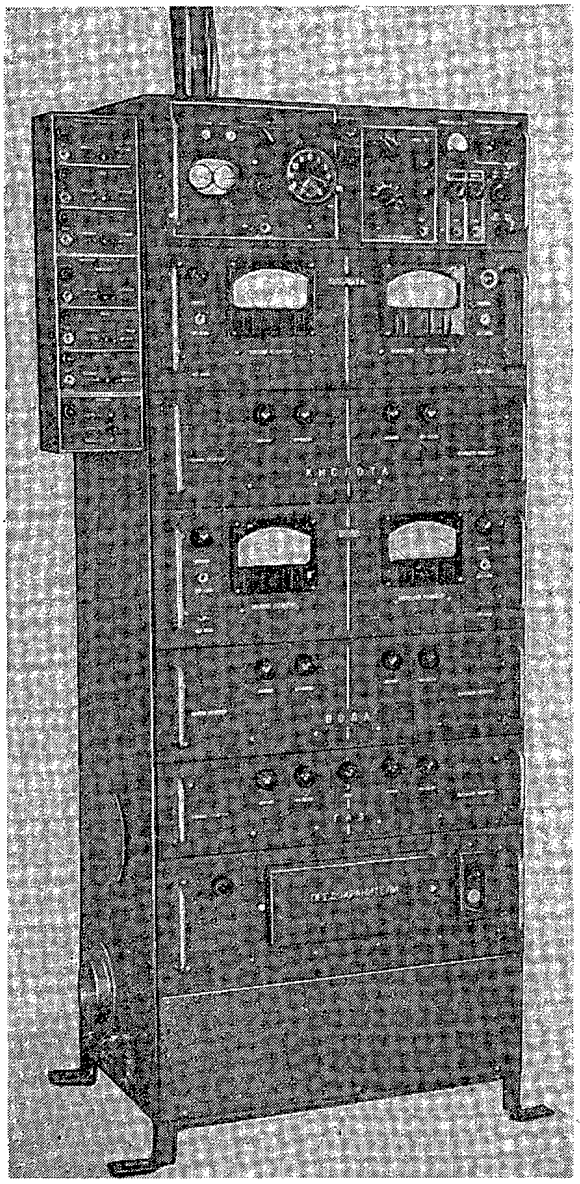

Fig. 4. General view of the automatic control device.

The pulse regulator consists of a contactless system, which is based entirely on semiconductor elements. The pulse regulator output signal is fed to the power amplifier and then to the servomechanism. The servomechanism consists of a needle valve, which is driven by a D-83 motor with a shorted rotor. The motor drives the valve through a mechanical reductor with a gear ratio of 100: 1. The direction of the motor's rotation is reversed by changing the phase of the voltage supplied to the control winding. The error in stabilizing the liquid flow does not exceed 2%.

The high temperature which arises in the reaction zone due to the fact that the process is exothermic (the temperature can attain 180-200°C in the reaction zone) is used for determining the position of the reaction zone. A four-arm ac bridge, which consists of two thermoresistors and two fixed resistors, serves as the data transmitter in establishing the reaction-zone position. The thermoresistors are placed in special quartz pins, which are inserted into the reaction vessel. (In order to provide better thermal contact with the reaction-vessel walls, the pins are filled with D-2 oil.)

The bridge is adjusted in such a manner that, for the normal position of the reaction zone, no current passes through the load diagonal. If the reaction zone is shifted from its normal position, the ac voltage supplied by the data transmitter is fed to the regulator, which is similar to the liquid-flow pulse regulator (with the exception of the phase-detecting converter, which is not required here). The regulator's reversive motor causes the valve to rotate, whereby the amount of gas that is supplied to the reaction vessel is varied.

The shifting of the reaction zone as a consequence of changes in the gas flow is characterized by great inertia, and it depends on the variation in the gas flow. Therefore, a correct choice of the pulse control time is of great importance. The reaction-zone position can be maintained with an accuracy to ± 10 mm. In the case of any malfunctioning in the device or in the regulating system, the control and signaling unit is connected.

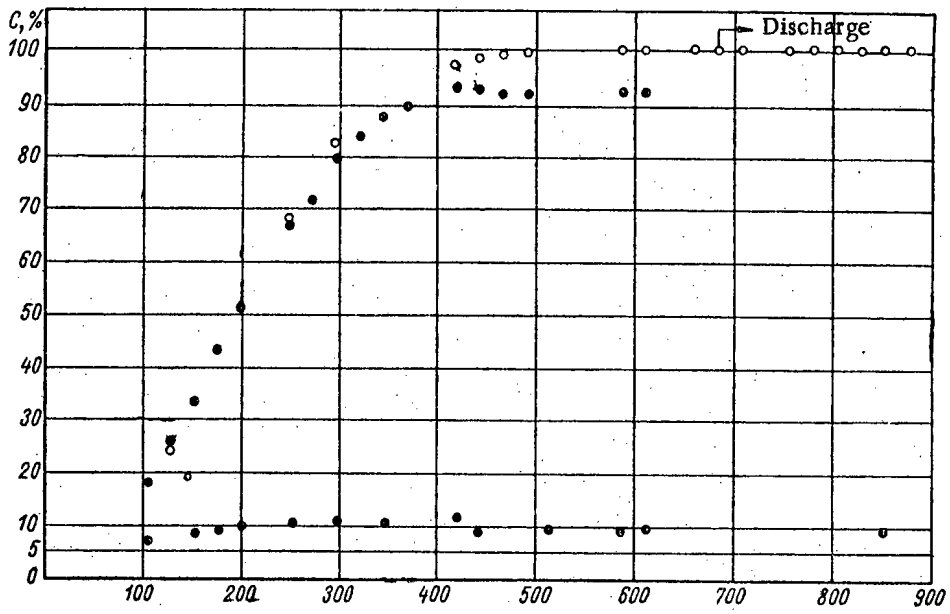

Fig. 5. Establishment of equilibrium in the first and the second column of the cascade. ●) Measurements with respect to N_2; ○) measurements with respect to NO.

Parameters of the First and the Second Column of the Cascade.

Parameters	First column	Second column
Diameter, mm	26	9
Length, cm	810	575
Packing: Levin spirals; dimensions, mm	2.5 × 1.8	1.5 × 1.5
Charge rate, $\frac{cm^3 \cdot 10M\ HNO_3}{min}$	17	0.8
Concentration of N^{15} in separating 0.55 nitrogen per day	9.2	99.8
Pressure drop, mm Hg	88	20

Remark. The separation factor of the cascade is 140,000.

The general view of the automatic control device is shown in Fig. 4.

Isotope Analysis of N^{15} Concentrates

We used N_2 and NO compounds in the isotope analysis of the enriched nitrogen samples. The measurements were performed by means of an MS-1 mass spectrometer, which was constructed in the laboratory [5]. The possible systematic measurement errors were eliminated by calibrating the mass spectrometer by using isotopic neon mixtures.

In the isotope analysis of N_2, an accurate determination of the isotope ratio N^{14}/N^{15} with respect to atomic ion peaks was difficult due to the presence of twice-ionized molecular ions. The presence of a considerable mass spectrometer background on the line with the mass number 28 can cause an error in determining the N^{15} content with respect to this line. Due to this, the measurements were performed with respect to lines 29 and 30 ($N^{15}\ N^{14}$ and $N^{15}N^{15}$). In using nitrogen as the product to be analyzed, we were able to secure an accuracy of ± 0.02% in measuring the percentage of nitrogen isotopes. In measuring nitrogen isotope concentrations in the NO compound, the N^{15}/N^{14} ratio was determined by using the formula

$$\frac{N^{15}}{N^{14}} = \frac{N^{15}O^{16} + N^{15}O^{18}}{N^{14}O^{16} + N^{14}O^{18}}.$$

The heights of the peaks corresponding to $N^{14}\ O^{17}$ and $N^{15}O^{17}$ ions were negligibly small.

The results obtained in measuring nitrogen isotope ratios in NO specimens that were 70%-enriched with N^{15} were in satisfactory agreement with the results of measurements performed on corresponding N_2 specimens. The accuracy in measuring the percentage of isotope components was 0.2%. For higher N^{15} concentrations, considerable discrepancies between the measurement results for N_2 and NO were observed. The differences between the actual N^{15} concentration values and those measured with respect to NO can probably be explained by the dissociation of NO molecules in the ion source and the superposition of $(N^{15}\ N^{15})^+$ ions, which appear as a result of the recombination of N^{15} fragments, on the line 30 $(N^{14}\ O^{16})^+$.

The basic cascade parameters are given in the table.

Figure 5 provides data on the establishment of equilibrium in the first and second column of the cascade.

The dependence of the N^{15} concentration in the lower portion of the second column on the amount separated out is given below:

Nitrogen discharge, g/day	N^{15} concentration
0,55	99,8
0,69	64
0,84	50

In the reaction vessels which we used, the HNO_3-loss with the H_2SO_4 discharged from the reaction vessels was equal to $\sim 2.7 \cdot 10^{-5}$ g per 1 ml H_2SO_4, which constituted 3-4% of the transfer in the cascade.

The authors hereby express their gratitude to V. A. Vlasenko, R. V. Tishchenko, R. M. Sakandelidze, D. K. Puradashvili, G. L. Partsakhashvili, L. V. Ermakova, A. M. Gasparov, M. S. Mikhelashvili, and L. I. Chernova for their help in the work and also to S. V. Bubnov and I. A. Kuras, who performed the constructional work.

LITERATURE CITED

1. W. Spindel, T. Taylor. J. Chem. Phys. 23, 981 (1955); 24, 626 (1956); Trans. N. Y. Acad. Sci. 19, 3 (1956); T. Taylor, W. Spindel. Proceedings of the International Symposium on Isotope Separation. Amsterdam, North-Holland Publishing Company, 1958, p. 158; L. Kauder, T. Taylor, W. Spindel. J. Chem. Phys. 31, 232 (1959).
2. G. Begun, J. Drury, E. Joseph. Industr. and Engng. Chem. 51, 1035 (1959).
3. W. Spindel, J. Chem. Phys. 22, 1271 (1954).
4. I. G. Gverdtsiteli et al., Soobshch. AN Gruz. SSSR, 24, 153 (1960).
5. K. G. Ordzhonikidze and V. Shyuttse, Zh. Éksperim. i Teor. Fiz., 29, 479 (1955).

All abbreviations of periodicals in the above bibliography are letter-by-letter transliterations of the abbreviations as given in the original Russian journal. ***Some or all of this periodical literature may well be available in English translation.*** **A complete list of the cover-to-cover English translations appears at the back of this issue.**

THE PROPAGATION IN AIR OF GAMMA RADIATION FROM A MOMENTARY POINT SOURCE

O. I. Leipunskii, A. S. Strelkov, A. S. Frolov, and N. N. Chentsov

Translated from Atomnaya Énergiya, Vol. 10, No. 5, pp. 493-500, May, 1961
Original article submitted July 7, 1960

In this article the Monte Carlo method is used to solve the problem of the propagation in an infinite air medium of gamma quanta with an initial energy of 1 Mev from a momentary isotropic point source. We obtain the radiation intensities as functions of time for gamma radiations arriving at the observation point from various solid angles, as well as the time-energy spectra of the intensity of the scattered gamma radiation at various distances from the source. By integration of the time distributions with respect to time we obtained the values of the buildup factors and the differential energy spectra of the scattered gamma radiation for a continuously acting source, as well as the angular distribution of the intensity and the angular energy spectra of the intensity of the scattered radiation for three distances of the observation point from the source.

For the Monte Carlo method of calculation of the problem of the propagation in an infinite air medium of a gamma radiation pulse of infinitely small duration (δ-pulse) from a point source, we took the initial energy of the gamma radiation equal to 1 Mev and the density of air as $1.29 \cdot 10^{-3}$ g/cm^3. The values of the total interaction factor of the gamma radiation with air and the cross-section pair-generation values of the Compton and photoelectric effects, both of which were necessary in the calculations, were taken from [1] and [2].

To solve the problem, we made an exact model of the motion of the gamma quantum emitted by the source. The direction of motion of the quantum after each collision was found by a random process by the Klein-Nishina indicatrix. A special procedure was developed for the rapid solution of the resulting transcendental equation. The absorption of the quanta by the medium was found not by a random process but by using the weighted multiplier of [3], so that a packet of quanta moved along each trajectory. The trajectory of the packet was tracked up to a weight equal to 10^{-4} times the initial weight. After each collision we calculated according to [4] the fraction of the quantum packet which, moving without collisions along the randomly determined direction, would reach a sphere of radius R. Such a record of gamma radiation was made simultaneously for various radii R_k. The proposed procedure made it possible to obtain from a comparatively small number of trajectories an acceptable description of the process of propagation of the gamma pulse up to distances equal to eight or ten times the mean free path of the initial radiation.

The draw of random parameters was carried out by a sequence of pseudorandom numbers of the type proposed in [5], generated by a program. In the version of the problem described here the number of tests was 1500. For an estimate of the precision we also determined the number of gamma quanta passing through each sphere of radius R_k, as well as the mean error of this quantity.

From the calculation we found the values Φ_{kjim}, which represented for a given distance R_k the values of the energy transmitted in the time $t_j - t_{j+1}$ through a unit area perpendicular to the flux by gamma quanta with energy $E_i - E_{i+1}$, forming an angle of $\theta_m - \theta_{m+1}$ between the direction of motion and the radius vector of the observation point. The time zero for each observation point was taken to be the time at which the direct radiation arrived at that point. On the basis of the Φ_{kjim} we found the corresponding values of the time-energy angular intensities of radiation $I^0_{kjim} = \frac{\Phi_{kjim}}{\Delta t_j \Delta E_i \Delta \Omega_m}$. In the calculation the values of R_k, t_j, E_i and θ_m were taken equal to the following: 1) R_k = 250, 500, and 1000 m, which correspond to values of $\mu_0 R_k$ equal to 2.03, 4.06, and 8.12 times the mean free path; 2) t_j = 0, 0.125, 0.250, 0.500, 1.00, 1.50, 2.00, 3.00, 4.00 and ∞ μsec; 3) E_i = 0, 0.0625, 0.125, 0.250, 0.500, 1.00 and 2.00 Mev; 4) θ_m = 0, 10, 40, 90, and 180°. The remaining values pertaining to the propagation of the gamma pulse were found

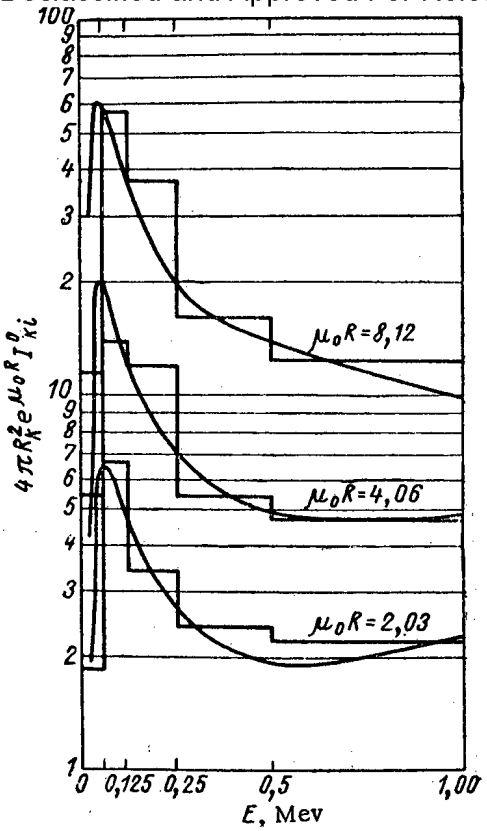

Fig. 1. Differential energy spectra of scattered gamma radiation with initial energy of 1 Mev for a steadily acting source of gamma quanta. The smooth curves show the data of [6].

R_k, m ($\mu_0 R_k$)	250 (2.03)	500 (4.06)	1000 (8.12)
Calculation by the Monte Carlo Method	3.69	7.57	21.8
Calculation by the method of [6]	3.6	7.5	18.6

by summing the values of Φ_{kjim} or I^0_{kjim} with respect to the variables which were of interest to us. The results of the calculation quoted below refer either to one gamma quantum emitted in a pulse (for functions of time) or to a source with power equal to 1 quantum per second (functions obtained for a constant source).

In order to check the correctness of the calculations by the integration of I^0_{kjim} we found the values of the buildup factors (Table 1) and the differential energy spectra of the intensity of scattered gamma radiation (Fig. 1), which were compared with the results of [6]. The comparison showed fairly good agreement of the results, which in turn corroborates the correctness of the calculation performed.

Let us consider the data obtained for a δ-source. Figs. 2, a, b, and c show the variation of the intensity of the scattered gamma radiation with time. The unit of intensity was taken to be the intensity after a time of 0-0.125 μ sec; the absolute value of the intensity in this interval of time in the calculation over the whole area of the sphere ($4\pi R^2 I^0_{k1}$) is equal to 1.43 Mev per μ sec for R = 250 m, 9.41 for R = 500 m, and 0.0088 for R = 1000 m. The intensity of the primary radiation is not shown in Fig. 2, since it would be a δ-function with infinite amplitude. A comparison of Figs. 2 a, b and c shows that as the observation point becomes more distant, the pulse is stretched (at least to the distance $\mu_0 R = 8.12$). The time required for the intensity to decrease to 0.1 times its initial value for distances of 250, 500, and 1000 m is equal respectively to 0.5, 1.0, and 1.5 μ sec. Such a stretching of the pulse can be explained if we consider that at great distances the dominant radiations of the spectrum begin to be the soft, multiply scattered gamma quanta which have traveled a longer way and arrived at the observation point with a greater delay (with respect to the time of arrival of the direct radiation). This is corroborated by the calculated time-energy spectra of the intensity of scattered gamma radiation (Figs. 3 a, b, and c). The quantity $4\pi R_k^2 e^{\mu_0 R_k} I^0_{kjt}$ is proportional to the intensity of the radiation with energy $E_j - E_{j+1}$ (calculated on the basis of a unit interval of energy) in the interval of time $t_j - t_{j+1}$. The values of the time intervals are shown in the upper part of the figure. It can be seen from Fig. 3 that for a given time interval the form of the spectra at distances greater than 250 m remains approximately constant. As was to be expected, as the time increases, the predominant radiation in the spectra begins to be the soft, multiply scattered radiation. Beginning with t = 1 μsec, practically no radiation of energy greater than 0.25 Mev remains in the spectra. The change in energy (averaged over the spectrum) of the scattered gamma radiation with time is shown in Figs. 4a, b, and c. The smooth curve in Fig. 4a shows the change in the energy of gamma radiation with an initial energy of 1 Mev, calculated from the mean Compton scattering angles and the mean lifetimes between successive scatterings:

$$E_{n+1} = E_n \overline{\cos\theta(E_n)}; \quad \tau_{n+1} = \frac{\lambda_n}{c} = \frac{1}{\sigma_k(E_n)\varrho_{air}\, c}.$$

Comparison shows that at all time the hardness of the radiation averaged over the spectrum is less than the mean radiation hardness computed from the values E_{n+1} and τ_{n+1}. In addition, it can be seen from Fig. 4 that beginning with t = 1-1.5 μsec the mean hardness of the radiation remains practically unchanged, with a value equal to 50-60 kev.

The variation of the intensity of the scattered gamma radiation with time for different solid angles is shown in Fig. 5a, b, and c. The ordinate axis of this figure shows the ratio of the intensity in a given solid angle (defined by

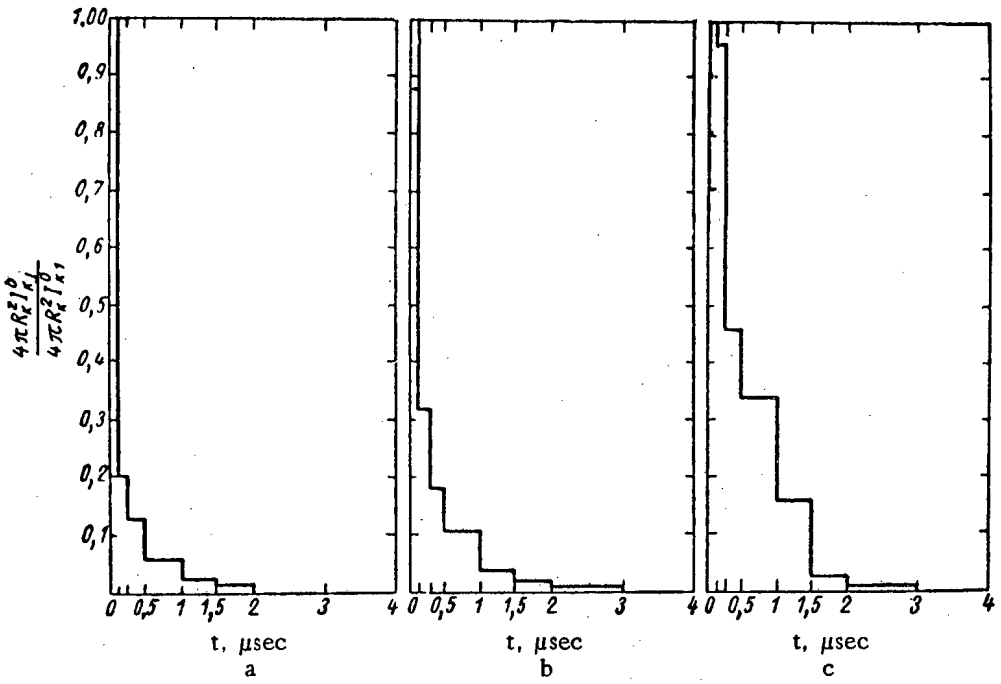

Fig. 2. Intensities of scattered gamma radiation as functions of time for three distances (in meters) of the observation point from the source: a) 250; b) 500; c) 1000.

the values $\theta_m < \theta < \theta_{m+1}$) for a given interval of time calculated on the basis of a unit solid angle to the maximum intensity observed in the given solid angle. The figure shows the values of maximum intensity for each of the angular intervals. Comparing the time dependence of the intensity in a definite interval of angles θ (or, which is the same thing, in a given solid angle at various distances from the source), we arrive at the conclusion that the decrease of intensity in solid angles defined by $\theta < 90°$ is delayed with increased distance. The time dependence of radiation intensity from the rear half-space shows a maximum which moves in the direction of longer times as the distance from the observation point increases.

With respect to the time-energy angular spectra of the intensity of scattered radiation the following remarks may be made: As the distance increases, the corresponding intensities decrease in absolute value. For given intervals of time and solid angle the spectra are approximately similar for different R_k. With increasing time and θ, for a given R_k the spectra become softer.

Let us now consider the data on the field of a steadily acting source which we may obtain from the solution of the δ-source problem. Two characteristics of the steady-source field, the buildup factors and the differential energy spectra of the intensity of the scattered gamma radiation, have already been considered above. Two other important characteristics, about which there is comparatively little information at the present time, are the angular distribution of intensity and the angular differential spectra of intensity of the scattered radiation.

Data on the angular distribution of gamma radiation intensity for various distances from the source are shown in Table 2 and Table 3.

TABLE 2. Angular distribution of intensity of scattered gamma radiation.

Angle θ, deg	Distance from source, meters		
	250 ($\mu_0 R$=2,03)	500 ($\mu_0 R$=4,06)	1000 ($\mu_0 R$=8,12)
0—10	16,9	13,5	10,4
10—40	37,1	37,7	32,9
40—90	27,8	32,3	28,9
90—180	17,6	16,5	27,7

TABLE 3. Angular distribution of the total intensity of gamma radiation.

Angle θ, deg	Distance from source, meters		
	250 ($\mu_0 R$=2,03)	500 ($\mu_0 R$=4,06)	1000 ($\mu_0 R$=8,12)
0—10	39,3	24,9	14,5
10—40	27,1	32,7	31,4
40—90	20,7	28,0	27,6
90—180	12,8	14,3	26,5

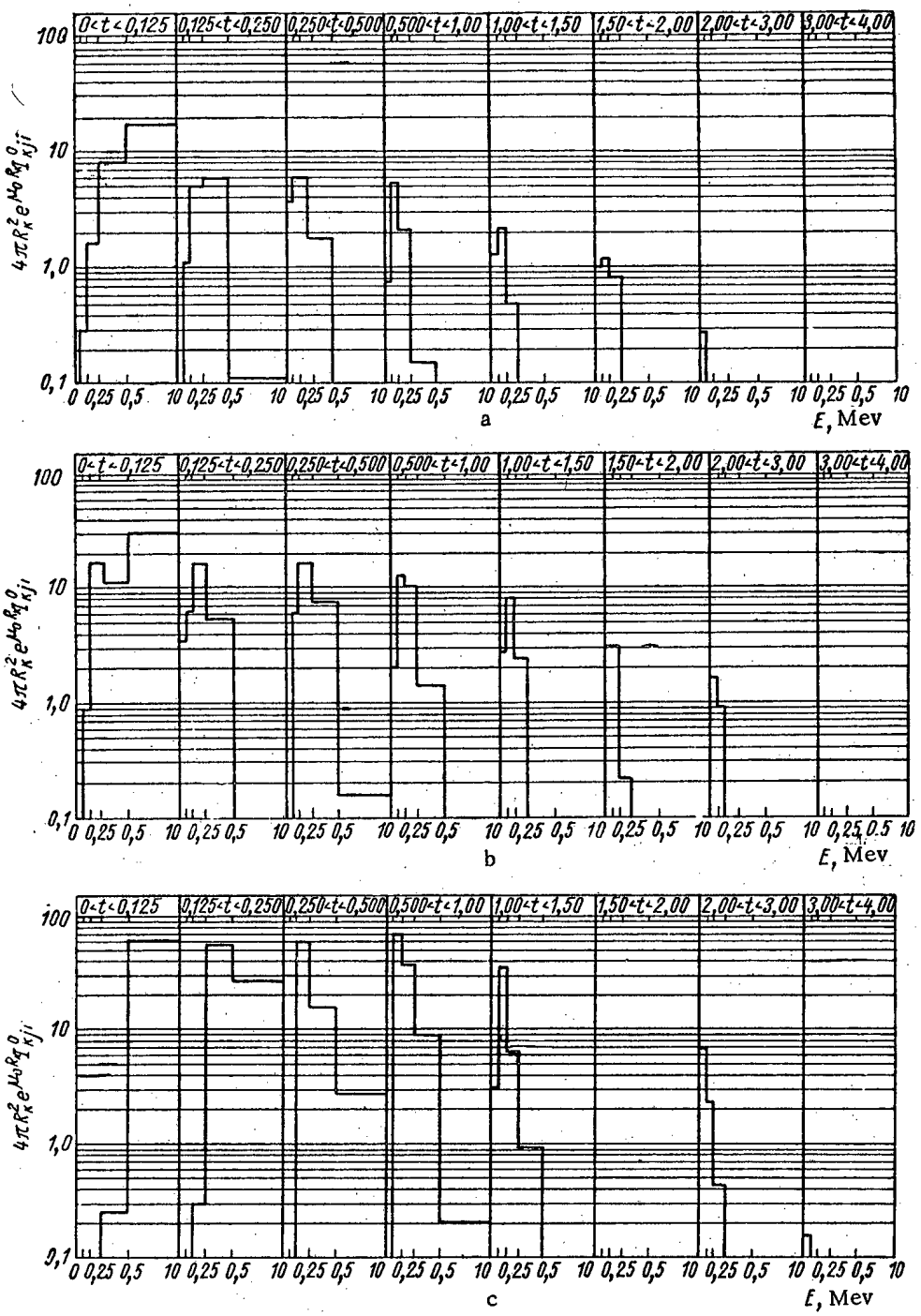

Fig. 3. Time-energy spectra of the intensity of scattered gamma radiation for three distances (in meters) of the observation point from the source: a) 250; b) 500; c) 1000.

Table 2 shows the fraction (in percent) of the intensity of the scattered gamma radiation arriving from a given solid angle as compared to the total intensity of scattered radiation at the observation point $\left(\frac{I^0_{sc}(\Omega)}{I^0_{sc}} 100\%\right)$; Table 3 shows the same data for the total intensity of radiation (including the direct). The solid angles $\Omega = 2\pi(\cos\theta_m - \cos\theta_{m+1})$ under consideration are defined by the values of θ shown in the first columns of the tables. The angular distribution of the intensity of scattered radiation obtained by the calculation may be compared with the data found

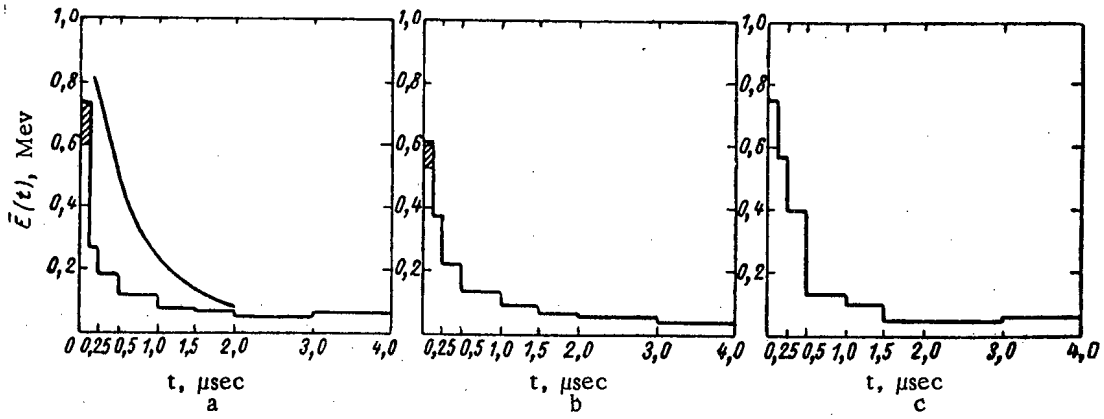

Fig. 4. Mean energy of scattered gamma radiation as a function of time for three distances (in meters) of the observation point from the source: a) 250; b) 500; c) 1000. The shaded parts of the histogram show the increase in hardness when the direct radiation is considered.

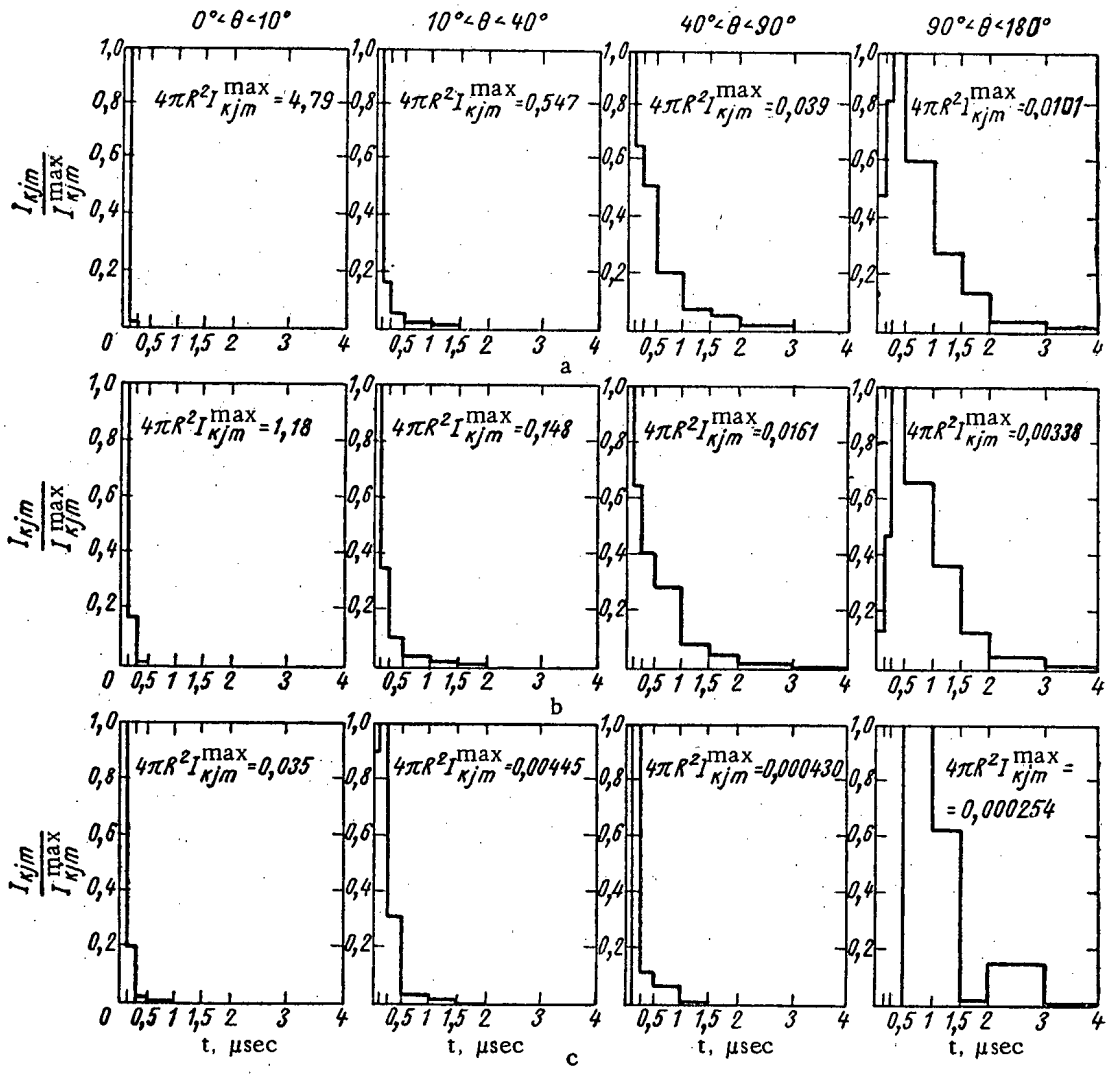

Fig. 5. Intensity of scattered gamma radiation as a function of time for various solid angles and three distances (in meters) of the observation point from the source: a) 250; b) 500; c) 1000.

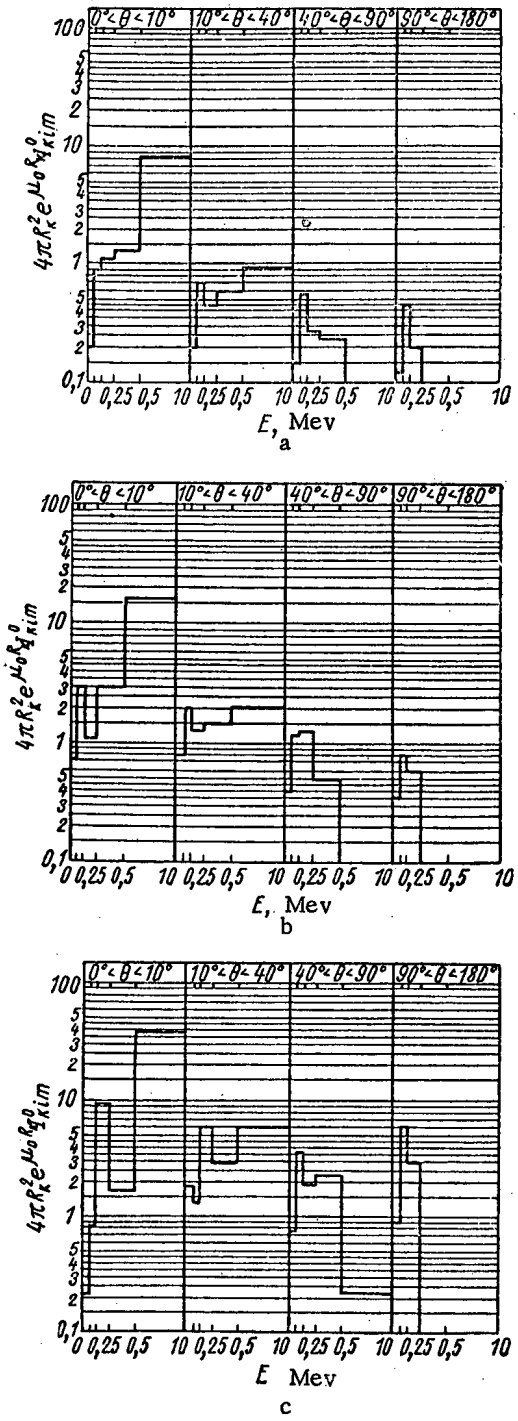

Fig. 6. Angular differential spectra of intensity of scattered gamma radiation with an energy of 1 Mev from a steadily acting source of gamma quanta for three distances (in meters) of the observation point: a) 250 ($\mu_0 R = 2.03$); b) 500 ($\mu_0 R = 4.06$); c) 1000 ($\mu_0 R = 8.12$).

in the literature. Starting with the angular distribution of the scattered radiation dose of a Co^{60} source measured in water [7], we can calculate the percentage of the scattered radiation dose coming from solid angles considered in the present article by comparison with the total scattered radiation dose. For $\mu_0 R = 2$ such a calculation gives the following values: for θ changing from 0 to 10° the fraction is 29%; for 10-40° it is 38%; for 40-90° it is 25%; and for 90-180° it is 8.7%.

If we take into consideration a certain difference in the initial energy of the gamma radiation, the perturbing action of the shielding cones, and also the behavior of the electron transformation factor as a function of radiation energy, we may consider the agreement of our results with the results of [7] entirely satisfactory*.

The angular differential spectra of the intensity of scattered gamma radiation of a steadily acting source are shown in Fig. 6. Comparing the spectra at various distances from the source, it can be observed that in the interval of distances $\mu_0 R = 2.03$ to 8.12 the spectra change very little, which indicates the establishment of equilibrium.

For an estimate of the precision of the results obtained from the calculation, we calculated in addition the value of the total intensity of radiation passing through a sphere of radius R_k as well as the mean error in this quantity. Starting from this, the precision of the calculation of the values of the buildup factors can be estimated at 2-5% for distances of 250 and 500 m, and at 15% for a distance of 1000 m. The estimate of precision of the time, angular and other intensity distributions was made by a comparison of the values obtained for 500, 1000, and 1500 tests. Starting with such a comparison, we can arrive at the conclusion that the precision of the calculation of the time dependence of the intensity is about 15-20% up to $t = 1\mu$ sec and about 40-50% after $t = 1\mu$ sec.

The precision of the calculation of the time-energy spectra at distances of 250 and 500 m from the source up to time $t = 1$-1.5 μ sec is about 20-30%; after $t = 1.5\mu$ sec the spectra should be considered approximate since the error in the calculation may be 50% and more. The same can be said with respect to the time dependence of the intensity for various solid angles.

*After this article had been sent to the editors, [8] was published, which studies the angular distribution of the intensity of scattered radiation from a Co^{60} source placed in a semi-infinite aqueous medium. A comparison of the results of the present article which pertain to the forward half-space and the results of [8] shows good agreement of the values of angular distribution of the intensity of scattered radiation. The maximum discrepancy in the ratio of the radiation moving in a given solid angle to scattered radiation coming from the entire forward half-space is about 25% (for $\mu_0 R = 4.06$ and the interval of angles θ equal to 40-90°), which can be explained by the difference in the geometry of the experiment of [8] (semi-infinite space) and the calculation (infinite space). (Remark at proof.)

The precision of angular distributions of intensity and angular energy spectra obtained for a steady source is about 30%.

In conclusion the authors express their deep gratitude to I. M. Gel'fand for his attention to the work and his collaboration in its execution.

LITERATURE CITED

1. "Shielding of Nuclear Reactors," edited by T. Rockwell [Russian translation] (Moscow, Foreign Literature Press, 1958), chap. 10.
2. K. Zigban. Beta and gamma spectroscopy [Russian translation] (Moscow, Foreign Literature Press, 1959) (Supplement I).
3. I. M. Gel'fand and others, Proceedings of the Second International Conference on the Peaceful Uses of Atomic Energy [in Russian] (Geneva, 1958). Report of Soviet Scientists, Vol. 2 (Moscow, Atomizdat, 1959), p. 628.
4. M. Berger, J. Res. Nat. Bur. Standards 55, No. 6, 343 (1955).
5. M. M. Korobov, Doklady Akad. Nauk SSSR, 115, No. 6, 1062 (1957).
6. H. Goldstein, J. Wilkins, Rept. U. S. Atomic Energy Comm., No. 40, 3075 (1955).
7. V. I. Kukhtevich, S. G. Tsypin, B. P. Shemetenko, Atomnaya Énergiya 5, No. 6, 638 (1958).
8. Yu. A. Kazanskii, Atomnaya Énergiya 8, No. 5, 432 (1960).

All abbreviations of periodicals in the above bibliography are letter-by-letter transliterations of the abbreviations as given in the original Russian journal. ***Some or all of this periodical literature may well be available in English translation.*** **A complete list of the cover-to-cover English translations appears at the back of this issue.**

LETTERS TO THE EDITOR

EMISSION OF THE BEAM AND CONTROLLING THE ENERGY IN A CYCLOTRON WITH AZIMUTHAL VARIATION OF THE MAGNETIC FIELD

A. A. Arzumanov, R. A. Meshcherov, E. S. Mironov, L. M. Nemenov, S. N. Rybin and Ya. A. Kholmovskii

Translated from Atomnaya Énergiya, Vol. 10, No. 5, pp. 501-502, May, 1961
Original article submitted March 15, 1961

The study was made on the 1½-meter cyclotron of the I. V. Kurchatov Institute of Atomic Energy, Academy of Sciences, USSR. The azimuthal variation of the magnetic field intensity with a depth of about ± 15% was provided

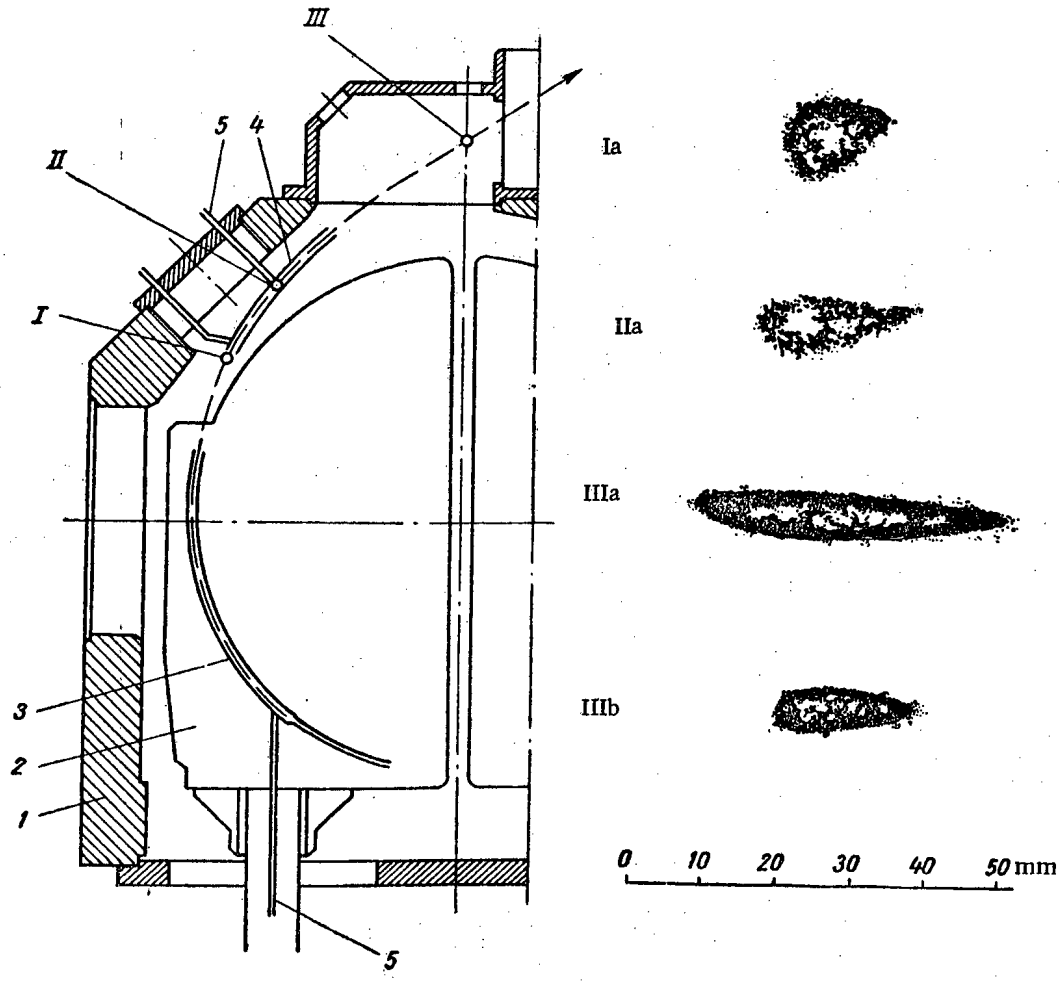

System of emission and traces of beam: 1) accelerating chamber; 2) duant; 3) internal part of the deflector; 4) external part of deflector; 5) high tension leads; I, II, III) points where Plexiglas discs are mounted; Ia, IIa, IIIa) traces of the beam with the action of only the internal part of the system; IIIb) a trace with the mutual action of the internal and external parts of the system. The linear scale refers to the photograph of the beam traces.

by three sectors with an angular spread of ~ 60° [1-3]. On the inside surface of each lid of the accelerating chamber there were circular windings, cooled by water. The windings had individual electric feed from motor-generators. This system of windings can correct the mean value of the magnetic field intensity along the radius, providing acceleration and emission of ions over a wide range of values of magnetic field intensity. For correction of the "mean plane" of the magnetic field and for controlling the first harmonics of the azimuthal heterogeneity, current windings were also used.

Experiments on the acceleration and emission of the beam were carried out for five values of the magnetic field intensity: 5; 10; 13.6; 14.7 and 17 koe. Protons were accelerated to an energy of ~ 5 Mev and ions of molecular hydrogen were accelerated to energies of ~ 10; 21; 24 and 31.5 Mev. The frequency of the circuit was measured by moving the short-circuiting elements of the resonance lines. A "slit" type source of ions was used [4]. The beam of ions was emitted from the accelerating chamber by a deflector with a heterogeneous electric field [5]. The coefficient of emission in various systems of acceleration varied from 25 to 60%, the current of ions in the emitted beam being 50-400 μa. The experiments were carried out under impulse conditions with a duty ratio of about 10-100.

The deflector consists of two parts. The first part is placed within the duant; the second part is placed outside the duant. The first part of the deflector consists of a section with flat electrodes with a 25° angular spread and a section with electrodes having a hyperbolic cross section with an angular spread of 65°. The second part has electrodes with hyperbolic cross sections with an angular spread of 35°. The electric feed of the deflector is provided by two high-voltage rectifiers.

The emission of the beam was studied both with the mutual action of the internal and external parts of the sytem and with the external part removed. The coefficient of emission in both cases remained practically constant. The figure gives photographs of the beam traces on the Plexiglas discs placed at different points along the path of the beam. The deflector as a whole was studied at magnetic field intensities of 5 and 10 koe. With a magnetic field intensity of 10 koe the voltage at the input of the internal part was 23 kv, and the input of the external part was 30 kv. The use of such a system makes it possible to lead beams of ions from the accelerating chamber with a small divergence, which makes it possible to use magnetic quadrupole lenses with a small aperture without loss in the ion-beam intensity. Furthermore, the small dimensions of the beam at the exit from the field of scatter of the main magnet made it possible to arrange the input slit of the magnetic analyzer at this point.

In conclusion the authors would like to thank L. F. Kondrashev and S. I. Prokof'ev for their valuable help in preparing the experiments.

LITERATURE CITED

1. J. A. Zavenyagin, R. A. Metshcherov, E. S. Mironov, L. M. Nemenov, J. A. Kholmovskij. Proceedings of the Intern. Conf. on High-Energy Accelerators and Instrumentation. CERN, 1959, p. 225.
2. R. A. Meshcherov, E. S. Mironov, L. M. Nemenov, S. N. Rybin and Yu. A. Kholmovskii. Atomnaya Énergiya, 8, No. 3, 201 (1960).
3. R. A. Meshcherov and E. S. Mironov, Atomnaya Énergiya, 10, No. 2, 127 (1961).
4. I. I. Afanas'ev, L. F. Kondrashev, L. N. Mikhailov and A. I. Nastyukha. Pribory i tekhnika eksperimenta, No. 6, 25 (1959).
5. A. A. Arzumanov and E. S. Mironov, Atomnaya Énergiya, 6, No. 2, 202 (1959).

All abbreviations of periodicals in the above bibliography are letter-by-letter transliterations of the abbreviations as given in the original Russian journal. *Some or all of this periodical literature may well be available in English translation.* A complete list of the cover-to-cover English translations appears at the back of this issue.

CsI (Tl) SCINTILLATORS FOR RECORDING α-PARTICLES

L. M. Belyaev, A. B. Gil'varg and V. P. Panova

Translated from Atomnaya Énergiya, Vol. 10, No. 5,
pp. 502-503, May, 1961
Original article submitted October 17, 1960

For detecting α-particles, scintillators of CsI monocrystals activated with thallium are used. The paper [1] describes a CsI(Tl) detector for recording α-particles which has low sensitivity to the γ-background. The separate recording of α-particles and the γ-background is based on the different duration of scintillations in the CsI(Tl) crystal caused by α-particles (0.42 μ sec) and electrons (0.7μ sec). In [2] a scintillation spectrometer was used with a CsI(Tl) crystal of diameter 11.5 mm and thickness 1 mm; the rseolving power for α-particles of Po^{210} was 7%. In [3] when using a crystal of CsI(Tl) measuring 5 × 5 × 0.3 mm with α-particles of Po^{210} a 3.5% resolution was obtained. In [4] for α-particles with an energy of 8 Mev when using CsI(Tl) crystals of 25 mm diameter and thickness 2 mm resolution of about 4-5% was obtained and of 2.6% only for one crystal.

We studied the possibility of developing from CsI(Tl) crystals scintillators of larger dimensions (diameter 30-55 mm) with good resolving capacity for detecting, spectrometry, and other work with α-radiation.

To prepare thin scintillators we used crystals of CsI(Tl) grown in the Institute of Crystallography, Academy of Sciences, USSR and also crystals produced industrially in this country.

Thin monocrystalline discs of CsI(Tl) with carefully polished end surfaces were mounted with Canada balsam on a glass backing of thickness 1.5-2 mm.

The polishing was done with cerium oxide crocus on a rotating ebonite disc tightly stretched with natural silk and slightly moistened with ethylene glycol [5].

The characteristics of the CsI(Tl) scintillators were measured on a single-channel scintillation spectrometer with specially chosen FÉU-24 and FÉU-29 photomultipliers. In the investigation the moments were found which have an important effect on the spectrometric parameters. For CsI(Tl) scintillators of thickness 0.4 and 0.2 mm and diameter 30, 40, 50, 55 mm during excitation of their whole surface with α-particles of Pu^{239} (Pu^{239} was applied on a brass backing of 70 mm diameter, the α-particles have a 5% energy scatter) we obtained a spectral resolution of 14-22% on the FÉU-24 and 11-18% on the FÉU-29. This poor resolution may be due to both the quality of the scintillator (light yield and homogeneity) and the heterogeneity of the photocathode of the photomultiplier.

By moving an Am^{241} source of α-particles of diameter 3 mm over the scintillator fastened on the photomultiplier, we found the degree of heterogeneity of the scintillator-photomultiplier system. The measurements showed that when the source is moved from the center to the periphery the peak from the α-particles of Am^{241} is displaced in value by 30% toward smaller amplitudes and the resolution deteriorates correspondingly (see the figure).

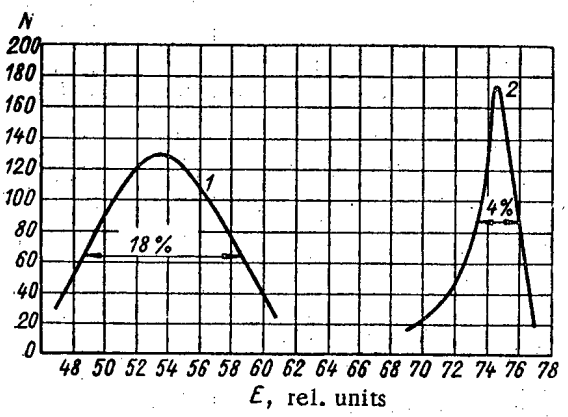

Spectral resolution of α-particles of Am^{241}: 1) at a distance of 20 mm from the center of the scintillator-photomultiplier; 2) at the center of this system.

All the alkali halide crystals, including CsI(Tl), have a certain heterogeneity of the scintillation properties due to the uneven distribution of activator in them [6]. The value of the light flash of the scintillator will depend on the point at which α-particles are incident on it. When measuring the degree of heterogeneity of thin scintillators it was found that the maximum scatter of the light yield values of separate sections of the surface does not exceed 4% for any of the scintillators which we prepared. The spectral resolution varies by 0.4-0.5%.

We evaluated the relative difference in the sensitivity of separate sections of the FÉU-29 photocathode. At a distance of 15 mm from the center of the photocathode the amplitude of the peak from the Am^{241} α-particles decreases by 25-30%. When using a thin scintillator the region of the photocathode adjoining the place of formation of the light flash works preferentially. It therefore follows from the data given above that the

main reason for the error in the spectrometric measurement of α-particles is the heterogeneity of the photomultiplier photocathode. The use of a light pipe should reduce the error arising due to the uneven sensitivity of the photocathode.

Later, all comparative measurements of thin scintillators were carried out during the excitation of their central part over the center of the photomultiplier photocathode by a source of Am^{241} α-particles of diameter 3 mm. We prepared and studied fourteen thin CsI(Tl) scintillators of diameter 30-55 mm. The following results were obtained:

Diameter of scintillator, mm	Spectral resolution for Am^{241} α-particles, %
30	3.5-4.0
40	4.0-4.5
50	5.5-6.3
55	5.2-6.3

It was found that the spectrometric parameters of scintillators depend on the thickness of the scintillators and the quality of the treatment of their surfaces. When the thickness of the disc (with diameter 30 mm) is changed from 2 to 0.2 mm the resolution improves from 4.2 to 3.5%. A scintillator whose surface was only ground had a spectral resolution of 4.5%; after careful polishing its light yield increased by 5% and the resolution was 4.1%.

LITERATURE CITED

1. I. Robertson, A. Ward. Proc. Phys. Soc. 73, No. 3, 523 (1959).
2. M. Halbert. Phys. Rev. 107, No. 3, 647 (1957).
3. H. Knoepfel, E. Loepfe, P. Stoll. Helv. phys. acta 30, 521 (1957).
4. J. Fleury et al. J. Phys. et la Radium 21, No. 5, 480 (1960).
5. O. Swelman. Rev. Scient. Instrum. 29, No. 9, 749 (1958).
6. L. M. Belyaev, V. A. Perl'shtein and V. P. Panova, Kristallografiya 2, No. 3, 437 (1957).

SCINTILLATION GLASSES WITH INCREASED LIGHT YIELD FOR DETECTING NEUTRONS

V. K. Voitovetskii and N. S. Tolmacheva

Translated from Atomnaya Énergiya, Vol. 10, No. 5,
p. 504, May, 1961
Original article submitted August 1, 1960

The luminescence yield of glasses actived with cerium increases with the content of Ce(III) [1]. However, when glasses are boiled in a neutral medium the introduction of a large amount of cerium does not lead to positive results, since the equilibrium between the Ce(IV) and Ce(III) moves sharply toward Ce(IV). The greatest scintillation efficiency is shown by lithium silicate glasses containing 0.01-0.015 of cerium [2, 3]. Glasses containing 0.05 of cerium, boiled in a neutral medium, were colored, which pointed to the presence of Ce(IV) in them.

Boiling in a reducing medium helped to keep a larger part of the activator in the trivalent state, which made it possible to increase the Ce concentration to 0.1 without coloring the glass. These glasses were prepared from specially pure materials; the Fe_2O_3 content did not exceed 10^{-3}%. Rigid reducing conditions were achieved by adding graphite powder to the charge and observing a special system of boiling.

Alundrum crucibles with the charge were placed in a Silit furnace at a temperature of 1250-1270°C; over the course of 1 hr the temperature was raised to 1370-1400°C, and the boiling was continued until the vitreous mass

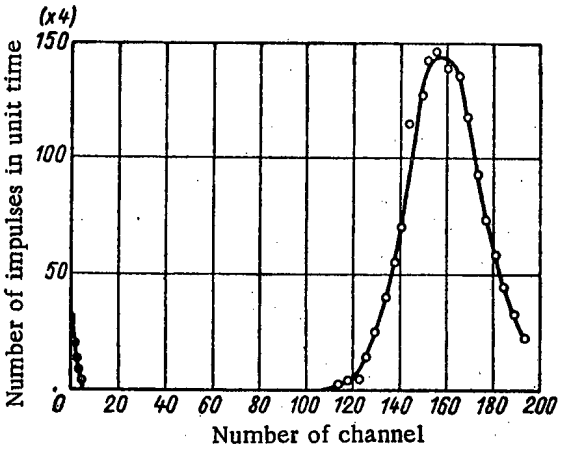

The differential amplitude spectrum of voltage impulses at the output of a scintillation counter with glass of the composition $Li_2O \cdot 3SiO_2 \cdot 0.08Al_2O_3 \cdot 0.1CeO_2$: ○ – thermal neutrons; ● – noise of photoelectron amplifier (FEU-S).

became light. (For some compositions of glasses the process of lightening was speeded up when the temperature was briefly increased to 1460°C.) The glasses were stamped in a cold mold in the form of 3.5-4 cm diameter discs. The glasses were annealed in a muffle furnace at 500°C.

The scintillation efficiency of thin glasses of composition $Li_2 \cdot 3SiO_2 \cdot 0.08\ Al_2O_3$ is practically constant within the limits of change in the cerium concentration from 0.05 to 0.1 and with excitation by electrons it is 8-9% of the scintillation efficiency of NaI(Tl) crystals. For glasses of thickness ~ 1cm the optimum concentration of cerium is 0.05-0.06. The ratio of the light yields of glass of this composition for electrons and products of the reaction of neutrons with Li^6 is 3.4-3.7*.

The figure shows the amplitude spectrum of voltage impulses at the output of a scintillation counter with glass of composition $Li_2O \cdot 3SiO_2 \cdot 0.08\ Al_2O_3 \cdot 0.1\ CeO_2$, obtained during the excitation of scintillations by products from the reaction of thermal neutrons with Li^6. The half-width of the peak is 22.5%.

Further increase in the scintillation efficiency is possible on transferring to more complex glass compositions. The scintillation efficency of thin glass of composition $Li_2O \cdot 0.5\ CaO \cdot 4SiO_2 \cdot 0.13\ Al_2O_3 \cdot 0.1CeO_2$ is 11% with respect to the scintillation efficiency of a crystal of NaI(Tl) and within certain limits it is independent of the content of Al_2O_3 (0.08-0.20) and cerium (0.06-0.10). With increase in the thickness of glass the optimum region of cerium concentration narrows and approaches a value of 0.06.

LITERATURE CITED

1. O. G. Karapetyan, Izv. AN SSR, XXIII, 1382 (1960).
2. V. K. Voitovetskii, N. S. Tolmacheva and M. I. Arsaev. Atomnaya énergiya, 6, No. 3, 321 (1959).
3. V. K. Voitovetskii and N. S. Tolmacheva, Atomnaya énergiya, 6 No. 4, 472 (1959).
4. L. Bollinger, G. Thomas, R. Ginther. Rev. Scient. Instrum. 30, 1135 (1959).

*In [4] there are descriptions of scintillation glasses for detecting neutrons containing boron. The scintillation efficiency of these glasses during excitation by electrons reaches 5-7%. However, when detecting neutrons the scintillation efficiency is determined not only by this value but also by the ratio of the light yields for electrons and products of the reaction of neutrons with nuclei of the absorbing material and also by the energy of the reaction. The scintillation efficiency of boron-containing glass for neutrons is 7-12 times less than that of lithium glasses. The ratio of light yields for electrons and reaction products for lithium glasses is 3.4-3.7; for boron-containing glasses it is 9-13; the energy of reaction in the first case is 4.79 Mev; in the second case it is 2.3 Mev. Therefore, in the distribution of voltage impulses at the output of the scintillation counter when detecting thermal neutrons, given in [4], the left slope of the peak falls even into the region of noise. For this reason a scintillation counter with boron-containing glass with the same intensity of the γ-background will record in the region of the peak many more impulses from γ-radiation than a counter with lithium glass.

A METHOD OF DETECTING α-PARTICLES AND FISSION FRAGMENTS BY A SCINTILLATION COUNTER ON A BACKGROUND OF INTENSIVE β - OR γ -RADIATION*

V. K. Voitovestskii and I. L. Korsunskii

Translated from Atomnaya Énergiya, Vol. 10, No. 5,
pp. 505-506, May, 1961
Original article submitted August 1, 1960

In some experimental and technical problems the necessity arises of recording fission fragments or α-particles with a scintillation counter in the presence of very intense β - or γ -radiation. In this case even when using the most suitable scintillator of ZnS (Ag, Ni) of optimum thickness, making it possible to obtain a maximum value for the ratio of amplitudes of impulses from the α-particles and electrons, repeated applications of impulses from the electrons give false readings.

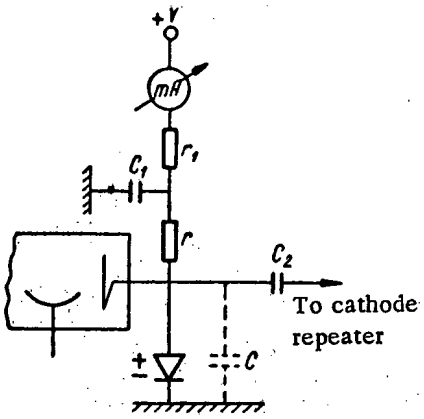

Fig. 1. Circuit for connecting diode at the output of the photomultiplier.

The permissible limits of the background of γ -radiation and electrons can be considerably increased if the constant resistance R at the output of the photomultiplier is replaced by a nonlinear element (in an α-particle counter $RC > \tau$, where C is the output capacity of the photomultiplier relative to the ground, τ is the time constant of deexcitation of the scintillator). A crystal diode can be used as the nonlinear element. Figure 1 shows a circuit for connecting the diode at the photomultiplier output (the negative impulse is taken from the photomultiplier; if the positive impulse is taken, then the diode is placed in the circuit of the dynode)**. By selecting a working point on the characteristics of the diode it is possible to arrange conditions under which the voltage impulses from the intensive scintillations hardly change compared with the impulses with a constant resistant R. The amplitude of these impulses, like the amplitude of impulses with a resistance R, will be determined by the total number of photoelectrons corresponding to the scintillation ($R_1C \simeq RC > \tau$, where R_1 is the effective resistance for a large current impulse). The number of repeated applications of the voltage impulses from the scintillations of weak intensity will then be sharply reduced, since the form of these impulses repeats the form of current impulses and their amplitude and duration are sharply reduced compared with the amplitude and duration of impulses at a constant resistance R ($R_2C \ll \tau$, where R_2 is the resistance of the diode at the working point).

For a scintillation detector of α-particles with a germanium diode at the photomultiplier output [scintillator ZnS (Ag, Ni)] in a parametric dependence on the current i passing through the diode, a family of characteristics was plotted: $\frac{a_1}{a_0} = f(a_0)$, where a_0 is the amplitude of the voltage impulse of the voltage impulse caused by an α-particle with constant resistance R at the output of the photomultiplier and a_1 is the amplitude of a voltage impulse with a diode at the photomultiplier output from the current impulse of the same value. These characteristics make it possible to correctly select the working conditions of the circuit. They were obtained with an amplitude discriminator having a discrimination range of 0.01-20 v [2]. The value of a_0 was varied by changing the voltage on the photomultiplier. Due to the scatter of the voltage impulses with respect to amplitude the value of a_0 was determined as the level of discrimination corresponding to a certain constant count rate of impulses. In a semilogarithmic scale Fig. 2 shows the characteristics $\frac{a_1}{a_0} = f(a_0)$ for the FEU-19 photomultiplier with the DGTs-2 diode.

* The work was done in 1952.

** In the Scherr telephone recorder for α-particles [1] the crystal diode is connected in parallel with the primary winding of the transformer, serving as the load of the photomultiplier; the telephone is connected in the secondary circuit of the transformer. In this circuit the diode makes it possible to improve the contrast between the clicks in the telephone from the α-particles and the constant noise from the dark current of the photomultiplier.

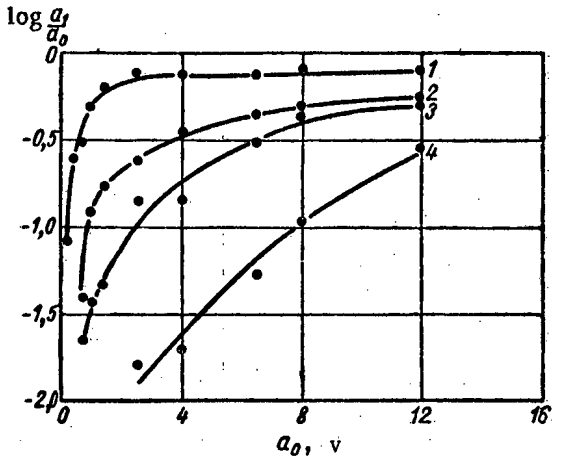

Fig. 2. Characteristics $\frac{a_1}{a_0} = f(a_0)$ for an FÉU-19 photomultiplier with a DGTs-2 diode. The value of the current passing through the diode is (ma) 1)0.01; 2)0.05; 3)0.1; 4)0.3.

When recording α-particles with a scintillation counter with this output circuit when the oscillator is acted on by 10^{10} β-particles in 1 sec (electrons of In^{116m} with $E_{max} \simeq 1$ Mev) there are no false readings from the applications of impulses. For photomultipliers which permit large currents at the output (FUÉ-11, etc.) the limiting value of the electron background can be increased still more. The limiting value of the background can also be increased if photomultipliers are used with a low output capacity and good time characteristics, which makes it possible to obtain the required reduction in probability of repeated applications with a smaller mean output current.

Under conditions of varying background intensity, to prevent the working point of the diode from being displaced, the selected value of the current passing through the diode is kept constant by means of a simple stabilization circuit.

LITERATURE CITED

1. R. Scherr. Rev. Scient. Instrum., 18, 10 (1947).
2. A. Van Rennes. Nucleonics 10, No. 7, 20 (1952).

PREPARING AND USING RESONANCE POLARIZED NEUTRONS

A. D. Gul'ko and Yu. V. Taran

Translated rom Atomnaya Énergiya, Vol. 10, No. 5,
pp. 506-508, May, 1961
Original article submitted December 31, 1960

When polarized slow neutrons react with polarized nuclei, the reaction cross section differs from the cross section observed when the spins are randomly orientated. The absorption of polarized neutrons by polarized nuclei makes it possible to determine the spin J of the compound nucleus. When the absorption is caused by a single level (for example in resonance), the value of J for this level can be determined from the sign of the change in the transmission of neutrons by the target with change in the relative orientation of the spins of neutrons and nuclei.

The relative cross section of polarized nuclei for polarized neutrons is given by the formula

$$\sigma = \sigma_0 (1 + f_I f_n f_N), \quad (1)$$

where σ_0 is the cross section in the absence of polarization; f_n is the neutron polarization; f_N is the nuclear polarization; $f_I = I(I+1)$ for $J = I + \frac{1}{2}$; $f_I = -1$ for $J = I - \frac{1}{2}$ and I is the spin of the polarized nucleus. The relative change in transmission of neutrons by the target with treatment of the relative orientation of the spins is approximately described (if f_N is fairly small) by the expression

$$\Delta t/\bar{t} \simeq 2\Phi f_I f_n f_N N \sigma_0, \quad (2)$$

where N is the thickness of the target (nuclei/cm^2) and Φ is the efficiency of reorientation of the neutron spins.

This method was used in [1, 2] to determine the spins of resonance levels of In^{115} and Eu^{151}. The sign of the change in transmission gives the spin of the studied level of the compound nucleus.

Figure 1 shows the arrangement of units in the polarization neutron spectrometer described in [1]. The apparatus consists of the following parts: a polarizer and a neutron monochromator together with a collimating device; devices for turning the neutron spins and their reorientation, a cryostat for the polarization of nuclei and a neutron detector.

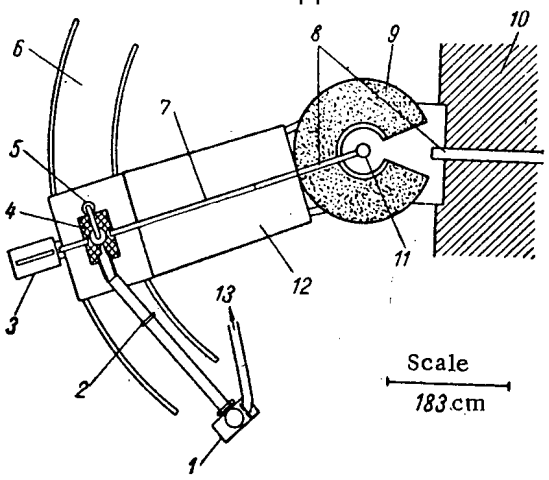

Fig. 1. Schematic plan of polarization neutron spectrometer:1) auxiliary pump; 2) evacuation line; 3) detector; 4) magnet and Dewar flask; 5) diffusion pump; 6) rails; 7) copper discs; 8) collimators; 9) rotating shield; 10) reactor shield; 11) magnet and cobalt crystal; 12) platform; 13) to initial-vacuum pump.

The neutron beam is monochromatized and polarized in the vertical direction with Bragg reflections from the planes (III) of a cobalt-iron monocrystal (92% cobalt and 8% iron) [3, 4]. The crystal is placed between the poles of an electromagnet in a field of ~ 6,000 oe intensity. The magnet can rotate about the vertical axis; there is also fine adjustment of the inclination of the crystal planes. The neutron beam incident on the polarizer is collimated by a slit collimator of the Solerovskii type with an angular divergence of 15'. The reflected beam passes through a similar collimator with an angular divergence of 13.5'. The second collimator is only necessary at small angles of reflection.

The orientation of the neutron spins between the polarizer and the target is controlled by a magnetic field of 25-oe intensity, which is produced by passing a 300-a current through copper discs placed along the neutron beam. Since the nuclei of the target were polarized in the horizontal direction, the neutron spins must be rotated through 90°. For this purpose the discs are bent at 90° over a length of 244 cm. The reorientation of the neutron polarization is achieved in the following way [5]. The polarized neutron beam passes through an aluminum disc of 2 mm thickness. To obtain one orientation of the neutron spins, the magnetic fields on both sides of the disc have the same direction. To obtain the opposite orientation of the neutron spins, a several hundred-ampere current is passed through the disc and the direction of the magnetic field in the polarizer is changed and also the sections of the copper discs between the polarizer and the aluminum disc. At a distance of 2 mm (thickness of the disc) the magnetic field is reversed and the neutron spins are not able to turn. The polarization of the neutrons is measured by the shim method (by a depolarizing iron disc) and by the method of double reflection [6]. The analyzer was another cobalt crystal placed in the gap of the permanent magnet with a field intensity of 2300 oe. The measurements showed that the polarization of the neutron beam was ~95% and the efficiency of spin reorientation was ~90%.

The nuclei are polarized by reducing the temperature of the specimen T to a few hundredths of one °K and by placing it in a strong magnetic field H [7]. The nuclear polarization

$$f_N = \frac{1}{3}\frac{I+1}{I}\frac{\mu H}{kT}, \qquad (3)$$

if $\mu H/KT \ll 1$. Here μ is the magnetic moment of the nucleus, k is the Botlzmann constant. Although this method gives a small polarization (a few percent) it is nevertheless useful because a target is obtained consisting only of the investigated nuclei. The apparatus for polarizing the target nuclei is shown in Fig. 2. A 19,000-oe intensity field in the 51-mm magnet gap is used both to magnetize the paramagnetic cooling salt and to polarize the specimen. Thermal contact between the specimen and the bottom layer of the cooling salt (chrome-potassium alum) is provided by silver wires. A lead wire connects the bottomlayer of the salt with the upper layer (iron-ammonium alum). This two-stage combination of salt-specimen in the magnetic field is cooled to 1°K with liquid helium. The combination is then slowly raised until the cooling salts are no longer in the magnetic shield. The lead wire serves as a thermal key, providing thermal contact between the salt when it is in the magnetic field and breaks it when it is in the magnetic screen, since it becomes superconducting. It takes 30 min to rise a distance of 140 mm. The temperature of the bottom layer of the salt is determined from its susceptibility by means of mutual induction coils. Over a period of 90 min the mean temperature was ~ 0.04°K. A rate of heating of 0.015°K/hr at 0.04°K corresponded to a heat flow of 200 erg/min.

The neutron detector is a $B^{10}F_3$ counter of diameter 2.5 cm and length 56 cm filled to a pressure of 120 cm.

The transmission of the neutron beam of the studied energy is measured alternately for two relative orientations of the spins of neutrons and nuclei every 5 min. The results of the measurements on the first three resonances in In^{115} are shown in the table. The observed changes in the transmission were corrected for the presence of potential scattering. For resonance at 3.86 ev a correction was made to allow for the effect of resonance at 1.46 ev. The corrected values were used for the calculation with formula (2) of the mean nuclear polarization during the experiment. Formula (3) was used to calculate the mean temperature of the indium specimen. The last column gives the measured mean

Results of Measurements with In^{115}

Resonance E_0, ev	Spin J	Relative change in transmission of neutrons by the target: observed	Relative change in transmission of neutrons by the target: corrected	Nuclear polarization $\bar{f}_N$, %	Mean temperature of specimen $\bar{T}$, °K (calculated)	Mean temperature of bottom layer of cooling salt $\bar{T}$, °K (measured)
1,46	5	10,5±2,2	10,9	2,4	0,064	0,039
3,86	4	−6,7±1,0	−9,1	3,0	0,052	0,033
9,10	5	2,9±0,9	3,3	2,5	0,062	0,043

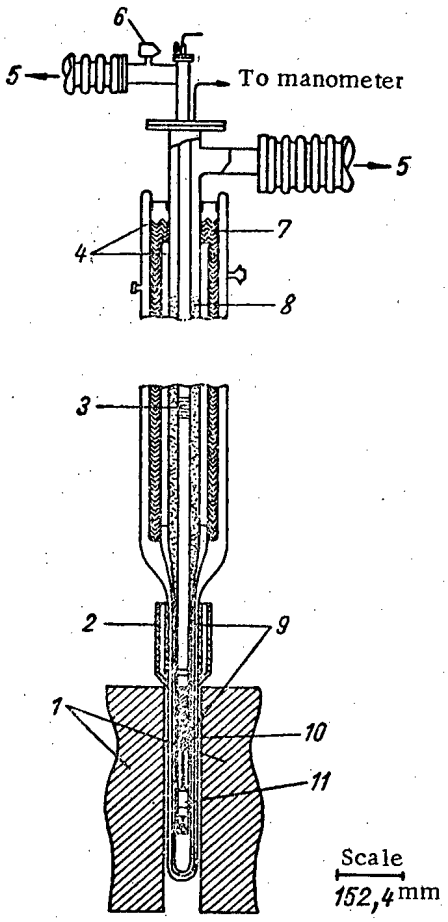

Fig. 2. Apparatus for nuclear polarization: 1) magnetic pole pieces; 2) magnetic shield; 3) thermal radiation shield; 4)vacuum; 5)to pump; 6)ionization manometer; 7)liquid nitrogen; 8)liquid helium; 9) sensitive measuring coils; 10)cooling salts; 11)specimen under investigation.

temperature of the bottom layer of the cooling salt. A control experiment on resonance at 1.46 ev with the specimen at room temperature gave a value of $\Delta t/\bar{t} = (0.06 \pm 1.15)\%$. This shows that the values of $\Delta t/\bar{t}$ given in the table are due to the polarization of the specimen. The measured values of the spins of resonance levels of In^{115} agree with results obtained in other work. This method was used to measure spins of resonances at 0.327 and 0.461 ev in Eu^{151} [2], which were equal to 3 and 2 respectively.

In conclusion it should be mentioned that this method for determining spin states of resonances has the advantage that the experimental results are easily interpreted. Its disadvantages are the difficulties in obtaining polarized and monochromatic neutrons with energy greater than 20 ev and difficulties in polarizing nuclei with magnetic moments less than the two nuclear magnetons.

LITERATURE CITED

1. A. Stolovy. Phys. Rev. 118, 211 (1960).
2. A. Stolovy. Bull. Amer. Phys. Soc. 5, No. 4, 294 (1960).
3. R. Nathans, A. Paoletti. Phys. Rev. Letter. 2, No. 6, 254 (1959).
4. R. Nathans et al. J. Phys. Chem. Solids 10,138 (1959).
5. R. Haas, L. Leipuner, R. Adair. Phys. Rev. 116, 1221 (1999).
6. C. P. Standord et al. Phys. Rev. 94, 374 (1954).
7. J. Dabbs, L. Roberts, S. Bernstein. Phys. Rev. 98, 1512 (1955).

RADIATION CAPTURE CROSS SECTIONS OF NEUTRONS WITH ENERGIES OF 0.03-2 Mev BY THE ISOTOPES Mn^{55}, Cu^{65}, Ba^{138}, Th^{232}

Yu. Ya. Stavisskii and V. A. Tolstikov

Translated from Atomnaya Énergiya, Vol. 10, No. 5,
pp. 508-511, May, 1961
Original article submitted October 29, 1960

The radiation capture cross sections of neutrons for some isotopes have been measured by the activation method described in [1-3]. The reference cross sections used were the cross sections of U^{235} fission and the capture sections of thermal neutrons [4]. The intermediate standard cross section was the radiation capture cross section of fast neutrons of I^{127}, which we measured relative to the cross section of U^{235} fission [5].

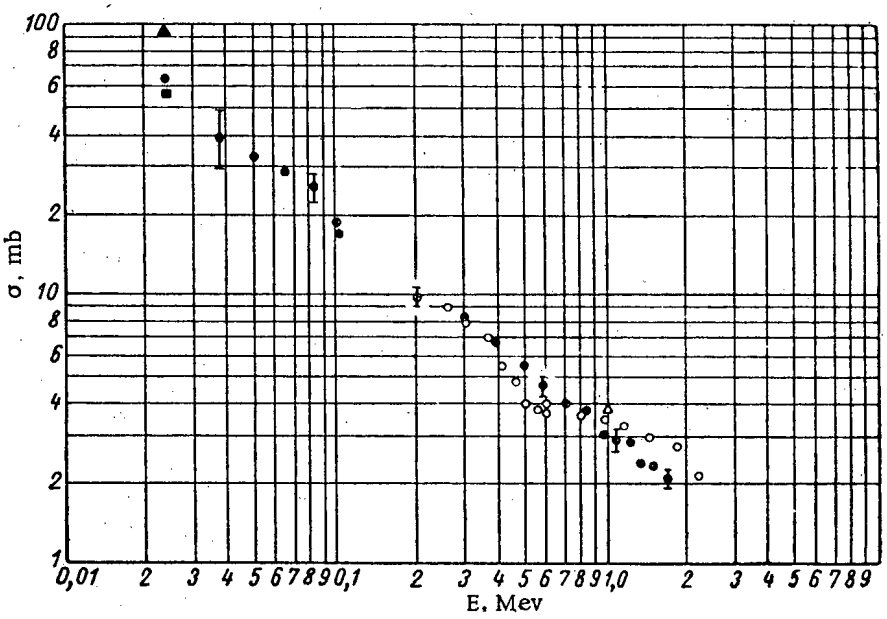

Fig. 1. Dependence of the radiation capture cross section of fast neutrons by isotope Mn^{55} on the neutron energies. Data of investigations: ●-present; ○-[6]; ▲-[9]; ■-[8]; △-[7].

The results of our measurements together with the results of other authors are given in Fig. 1-4. The mentioned errors are the mean square errors in the experiment and the errors in the U^{235} cross section.

In contrast to [6] where it was found that the radiation capture cross sections of neutrons by manganese remain constant in the energy region 600-900 kev, the cross sections which we obtained decrease smoothly with energy over the whole studied range of neutron energies.

The radiation capture cross sections of neutrons by even-even nuclei of Ba^{138}, Th^{232} and uneven-even nuclei of Cu^{65} remain constant over a fairly wide range of neutron energies, and in the Ba^{138} cross section there is a wide maximum. This points to the important role of neutrons with $l > 0$. In the opposite case the cross sections would fall with reduction in energy according to the law $1/E$ [7].

The values of the neutron energies for which the cross sections begin to fall rapidly are well correlated with the position of excited levels of the corresponding nuclei-targets ($1120(^5/_2-)$, $1490(^7/_2-)$ kev for Cu^{65}; $1420\ (2^+)$ kev for Ba^{138}). Our calculations of the dependence of neutron radiation capture cross sections on energy according to the statistical theory of nuclear reactions and models of a semitransparent nucleus with a diffuse edge and a black nucleus indicate that the dependence of $\sigma\ (n,\gamma)$ on the neutron energy is largely determined by the contribution of the neutron waves with $l > 0$ and concurrence with inelastic scatter.

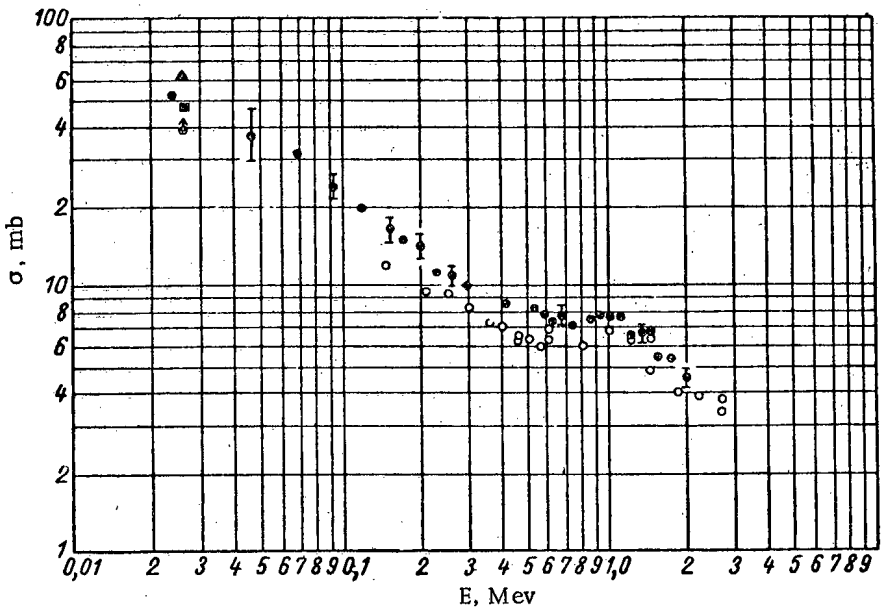

Fig. 2. Dependence of radiation capture cross section of fast neutrons by isotope Cu^{65} on the neutron energies. Data of investigations: ○-present; ◉-present (photoneutrons); ○-[6]; ■-[8]; ▲-[9].

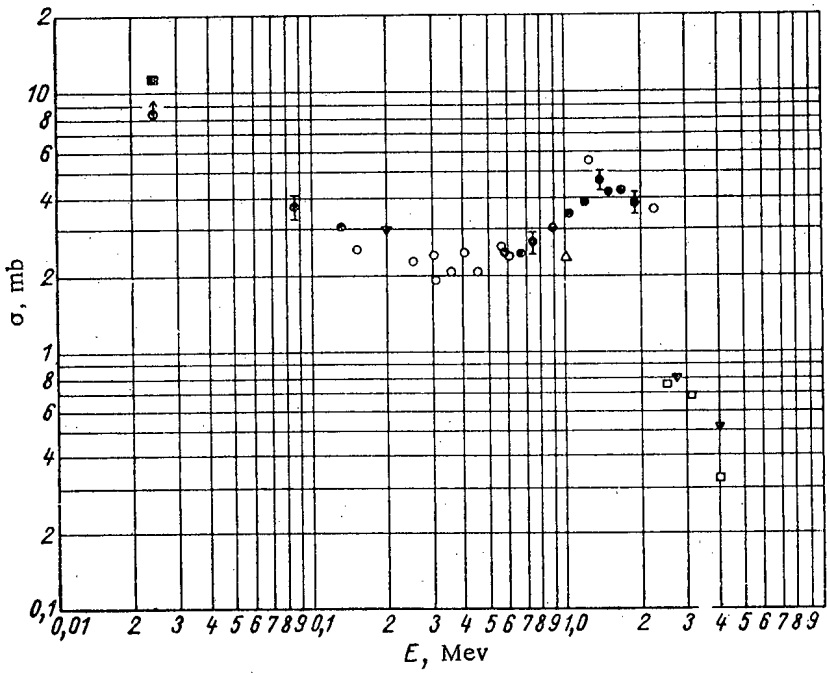

Fig. 3. Dependence of radiation capture cross section of fast neutrons by a Ba^{138} isotope on the neutron energies. Data of investigations: ●-present; ◉-present (photoneutrons); ○-[6]; ■-[8]; △-[7]; ▼-[10]; □-[11].

The reduction in the capture cross section for Th^{232} when $E_n > 900$ kev is also due to concurrence with inelastic scatter and fission.

The authors would like to thank A. I. Leipunskii, O. D. Kazachkovskii and V. S. Stavinskii for their interest in the work and for their valuable discussions.

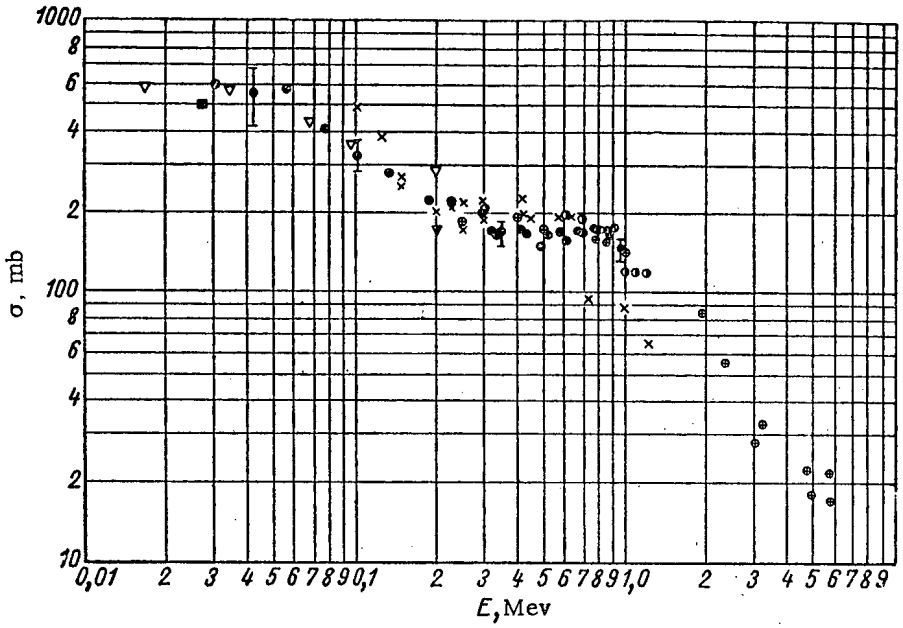

Fig. 4. Dependence of radiation capture cross section of fast neutrons by a Th^{232} isotope on the neutron energies. Data of investigations: ●-present, ■-[9]; ⊕-[12]; ◑-[13]; ×-[14]; ▽-[15]; ▼-[10].

LITERATURE CITED

1. Yu. Ya. Stavisskii and V. A. Tolstikov, Atomnaya énergiya, 7, No. 3, 259 (1959).
2. Yu. Ya. Stavisskii and V. A. Tolstikov, Atomnaya énergyia, 9, No. 5, 401 (1960).
3. Yu. Ya. Stavisskii and V. A. Tolstikov. Measuring cross sections of radiation capture of fast neutrons by the isotopes V^{51}, Mn^{55}, Nb^{93}, Mo^{100}, W^{189}, Tl^{205}, Th^{232}. Report to the second All-Union Conference on Nuclear Reactions at Low and Medium Energies (Moscow, July, 1960).
4. D. Hughes, R. Schwartz. Neutron Cross Section. N. Y., McGraw-Hill Book Co., 1955.
5. Yu. Ya. Stavisskii, V. A. Tolstikov and V. N. Kononov. Atomnaya énergiya, 10, No.2, 158 (1961).
6. A. Johnsrud, M. Silbert, H. Barschall. Phys. Rev. 116, 927 (1959).
7. D. Hughes, R. Gart, D. Levin. Phys. Rev. 91, 1423,(1953).
8. R. Macklin, N. Lazar, W. Lyon. Phys. Rev. 107, 504 (1957).
9. V. Hummel, B. Hamermesh. Phys. Rev. 82, 67 (1951).
10. A. I. Leipunskii et al, Transactions of the Second International Conference on the Peaceful Use of Atomic Energy (Geneva, 1958). Reports of Soviet Scientists, Vol. 1. Moscow, Atomic Energy Press, 1959, p. 136.
11. Yu. V. Gofman, Appendix to "Ukr. fiz. zh.", III, No. 1, 14 (1958).
12. D. Hughes, R. Schwartz. Neutron Cross Section. N. Y., McGraw-Hill Book Co., 1955 (data from University of California).
13. J. Barry, L. O'Connor, J. Perkin. Proc. Phys. Soc. 74, No. 480, 685 (1959).
14. R. Hanna, B. Rose. J. Nucl. Energy, 8, 197 (1959).
15. D. Hughes, R. Schwartz. Neutron Cross Section. N. Y., McGraw-Hill Book Co. 1955 (data from Los Alamos Laboratory).

All abbreviations of periodicals in the above bibliography are letter-by-letter transliterations of the abbreviations as given in the original Russian journal. *Some or all of this periodical literature may well be available in English translation.* A complete list of the cover-to-cover English translations appears at the back of this issue.

PASSAGE OF NEUTRONS WITH ENERGIES OF 0.5 and 1.0 Mev THROUGH WATER AND MIXTURES OF WATER WITH HEAVY COMPONENTS

V. I. Kukhtevich and B. I. Sinitsyn

Translated from Atomnaya Énergiya, Vol. 10, No. 5,
pp. 511-513, May, 1961
Original article submitted October 29, 1960

The authors of the present paper have measured the spatial distribution of thermal and epicadmium neutrons formed by moderating neutrons with energies of 0.5 and 1.0 Mev in water, and have determined the removal cross section σ_{rem} of carbon, iron, and lead for neutrons with these initial energies. The data of the measurements have been compared with theoretical calculations made by Holte, Ref. [1]. The spatial distribution in water of neutrons of 1.0 Mev energy moderated to thermal energies has been measured in Ref. [2]. The results of the measurements have likewise been compared with Holte's calculations. Satisfactory agreement was obtained between the experimental and calculated data. At a distance of 34 cm from the source, the disagreement did not exceed 40%.

In the present paper the measurements were made in semi-infinite geometry. A rectangular steel tank full of water, with the dimensions 110 × 110 × 120 cm and wall thickness 3 mm, was placed 8 cm in front of the neutron source. In measuring the removal cross sections, the test substance was placed between the source and the front wall of the tank. The detector was a proportional BF_3 counter, 0.9 cm in diameter and 7 cm long. It was placed in a thin-walled tube of organic glass and could be moved about inside the water tank. To exclude any effect of the diffusion of thermal neutrons on the detector indications, the counter was surrounded by a cadmium shield 0.9 mm thick. Between the walls of the shield and the walls of the counter, a space was left, 0.7 cm thick, filled with polyethylene to increase the sensitivity. The measurements of the removal cross section were made with a counter covered with a cadmium shield.

The neutrons of energy 0.5 and 1.0 Mev were obtained from the $T(p,n)He^3$ reaction on a Van de Graaf accelerator. A thin tritium-zirconium target of thickness 0.172 mg/cm^2 was used. The test substance had cross-sectional dimensions 60 × 60 cm and thickness as follows: carbon-6 cm, iron-4.88 cm, lead-3.94 cm.

Removal Cross Sections for Neutrons (in barns)

Element	Neutron energy, Mev	
	0,5	1,0
Carbon	3,16±0,25	2,08±0,23
Iron	2,36±0,47	1,07±0,11
Lead	1,22±0,78	2,87±0,63

The results of the measurements are given in Fig. 1 and 2 and in the table. The mean error in the values of the removal cross sections was 14% for E_n = 1.0 Mev, and 33% for E_n = 0.5 Mev. One should note the good agreement between the values of the removal cross section of iron at 1.0 Mev given in Ref. 3, σ_{rem} = 1.1 barn, with the value σ_{rem} = 1.07 + 0.11 barn obtained in the present experiment.

Figure 1 gives the results of measurements of the spatial distributions of epicadmium netutrons in water for original neutron energies of 0.5 and 1.0 Mev. Curves are drawn in the same figure of Holte's calculation of the spatial distribution of neutrons with a final energy of 1 ev. The curves are normalized at the point x = 30 cm. The agreement between the experimental and the calculated results lies within the limits of error of the experiment except for the results at distances x < 6 cm.

To compare the results of the measurements of the spatial distribution of thermal neutrons in water with Holte's theoretical calculations, a number of transformations were made. First of all, the distribution of the density of neutrons of energy 1 ev in water, obtained from Holte's calculations, was taken as the density of sources for the birth of thermal neutrons diffusing in water, with the diffusion length L = 2.72 cm, Ref. [2]. The diffusion correction is most easily made for an infinite plane source. Therefore, the results of Holte's calculations for an isotropic point source (as well as the results of our experiment) were transformed to results for an infinite plane isotropic source using the formula

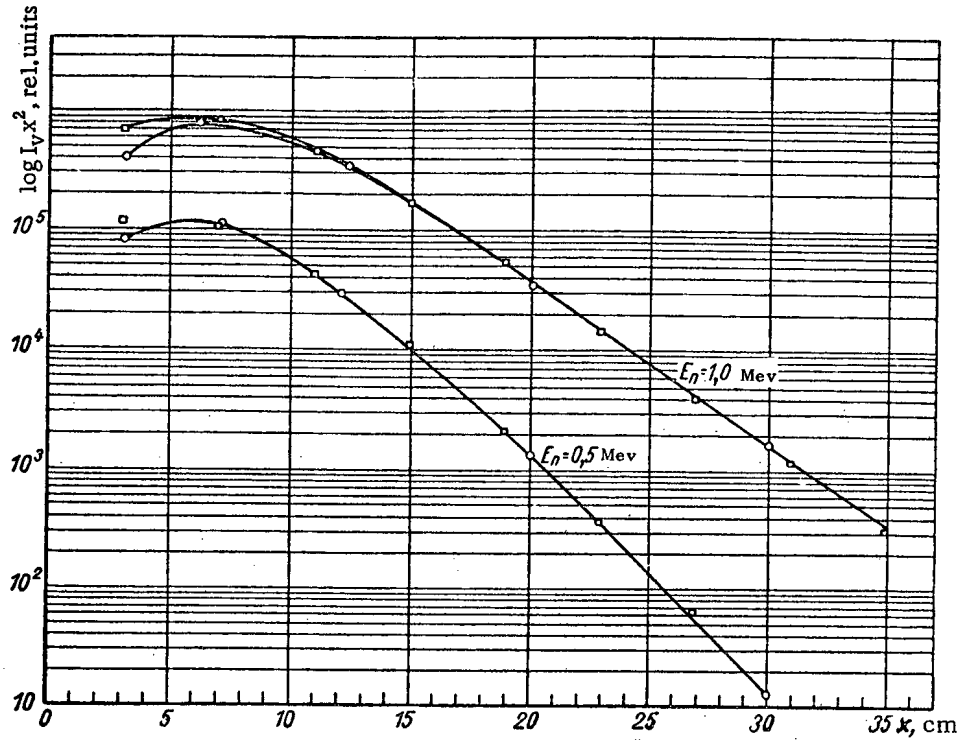

Fig. 1. Spatial distribution of epicadmium neutrons in water; □-measurements with a BF_3 counter in a cadmium shield; ○-results of Holte's calculations [1].

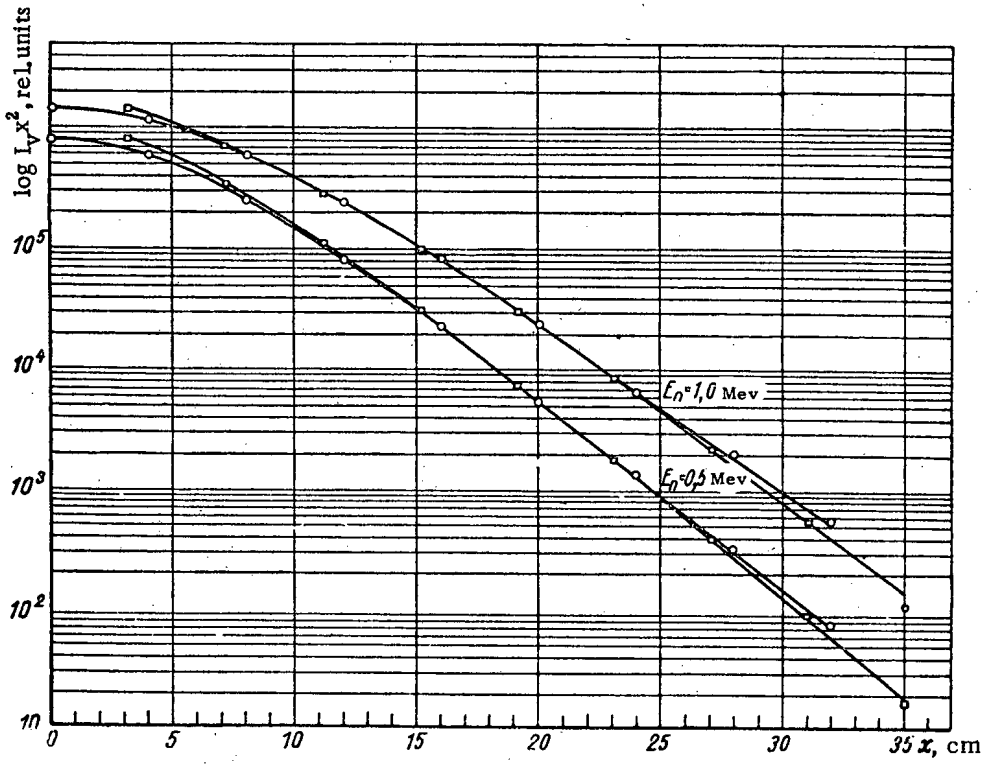

Fig. 2. Spatial distribution of thermal neutrons in water from a plane isotropic source: □-measurements with a BF_3 counter; ○-results of Holte's calculations [1], taking account of diffusion.

$$C(z)=2\pi\int_{z}^{\infty} C(x)\,x\,dx,$$

where C (x) is the distribution function of neutrons from an isotropic point source.

The diffusion correction was made from the expression

$$F(r)=K\int_{-\infty}^{\infty} C(z)\,e^{-|r-z|/L}\,dz,$$

where K is the normalizing factor to the experimental curve.

The results of comparing the experimentally measured distribution of thermal neutrons with the calculated values for neutron energies of 0.5 and 1.0 Mev are given in Fig. 2. The curves are normalized at the point x = 20 cm. The results are in satisfactory agreement, and are within the limits of accuracy of experiment and theory. At short distances (10 cm and less) disagreement in the results is observed, reaching 15% at x = 3 cm although in this region the statistical error does not exceed 1-2%. The disagreement may be explained by the fact that in the experiment no account was taken of a number of factors which are important at small distances, thus: the medium is not infinite near the source; the effect of the 3-mm thick front wall of the tank; the effect of the scattered neutron background; and the inaccuracy of the detector. These same factors apply to the measurement of the spacial distribution of epi-cadmium neutrons.

The statistical error in the measurement of the spacial distributions vary from 1 to 2% near the source, to 30 to 35% at distances from the source of 30 to 35 cm.

The authors express their obligation to S. G. Tsypin for his part in discussing the results of the work as well as to E. T. Bondarev who did a large amount of work in preparing the experiment.

LITERATURE CITED

1. G. Holte. Arkiv fys. 8, 165 (1954).
2. K. Shure, P. Roys. Nucl. Sci. Engng. 2, 170 (1956).
3. Protection of nuclear reactors [Russian translation]. Edited by T. Rockwell. Moscow, Izd-vo Inostr. Lit. 1958.

DISTRIBUTION OF NEUTRONS IN MEDIA WITH A CYLINDRICAL INTERFACE BOUNDARY AND OFF-AXIS SOURCE DISTRIBUTION

A. E. Glauberman, V. B. Kobylyanskii, I. I. Tal'yanskii

Translated from Atomnaya Énergiya, Vol. 10, No. 5,
pp. 513-515, May, 1961
Original article submitted October 11, 1960

In [1] the solution is given to the problem of the distribution of the neutrons from a point source of fast neutrons located on the axis of a crevice. But depending on the location of the source, the medium outside the crevice will exert more or less influence on the neutron flux inside the crevice.

Let the source be located a distance a from the axis of the crevice. We shall let the z axis be directed along the axis of the crevice, and the plane z = 0 and θ = 0 we take such that the z and θ coordinates of the source are equal to zero and r = a. The radius of the crevice is designated by R. To solve the problem, we used the two-group approximation, wtih fictitious sources on the boundary separating the media [1].*

In our coordinate system, in the present case, the density of fast neutron sources ρ_{1c} takes the form

* The nomenclature is the same as in [1].

$$\left.\begin{aligned} \varrho_{1c} &= \frac{Q}{4\pi r}\,\delta(r-a)\,\delta(\Theta)\,\delta(z);\\ \delta(r-a) &= r\int_0^\infty \lambda J_m(\lambda_r)\,J_m(\lambda a)\,d\lambda;\\ \delta(z) &= \frac{1}{2\pi}\int_{-\infty}^{\infty} e^{i\eta z}\,d\eta;\\ \delta(\Theta) &= \frac{1}{2}\sum_{m=-\infty}^{\infty} e^{i\Theta m}, \end{aligned}\right\} \tag{1}$$

where J is a Bessel function. The integral representations which we have written for the δ-functions allow us to find the flux of fast neutrons by a method similar to that used in [1]. Calculation gives

$$\varphi_{1c}(r,\Theta,z) = \frac{Q}{2\pi}\int_{-\infty}^{\infty}[K_0(\xi_{1c}a)+A_0(\eta)]\,I_0(\xi_{1c}r)e^{i\eta z}d\eta + \frac{Q}{\pi}\sum_{m=1}^{\infty}\int_{-\infty}^{\infty}[K_m(\xi_{1c}a)+A_m(\eta)]\,I_m(\xi_{1c}r)$$
$$\times\cos m\Theta e^{i\eta z}\,d\eta \quad (\text{for } r<a); \tag{2}$$

$$\varphi_{1c}(r,\Theta,z) = \frac{Q}{2\pi}\int_{-\infty}^{\infty}[K_0(\xi_{1c}r)\,I_0(\xi_{1c}a)+I_0(\xi_{1c}r)\,A_0(\eta)]e^{i\eta z}\,d\eta +$$
$$+\frac{Q}{\pi}\sum_{m=1}^{\infty}\int_{-\infty}^{\infty}K_m(\xi_{1c}r)\,I_m(\xi_{1c}a)+I_m(\xi_{1c}r)\,A_m(\eta)]\cos m\Theta e^{i\eta z}\,d\eta \quad (\text{for } r>a), \tag{2'}$$

where

$$A_\mu(\eta) = K_\mu(\xi_{1c}R)\,f_\mu^{(1c)}(\eta) \tag{3}$$

and

$$\varphi_{1r}(r,\Theta z) = \frac{1}{2\pi}\int_{-\infty}^{\infty}K_0(\xi_{1r}r)\,B_0(\eta)\,e^{i\eta z}\,d\eta + \frac{1}{\pi}\sum_{m=1}^{\infty}\int_{-\infty}^{\infty}K_m(\xi_{1r}r)\,B_m(\eta)\cos m\Theta e^{i\eta z}\,d\eta, \tag{4}$$

where

$$B_\mu(\eta) = I_\mu(\xi_{1r}R)\,f_\mu^{(1r)}(\eta). \tag{5}$$

Here $\xi_{1\alpha}=\sqrt{\eta^2+\varkappa_{1\alpha}^2}$, and the functions $f_\mu^{(1\alpha)}(\eta)$ take the form

$$\left.\begin{aligned} f_\mu^{(1c)} &= \frac{QI_\mu(\xi_{1c}a)\,[D_{1r}\xi_{1r}K_\mu(\xi_{1c}R)\,K'_\mu(\xi_{1r}R)-D_{1c}\xi_{1c}K_\mu(\xi_{1r}R)\,K'_\mu(\xi_{1c}R)]}{K_\mu(\xi_{1c}R)\,[D_{1c}\xi_{1c}I'_\mu(\xi_{1c}R)\,K_\mu(\xi_{1r}R)-D_{1r}\xi_{1r}I_\mu(\xi_{1c}R)\,K'_\mu(\xi_{1r}R)]};\\ f_\mu^{(1r)} &= \frac{QI_\mu(\xi_{1c}a)\,[D_{1c}\xi_{1c}K_\mu(\xi_{1r}R)\,K'_\mu(\xi_{1c}R)-D_{1r}\xi_{1r}K_\mu(\xi_{1c}R)\,K'_\mu(\xi_{1r}R)]}{I_\mu(\xi_{1r}R)\,[D_{1c}\xi_{1c}I'_\mu(\xi_{1c}R)\,K_\mu(\xi_{1r}R)-D_{1r}\xi_{1r}I_\mu(\xi_{1c}R)\,K'_\mu(\xi_{1r}R)]}. \end{aligned}\right\} \tag{6}$$

The expression for φ_{1c} (2') at a = 0 coincides with the corresponding expression in [1].

The flux of slow neutrons is found from the equations

$$\Delta\Phi_{2\alpha}-\varkappa_{2\alpha}^2\Phi_{2\alpha} = -\varkappa_{12\alpha}^2\varphi_{1\alpha}, \tag{7}$$

where the index α is characteristic of the medium.

After calculation we obtained the following expressions for $\varphi_{2\alpha}$:

$$\varphi_{2c}(r,\Theta,z) = \frac{\varkappa_{12c}^2}{\varkappa_{2c}^2-\varkappa_{1c}^2}\varphi_{1c} + \frac{1}{2\pi}\int_{-\infty}^{\infty}I_0(\xi_{2c}r)\,K_0(\xi_{2c}R)\,\frac{C_0^{(a)}D_{0a}^{(r)}+C_0^{(a)}D_{0b}^{(r)}}{D_{0a}^{(c)}D_{0b}^{(r)}+D_{0a}^{(r)}D_{0b}^{(c)}}\,e^{i\eta z}\,d\eta$$

$$+\frac{1}{\pi}\sum_{m=1}^{\infty}\int_{-\infty}^{\infty} I_m(\xi_{2c}r)\,K_m(\xi_{2c}R)\,\frac{C_m^{(a)}D_{ma}^{(r)}+C_m^{(a)}D_{mb}^{(r)}}{D_{ma}^{(c)}D_{mb}^{(r)}+D_{ma}^{(r)}D_{mb}^{(c)}}\cos m\Theta e^{i\eta z}\,d\eta;$$

$$\varphi_{2r}(r,\ \Theta,\ z)=\frac{\varkappa_{12r}^2}{\varkappa_{2r}^2-\varkappa_{1r}^2}\varphi_{1r}+\frac{1}{2\pi}\int_{-\infty}^{\infty} I_0(\xi_{2r}R)\,K_0(\xi_{2r}r)\,\frac{C_0^{(b)}D_{0a}^{(c)}+D_{0b}^{(c)}C_0^{(a)}}{D_{0a}^{(c)}D_{0b}^{(r)}+D_{0a}^{(r)}D_{0b}^{(c)}}\,e^{i\eta z}\,d\eta \tag{8}$$

$$+\frac{1}{\pi}\sum_{m=1}^{\infty}\int_{-\infty}^{\infty} I_m(\xi_{2r}R)\,K_m(\xi_{2r}r)\,\frac{C_m^{(b)}D_{ma}^{(c)}+C_m^{(a)}D_{mb}^{(c)}}{D_{ma}^{(c)}D_{mb}^{(r)}+D_{ma}^{(r)}D_{mb}^{(c)}}\cos m\Theta e^{i\eta z}\,d\eta,$$

where

$$C_\mu^{(a)}(\eta)=\frac{\varkappa_{12r}^2}{\varkappa_{2r}^2-\varkappa_{1r}^2}K_\mu(\xi_{1r}R)\,B_\mu(\eta)-\frac{\varkappa_{12c}^2}{\varkappa_{2c}^2-\varkappa_{1c}^2}[QI_\mu(\xi_{1c}a)\,K_\mu(\xi_{1c}R)+K_\mu(\xi_{1c}R)\,A_\mu(\eta)];$$

$$C_\mu^{(b)}(\eta)=\frac{D_{2r}\varkappa_{12r}^2}{\varkappa_{2r}^2-\varkappa_{1r}^2}\xi_{1r}K'_\mu(\xi_{1r}R)\,B_\mu(\eta)-\frac{D_{2c}\varkappa_{12c}^2}{\varkappa_{2c}^2-\varkappa_{1c}^2}[Q\xi_{1c}I_\mu(\xi_{1c}a)\,K'_\mu(\xi_{1c}R)+\xi_{1c}I'_\mu(\xi_{1c}R)\,A_\mu(\eta)]; \tag{9}$$

$$D_{\mu a}^{(c)}=I_\mu(\xi_{2c}R)\,K_\mu(\xi_{2c}R);\qquad D_{\mu b}^{(c)}=D_{2c}\,\xi_{2c}\,I'_\mu(\xi_{2c}R)\,K_\mu(\xi_{2c}R);$$

$$D_{\mu a}^{(r)}=I_\mu(\xi_{2r}R)\,K_\mu(\xi_{2r}R);\qquad D_{\mu b}^{(r)}=D_{2r}\xi_{2r}I_\mu(\xi_{2r}R)\,K'_\mu(\xi_{2r}R).$$

Analysing Φ_{2c}^{*} as a function of a, it can be shown that, as we might expect, the contribution of neutrons moderated inside the crevice to φ_{2c} increases with increasing a. Therefore, the use of off-axis sources can give more accurate information on the material surrounding the crevice.

LITERATURE CITED

1. A. E. Glauberman, I. I. Tal'yanskii. Atomnaya énergiya, III, No. 23 (1957).

RADIATION FROM A VOLUME SOURCE IN THE PRESENCE OF SURFACE ACTIVITY

E. E. Kovalev and D. P. Osanov

Translated from Atomnaya Énergiya, Vol. 10, No. 5,
pp. 515-517, May, 1961
Original article submitted July 3, 1960

In considering the radiation from extended sources, it is usual to assume that surface activity is absent, [1] and [2]. However, for real volume sources, this assumption is not met. In many cases after absorbtion, the radioactive substances go through the liquid or gaseous phase of the volume source, on to the surface of a solid phase, that is, of some absorber such as a glass vessel. The radiation from this material distributed over the surface may amount to a considerable part of the radiation from the real source.

We shall introduce the concept of a dose factor for the surface activity S, defined as the ratio of the dose strength of γ-radiation of the volume source in the presence of surface activity to the dose strength under the same conditions, but without surface activity. This definition is convenient, since it allows us to use the expressions for the yield of γ-radiation from the different volume sources under real conditions, i.e., in the presence of surface activity, if we introduce S into these relationships in the form of a coefficient. In accordance with this definition

$$S=\frac{P}{P_1}=\frac{P_1+P_s}{P_1}, \tag{1}$$

where P is the dose strength of γ-radiation from the volume source at the point A in the presence of surface activity; P_1 is the dose strength of γ-radiation from the volume source, neglecting the surface activity; P_S is the dosage contribution of the surface activity to the yield of γ-radiation.

The following considerations deal with a cylindrical source, in the volume of which, in the form of a solid, liquid, or gas, and on the lateral surface of the walls of which there is a thin layer of uniformly distributed radioactive substance, Fig. 1. The radiation from the material distributed over the surface, P_2, is attenuated by a definite amount in the volume of the cylindrical source, so that

$$P_s = f_2 P_2; \tag{2}$$

here f_2 is the coefficient giving the attenuation of the γ-radiation from the materials located on the surface of the cylindrical source. If the active substance is distributed through the volume of the cylindrical source in the form of a gas, then $f_2 \simeq 1$ and $P_S = P_2$. In this case, the radiation from the cylindrical source is equal to the sum of the activity contributions from the volume P_1 and from the surface P_2. The coefficient f_2 is independent of the density of the surface activity, but it is affected by the spectral composition of the γ-radiation and the geometrical and physicochemical parameters of the source.

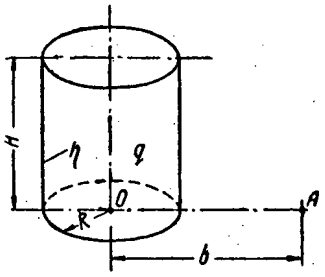

Fig. 1. Fundamental parameters of the cylindrical source.

The radiation yield from an extended source is conveniently expressed in terms of the radiation from a point source using a geometrical factor G. In our case

$$\left.\begin{aligned} P_1 &= P_0 Q_1 G_1 f_1 \text{ (for a solid cylinder);} \\ P_s &= P_0 Q_2 G_2 f_2 \text{ (for a hollow cylinder filled with absorbing material).} \end{aligned}\right\} \tag{3}$$

Here P_0 is the dose strength from a point source of unit activity, Q_1 and Q_2 are the total activities of a solid and a hollow cylinder respectively, f_1 is the self-absorbtion factor for a solid cylinder.

Using Eq. (3) and expressing the total activity in terms of the specific activity q for a solid cylinder and the density of the surface activity η for a hollow cylinder, (see Fig. 1), Eq. (1) may be arranged in the following form:

$$S = 1 + \frac{2}{R}\frac{\eta}{q}\frac{f_2}{f_1}\frac{G_2}{G_1}, \tag{4}$$

where R is equal to the radius of the cylinder. Equation(4) makes it possible to calculate the dose factor of the surface activity for various cylindrical sources if we know the ratio of the density of the surface activity to the specific activity of the cylindrical volume, η/q and the values of f_2/f_1 and G_2/G_1, which depend on the geometric and physicochemical parameters of the source.

The value of η depends on the specific activity q, on the nature of the processes taking place in the volume of the cylindrical source and on the physicochemical properties of the surface and cannot be determined unambiguously ahead of time.

Thus to find the dose factor of the surface activity S, we must find the ratio $\alpha = f_2 G_2 / f_1 G_1$. In calculating α we used the values f_1, f_2, G_1, and G_2 from [3–6]. The values of α were determined for points lying at a distance b (see Fig.1) from the axis of the cylinder in the plane of the lower base. It is obvious that these results are applicable to any cross-sectional plane of the cylinder which is parallel to the plane of the base.

Figure 2 shows the values of α as a function of the parameters P = b/R and μR. The variation of α with the relative height of the cylindrical source, K = H/R, over the range $0.5 \leq K \leq 5$, was seen to be slight. This made it possible, in constructing nomograms, to use values of α averaged for different values of K. Here the error did not exceed 10%.

From the calculated values of α we obtained an approximate formula connecting α with the parameters P and μR:

$$\alpha = 0{,}5\,(1 + 0{,}75\mu R)\left(1{,}5 + \frac{1}{P}\right). \tag{5}$$

This formula makes it possible to calculate the value of α with an error not greater than 10% over the range $0 \leq \mu R \leq 5$, $0.5 \leq K \leq 5$, $1.25 \leq P \leq 10$, and with an error not greater than 20% over the range $5 \leq \mu R \leq 10$, $3 \leq K \leq 5$, $1.25 \leq P \leq 10$. Using Eq. (5), Eq. (4) may be rewritten as

$$S = 1 + \frac{1 + 0{,}75\mu R}{R}\left(1{,}5 + \frac{1}{P}\right)\frac{\eta}{q}. \tag{6}$$

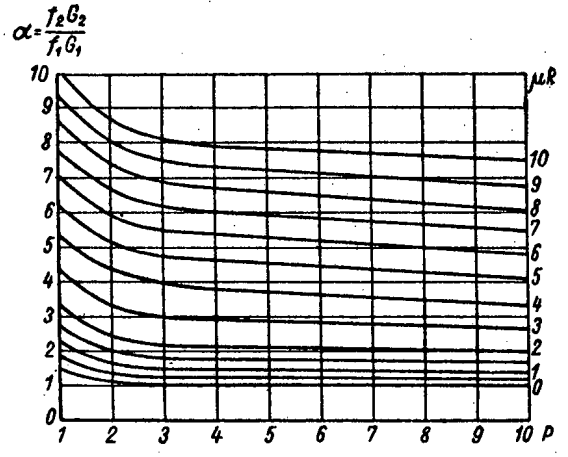

Fig. 2. $\alpha = f_2G_2/f_1G_1$ as a function of P = b/R and μR.

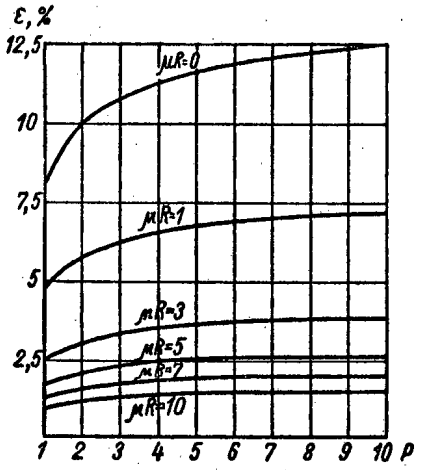

Fig. 3. Nomogram for determining the limiting ratio of the total surface and volume activities, ε %.

If we introduce the ratio ε of the total surface activity to the total volume activity of the source, the expression for the dose factor of the surface activity takes the more general form

$$S = 1 + \frac{1 + 0{,}75\mu R}{2}\left(1{,}5 + \frac{1}{P}\right)\varepsilon. \qquad (7)$$

Equation (7) may be used for practical calculation of the γ-ray yield from a cylindrical source including the surface activity. It should be noted that this formula has been derived for the case that the spectral distribution of the radiation from the substance adsorbed on the surface of the cylindrical source and from that distributed in the volume is identical. This condition is not always met. As an example of this, we may take selective adsorption by the walls of the source in the presence of a mixture of radioactive isotopes in the cylindrical volume. If, in this case, we know the coefficients of selective adsorption, S may be calculated from Eq. (7), applying it to each component of the mixture.

We shall now show, in a concrete case, how the surface activity affects the radiation from a cylindrical source. Take a cylinder with R = 10 cm, filled with a solution of a salt of Co^{60} at a density ρ = 1.2 g/cm^3 (μ = 0.076 cm^{-1}). As a result of adsorption, surface activity is formed on the walls of the cylinder.

Value of S as a function of ε are given below for a distance of 150 cm from the axis of the cylinder (R = 100 cm, μR = 7.6, p = 1.5):

$\bar{\varepsilon}$, %	0	5	10	20	30	40	50	60	70	80	90	100
S	1,00	1,36	1,73	2,45	3,18	3,90	4,63	5,35	6,08	6,80	7,52	8,25

Thus the effect of adsorbed acitivity on the radiation from a cylindrical source may be very considerable and it is obviously necessary to take account of adsorption in calculating the γ-radiation yield.

The results given also make it possible to determine how to use a source so that the effect of adsorbed activity on the γ-radiation yield will be minimized. We shall assume that an increase in γ-ratios of 10% from adsorption (S = 1.1) is unimportant. Then we can write the following inequality:

$$\varepsilon \leqslant \frac{0{,}2}{1 + 0{,}75\mu R\left(1{,}5 + \frac{1}{P}\right)}. \qquad (8)$$

The limiting values of ε corresponding to a 10% increase in dosage from adsorption were calculated from Eq. (8) and are given in the nomogram, Fig. 3. Using the nomogram it is easy to find, for example, that for a source with the parameters μR = 10 and P = 10, the limiting value of the ratio of adsorbed activity to the activity in the solution is about 1.5%. For small values of μR, this limiting value reaches 10%. Knowing the limiting value of ε for a concrete cylindrical source, we can find the operating conditions for the source (the selection of raw material, the degree and frequency of deactivation required, etc.) which give the minimum increase in γ-radiation from adsorbed activity.

LITERATURE CITED

1. G. V. Gorshkov. Gamma-radiation of radioactive bodies [in Russian] Leningrad State University Press, 1956.
2. Protection of Nuclear reactors[Russian translation], edited by T. Rockwell, Moscow, Izd-vo Inostr. Lit. 1958.
3. V. I. Popov, Collection: "Apparatus and methods of measuring radiation," Ed. 2, Moscow, Atomizdat, 1960, p.7.
4. E. E. Kovalev, D. P. Osanov. Biofizika 6, No. 5, 630 (1960).
5. E. E. Kovalev, V. I. Popov. Apparatus and technique of experimentation [in Russian] No. 3, 63 (1959).
6. Radium Dosage. The Manchester System, Livingstone Ltd. Edinburg, 1947.

MEASUREMENTS OF THE SPECTRA AND TEMPERATURE OF THE NEUTRON GAS IN A GRAPHITE-WATER REACTOR

E. Ya. Doil'nitsyn and A. G. Novikov

Translated from Atomnaya Énergiya, Vol. 10, No. 5,
pp. 517-519, May, 1961
Original article submitted January 17, 1961

Knowing the spectra of thermal neutrons established in different moderators is a matter of fundamental importance when making calculations on reactors which use the moderators in question. This paper describes the experimental measurement of the spectra of the thermal neutrons in a graphite-water reactor at different graphite temperatures from 300 to 800°K. A comparison is made between the temperature of the neutron gas and the temperature of the graphite.

The spectral measurements were made with a mechnical neutron selector having a 256-channel time analyzer. The neutron energy range was 1-0.015 ev. The neutron beam was taken from the graphite edge of the active zone through a special 50-mm diameter test hole. In the measurements we used a mechanical chopper, [1] with a pertinax rotor and a one-slit collimator which passed neutrons coming only from the central part of the surface emitting the beam. The measurements were made at a chopper speed of 1500 rpm with a flight distance of 7 m. The resolution of the selector was 15 microseconds per meter; the width of the analyzer channel was 32 microseconds. The corrections of distortion of the spectrum at this resolution were insignificant. At an energy of 0.025 ev the correction to the transmission function was 7.5%. The neutron detector had an efficiency of about 8%. The background in the selector was 2-3% of the total effect. Corrections for the geometrical conditions of the experiment amounted principally to the distortion of the beam spectrum from absorbtion of thermal neutrons by the nitrogen of the air in the path of the beam, which amounted to 12 meters. Since the effective neutron scattering cross section of the graphite is independent of energy in the range of the experiment and the diameter of the test hole is small, it may be assumed that the spectrum of the neutrons in the beam is the same as the spectrum in the reactor.

Figure 1 shows the neutron spectrum at 0.05% reactor power. Within the accuracy of the experiment, the spectrum of thermal neutrons in the region from 0.1 ev to the lower limit of measurement corresponded with the Maxwellian distribution in all measurements both on the cold as well as the strongly heated graphite at 70% reactor power.

The temperature of the neutron gas was determined from the results of the spectral measurements as well as by the boron-filter method. Figure 2 gives the results of these measurements at 0.05, 15, 20, 50 and 70% reactor power. The difference between the temperature of the neutron gas and the temperature of the moderator found in our measurements can be described by the expression

$$T_N - T_{GR} = 0{,}8T_{GR}^{0{,}72}. \quad (1)$$

Within the limits of accuracy of the measurements over the range 300-800°K, Eq. (1) is in satisfactory agreement with the equation found in [2]:

$$\frac{T_N - T_{GR}}{T_{GR}} = C\frac{\sum_a}{\xi\sum_s}, \quad (2)$$

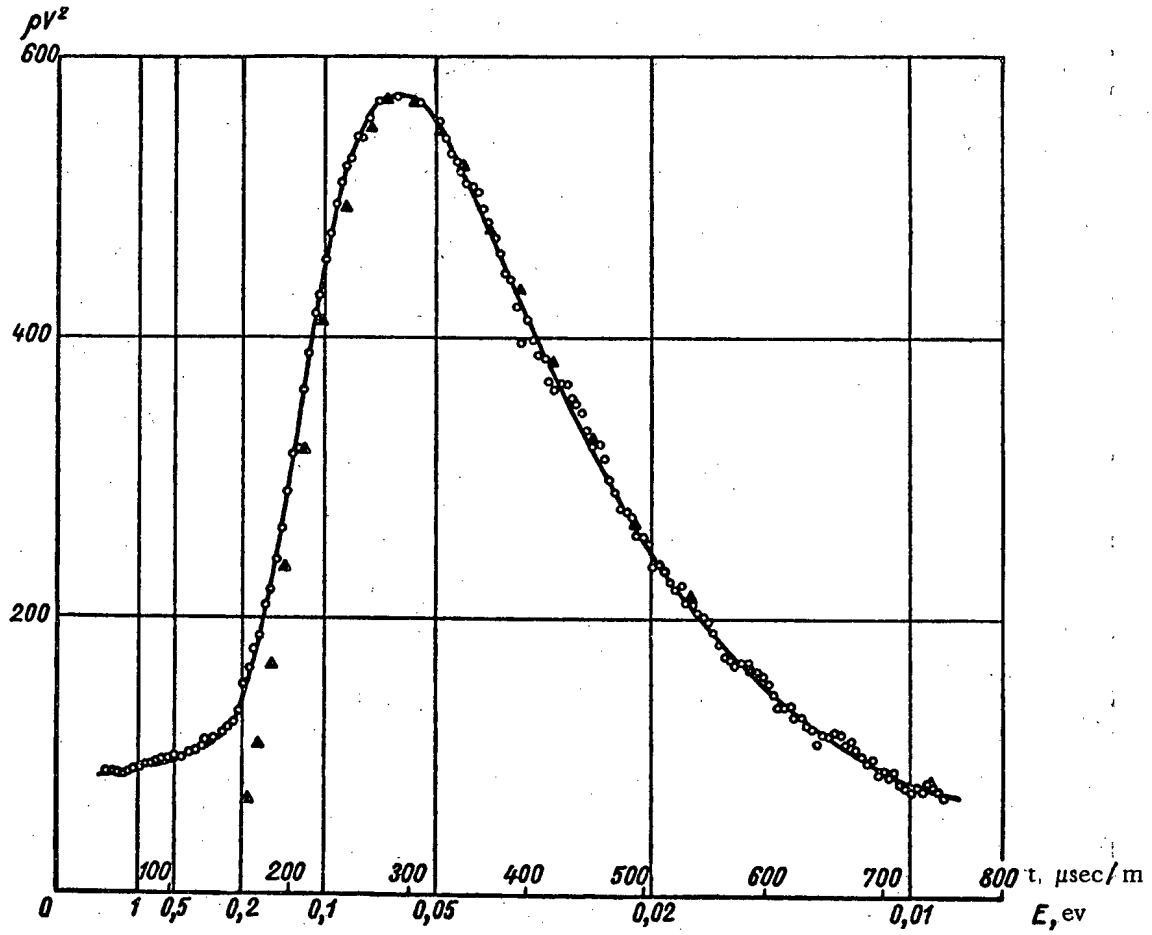

Fig. 1. Neutron spectrum at 0.05% reactor power: O-experimental data; ▲-Maxwellian distribution at a temperature of 350°K.

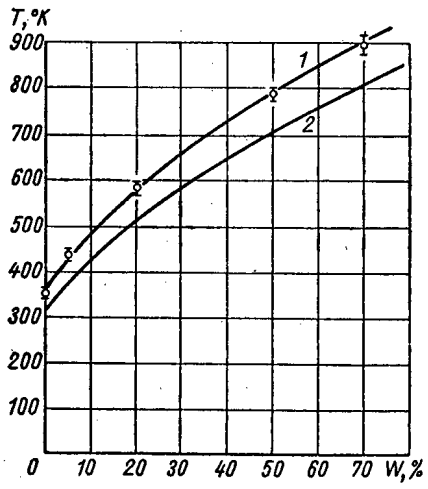

Fig. 2. Temperature of the neutron gas, T_n (curve 1), and the temperature of the graphite layer, T_{gr} (curve 2), as a function of reactor power.

where $\frac{\Sigma_a}{\xi\Sigma_s}$ is the ratio of absorbtion to moderation in the medium.

The calculations from the data of [3] give low values for the temperature of the neutron gas as compared with our experimental data.

LITERATURE CITED

1. V. V. Vladimirskii, V. V. Sokolovskii. Transactions of the Second International Conference on the Peaceful Uses of Atomic Energy [in Russian] (Geneva, 1958). Reports of Soviet Scientists, Vol. 1, Moscow Atomizdat, 1959, p. 520.
2. E. Koén. Materials from the International Conference on the peaceful uses of atomic energy (Geneva, 1955) [in Russian], Vol. 5, Moscow, Academy of Sciences Press, U.S.S.R., 1958, p. 487.
3. G. Leibfried. Nucl. Sci. Engng, 4, No. 4, 570 (1958).

PLOTTING OF ENTROPY DIAGRAMS BY USING EXPERIMENTAL DATA ON THE VELOCITY OF SOUND.

I. I. Novikov and Yu. S. Trelin

Translated from Atomnaya Énergiya, Vol. 10, No. 5,
pp. 519-521, May, 1961
Original article submitted February 6, 1961

Thermodynamic diagrams and coolant tables are necessary for reactor thermal calculations.

The existing methods for calculating and plotting thermodynamic diagrams are based on the use of experimental data on the compressibility and specific heat of coolants or of data on their specific heat and the adiabatic throttling effect. These calculation methods are cumbersome and, in many cases, also insufficiently accurate, especially near the saturation curve and in and beyond the critical regions. This is connected with the fact that there are virtually no detailed experimental data on the specific heat and adiabatic throttling for the majority of materials.

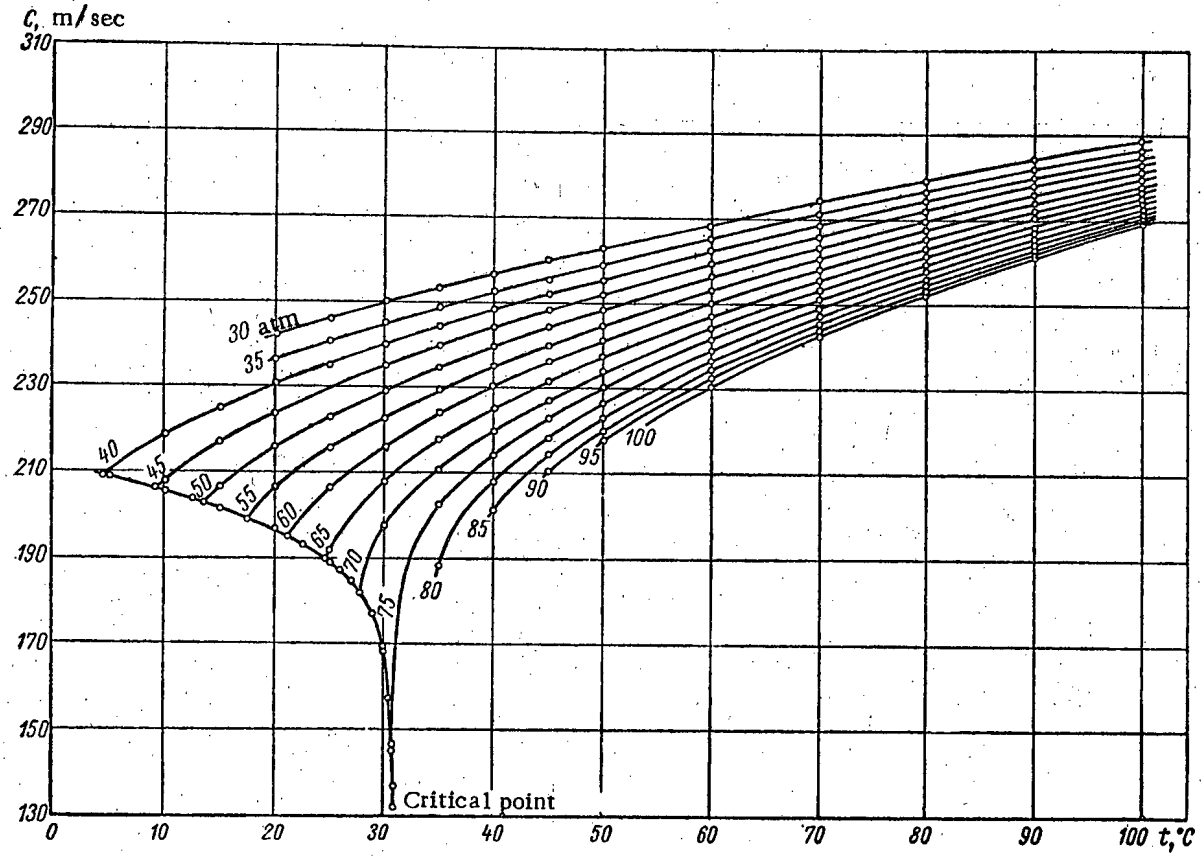

Fig. 1. Velocity of sound in superheated and saturated CO_2 vapors.

The authors of the present article have developed a new method for plotting entropy diagrams. This method is based on utilizing experimental data on the velocity of sound-propagation in the coolant, whereby accurate diagrams of this type can be quickly produced.

The essence of the method consists in the following.

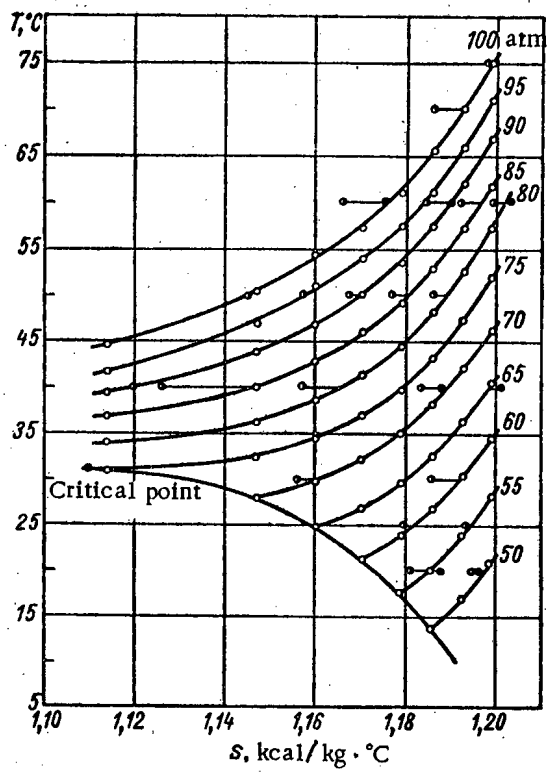

Fig. 2. T vs s diagram for CO_2, which was plotted by using data on the velocity of sound. O) Data calculated with respect to the velocity of sound; ●) theoretical data borrowed from D. D. Kalafata and L. Z. Rumshiskii; O) theoretical data borrowed from Katkhe.

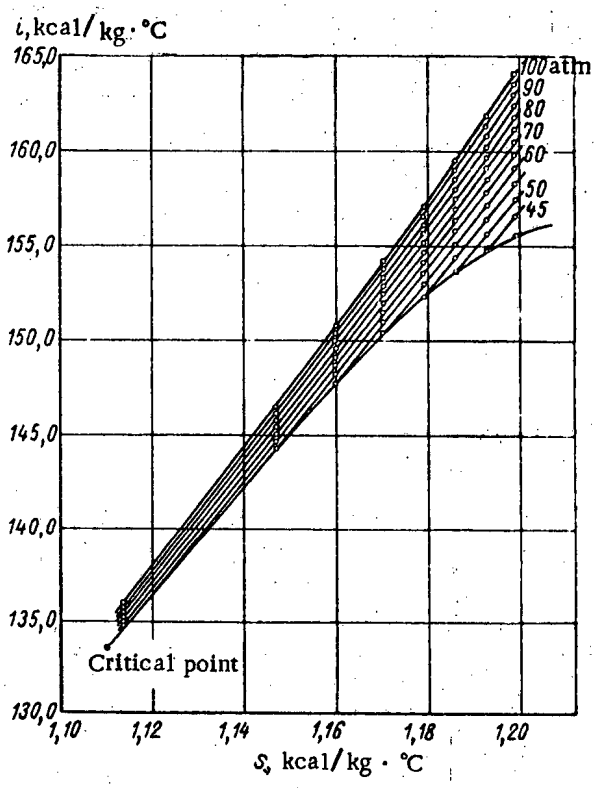

Fig. 3. Diagram of i vs s curves for CO_2, which was plotted with respect to data on the velocity of sound.

As is known, the propagation of sound waves in a substance is accompanied by an isentropic change in the state of the substance, due to which the velocity of sound is given by

$$c = \sqrt{-gv^2\left(\frac{\partial p}{\partial v}\right)_s}. \qquad (1)$$

After measuring the velocity of sound and having data on the compressibility of the substance, the value of the partial derivative $(\partial p/\partial v)_s$ can readily be calculated:

$$\left(\frac{\partial p}{\partial v}\right)_s = -\frac{c^2}{gv^2}; \qquad (2)$$

correspondingly, the relationships between changes in volume and pressure and enthalpy for s = const are given by

$$\Delta v = \left(\frac{\partial v}{\partial p}\right)_s \Delta p; \qquad (3)$$

$$\Delta i = v\Delta p. \qquad (4)$$

By means of these expressions and by using the experimentally found values of the derivative $(\partial v/\partial p)_s$, we can calculate the changes in specific volume and enthalpy for a given pressure variation along any of the isentropic curves, and, consequently, determine the v, i, and p values at each point of the isentropic curve. This makes it possible to plot isentropic diagrams by using the experimental data directly, which was not possible before when other methods were used, since the isentropic parameters were in those cases determined by calculation with respect to the initial data (for instance, with respect to compressibility and specific heat).

Considering that, as a result of the advances made in measurement techniques, the measurement of the velocity of sound in a wide range of pressures and temperatures is presently a relatively simple problem in comparison with the determination of specific heat and that it can be performed with a high degree of accuracy (within 0.1-0.3%), while the compressibility of substances can be determined experimentally with an even greater accuracy, it is clear that the proposed method has considerable advantages in comparison with other methods from the point of view of accuracy. The velocity of sound is measured at such frequencies that the dispersion effect is not pronounced. The accuracy of the diagrams can be judged by comparing the measured sound-velocity values with those calculated with respect to the available thermodynamic tables and diagrams.

For plotting of T vs s and i vs s diagrams, it is necessary to know the entropy and the enthalpy values for the liquid and gaseous phases on the saturation curve. These values are known with a high degree of accuracy for almost all substances.

In order to determine the advantages and disadvantages of the new method, we plotted entropy diagrams for CO_2. For this, we first measured the velocity of sound in CO_2 on the saturation curve and in superheated vapor [1 and 2].

The measurements were performed in the pressure region from 4 to 100 atm and in the temperature region from 5 to 100°C at ultrasound frequencies of 500 and 1500 kc. The subsequent analysis of the measurement results made it possible to establish the dependence of the velocity of sound on frequency, which was valid only at pressures below 30 atm for superheated and saturated vapors and a frequency of 500 kc. The results of sound measurements are given in Fig. 1, which shows the isobaths of the thermodynamic (i.e., in the absence of dispersion) velocity of sound. The measurement accuracy was 0.25%.

The entropy and enthalpy values on the saturation curve were borrowed from [3], and the density values were borrowed from [4-6].

The parameters for each subsequent point of the isentropic curve were calculated according to the initial-point parameters by using the method of successive approximations. In this, the relative error of volume calculations did not exceed 0.7%, while the specific heat error did not exceed 0.03%. Figures 2 and 3 shows the T vs s and i vs s diagrams which we plotted. A comparison between these diagrams and the available diagrams (data borrowed from D. D. Kalafata and L. Z. Rumshiskii [7]), which were obtained by calculation with respect to compressibility data, indicates that the greatest discrepancy is found near the critical point; it attains 2-3% on the T vs s diagram and 5-7% on the i vs s diagram. The entropy diagrams thus plotted proved that the proposed new method involves very simple mathematical operations and that it secures highly accurate diagrams. The comparative simplicity with which the initial experimental data can be obtained promises that this method of plotting entropy diagrams will be successfully used in practice.

LITERATURE CITED

1. I. I. Novikov and Yu. S. Trelin, Zhurnal Prikladnoi Mekhaniki i Tekhnicheskoi Fiziki, No. 2, 112 (1960). Siberian Branch, Academy of Sciences, USSR.
2. Yu. S. Trelin, Collection: Ultrasound Application in the Investigation of Matter [in Russian] (Moscow Regional Pedagogical Institute, Moscow, 1961) Vol. 13, p. 123.
3. R. Plank and J. Kuprianoff, Zs. Techn. Phys., 3, 93 (1929).
4. A. Michels and C. Michels, Proc. Roy. Soc., 153A, 201 (1936).
5. A. Michels, C. Michels, and B. Blaisse, Proc. Roy. Soc., 160A, 358 (1937).
6. K. MacCormack, W. Schneider. J. Chem. Phys., 18, 1269 (1950).
7. Thermophysical Properties of Matter [in Russian] (Gosénergoizdat, Moscow, 1956), p. 42; ed. by N.B.Vargaftik.

All abbreviations of periodicals in the above bibliography are letter-by-letter transliterations of the abbreviations as given in the original Russian journal. *Some or all of this periodical literature may well be available in English translation.* A complete list of the cover-to-cover English translations appears at the back of this issue.

STEADY-STATE BOILING OF VOLUME-HEATED LIQUIDS

V. K. Zavoiskii

Translated from Atomnaya Énergiya, Vol. 10, No. 5,
pp. 521-523, May, 1961
Original article submitted September 1, 1960

The present article describes some regularities in the boiling of volume-heated liquids, which takes place when the heat sources are continuously distributed throughout the liquid volume.

In a previous paper [1], it was shown that under steady-state boiling conditions, the radius of a moving vapor bubble is determined by the expression

$$R=(kau)^{1/3}\left(\frac{c\gamma'}{r\gamma''}\Delta Tt\right)^{2/3}, \tag{1}$$

where k is a constant coefficient, γ', c, and a are the density, specific heat, and the diffusivity coefficient of the liquid, respectively, r is the vapor generation heat, γ'' is the vapor density, u is the relative bubble velocity in the liquid, ΔT is the overheating, i.e., the difference between the liquid temperature and the vapor temperature, and t is the time during which the bubble dwells inside the boiling liquid. This equation was derived under the assumption that the velocity with which the bubbles move and the liquid over-heating are constant.

It follows from Eq. (1) that the rate of growth of the moving bubble is mainly determined by the rate at which heat is supplied to it by convection.

We shall use expression (1) for determining the distribution of vapor bubbles with respect to their dimensions. If we consider intensive boiling, for which the motion speed of the liquid considerably exceeds the speed with which the bubbles rise in a stationary liquid, we can introduce a certain average time τ during which the bubble dwells in the liquid. Under these conditions, the value of τ will be independent of the bubble's "age" and, consequently, of its dimensions, since the displacement velocity of the bubbles will be mainly determined by the speed with which the liquid moves.

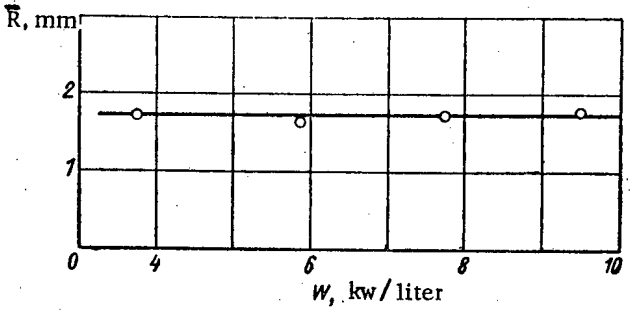

Fig. 1. Dependence of the average vapor-bubble radius on specific power.

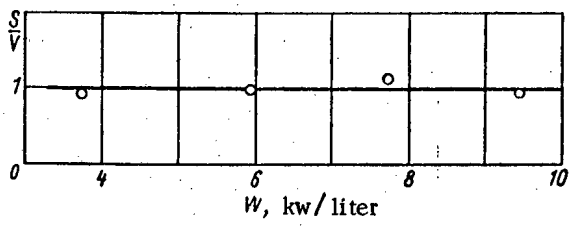

Fig. 2. Dependence of the ratio of the total phase boundary surface to the total vapor volume on specific power.

Lt P(t) be the probability that the bubble will not leave the liquid volume during the time t. If we assume that the bubbles are generated with equal probability at any instant of time, then the probability that there will be in the liquid a bubble whose age will be in the interval from t to t + dt will be equal to

$$P(t)\,dt=\frac{1}{\tau}e^{-\frac{t}{\tau}}dt, \tag{2}$$

while

$$\int_0^\infty P(t)\,dt = 1.$$

In this, the processes of fragmentation and combination of bubbles are not taken into account. Equation (2) expresses the distribution of vapor bubbles with respect to age. We shall now find the distribution of bubbles with respect to size. For this, we shall substitute the bubble radius R for the independent variable t. Let $f(R)$ be the function expressing the distribution of bubbles with respect to the radius. If the radius element dR corresponds to the above-considered time element dt, we have

$$f(R)dR = P(t)\,dt, \tag{3}$$

Hence, by taking into account expressions (1) and (2), we obtain

$$f(R)\,dR = {}^3/_2 \alpha R^{1/2} e^{-\alpha R^{3/2}}\,dR, \tag{4}$$

where

$$\alpha = \frac{1}{\tau}\left(\frac{1}{kau}\right)^{1/2}\left(\frac{r\gamma''}{c\gamma'}\right)\frac{1}{\Delta T}. \tag{5}$$

From expression (4), considering that α = const (according to the above-mentioned paper), we find the value of the most probable bubble radius:

$$R_{\text{prob}} = \left(\frac{1}{3\alpha}\right)^{2/3}. \tag{6}$$

Let us introduce the new variable

$$x = \frac{R}{R_{\text{prob}}}. \tag{7}$$

Expression (4) will then assume the following form:

$$f(x)\,dx = {}^1/_2 x^{1/2} e^{-1/3 x^{3/2}}\,dx, \tag{8}$$

while

$$\int_0^\infty f(x)dx = 1.$$

Hence, it is obvious that the function of the distribution of vapor bubbles with respect to size is completely defined if the most probable bubble radius is known.

Let us now determine the ratio of the average bubble radius to the most probable radius:

$$\frac{\overline{R}}{R_{\text{prob}}} = \bar{x} = 3^{2/3}\Gamma\left(1+\frac{2}{3}\right) \simeq 1{,}87, \tag{9}$$

where $\Gamma\left(1+\frac{2}{3}\right)$ is the γ-function.

Let us find the ratio of the total surface of vapor bubbles to their total volume:

$$\frac{S}{V}=\frac{4\pi\overline{R^2}n}{{}^4/_3\pi\overline{R^3}n},$$

where n is the number of bubbles in the liquid. By taking into account expressions (7) and (8), we obtain

$$\frac{S}{V}=\frac{3}{R_{\text{prob}}}\frac{\overline{x^2}}{\overline{x^3}}=\frac{0{,}72\Gamma\left(1+\frac{4}{3}\right)}{R_{\text{prob}}}$$

or

$$\frac{S}{V}\simeq\frac{0{,}86}{R_{\text{prob}}}. \tag{10}$$

The experimental verification of the obtained relationships was performed by means of the device described in the above-mentioned paper. Water in a rectangular glass vessel was heated under atmospheric pressure by transmitting an electric current through it. The water volume was from 2 to 3 liters, and the power supply varied approximately from 4 to 10 kw/liter. The longitudinal and transverse dimensions of the bubbles which were located in the visible portion of the boiling liquid volume were measured on photographs which were taken through the front wall of the vessel. The volume of each bubble as an ellipsoid of rotation and the radius of the equivalent sphere were then calculated.

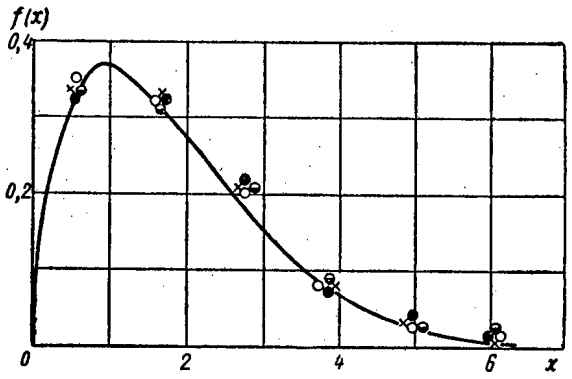

Fig. 3. Distribution of vapor bubbles with respect to size for different boiling powers (kw/liter): ⊜ – 3.8; × – 5.9; O – 7.7; ● – 9.5.

The average vapor-bubble radius was calculated with respect to the measurement data for the power interval under investigation, and a straight line was drawn through the obtained points by using the method of least squares (Fig.1). It is obvious from the figure that, under these experimental conditions, the average radius is independent of the power applied; it is approximately equal to 1.7 mm. By substituting this value in expression (9), we obtain the value of the most probable bubble radius, which is equal to 0.9 mm.

After this, the surface of each measured bubble was calculated, and the ratio of the total phase boundary surface to the total vapor volume was found (Fig.2). It appeared that, in steady-state boiling, this ratio does not depend on the power applied, and that it is approximately equal to 1.0. By using expression (10), we find $R_{\text{prob}} \simeq$ 0.86 mm, which, within the limits of experimental errors, coincides with the probable radius value which was calculated above with respect to the average radius.

Figure 3 shows the experimental distribution of vapor bubbles with respect to size. The curve corresponds to expression (8), while the R_{prob} value was assumed to be equal to 0.9 mm. It is obvious from the figure that, in steady-state boiling, the distribution of bubbles with respect to size virtually does not change with an increase in the power supply.

LITERATURE CITED

1. V. K. Zavoiskii, Atomnaya Énergiya, 10, No. 3, p. 272 (1961).

CRITICAL THERMAL LOADS IN FORCED MOTION OF WATER WHICH IS HEATED TO A TEMPERATURE BELOW THE SATURATION TEMPERATURE

D. A. Labuntsov

Translated from Atomnaya Énergiya, Vol. 10, No. 5,
pp. 523-525, May, 1961
Original article submitted April 8, 1960

One of the possible methods for increasing the heat output of reactors consists in intensifying the heat exchange in the reactor core. However, there are limiting heat-flux densities, the so-called critical thermal loads, which arise when underheated (with respect to the saturation temperature) water or a water-vapor mixture moves through the operating channels of a heterogeneous reactor. For underheated water flows, the critical thermal loads are equal to several millions and sometimes tens of millions of kcal/m^2·hr.

List of Papers Used and the Basic Characteristics

Literature cited	Pressure, atm abs	Range of velocity changes, m/sec	Range of underheating variations, deg C	$q_{cr} \cdot 10^{-6}$ kcal/m^{2}hr
[8] *	1; 3; 5; 9	0,85—5,5	—	1,6—4,8
[7]	1	0,7—3	0—15	1,5—3,6
[4]	1—22	1,5—8	14—165	3,7—15,5
[13]	35	3,6—45	0—201	3,7—45
[9]	21; 41; 81; 110; 140; 180; 200	1—8	0—240	1—11
[1, 10] **	100; 170	1—3,5	0—80	2—10
[11, 12] **	141; 160; 180; 201	1,5—8	0—80	1—5,5

*Experiments characterized by very low vapor and water-vapor mixture content.
**Only selected characteristic experimental points were used.

When the critical load is attained, a practically instantaneous drop in heat transfer (crisis) takes place. The temperature of the heat-releasing surface increases and reaches values that are inadmissible from the point of view of thermal stability and strength conditions.

The essence of the heat transfer crisis in forced motion of an underheated liquid consists in the transition from the regime of bubble boiling in the near-wall boundary layer to the film-boilingregime, which is characterized by a very low intensity of heat transfer.

At the present time, a considerable amount of experimental data on critical thermal loads in water and water-vapor mixtures are available. The obtained data indicate that critical thermal loads are determined (at least in the first approximation) by the pressure, velocity, and the magnitude of under-heating at the crisis cross section; they are virtually independent of the length, diameter, and configuration of the operating channel [1-3]. The effect of channel dimensions becomes pronounced only for diameters that are less than 2 mm.

However, theoretical dependences of the critical thermal loads which would be valid for the entire range in which the basic parameters change are not yet available. The equations given in [3-5] pertain only to the low-pressure region (1-22 atm abs) or to the high-pressure region (140-210 atm abs), and they cannot be used for extrapolation for the intermediate region.

Considerable difficulties are encountered in attempting to derive a generalized formula by using similarity-theory methods due to the unavailability of a rational physical model of the process. This situation is also aggravated by the fact that there are almost no experimental data on critical loads in other liquids besides water. Some data [6] indicate that organic liquids are totally unsuitable for experimental investigations of the heat-transfer crisis, since their thermic decomposition starts in the neighbourhood of the critical regimes.

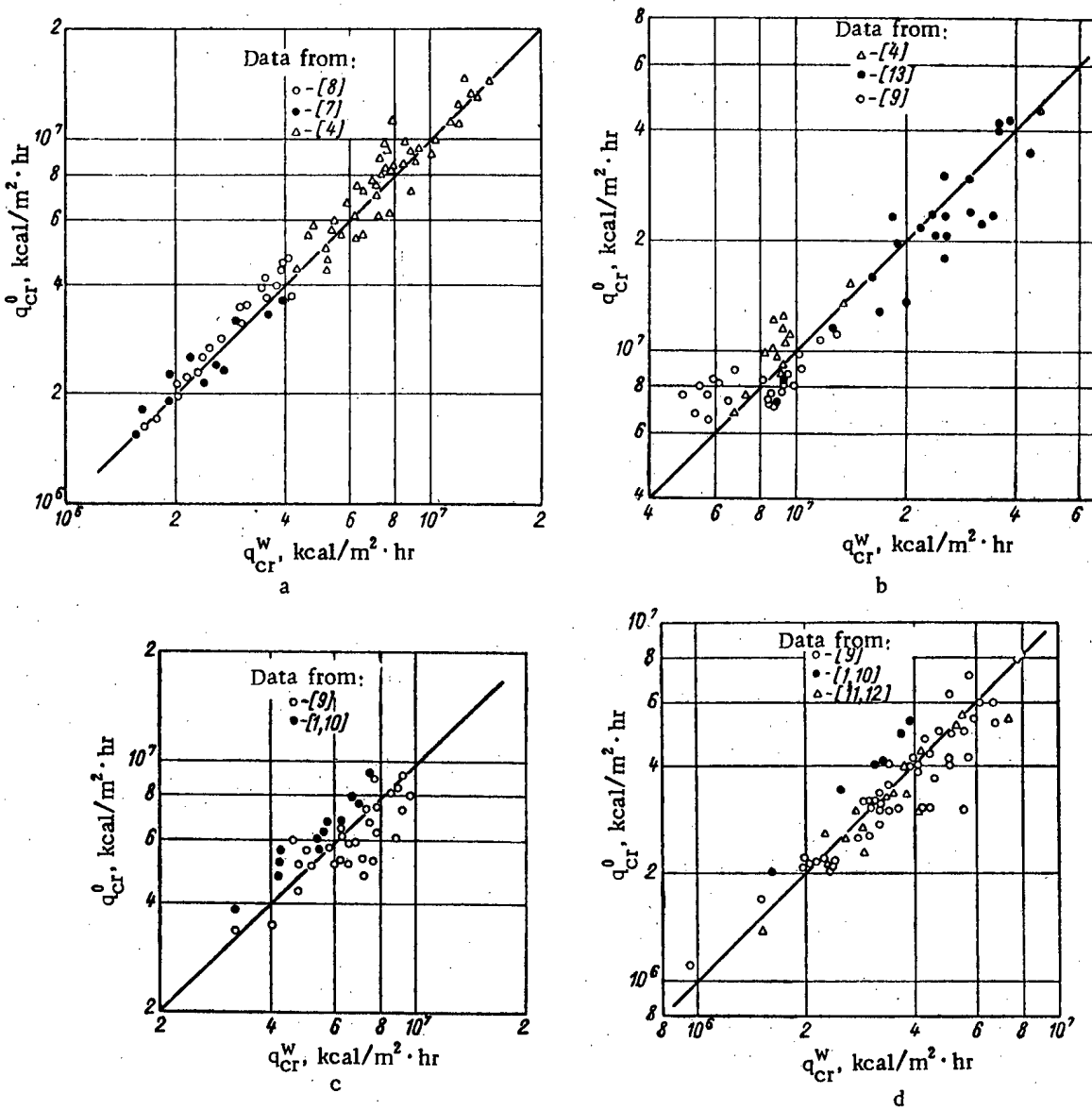

Comparison between critical loads q^w_{cr} in water that were calculated by using Eq. (2) and the experimental q^o_{cr} values for pressures equal to (atm abs): a) 1 – 10; b) 10 – 50; c) 50 – 120; d) 120 – 200.

The aim of the present paper is to find a single empirical formula for critical thermal loads that arise in the motion of underheated water and water-vapor mixtures with zero vapor content which would describe the known experimental data in the entire investigated range in which the determining quantities vary. The results obtained in the papers listed in the table were used for this purpose. The analysis of experimental data was performed on the basis of the following general functional dependence:

$$q_{cr} = f(w, p, \Delta t_{und}), \tag{1}$$

where w is the velocity of water (m/sec), p is the pressure (atm abs), and $\Delta t_{und} = t_s - t_l$ (°C) is the difference between the actual temperature and the saturation temperature. All values were reduced to the cross sections at the location where crisis arises. Since the heat transfer crisis represents to a certain extent a statistical process, the existing data are often characterized by a considerable spread.

A systematic determination of the effect of individual factors in the functional dependence (1) finally yielded the following formula:

$$q_{cr} = 1{,}25 \cdot 10^6 \varphi(p) \sqrt[4]{1 + \frac{2{,}5}{\varphi(p)} w^2 \theta(\Delta t_{und})} \text{ kcal/m}^2 \cdot \text{hr} \tag{2}$$

Here,

$$\varphi(p)=p^{1/3}\left(1-\frac{p}{p_{cr}}\right)^{4/3};$$

$$\theta(\Delta t_{und})=1+\frac{15}{\sqrt{p}}\frac{c_p}{r}\Delta t_{und}$$

where c_p and r are the specific heat of water and the vapor-generation heat on the saturation line at the water pressure, respectively.

The figure provides a comparison between the critical loads for water (q_{cr}^{w}) which were calculated according to this formula for different pressures and the experimental values q_{cr}^{o}.

In conclusion, it must be emphasized that the formula (2) for determining critical loads is applicable only in the range of the determining parameters that were used in the above experiments (see table). Extrapolation for the regions outside these limits must be performed with caution.

LITERATURE CITED

1. V. E. Doroshchuk and F. P. Frid, Teploénergetika, No. 9, 74 (1959).
2. B. A. Zenkevich, Atomnaya Énergiya, 4, No. 1, 74 (1958).
3. B. A. Zenkevich and V. I. Subbotin, Atomnaya Énergiya, 3, No. 8, 149 (1957).
4. V. S. Chirkin and V. P. Yukin, Zh. Tekhn. Fiz., No. 7, 1542 (1956).
5. S. S. Kutateladze and M. A. Styrikovich, Hydrodynamics of Gas-Liquid Systems [in Russian] (Gosénergoizdat, Moscow, 1958).
6. P. I. Povarnin, Collection: Investigations of Heat Transfer to Vapor and Water Which Boils in Tubes under High Pressures [in Russian] (Atomizdat, Moscow, 1958), p. 150; ed. by N. A. Dollezhal'.
7. S. S. Kutateladze and V. M. Borishanskii, Énergomashinostroenie, No. 2, 10 (1958).
8. E. K. Averin and G. N. Kruzhilin, Collection: Heat Transfer and Thermal Simulation [in Russian] (Izd-vo SSSR, Moscow, 1959), p. 239.
9. I. T. Alad'ev and L. D. Dodonov, Collection: Convective and Radiant Heat Transfer [in Russian] (Izd-vo AN SSSR, Moscow, 1960), p. 65.
10. V. E. Doroshchuk and F. P. Frid, Collection: Heat Exchange under High-Load and Other Special Conditions [in Russian] (Gosénergoizdat, Moscow, 1959), p. 23; ed. by A. A. Armand.
11. V. I. Subbotin et al., Collection: Investigations of Heat Transfer to Vapor and Water Which Boils in Tubes under High Pressures [in Russian] (Atomizdat, Moscow, 1958), p. 95; ed. by N. A. Dollezhal'.
12. V. I. Subbotin et al., Collection: Investigations of Heat Transfer to Vapor and Water Which Boils in Tubes under High Pressures (in Russian] (Atomizdat, Moscow, 1958), p. 120; ed. by N. A. Dollezhal'.
13. P. I. Povarnin and S. T. Semenov, Teploénergetika, No. 4, 72 (1959).

All abbreviations of periodicals in the above bibliography are letter-by-letter transliterations of the abbreviations as given in the original Russian journal. *Some or all of this periodical literature may well be available in English translation.* A complete list of the cover-to-cover English translations appears at the back of this issue.

INVESTIGATION OF METAL CORROSION IN THE EXPERIMENTAL CHANNEL OF THE IRT REACTOR

A. V. Byalobzheskii and V. D. Val'kov

Translated from Atomnaya Énergiya, Vol. 10, No. 5,
pp. 525-528, May, 1961
Original article submitted October 29, 1960

The behavior of corrosion pairs Zr – Al, Zr – Fe, and Fe – Al* in a 0.05 N NaCl solution for a thermal neutron flux of ~ 2×10^{12} neutrons/cm^2·sec was investigated in the IRT reactor of the I. V. Kurchatov Order of Lenin Institute of Atomic Energy [1].

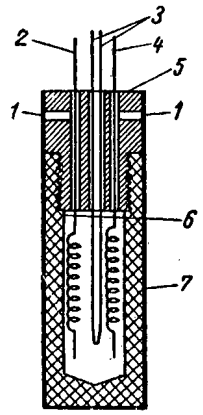

Fig. 1. Working cell. 1) Screws (zirconium); 2 and 4) specimens; 3) thermocouple (copper-constantan; coating: thin polystyrene layer); 5) plug (polystyrene); 6) electrolyte level; 7) frame (polystyrene).

The method of corrosion pairs was chosen because it made it possible to observe the behavior of metallic electrodes directly in the process of their irradiation in the reactor.

The investigations were performed in a cell, the diagram of which is shown in Fig. 1. The specimens were made of wire in the shape of spirals, and they all had an equal surface area, which was 3.5 cm^2. The specimens were degreased in acetone and were etched in special etching agents.** The specimens were then fastened in plug 5 by means of screws 1. The electrolyte in the amount of 3.5 cm^3 was then poured inside the frame 7 of the cell, and the plug was screwed in. The aluminum contact conductors, which were connected to specimens 2 and 4, formed a closed circuit through a sensitive microammeter. After the pair current assumed a steady-state value I_{st}, the cell was lowered into the channel, and the pair current was measured. The temperature of the electrolyte in the cell was simultaneously controlled by means of thermocouple 3. In order to determine the temperature effect, control experiments without irradiation were performed. In these cases, the working cell was placed in a thermostatically controlled device, where the heating conditions prevalent in the reactor were accurately reproduced.

Figure 3 shows the current density curves for the pairs under investigation in the reactor (curves 1, 2, and 3) and in the control experiments (dotted curve 1', 2', and 3'). The diagram also shows curves that indicate the character of the electrolyte heating in lowering the cell into the reactor (curve 4) and of the electrolyte cooling in withdrawing the cell from the reactor (curve 4'). The heating and cooling in the control experiments were performed in correspondence with these data.

In individual experiments, after the current attained the I_r value, which corresponded to the horizontal portion, the cell was kept in the reactor over a period of approximately 1.5 hr; in this, the I_r value did not change. Thus, it could be considered that I_r was the steady-state current density of a given corrosion pair in the reactor. In order to reduce the induced activity in the cell, the experiment duration was set at 20 min (the time necessary for attaining I_r).

A comparison between curves 1 and 3 and curves 1' and 3' indicates that the characteristics of the increase and decrease in the pair current were equal in the working and the control experiments. This indicates that the increase in the electrolyte temperature as a result of the absorption of radiation energy in the electrolyte is the basic factor determining the pair-current increase in the reactor. A comparison between the I_{st} and I_r values and similar indices that were obtained in the control experiments, which is given in the table, confirms this conclusion. It follows from the table that, for Zr – Fe and Fe – Al, a well-defined increase in the current density in the reactor (I_r) in comparison with the current density I_c that was obtained in control experiments could be observed. This difference is

*The metals mentioned first were used as cathodes.

** The etching agent composition was: for zirconium, concentrated HNO_3 (45 cm^3), concentrated HF (5 cm^3), and H_2O (45 cm^3); for aluminum, NaOH (10%), HNO_3 (30%); for iron, concentrated HCl.

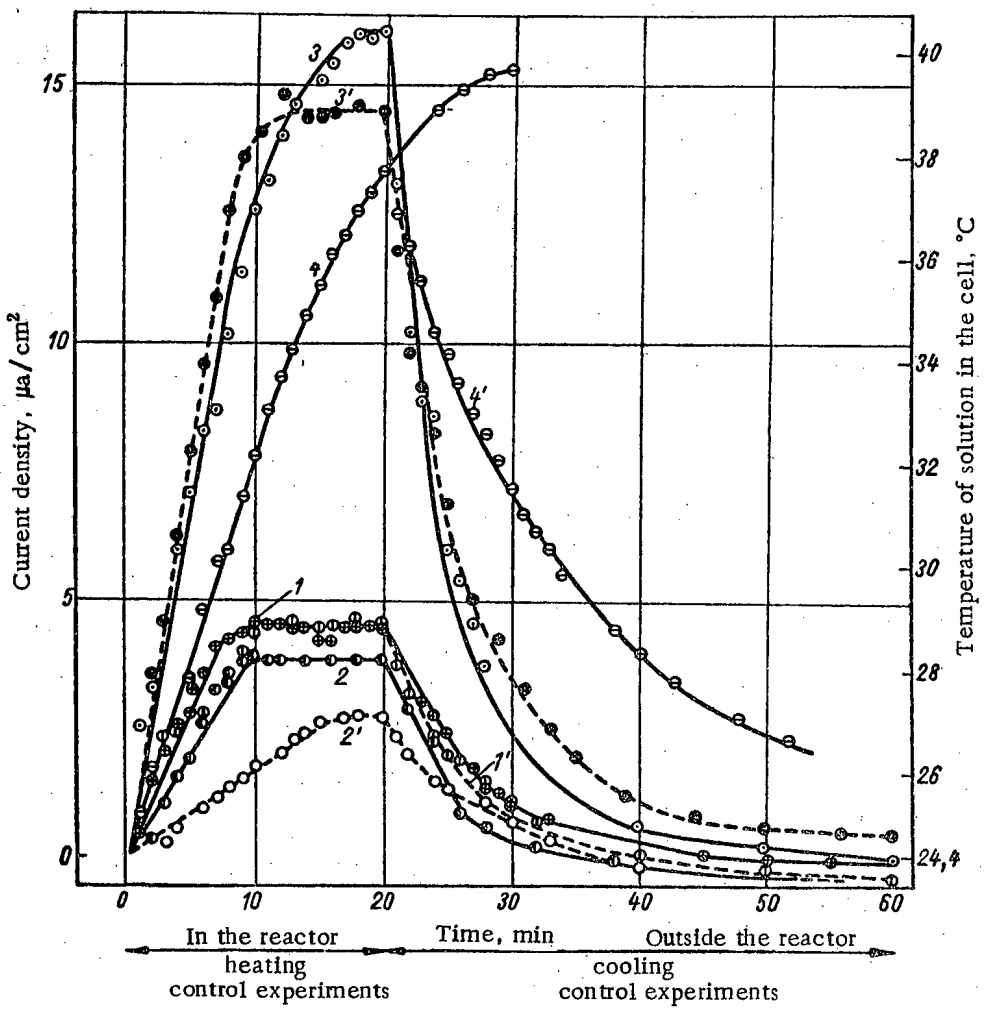

Fig. 2. Dependences of changes in the corrosion pair-current density and in the electrolyte temperature on the cell exposure time in the reactor and in the thermostat: 1) Zr–Al; 2) Zr–Fe; 3) Fe–Al. 1') Zr–Al; 2') Zr–Fe; 3') Fe–Al.

Comparative Data on the Behavior of Corrosion Pairs in the Experimental IRT Reactor and in Control Experiments Simulating the Reactor Temperature Conditions.

Corrosion pairs	Reactor experiments			Control experiments		
	Current density, μ a/cm²			Current density, μ a/cm²		
	Before insertion in the reactor (I_{st})	In the reactor (I_r)	Relative increase in the pair current density (I_r/I_{st})	at T_0 = 24.4°C ($I_{st\ c}$)	at T_c = 37.75°C (I_c)	Relative increase in the pair current density ($I_c/I_{st\ c}$)
Zr–Al	1.90	6.40	3.37	2.23	6.84	3.06
Zr–Fe	1.36	5.19	3.78	1.39	3.94	2.84
Fe–Al	13.48	29.60	2.22	13.91	27.41	1.97

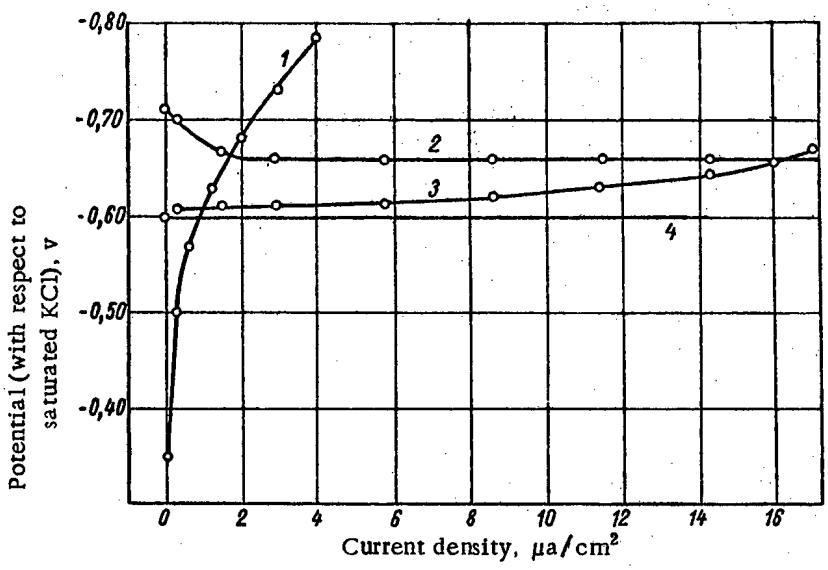

Fig. 3. Curves of the cathode and anode polarization of metals in 0.05 N NaCl at 25° C. 1) Cathode polarization of zirconium; 2) anode polarization of aluminum; 3) cathode polarization of iron; 4) anode polarization of iron.

especially noticeable in the case of the Zr–Fe pair. The kinetic curves for this pair (see Fig. 2) also show a considerable difference between the characteristics of the pair current density variation in the reactor (curve 2) and in the control experiment (curve 2'). The difference between the behavior of pairs is due to the action of water-radiolysis products, which can act as effective cathode and anode depolarizers in electrochemical processes [2].

Figure 3, which shows the obtained polarization curves for electrodes consisting of corrosion pairs, indicates that for all pairs the cathode reaction rate is the decisive factor. Consequently, the increase in the pair current density due to the water-radiolysis products can be caused only by their cathode-depolarizing action. In the radiolysis of aqueous solutions, OH and HO_2 radicals among the short-lived products and hydrogen peroxide among the long-lived products act as cathode depolarizers. Since the ionizing radiation intensity in the experimental channel of the IRT reactor is comparatively low and, consequently, the amount of radiolysis products that are formed in the near-electrode diffusion layer is small, the direct action of these products should not greatly affect the increase in the pair current density, while, against the background of the intensifying action of the temperature factor, this action may be not detected at all, which happened in the case of the Zr–Al pair.

However, such an action of radiolysis products occurs only in the case where the solution does not contain readily oxidizable substances, which, in their oxidized state, can play the role of vigorous cathode depolarizers. Such substances, if they are sufficiently stable, can act as accumulators of the oxidizing properties of the water-radiolysis products. In this case, the utilization factor of the water-radiolysis oxidizing component for cathode depolarization will obviously sharply increase (although not directly, but through the intermediate oxidation reaction of the additional reagent). This situation is actually encountered in the operation of the Zr–Fe pair. In this pair, iron represents the anode, and it passes into the solution in the form of bivalent ions:

$$Fe \longrightarrow Fe^{2+} + 2\bar{e}. \qquad (1)$$

As a result of interaction with the radiolysis products, Fe^{2+} is transformed into Fe^{3+}:

$$\left.\begin{aligned} &Fe^{2+} + OH \longrightarrow Fe^{3+} + OH^-; \\ &2Fe^{2+} + 3H_2O_2 \longrightarrow 2Fe^{3+} + 2H_2O + 2OH^- + O_2; \\ &2Fe^{2+} + 2HO_2 \longrightarrow 2Fe^{3+} + 2OH^- + O_2. \end{aligned}\right\} \qquad (2)$$

As is known [3], trivalent iron is, however, a good cathode depolarizer:

$$Fe^{3+} + \bar{e} \rightarrow Fe^{2+} \quad (3)$$

Thus, the presence of iron ions in the electrolyte produces a considerable corrosion effect (~ 25-30%) in the Zr–Fe pair due to the depolarizing action of the corrosion medium radiolysis products.

It is our pleasant duty to thank Yu. F. Chernilin and the members of his team for their help in performing the experiments.

LITERATURE CITED

1. V. V. Goncharov et al., Transactions of the Second International Conference on the Peaceful Uses of Atomic Energy (Geneva, 1958). Reports by Soviet Scientists [in Russian] (Atomizdat, Moscow, 1959) Vol. 2, p. 243.
2. A. V. Byalobzheskii and V. D. Val'kov, Collection: Investigations of Metal Corrosion [in Russian] (Izd-vo AN SSSR, Moscow, 1959), Vol. 5, p. 130.
3. N. D. Tomashov, Theory of Corrosion and Metal Protection [in Russian] (Izd-vo AN SSSR, Moscow, 1959), p. 448.

DETERMINATION OF THE ISOTOPIC COMPOSITION OF LITHIUM BY ACTIVATION ANALYSIS

L. P. Bilibin, A. A. Lbov, and I. I. Naumova

Translated from Atomnaya Énergiya, Vol. 10, No. 5,
pp. 528-529, May, 1961
Original article submitted November 21, 1960

The determination of isotopic composition is largely based on mass spectrometry at the present time. Papers have appeared in recent years on the determination of isotopic composition by activation analysis; for example, determination of the isotopic composition of lithium from tritium [1,2]. The isotopic compositions of uranium and other elements may be determined by the activation method. The authors of the present work propose an express method for determining the isotopic composition of lithium which does not require complex apparatus and gives quite satisfactory accuracy.

The reactions $Li^6(n, \alpha)T$ (proceeding with thermal neutrons with a cross section of $930 \cdot 10^{-24} cm^2$) and $O^{16}(T,n)F^{18}$ are used for activation analysis of Li^6. Li^6 is determined through F^{18} ($T_{1/2}$ = 112 min, $E_{\beta+}$ = 0.649 Mev). These reactions were used previously for determining small amounts of oxygen in beryllium [3] and other materials [4]. These reactions were used in the present work for determining the Li^6 content of a mixture of lithium isotopes with an unknown content of Li^6 and Li^7.

The procedure described requires the same chemical compound containing lithium and oxygen atoms for the working and standard samples. Lithium carbonate was chosen as the compound. The requirements for the chemical compound may be reduced to the following:

1) simple preparation of the required compound from other chemical compounds;

2) simple preparation of targets for measurement;

3) adequate content of oxygen within the range of a triton;

4) absence of positron activity and γ-activity with $E_\gamma \geq 0.5$ Mev due to (n, γ)-reactions on other components of the compound.

The method of determining the isotopic composition of lithium was as follows. The lithium compound analyzed was converted to the carbonate [5]. For irradiation and measurement, the lithium carbonate samples were pressed into

tablets 8 mm in diameter and weighing 40 mg. The tablets were inserted into polyethylene cassettes and placed in the reactor channel at distances of 1 cm from each other.

In our work, we normally irradiated ten cassettes in a polyethylene container at one time; three of these cassettes contained a natural mixture of lithium isotopes for a standard and for checking for a change in the neutron flux along the channel, while seven contained working samples with unknown Li^6 content.

In the simultaneous irradiation of samples of a natural mixture of lithium isotopes and samples enriched to 98.8% in Li^6, there was a substantial reduction in the activity of F^{18} per mg of Li^6 for the enriched samples, which was evidently connected with a self-shielding effect. To eliminate this effect in the analysis of samples enriched in Li^6, we used isotope dilution and, for this purpose, to the lithium carbonate of unknown isotopic composition was added 2-20 times the amount of "chemically pure" or "analytical" grade lithium carbonate of natural isotopic composition. The materials were mixed either directly in an agate mortar or by solution in water with subsequent evaporation with stirring.

The positron activity of F^{18} and the annhilation γ-quanta (E_γ = 0.51 Mev) were measured on an end-window β-counter and a single-channel scintillation γ-spectrometer with a NaI (Tl) crystal, respectively. The γ-spectrometer allowed both analysis of the γ-radiation over the range of 0.06-2.5 Mev and an integral count at the spectrometer "gate" with a width adequate to pick out the photopeak of the F^{18} annihilation γ-quanta. With a thermal neutron flux of $\sim 4 \cdot 10^{11}$ neutrons/cm^2 · sec and an irradiation time of 5 min, 4 hr after irradiation, samples of natural lithium carbonate had a γ-activity in the photopeak of ~500 counts/min at an efficiency of ~0.07. The slope of decay curves, plotted on the γ-spectrometer with the gate equal to the width of the photopeak at 0.51 Mev, corresponded to $T_{\frac{1}{2}}$ = 112 min.

The Li^6 content of the unknown mixture was determined from the expression

$$\eta = k\eta_0 (1 - 2{,}7 \cdot 10^{-4}\eta) \left[\frac{n_2}{n_1} \left(\frac{1+k}{k} \right) - 1 \right],$$

where η_0 is the Li^6 content of the natural mixture (in percent of number of atoms), k is the dilution factor, equal to the ratio of the weights of natural and enriched lithium carbonate in the mixture prepared (working sample), and n_2 and n_1 are the activities per unit weight of target for the working and standard samples respectively. *

Weight of Li^6 in tablet, mg	0.45	0.65	1.45	2.10	6.8
Activity per mg of Li^6, relative units	1.00	0.99	1.02	0.95	0.65

In the table to the right we give experimental data showing the effect of self-shielding at different Li^6 content in the sample.

As the data presented show, with several milligrams of Li^6 in the sample, the activity was reduced by tens of percents. Therefore the dilution factor chosen was such that self-shielding had no effect on the analysis. For a sample containing 100% of Li^6, this was the case with a dilution factor of $k \geq 3$. Then the Li^6 content of a tablet 8 mm in diameter and 40 mg in weight did not exceed 2 mg.

The accuracy of the determination of Li^6 with measurements on a γ-spectrometer could be raised to 3-4%, while the sensitivity of the method under our conditions was 10^{-6}–10^{-7} g of Li^6. The virtues of the method given are its simplicity and the possibility of carrying out all analyses in half an hour, without the time for transportation of the samples from the reactor.

In addition to using thermal neutrons from a reactor, we also irradiated tablets of natural lithium carbonate (and mixtures with enriched carbonate), 20 mm in diameter and ~500 mg in weight, with neutrons with E = 14 Mev, slowed in a paraffin block (~20 cm in diameter and ~30 cm in height). The tablets were arranged at a distance of ~10 cm from the tritium target; the neutron flux with E = 14 Mev was $\sim 10^9$ neutrons/sec and the irradiation time was 3 hr. Half an hour after irradiation, the β-count of F^{18} on a natural mixture of isotopes was ~100 counts/min. It was impossible to use a Po–Be source under these conditions because of its relatively low intensity ($\sim 10^8$ neutrons/sec).

* The term $2.7 \cdot 10^{-4}$ is a small correction.

LITERATURE CITED

1. L. Kaplan, K. Wilzbach. Analyt. Chem., 26, No. 11, 1797 (1954).
2. E. Piccioto, M. Styvendael. Compt. rend. Acad. sci Paus., 232, 855 (1951).
3. R. Osmond, A. Smales. Analyt. chim. acta, 10, No 2, 117 (1954).
4. A. A. Lbov and I. I. Naumova, Atomnaya energiya, 6, No. 4, 468 (1959).
5. G. Brauer. Handbook of Preparative Inorganic Chemistry [Russian translation] (IL, Moscow, 1956), p. 446.

ELECTROCHEMICAL REDUCTION OF U (VI) FROM HYDROCHLORIC ACID SOLUTIONS USING CATIONITE MEMBRANES

B. N. Laskorin and N. M. Smirnova

Translated from Atomnaya Énergiya Vol. 10, No. 5,
pp. 530-531, May, 1961
Original article submitted October 17, 1960

For the electrochemical reduction of rich hydrochloric acid solutions of uranium, we used the electrodialysis method with cationite membranes (Fig. 1). The cationite membrane divides the electrolyzer into cathode and anode chambers. The hydrochloric acid solution of uranium is added to the cathode part of the apparatus and is reduced. The cationite membrane separates the anode chamber with the oxidizing medium from the cathode part with the reducing medium; in addition, the membrane prevents transfer of chlorine ions from the catolyte to the anolyte. Dilute sulfuric acid is poured into the anode part of the electrolyzer. This apparatus makes it possible to reduce U(VI) to U(IV) from hydrochloric acid solutions with liberation of chlorine at the anode [1,2].

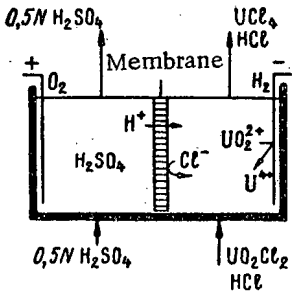

Fig. 1. Diagram of the electrochemical reduction of hydrochloric acid solutions of uranium.

During reduction the following reactions may take place at or near the cathode:

$$UO_2^{2+} + 2\bar{e} + 4H^+ \rightarrow U^{4+} + 2H_2O;$$
$$UO_2^{2+} + \bar{e} \rightarrow UO_2^+;$$
$$2UO_2^+ + 4H^+ \rightarrow U^{4+} + UO_2^{2+} + 2H_2O;$$
$$UO_2^+ + \bar{e} \rightarrow UO_2;$$
$$UO_2 + 4H^+ \rightarrow U^{4+} + 2H_2O;$$
$$U^{4+} + \bar{e} \rightarrow U^{3+};$$
$$UO_2^{2+} + 2U^{3+} \rightarrow 4H^+ \rightarrow 3U^{4+} + 2H_2O.$$

Decomposition of water takes place at the anode:

$$H_2O \rightarrow 2H^+ + {}^1/_2O_2 + 2\bar{e}.$$

The cation-exchange membrane allows the mobile hydrogen ions to pass from the anolyte to the catholyte, which also assists the reduction process.

We used a 0.5 N solution of sulfuric acid as the anolyte. The investigations were carried out in sectional electrolyzers of organic glass, with chamber volumes of 100, 200 and 400 ml respectively. Acheson graphite was used for the electrodes. We used membranes of KU-2 resin and various plastics, and also an American Amberplex S-1 and a British Permaplex S-10 membrane. Hydrochloric acid solutions obtained after regeneration of ion-exchange resins were reduced. The desorption solutions contained 90-140 g/liter of uranium, admixtures of iron and aluminum, and also sulfate ions and a varying amount of free hydrochloric acid.

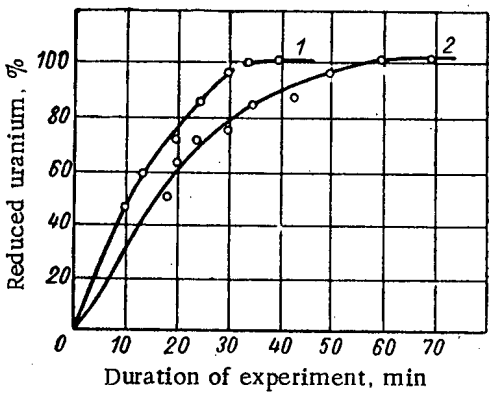

Fig. 2. Kinetics of the reduction of U(VI) to U(IV) in a hydrochloric acid solution containing 90 g/liter of uranium and 1.85 g-equiv/liter of hydrochloric acid, at current densities of 40 ma/cm^2 (curve 1) and 20 ma/cm^2 (curve 2).

By means of special experiments it was shown that there is no increase in the sulfate-ion concentration during the electrochemical reduction of uranium by this method. Transfer of uranium to the sulfuric acid anolyte as a result of diffusion is negligible; when a catholyte containing 90 g/liter of uranium is used, the amount of uranium transferred does not exceed 10 mg/liter. During the reduction process only a little chlorine is liberated at the anode.

At a low acid concentration, hydrochloric acid solutions of U(IV) are readily hydrolyzed, with formation of various soluble and insoluble products, which may have a marked influence on electrode processes.

According to our determinations, U(VI) is reduced with difficulty to U(IV) from 0.1-0.2 N hydrochloric acid solutions. In 0.3 N hydrochloric acid, reduction takes place with simultaneous formation of a green precipitate in the cathode "compartment." In 1.5, 1.6, 1.8, 2.5 and 3.7 N solutions, containing 90-140 g/liter of uranium, precipitates are formed in the cathode compartment during reduction. Reduction of U(VI) to U(IV) is 98-100%. The reduction time depends on the current density.

To investigate the relation between the reduction kinetics of uranium in the cathode compartment and the current density, we used a solution containing 90 g/liter of uranium per 1.85 g-equiv/liter of hydrochloric acid, 0.050 g/liter of iron and 10.5 g/liter of sulfate ions. During reduction, samples were taken from the cathode compartment at specific intervals, and their U(IV) and U(IV) + U(VI) contents were determined. The results are given in Fig. 2.

From Fig. 2 it is seen that U(VI) is completely reduced to U(IV) at the graphite cathode. At a current density of 20 ma/cm^2, reduction is completed in 70 min, while at a current density of 40 ma/cm^2 the reduction time is reduced to 40 min. In the first case the uranium yield per unit current density is 99%; in the second it is 98%. In the first case the energy consumed on the reduction of 1 kg of uranium is 0.7 kw·hr; in the second it is 1 kw·hr.

Similar results were obtained for solutions containing 140 g/liter of uranium. At a current density of more than 40 ma/cm^2 the cathode potential becomes more negative, conditions for the liberation of hydrogen at the cathode are established and the yield of U(IV) per unit current density inevitably falls. Thus, at a current density of 70 ma/cm^2 (without mixing of the catholyte) a yield of about 60% U(IV) was obtained at the graphite cathode.

It is known that maximum overvoltage of hydrogen is observed at lead electrodes. At the present time, for the fabrication of the electrodes, tests are being carried out with lead - silver - antimony alloys, stable in hydrochloric acid. The use of these alloy electrodes will make it possible to carry out the reduction of uranium with a high current yield and at high current densities.

It must be noted that simultaneous electrochemical reduction and precipitation of uranium tetrafluoride in the proposed apparatus is impossible because no ionite membranes withstand heating above 50-60°C, a higher temperature being required for the precipitation of the macrocrystalline uranium tetrafluoride [2]. Therefore the precipitation of the tetrafluoride was carried out after the reduction of uranium. The uranium yield as the tetrafluoride depends on its degree of oxidation, i.e., on the time interval between the stages of reduction and precipitation. According to preliminary data, the yield of uranium as tetrafluoride reached 93-98%. With a continuous process the uranium yield undoubtedly increases.

LITERATURE CITED

1. Higgins, Neill, and McNeese. Proc. 2nd International Conference on the Peaceful Uses of Atomic Energy (Geneva, 1958). Selected Reports of Foreign Scientists [in Russian], 7, Moscow, Atomizdat, 1959, p. 468.
2. Mason and Parsy. Proc. 2nd International Conference on the Peaceful Uses of Atomic Energy (Geneva, 1958). Selected Reports of Foreign Scientists [in Russian], 7, Moscow, Atomizdat, 1959, p. 451.

GAMMA-SPECTROMETRIC DETERMINATION OF SMALL AMOUNTS OF URANIUM, THORIUM, AND POTASSIUM IN ROCKS

N. P. Kartashov

Translated from Atomnaya Énergiya Vol. 10, No. 5,
pp. 531-533, May, 1961
Original article submitted September 19, 1960

Problems of the selection of the optimum energy ranges and the accuracy of the γ-spectrometric method of the separate determination of two natural emitters – uranium and thorium – were examined in [1]. Below, an examination is made of the possibility of the separate γ-spectrometric determination of the contents of potassium and equilibrium uranium and thorium, uniformly distributed in a rock. The necessity for such an analysis arises during radiometric investigations of rocks and weakly active ores, in which the γ-radiation intensity of potassium is commensurate with the γ-radiation intensity of uranium and thorium. The calculation procedure is similar to that employed in [1] and is not described here.

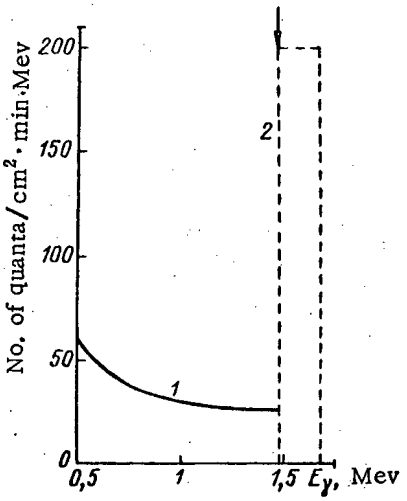

Fig. 1. Spectrum of the γ-radiation of K^{40} distributed in a rock: 1) dispersed γ-radiation; 2) primary γ-radiation.

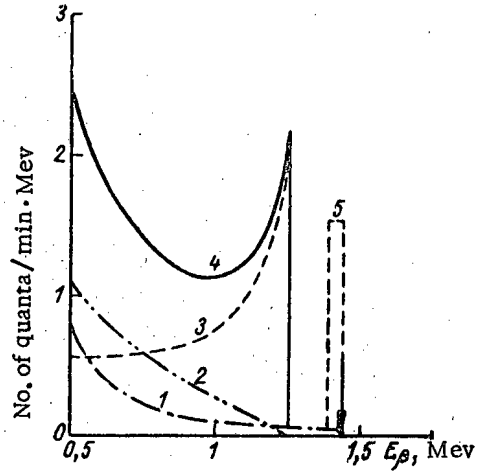

Fig. 2. Spectrum of secondary β-particles formed in a NaI(Tl) crystal by the γ-radiation of potassium in a rock.

Figure 1 gives the γ-spectrum, including both the primary and the dispersed γ-radiation with an energy of $E_\gamma \geq 0.5$ Mev, produced in an infinite homogeneous medium (rock) containing 1% of a natural mixture of potassium isotopes. As already noted [1], for a semi-infinite medium the appearance of the spectrum in the region examined hardly changes, while the absolute values of the intensity are reduced by half.

The initial part of the spectrum, corresponding to γ-quanta with an energy of $E_\gamma < 0.5$ Mev, is not considered because of its marked dependence on the composition of the rocks.

Figure 2 shows the spectral distribution of the β-particles formed per minute, calculated per 1 gram of NaI(Tl) crystal, by the γ-radiation of potassium in a rock with a potassium content of 1%. Curves 1 and 2 correspond to the photoelectrons and recoil electrons from a continuous spectrum of dispersed γ-rays; curve 3 corresponds to the recoil electrons from the γ-rays of the primary monochromatic line; curve 4 corresponds to the total distribution density of the β-particles in the continuous spectrum (to the sum of the ordinates of curves 1-3). The area bounded by the dotted line 5 expresses the number of monochromatic β-particles, formed during the process of photoabsorption of the γ-quanta of the primary spectral line of potassium. The true energies of the monochromatic γ- and β-particles are noted by arrows.

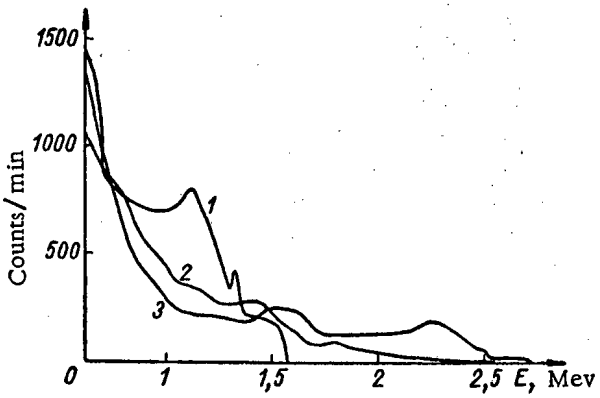

Fig. 3. Calculated scintillation γ-spectra for a spectrometer with a NaI(Tl) crystal at a window width of 0.25 Mev.

Numerical Values of the Coefficients Obtained by Graphical Integration of the Selected Ranges of the Spectra of Secondary β-Particles

Level of discrimination, Mev				
Lower	Upper	a	b	c
0.8	1.2	7.50	2.18	24.2
1.3	1.9	3.86	2.00	4.00
2.0	2.5	0.23	1.18	0.00

The theoretical appearance of the spectrum of K^{40}, recorded by a γ-spectrometer with an NaI(Tl) crystal of weight 50 g, is given in Fig. 3, together with analogous spectra of uranium and thorium, given in [1]. For ease of comparison of the spectra, during this calculation the content of the natural mixture of potassium isotopes in the rock was taken as 46.95% (curve 1), which corresponds to the potassium equivalent of the calculated values of the uranium content (0.01%, curve 2) and thorium content (0.023%, curve 3) with respect to the integral γ-radiation intensity. As may be seen from Fig. 3, in spite of the uniformity of the monochromatic lines of the primary γ-radiation, the spectra of uranium, thorium and potassium nevertheless remain fairly different from each other. Therefore the separate γ-spectrometric determination of the contents of all three natural emitters is possible.

In a similar way to separate two-component systems [1], the content of equilibrium uranium, thorium and potassium in a rock may be determined individually, from a system of three equations of the following type:

$$\left.\begin{aligned} a_1U+b_1Th+c_1K=I_1;\\ a_2U+b_2Th+c_2K=I_2;\\ a_3U+b_3Th+c_3K=I_3; \end{aligned}\right\} \quad (1)$$

where $I_{1,2,3}$ are the intensities of the γ-radiation, measured with a scintillation spectrometer at three essentially different discrimination levels; U, Th and K are the uranium, thorium and potassium contents; $a_{1,2,3}$, $b_{1,2,3}$ and $c_{1,2,3}$ are coefficients equal to the γ-radiation intensity recorded in rock with a unit content of uranium, thorium and potassium respectively at the three different discrimination levels. According to [1] and Fig. 2, for the separate three-component determination of the content of emitters we chose three spectral energy ranges: 1) 0.8-1.2 Mev; 2) 1.3-1.9 Mev and 3) 2.0-2.5 Mev. The choice of these ranges was determined by: 1) the maximum mutual variation of the counting rate of each of the γ-emitters during transition from one energy range to another and 2) the minimum variation of the counting rate of each of the γ-emitters during a slight displacement of the energy range. The numerical values of the coefficients given in the table correspond to measurements in a blasthole by a scintillation counter with a 50-g NaI(Tl) crystal at uranium, thorium and potassium contents of $1\cdot10^{-4}$%, $1\cdot10^{-4}$% and 1% respectively and taken as basic. After substitution of the coefficients the determinant of the system of equation (1) is equal to 65.8 and is ~60% of the largest of the diagonal derivatives of the coefficients. Therefore the system of equations (1) has a real solution.

The calculation shows that during the γ-spectrometric analysis of an acid rock of the granite type with a clarke content of the radioactive elements [2] ($3.8\cdot10^{-4}$% U, $13\cdot10^{-4}$% Th and 2.6% K) the relative root-mean-square errors in the determination of these contents will be

$$\delta_U=105\frac{1}{\sqrt{t}}\%;\quad \delta_{Th}=30,2\frac{1}{\sqrt{t}}\%;$$

$$\delta_K=46,0\frac{1}{\sqrt{t}}\%.$$

For a measurement time t = 10 minutes, this is δ_U = 33.2% δ_{Th} = 9.5% and δ_K = 14.5%. Uranium has the most regular spectrum of the secondary β-particles; therefore as a result of the difficulty of selecting the optimum range the accuracy of the determination of the uranium content is two to three times less than that for thorium and potassium. If there is a considerably greater amount of one of the emitters compared with the other two (with respect to the

γ-radiation intensity), the relative accuracy of its determination increases. Although the other components are determined with a considerably lesser relative accuracy, the solution of the problem of the nature of the anomaly does not give rise to difficulties. Thus, for example, during the γ-spectrometric analysis of a small anomaly, corresponding to contents of $5 \cdot 10^{-3}$% U, $13 \cdot 10^{-4}$% Th and 2.6% K, with t = 10 minutes, the errors will be $\delta_U = 4.8\%$, $\delta_{Th} = 12.7\%$ and $\delta_K = 29.2\%$, and the anomaly will be interpreted with certainty as a "uranium" anomaly.

LITERATURE CITED

1. G. M. Voskoboinikov and N. P. Kartashov. Atomnaya Énergiya, 6, 1, 42 (1959).
2. N. P. Kartashov. Izv. Vostochnogo filiala Akademii Nauk SSSR, No. 4-5, 63 (1957).

A NEW GENERAL-PURPOSE HIGH-PRECISION BETA-RAY SPECTROMETER

Translated from Atomnaya Énergiya, Vol. 10, No. 5,
pp. 534-536, May, 1961

A high-precision magnetic beta-ray spectrometer featuring automatic control and automatic recording has been built and tested at the Physics and Engineering Institute of the USSR Academy of Sciences (Fig. 1) [1].

The electron-optical system of the beta-ray spectrometer is similar to the optical system in a conventional spectrometer [2]. The use of an electron-optical system of this type has made it possible to design an instrument suitable for research of extended scope in the field of nuclear spectroscopy. Studies of continuous electron and positron spectra and internal conversion spectra can be carried out with the aid of this instrument, with precise determinations of the relative intensities of conversion lines. It provides high precision in relative measurements of the energies of conversion lines and the limits of continuous spectra. The spectrometer is also suited to research on photoelectron and recoil-electron spectra. The research applications referred to above are usually satisfied by means of several instruments of different design, each of which is designed for the solution of a limited range of problems.

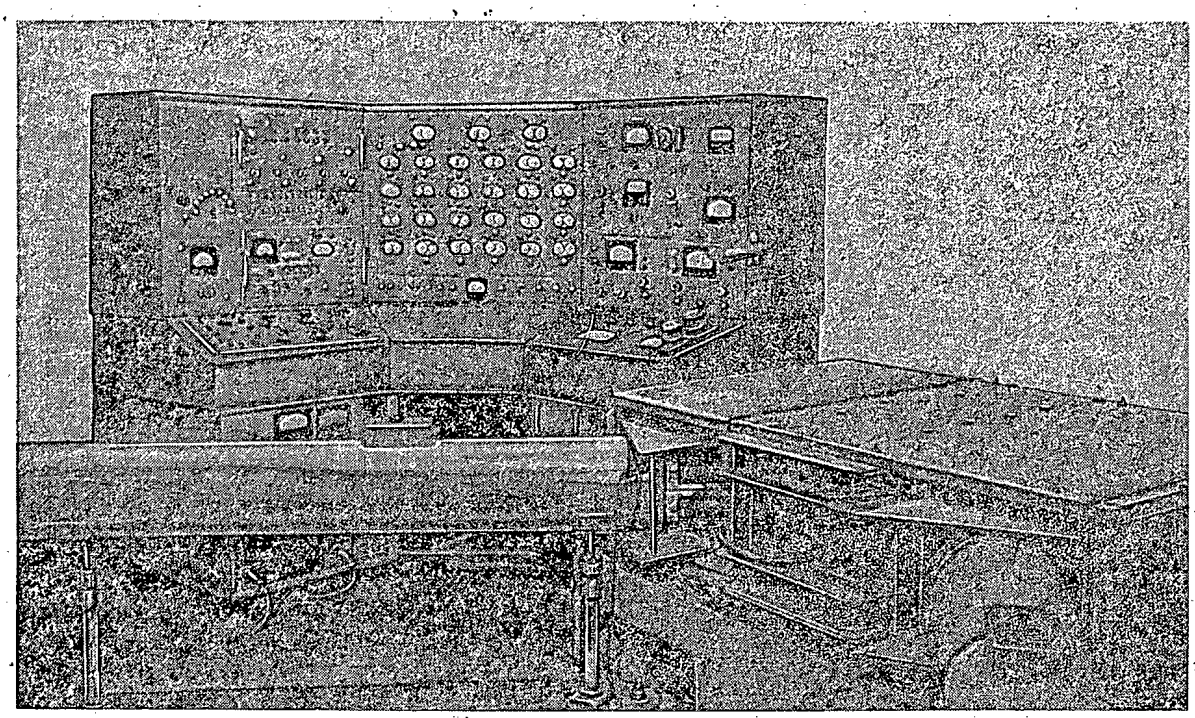

Fig. 1. General view of the general-purpose high-precision beta-ray spectrometer.

The spectrometer consists of a deflecting magnet (magnetic prism), two magnetic lenses (one focusing and one collimating lens), a vacuum system, a lens current and magnetic field stabilization systems, a dc biasing system, and an automatic control and recording system. The path of beta-rays in the spectrometer is illustrated diagrammatically in Fig. 2.

The individual electron optics components of the beta-ray spectrometer fulfill the same functions as the corresponding components of an optical spectrometer. The collimating lens shapes a parallel bundle of electrons of a determined energy emitted at each point of a radioactive source which is placed in the focal plane of the instrument.

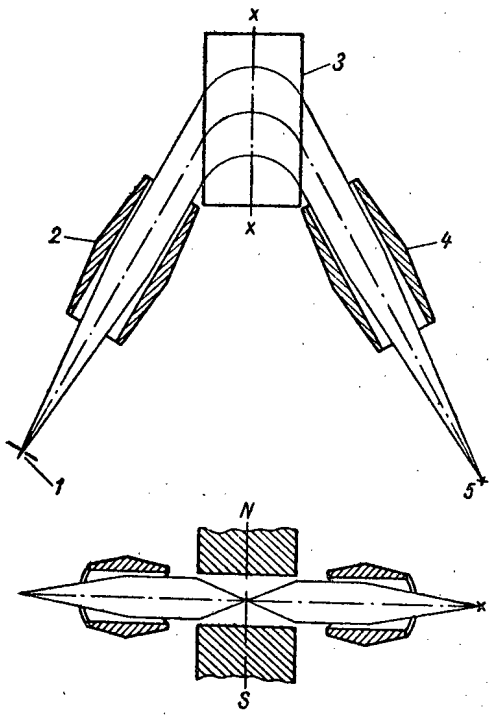

Fig. 2. Electron optics system of spectrometer: 1) entrance slit; 2) focusing lens; 3) deflecting magnet; 4) collimating lens; 5) radioactive source.

The magnetic prism performs the function of breaking down the electrons by velocities. The focusing lens establishes an electron image in the plane of the entrance lens. The focal length of the focusing lens is 120 cm.

The distance from the radioactive source to the center of the collimating lens may be varied from 120 to 30 cm while the instrument is in operation. The focal length of the lens may be varied simultaneously by increasing the current flowing through its winding. In a variant of equal length, the focal length of the collimating lens is 120 cm. The magnification of the entire system is then equal to unity. By varying the focal length of the collimating lens, solid angles ranging from 0.05 to 0.8% of 4π can be selected at will. Dispersion is retained as the solid angle is increased, but some loss of resolving power is entailed when the magnification becomes greater than unity.

One sole specification applies to the field distribution over the magnet pole gap: it must not be varied in the direction of the x axis. This is a major advantage of the spectrometer, the factor responsible for the high resolution attainable.

Short magnetic lenses of new design [3] are employed in the spectrometer. A field with an axial distribution close to bell-shaped is formed by a coil with distributed winding wound directly onto the vacuum tube of the spectrometer through which an electron beam passes. Lenses of this design have some advantages over short magnetic lenses of conventional design: Their field strength drops sharply beyond the winding; the lens may be shielded with greater ease than that with which limitations can be imposed on the scattered field and the beam is much less affected by stray fields; there is no longer any need to adjust the lens with respect to the optical axis of the system (the tube axis). Moreover, other conditions (focal length, amount of spherical aberration, etc.) being equal, available power and weight of lenses with distributed winding are several times less than in the case of lenses of ordinary design. The shields are made in the form of steel tubes with windings on top.

The design of the spectrometer vacuum system makes it possible to carry out the necessary controls and measurements of distance from the source to the center of the collimating lens without disturbing the vacuum during operation of the instrument.

The lens current and magnetic field stabilization system feeds a smoothly varying direct current to the windings of the lenses and magnet. Peak current value is obtained at an electron energy of 2.7 Mev. The field value at the magnet pole gap is intimately associated with the value of the current flowing through the lens windings and is kept constant to within 0.005% tolerance. Stabilization of the magnet gap field [4,5], rather than stabilization of the current in the windings as is usually the approach in magnetic spectrometer design, makes it possible to eliminate effects of hysteresis and nonlinearity in the magnetization curve of the magnet iron. This opens up possibilities for exact measurement of electron energy and obviates any need to adjust the instrument while the measurement of the spectrum is being taken. The spectrometer resolving power remains constant over the entire energy range. In the case of the variant with arms unequal, the collimating lens is fed from a separate current stabilizer coupled to the basic stabilization system such that the change in current in the collimating lens does not lead to a change in base current as the position of the source is varied, while the current in the collimating lens varies proportionally to base current when the value of the base current is changed.

The dc biasing system sets up a potential difference between the substrate of the radioactive source and the body of the instrument to accelerate or decelerate electrons emitted by the source. The use of electrical biasing makes it possible to measure separate portions of the spectrum without varying the field strength of the deflecting field or lens fields. Measurements of electron energy differences taken in this fashion allow the results to be expressed directly in electron-volts, with a very high degree of accuracy in the measurements.

Recording of electrons passing through the entrance slit is carried out by means of two gas-discharge counters placed beyond the slit and included in a coincidence circuit. In order to minimize the background of random coincidences, the counters are free to be positioned at distances up to 700 mm apart. The electrons passing through the first counter are thereupon focused by a short distributed-winding magnetic lens onto the entrance window of the second counter [6]. The lens winding is included in series in the supply circuit of the spectrometer lenses, so that electrons at the energy to which the spectrometer is tuned are focused in the area of the entrance window of the second counter. The background of random coincidences can be reduced to 5 counts per hour with a recording efficiency of 60-70% for electrons of higher than 300 kev energy by this method.

The automatic control system provides control of the spectrometer through programing and automatic recording of measurement data [7]. A variation of energy through a predetermined magnitude from one point to the next is carried out by the automatic control system which varies the base current value (and consequently the deflecting field) or the value of the bias voltage.

The following results were obtained from studying and testing the beta-ray spectrometer. The highest resolution was 0.014% when a solid angle 0.006% of 4π was used and the source size was 0.4 × 15 mm. The maximum solid angle used was 0.8% of 4π, with resolution of 0.11% and source size 1.5 × 15 mm. In addition, operation was feasible at intermediate values of solid angle and resolving power. For example, when the fraction of the solid angle used was 0.2 and 0.05% of 4π, the resolving power was 0.07 and 0.03% respectively (source size 1.5 × 15 mm).

The energy calibration of the spectrometer was done in terms of the 26th conversion lines of Ir^{192}, whose energies are known to high precision, and according to the F-line of thorium. The reproducibility of measurement data was checked for conversion-line energy and nonlinearity of the calibration curve. The probable error of relative energy measurements was 0.02%, the deviation from linearity on the part of the calibration curve did not exceed 0.2%. Checks were also made of resolution as a function of energy and of the reproducibility of instrumental half-width and line area in a series of measurements of the same conversion line. The resolution proved to be energy-independent over the range of interest (100-700 kev) to an accuracy consonant with the reproducibility of the instrumental half-width of the line. The reproducibility of the value of the line instrumental half-width is characterized by a relative probable error less than 5%. The reproducibility of the results of measurements of the area of conversion lines is characterized by a probable error of 2%.

A detailed description of the spectrometer will be published shortly.

At the present time, the "Fizpribor" instrument factory is engaged in the manufacture of a similar line of spectrometers with slightly improved characteristics.

V. M. Kel'man, B. P. Peregud, V. I. Skopina

LITERATURE CITED

1. V. M. Kel'man, B. P. Peregud, V. I. Skopina. Report to the X All-Union Conference on Nuclear Spectroscopy (Moscow, 1960).
2. V. M. Kel'man, D. L. Kaminskii. Zhur. éksptl. i teoret. fiz. 21, 555 (1951).
3. V. M. Kel'man, B. P. Peregud, V. I. Skopina. Zhur. tekhn. fiz., XXIX, 1219 (1959).
4. B. P. Peregud. Pribory i tekhnika éksp., No. 3, 64 (1957).
5. B. P. Peregud. Pribory i tekhnika éksp., No. 5, 64 (1958).
6. S. F. Antonova, S. S. Vasilenko, M. G. Kaganskii, D. L. Kaminskii. Zhur. éksptl. i teoret. fiz., 37, 667 (1959).
7. B. P. Peregud, K. B. Abramova. Pribory i tekhnika éksp., No. 2, 12 (1958).

All abbreviations of periodicals in the above bibliography are letter-by-letter transliterations of the abbreviations as given in the original Russian journal. *Some or all of this periodical literature may well be available in English translation.* A complete list of the cover-to-cover English translations appears at the back of this issue.

ION EXCHANGE EXTRACTION OF URANIUM FROM DENSE PULPS BY THE "FLOATING RESIN" TECHNIQUE*

Translated from Atomnaya Énergiya, Vol. 10, No. 5,
p. 540, May, 1961

Research and development work on equipment for ion exchange of uranium directly from pulp following acid leaching is being pursued in the Union of South Africa. In particular, a report has already been made public** on tests of a facility consisting of several pieces of equipment with air-intermixing of the Pachook type, in which the resin is evenly distributed in the pulp and the intense air-intermixing prevents separation of resin and pulp in the basic equipment.

A second method for contacting resin and dense pulp has been dubbed the "floating resin" technique. In this case, the resin in each column floats freely on the surface of relatively heavy pulp. Weak air mixing assures contact between the liquid phase and the ion exchange resin, which is necessary for rapid passage of uranium into the resin; however, this intermixing does not disrupt layers of resin floating on the pulp surface. The pilot plant consists of 14 chambers of rectangular cross section with the bottoms in the form of an inverted double-sloping top. The cross section through each chamber is 250 × 250 mm, and the chamber depth is 350 mm. There is a small airlift tube in each chamber to facilitate intermixing of pulp. The resin and pulp pass through all the chambers in countercurrent flow. The pulp transits from one chamber to the next through an opening in the common wall beneath the resin layers. Resin is transported in the opposite direction with the aid of a bucket conveyor. When the uranium content in the original pulp is 0.18 g/liter converted to U_3O_8, the retaining capacity of the resin for uranium is about 24 grams of U_3O_8 for each liter of swelled resin. The strongly basic anion exchange resin XE-198 of grain size 28 mesh was chosen for the experiments. The dwell time of the resin in each chamber was 60-70 min, and dwell time of the pulp was 20 min.

Resin losses were determined in a special apparatus under conditions close to those anticipated in actual production. In continuous operation over a 60-day period, 2.5 wt. % of the resin was lost.

A. Zarubin

CONFERENCE ON RADIATION EFFECTS IN MATERIALS

Translated from Atomnaya Énergiya, Vol. 10, No. 5,
pp. 540-542, May, 1961

A conference on effects of nuclear radiations on materials was held in Moscow in December, 1960. The gathering was organized under the auspices of the Divisions of Engineering and Physical-Mathematical Sciences of the USSR Academy of Sciences.

Over 500 delegates were in attendance at the conference; the number of reports delivered surpassed forty.

In a review paper, S. T. Konobeevskii surveyed the achievements in the field of research on radiation effects in solids and new experimental work geared toward improved knowledge of the mechanism of radiation effects on materials, both in the USSR and other countries. Emphasis was placed on the value of this research for plasticity and strength studies. The latter topic was also broached by G. V. Kurdyumov who, using copper, iron, and their alloys as

*J. South Afr. Inst. Mining and Metallurgy, 60, No. 12, 647 (1960).
**Atomnaya Énergiya, 9, No. 5, 430 (1960).

examples, showed that increased resistance of metal to deformation following irradiation is related to the enhanced strength of the lattice in blocking the motion of dislocations and to changes in grain substructure (breakup of mosaic blocks).

A report by S. M. Feinberg on the new SM-2 experimental reactor for research on radiation effects demonstrated the enormous experimental opportunities now opened up to research workers.*

The steels are the most important structural material for nuclear reactors. The effect of reactor radiation on the mechanical properties of structural steels was the subject of several papers. The effect of integral flux and of irradiation temperature on properties in tension and impact strength were investigated. N. F. Pravdyuk et al. described their findings on some low-carbon steels where the basic factor limiting the applications for the steels is the rise of the transition temperature in brittle to ductile transition. The authors noted that radiation damage in such materials as austenite steel, zirconium and its alloys, is less dangerous. In some cases, irradiation of austenitic steels even effects a slight improvement in properties. Results of irradiation of various steels in the ferrite-pearlite category and their welding compounds were reported (A. D. Amaev et al.) to the conference and also some researches on austenized and cold-hardened 1Kh18N9T stainless, as well as titanium-alloy and tungsten-alloy austenitic precipitation-hardened steel (A. V. Efimov, O. A. Kozhevnikov et al.). Irradiation exerts less effect on higher-strength steels. It was noted that the properties of precipitation-hardened steel also vary because of ageing processes during radiation exposure.

V. S. Lyashenko et al. reported on a change in the microstructure of U-7 and 3Kh13 steels under neutron bombardment, which they explained as the work of thermal spikes due to primary recoil atoms, in the first instance affecting the carbide component of the steels. In this context it is interesting to note the study submitted by I. M. Pronman et al., who showed that neutron bombardment of white cast iron and cementite in a flux of $5 \cdot 10^6$ neutrons/cm^2 at 65°C with subsequent annealing at 650°C leads to deterioration of the cementite. A similar phenomenon was observed following irradiation with electrons at 600°C. Studies of the effect of pile irradiation on some properties of avialite alloy and molybdenum were reported.

One interesting report (P. A. Platonov) dealt with relaxation of internal stresses under irradiation in nickel, nichrome, zirconium, steels of the pearlite class, and special spring steel. The relaxation is estimated from the bending deflection of planar specimens. Recovery, i.e., partial reversibility of the effect when stresses are relieved, is also observed. The recovery rate increases as the temperature. Some suggestions were advanced in this respect on the nature of radiation hardening. A similar phenomenon of stress relief in cold-deformed rolling of platinum, molybdenum, zirconium, copper, nickel, and bronze specimens was revealed in x-ray examinations in a reduction in the width of x-ray lines (B. M. Levitskii et al.). The recovery effect was also observed in irradiated materials (following gentle heating, partial return to the initial state was observed). The stress relaxation effect (studied in terms of deflection) was also observed in the case of gamma irradiation of specimens of iron-aluminum-chromium alloys, U-8 steel, and nickel (I. Ya. Dekhtyar, A. M. Shalaev).

A paper by Yu. I. Pokrovskii and associates reported the effect of large radiation doses (up to $5 \cdot 10^{20}$ neutrons/cm^2) on internal friction and modulus of elasticity in copper, magnesium, aluminum, and zinc. It was disclosed that radiation induces an increase in critical stress, i.e., the stress value at which a rapid increase in internal friction with amplitude sets in. Another paper, with zinc as example, showed that this stress may be identified with critical shear stress. The effect of irradiation on internal friction in a copper single crystal was also investigated (A.I. Zakharov).

A paper by S. T. Konobeevskii et al. on the effects of pile radiation on tinny bronze (8.2 A% tin) with 1 A% plutonium additive proved highly interesting. After irradiation of the alloy, in a heterogeneous state, by a flux of 10^{18} to 10^{20} neutrons/cm^2, a gradual transition of the heterogeneous structure to a homogeneous structure was observed. No process of a similar nature was observed in the same bronze with no plutonium added. This phenomenon is accounted for by invoking the concepts, developed earlier for U–Mo alloys, of temperature spikes due to fission fragments and their effect on the diffusion process. In the view of the authors of this paper, the data adduced signify that Brinkman displacement spikes caused by primary displaced atoms are inefficacious in radiation-diffusion phenomena.

Results of the effect exerted by fluxes up to $1.35 \cdot 10^{20}$ neutrons/cm^2 on electrical resistivity and on lattice periods of the ordered alloy Fe_3Al were reported to the Conference. The effect of gamma irradiation on the lattice period of the same alloy was investigated (S. D. Gertsriken and N. D. Plotnikova). S. M. Astrakhantsev and Yu. I. Konnov considered the effect of neutron radiation (dose $\approx 10^{17}$ neutrons/cm^2) on the K-state in the alloy Kh20N80,

* For a description of the SM-2 reactor design, cf. Atomnaya Énergiya 8, No. 6, 493 (1960).

noting that exposure of a nonhomogeneous solid solution led to degradation of the K-state, while exposure of a homogeneous solid solution resulted in the appearance of the K-state.

A report by S. T. Konobeevskii and F. P. Butor described a study of diffusion scattering in irradiated single crystals of silicon, corundum, molybdenum, and diamond. An explanation of the anomalous increase in the lattice period of diamond under irradiation attributed the effect to the formation of regions with a graphitic structure.

A paper authored by I. V. Telegina and E. V. Kolontsova dealt with studies of radiation damage in LiF and quartz single crystals. Fragmentation of LiF under neutron bombardment was disclosed.

Data were submitted (by É. L. Andronikashvili and associates) on radiation damage effects on microhardness, Martens hardness, and the microstructure of potassium chloride crystals. Radiation damage effects were correlated with data on the relationship between microhardness and the number of F-centers.

Papers were also submitted to the conference dealing with results of investigations in the area of annealing processes of stored energy accumulated in graphite under irradiation, and on the effect of neutron irradiation on electrical resistivity in iron, nickel, zirconium, titanium, molybdenum, and tungsten. The kinetics of annealing out the increase in electrical resistivity were also discussed in one of the papers.

A paper by A. V. Byalobzheskii offered a generalization of data on radiation effects on corrosion of metals and alloys. It was shown that an acceleration of the rate of corrosion is almost always related to radiolysis of the corrosion-supporting medium. Especially prominent activity is manifested by short-lived radiolytic products.

Delegates heard with interest a report (A. K. Kikoni et al.) on the stimulating effect of gamma radiation on the flotation process, accounted for in the authors' view chiefly by gamma irradiation of the flotation agent. Another report (S. V. Starodubstsev et al.) of interest dealt with changes in the adsorptive properties of silica gel subjected to gamma exposures.

Many of the reports dealt with gamma radiation effects on crystalline solids of various types.

The effect of gamma rays on ferromagnetic metals and alloys was discussed by I. Ya. Dekhtyar, A. M. Shalaev. Variation in the degree of long-range order in Fe_3Al and other alloys, in the coercive force in pure iron and nickel, were observed. The effect of gammas on semiconductor single crystals CdS and CdSe were studied (I. D. Konozenko et al.). The observed increase in the conductivity of CdS crystals exposed to gammas led to the use of CdS crystals as radiation sensors in x-ray and gamma-ray dosimeters. In a study of the effect of gamma radiation on electrical conductivity in amorphous boron and selenium, S. V. Starodubtsev et al. showed that amorphous selenium becomes converted to the crystalline form when bombarded by gammas. A change in the linear dimensions of the shear modulus of quartz and Rochelle salt exposed to gamma radiation was reported (S. V. Starodubtsev, S.A. Azizov et al.). Data were reported on luminescence in quartz (S.V. Starodubtsev and Sh. A. Vakhidov) and on changes in the properties of F-1000 and FM ferrites (É. I. Trinkler).

Some of the papers were devoted to problems arising in irradiation techniques and investigations of active specimens. Methods of dose determination for neutron bombardment and techniques for obtaining a high temperature in irradiated specimens by means of a special heat-insulating air gap were discussed (N. F. Pravdyuk, A.D. Amaev et al.). Mention was made (N. F. Pravdyuk, V. A. Nikolaenko et al.) of the possibility of determining integral flux of fast neutrons according to the variation in the lattice periods of diamond and SiC. Another paper advanced the suggestion of converting the neutron flux over a spectrum physically existing in a pile to some effective flux, by using Seitz estimates of the number of primary displaced atoms as a function of neutron energy. A radiography unit for investigating active specimens using a double diffraction reflection system with ionization and scintillation counting techniques was described in a paper by B. M. Levitskii et al. A basically similar facility was also discussed in another paper (B. V. Sharov et al.). A new technique basically different in principle for recording reflected rays was described by V. A. Nikolaenko et al. This facility uses an ionization chamber for the purpose; the effect of radioactive background is eliminated by appropriate compensating currents. A review paper on techniques for quantitative calculations of radiation damage, using electronic computers, was read by A. I. Orlov.

This conference bears witness to the intense interest, on the part of a large number of research workers, in problems of radiation damage to materials.

The proceedings of the conference will be published in symposium form by the Academy of Sciences of the USSR.

Yu. N. Sokurskii

RADIOISOTOPE APPLICATIONS IN EAST GERMANY*

Translated from Atomnaya Énergiya, Vol. 10, No. 5,
pp. 543-544, May, 1961

In November,1955 the Council of Ministers of the German Democratic Republic adopted a resolution entitled "Resolution on measures for peaceful exploitation of atomic energy," which contributed to laying the foundations for the development of isotope engineering in East Germany. This resolution was based on an "Agreement on collaboration between the USSR and the German Democratic Republic in the field of the physics of the atomic nucleus and uses of atomic energy for the needs of the national economy," signed in April 1955. According to the terms of this agreement, the Soviet Union took on as one of its obligations the rendering of its assistance to the German Democratic Republic in the form of deliveries of radioactive isotopes and training of specialists in various fields of nuclear interest. At the end of 1955, the very first attempts were made to utilize radioactive isotopes in medicine and agriculture. The first shipments of isotopes soon arrived from the USSR; many young scientists were sent on leave to the Soviet Union to study isotope applications in various branches of industry.

At the end of November,1955 the Commission on Isotopes held its first meeting. Since that time, the Commission has held 25 meetings and has conducted valuable work on promoting isotope applications. During the years 1956-1960, applications of radioactive isotopes climbed steadily and rapidly (see accompanying graph). It was during this period that the prerequisites were established for an extensive development of work in this important field of technical advances. The necessary radiation sources and labeled compounds were put into production; instruments for recording ionizing radiations were developed, equipment and accessories for handling radioactive materials were designed; specialists were expertly trained in isotope-handling techniques in the Soviet Union and in isotope courses given at institutes in the German Democratic Republic; the major problems encountered in radiation shielding were brought under legislative control. Starting with 1959, production of radioactive isotopes was stepped up at the Rossendorf reactor. It has been confirmed that the use of radioactive isotopes in some branches of industry, such as determination of weight per square meter of material, quality control of materials, and thickness determinations, have paid off in tremendous savings. After the necessary prerequisites had been established, the Commission on Isotopes of the Science Council for the Peaceful Uses of Atomic Energy and the Nuclear Research and Nuclear Industry Administrative Board therefore oriented its efforts toward promoting efficient use and assimilation of isotope techniques in industry on a broad scale.

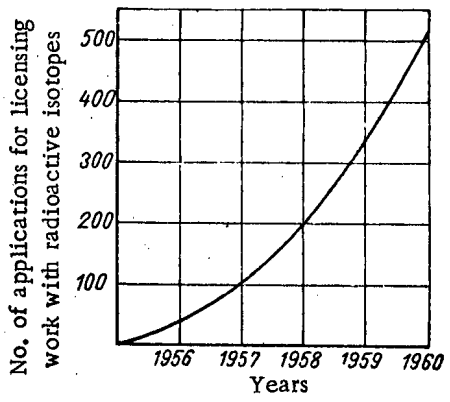

Increase in number of applications for work with radioactive isotopes (tentative data for 1960).

It should be noted that isotopes are being used still far below their potentialities in industry, and that the advantages inherent in isotope techniques for industry and engineering are nowhere near exhausted. At the present time, success in getting industry to adopt new techniques and in overcoming resistance to them, and in getting around their present limitations, depends on the extent to which isotope techniques will yield full economic returns and make a valuable contribution to the solution of the principal economic problem. The Soviet science and engineering exhibit "Atomic Energy for Peaceful Purposes" held in Leipzig in 1956 attracted a total of 83,000 visitors, while the East German mobile exhibit "Isotopes in the Service of Science and Engineering Progress" was visited by about 78,000 persons in the course of its 1959-1960 tour through the principal cities of the German Democratic Republic, acquainting broad layers of the population with radioisotope applications. Numerous books, pamphlets, and periodicals (including the new journal Isotopentechnik) are doing their part in deepening and expanding knowledge of atomic developments.

The Technikpalast engineering exhibit in Berlin is of enormous significance in spreading technical knowledge in the field of uses of isotopes. The program at the Technikpalast for keeping engineers up to date on the most important aspects of isotope applications dates back to November,1955.

*Based on an article by B. Winde, in Isotopentechnik, 1, No. 2, 33 (1960).

The collaborative efforts of Technikpalast staff members is also felt in the course of educational and lecture activities, in visits to productive enterprises, and in consultant services to publications. The success of these efforts is visible not only in the form of practical results, but also in the fact that the "Isotopes in Engineering and Industry" session at the Leipzig Technikpalast, in the course of five years up to November, 1960, had provided opportunities for 60 scientists and engineers to present information-packed reports on the results of applications of radioactive isotopes in industrial production and in scientific research.

V. P.

NEW RULES GOVERNING SHIPPING OF RADIOACTIVE MATERIALS

Translated from Atomnaya Énergiya, Vol. 10, No. 5,
pp. 544-545, May, 1961

The State Committee of the Council of Ministers of the USSR on the Uses of Atomic Energy and the State Health Inspection Team of the USSR on December 26, 1960 confirmed new rules governing the transportation and shipping of radioactive materials [1] which are now obligatory for all institutions, organizations, and enterprises under the jurisdiction of all ministries, government departments, and regional councils of the national economy engaged in the transportation, storage, and use of radioactive materials.

The rules were elaborated in conformity with health regulations covering handling of radioactive materials and sources of ionizing radiations [2] in the light of recommendations circulated by the International Atomic Energy Agency [3,4].

The rules set forth specifications covering packing for hauling of radioactive materials; in fulfillment of these requirements, radioactive materials must not be allowed to penetrate beyond the package under ordinary transportation, loading, unloading, and storage conditions, which should make it possible to consider packings manufactured in accordance with these specifications, such as sources of ionizing radiations which create no danger of radioactive contamination of the surrounding medium or of the means of transportation.

Just as under the terms of rules previously in effect[5], radioactive materials being transported from one place to another may be classified in three groups, according to the physical characterisitics of the radiations emitted. The first heading will embrace those radioactive materials which emit gamma photons along with alpha and beta particles (Co^{60}, I^{131}, Ir^{192}, Cs^{137}, etc.). The second heading includes radioactive materials which are neutron emitters or neutron-and-gamma emitters. The third group includes those substances emitting alpha and beta particles (Po^{210}, Sr^{90}, P^{32}, S^{35}, C^{14}, etc.).

To facilitate the organization of transportation of radioactive materials and of dosimetric and radioactive control measures, the rules stipulate four categories of shipping packings depending on the gamma dose rate and the neutron flux at the packing surface or at a distance of one meter from the surface.

The first category includes packings at whose surface the gamma dose rate does not exceed 0.4 mr/hr (or where the fast-neutron flux does not exceed 2 neutrons/cm^2·sec). The second category is for those packings at whose surface the gamma dose rate does not exceed 10 mr/hr (40 neutrons/cm^2·sec), or 0.4 mr/hr (2 neutrons/cm^2·sec) at a distance of 1 meter. The third category is for those packings at whose surface the gamma does rate does not exceed 200 mr/hr (800 neutrons/cm^2·sec), or 10 mr/hr (40 neutrons/cm^2·sec) at a distance of 1 meter. A special fourth category is set aside for those packings where the gamma dose rate only is normalized at a distance of one meter (50 mr/hr) and the corresponding neutron flux is 200 neutrons/cm^2·sec. Packings referred to the fourth category are licensed for service only on specially set aside transportation units or in specially set aside bays in the holds of seagoing and river vessels.

Packing specifications previously included in the rules are now supplemented with indications that the integrity of the primary volumes containing radioactive materials must not be impaired if the temperature is varied from + 50 to – 70°C or if atmospheric pressure varies from 1.0 to 0.2 atmospheres.

Containers approved for carrying radioactive materials are only those conforming with the technical conditions laid down by the State Committee of the Council of Ministers of the USSR on the Uses of Atomic Energy and the USSR State Health Inspection body.

The rules limit radioactive contamination of the external surfaces of containers. Contamination must not give rise to radiations larger than 200 alpha particles or 5000 beta particles from 150 cm^2 of surface area. The gamma dose rate must at the same time not exceed 0.4 mr/hr. To avert any possible radioactive contamination of the means of transportation used, warehouse areas, etc., the containers must be placed inside supplementary external packings free from radioactive contamination.

Rules provide for proper marking of containers, packing, carriers, and transportation units in a number of cases, and for placement of the radiation hazard symbol* [1, 2] and attachment of special labels [1] to packing and containers, to indicate the nomenclature and activity of the radioactive material contained therein and the category of packing.

When the above-mentioned basic requirements, plus several other requirements outlined in detail in the rules, are duly observed, packaged radioactive materials in the first, second, and third categories are approvable for shipping by air, railroad, water route, and truck, and for storage in conventional warehouses and depots with no need to separate them from other cargo; freight containing undeveloped x-ray film, moving-picture film, or photographic films and plates must of course be separated from containers with radioactive materials.

The number of containers allowable per single transportation unit or single warehouse bay or compartment is limited by the requirement of safety regarding radiations emitted from the packages during shipping and storage, as well as by safety considerations regarding possible accidents involving the means of transportation.

Packings in the first and second shipping categories may total up to 2000 millicuries of uncovered radioactive materials and up to 2000 curies of covered radiation sources. A single shipping container in the third shipping category may contain radioactive materials with activity totaling 200 curies in exposed form and unlimited activity for sealed sources.

The new standards envisage the possiblity of shipping containers with radioactive materials in general-purpose railroad-car, truck, and other common carriers, with requirements applying as in the case of the first, second, and third shipping categories.

The new safety standards direct particular attention to the safety of transportation workers and that of passengers; the annual exposure dosage for these persons is set at 0.5 roentgen per year [1,2].

Appendices to the rules furnish tables listing minimum exclusion distance for areas frequented by personnel from various amounts of packages belonging to the several shipping categories, and minimum distances for freight containing undeveloped x-ray, moving-picture, or photographic plates and film.

A supplement to the general regulations to be observed in shipping of radioactive materials outlines the concrete requirements governing shipping by various means of transportation.

Containers free of radioactive materials may be shipped in any means of transportation without restriction, provided only that the dose rate of any radiations left on the surface of the container not exceed 0.4 mr/hr, and that there be no radioactive contamination of the surface of any additional packing used. If these conditions are met, no radiation hazard symbol need be attached to the container, nor any labels.

Measures to be attended to in case the integrity of the shipping cases is impaired in an accident to the means of transportation or for any other reasons are considered in the rules, as well as public health requirements covering shipping of radioactive substances, and some miscellaneous requirements of pertinence.

In addition to the data already mentioned, the appendices to the rules also cite the critical tolerance levels for exposure and radioactive contamination, a list of recommended instruments for measuring radiation damage, dose rate and radioactive contamination, thicknesses of materials providing 10-fold and 100-fold attenuation of radiation, examples for determining minimum tolerable distances from shipping cases with activity, the radiation hazard symbol, blanks for labels and tags, and other material.

With the adoption of these new rules, the previously observed rules [5] and departmental instructions regulating shipping of radioactive materials expire.

Organizations engaged in and licensed for the shipping, loading, unloading, and temporary storage of shipping cases containing radioactive substances must, in the light of these new rules, revise their instructions, rules and re-

*A color insert of the symbol mentioned here was not reproduced because of its similarity to the symbol used in the United States -- Publisher's Note.

gulations to conform to the specific characteristics of locally prevailing conditions and to meet with the approval of public health inspection bodies.

The introduction of this new set of rules will contribute to improvement of safety in the shipping of radioactive materials and will also contribute to better organization of such work.

N. I. Leshchinskii, A. S. Shtan'

LITERATURE CITED

1. Rules governing shipping of radioactive materials. Moscow, Gosatomizdat, 1961.
2. Public health rules governing handling of radioactive materials and sources of ionizing radiations. Moscow, Gosatomizdat, 1960.
3. Safe handling of radioisotopes. Vienna, IAEA, 1958.
4. Rules governing shipping of radioactive materials. Vienna, IAEA, 1960.
5. Provisional health rules regarding shipping of radioactive materials. Moscow, Medgiz, 1959.

NEW REGULATIONS OF RADIATION SHIELDING ADOPTED IN WEST GERMANY*

Translated from Atomnaya Énergiya, Vol. 10, No. 5, pp. 545-546, May, 1961

The "Law on peaceful uses of atomic energy and protection against concomitant radiation hazard" (known as the "Atomgesetz") presently in effect in West Germany does not take up any concrete problems of radiation exposure hazard; it authorizes the federal government to legislate in manners pertaining to that field. In principle, the approval of the Parliament is required for the issuance of any such decrees and regulations, but since the essential modifications in the decrees and regulations consist in the replacement of physical, engineering, or biological quantities by other such quantities, issuance will be approved in advance without discussion in the Parliament. This order of procedure arose from the efforts to reflect the rapid development of science and engineering in executive decrees having the force of law within a reasonable time. The first batch of such decrees are those adopted on May 30, 1960, the "Regulations on radiation shielding," which consider in detail problems concerned with protection of personnel from harmful radiation effects. Other problems of radiation shielding still to be formulated in decree form were not included in the regulations for the time being.

The new regulations define a radioactive substance as a substance which spontaneously, i.e., without external stimulation, emits ionizing radiation. Such substances include neutron sources and other materials or objects containing radioactive substances or contaminated with such substances. The concepts of sealed and uncovered radioactive preparations are defined. The sealed category is defined to include those radioactive materials placed in a dense and firm nonradioactive enclosing medium which denies them access under ordinary conditions to the external surface of the enclosing medium. All other preparations are considered to be open or nonsealed.

The regulations establish the priority of shielding in handling of radioactive materials, including mining of raw materials, processing of same, fabrication of radiation sources, use and shipping of radiation sources and other preparations, and also disposal of radioactive wastes. A license is required for approval of work handling radioactive materials, and licensees must meet with certain requirements. Personnel authorized for direct work with radioactive materials or responsible for directing such work must be competent in the field of radiation shielding.

The rules also stipulate the priority prevailing in the insurance of persons working with radioactive substances. The use of radioactive materials in small quantities or in low concentrations well below any hazard level is exempt from any special license requirement. This also applies to chemical laboratories having not more than 100 grams of solid compounds containing natural uranium or thorium on their premises.

*J. Pfaffelhuler. Atomwirtschaft, 5, No. 9, 384 (1960).

Licensing for shipping is required in practice only when radioactive materials are being shipped through city streets and thoroughfares or in the use of common carriers on rivers and lakes.

The use of radioactive materials in any type of light source (instrument scales, dials, indicators, etc.) is permitted without licensing.

The purchase and sale of radioactive substances is affected by the new regulations in the sense of being permitted without need of special licensing, in contrast to previously valid regulations, but requiring that an obligatory official form be filled out. Only those persons duly licensed to handle radioactive substances of the stiupulated form and in the stipulated quantities are permitted to engage in thesale of such substances.

The regulations prescribe approved designs of devices with sealed radioactive preparations preventing the sealed-in radiation from exceeding tolerance dose limits for the surrounding area and personnel. When this condition is met, no further special permission is needed to use the equipment and only an official declaration is required in a sale of the device.

The concept of control zone, in which any worker on duty for forty hours a week has a chance of acquiring a dose larger than 1.5 rem per year, and the zone of observation, which shares its inner boundary with the outer boundary of the control zone, are introduced. The outer boundary of the observation zone lies at the point where there is a possibility of acquiring a dosage higher than 0.15 rem per year on prolonged exposure. If dosimeters positioned inside that zone show readings corresponding to higher than 0.5 rem annually, immediate steps must be taken. Young persons below and up to 18 years of age, pregnant or nursing women are not allowed to handle unsealed radioactive products or to be present in a control zone, the only exception being medical treatment.

The critical radiation tolerance dose for anyone handling radioactive substances is set, on a lifetime basis, according to the formula $D = 5 (N - 18)$, where D is the dose in rem, N is the age of the worker in years. No weekly dose is set. The dose acquired from 13 weeks of continuous work must not exceed 3 rem, under the further condition that not more than 5 rem exposure per year be permitted. If the accumulated dosage from previous exposure is known to precision, and does not exceed the lifetime tolerance level, then 3 rem are allowable for each 13-week interval, corresponding to 12 rem annually.

The rules call for disposing of radioactive wastes whose activity exceeds the critical tolerance level in special burial or storage sites designed for that express purpose.

All clauses under the regulations apply with equal vigor to nuclear fuel, which is classified for the purpose of the regulations under radioactive substances in general. Several sections of the regulations provide detailed illustration of juridical problems of interest.

V. P.

RADIOACTIVE ISOTOPES IN TRACER MONITORING OF SEEPAGE FLOW PATTERNS

Translated from Atomnaya Energiya, Vol. 10, No. 5,
pp. 546-549, May, 1961

Radioisotope tracer techniques are coming into their own as useful tools in the solution of numerous problems relating to seepage flow patterns in hydraulic engineering construction work. The use of radiotracer techniques aids in monitoring the effective speed of seepage flow into earthdams, dams, banks of water reservoirs, canals, etc. The radioactive tracer technique may also be called upon to map out the pathways of seepage into the foundations of hydraulic engineering constructions.

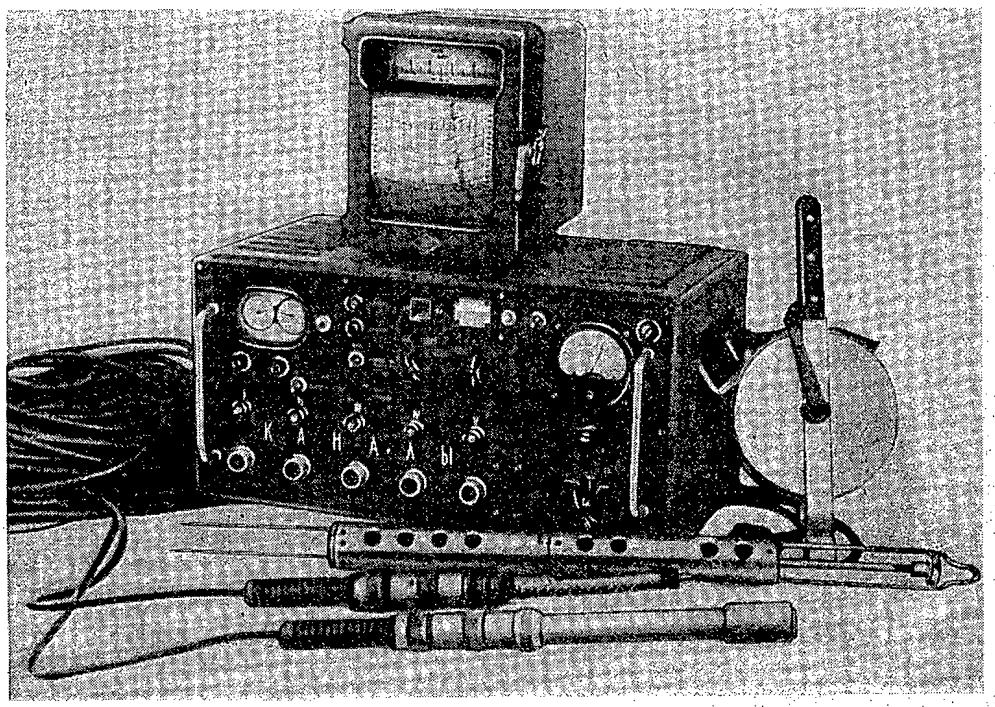

Fig. 1. Set of equipment for tracer monitoring of seepage flow.

The use of radioactive tracers to monitor the behavior and efficiency of various types of structures built to combat seepage is of particular significance. We must include here such questions as the appearance of low-density pervious zones in earthfill dams, upstream blankets constructed with poor workmanship, searches for "leaky windows" in grout curtains and sheetpile cofferdams, etc. In these cases, determination of effective speeds and flow-rates of seepage opens the way for estimating the extent of damage in such zones and indicating the measures to be taken in coping with it. The tracer method also makes it possible to determine the filtration constant in earthfill dams and hydraulic levees.

In this way, the tracer technique can be put to work to obtain a true picture of seepage behavior in the footings of a structure.

Recognizing the high efficiency of the technique, the Moscow branch of the Orgénergostroi power construction institute undertook to develop procedures for utilizing radioactive tracers to full advantage in civil engineering work and successfully designed a line of field equipment for tracer monitoring of seepage.

The essence of the tracer technique employed in seepage studies consists in introducing a certain quantity of tracer compound into a drillhole known as the injection hole. The problem subsequently reduces to one of recording radiations from the radiation compounds entrained in the seepage flow, using a series of control drillholes for the purpose.

Comparative Evaluation of Tracer Compounds

Isotope	Compound	Adsorption characterstics	Maximum radiation energy, Mev	Half-life, days
P^{32}	NaH_2PO_4	Intense sorption on sand, hole filter, and body of probe	1.7 (β)	14.3
$Zr^{95} + Nb^{95}$	$Zr(C_2O_4)_2$	Weakly sorbed	0.84 (β) 0.92 (γ)	6.5
I^{131}	NaI, KI	Practically no sorption, traces of activity easily washed free by water flow	0.82 (β) 0.72 (γ)	8.14

Depending on the nature of the problem posed, on the procedure followed to solve it, and the method resorted to in recording tracer emissions, various types of observations can be performed. To determine the direction of flow of a stream, observations are carried out using several control holes at which the tracer might show up. To determine rates of flow of a stream and the seepage coefficient, observations are made of the rate at which the tracer is diluted in the injection hole or of the time it takes the tracer to reach a given control hole. The injected tracer must flow along with the same direction as the stream and at the same speed. This is a fundamental requirement for tracers in this application.

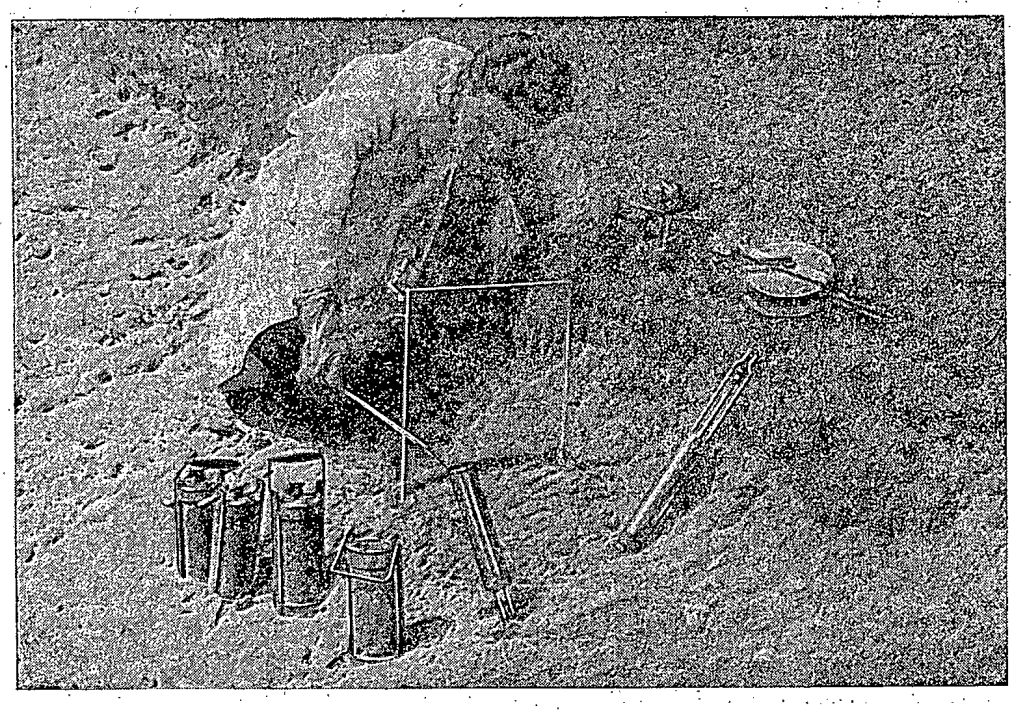

Fig. 2. Loading mechanical attachment for radioactive isotope I^{131} capsule.

In order to derive satisfactory results from the radioactive tracer method, the appropriate radioactive substance for the soil environment studied must be selected correctly, and care must be exercised in the choice of the radiation recording system.

Radioactive tracers now in use for monitoring seepage in hydraulic levees must conform to the following requirements:

1) The tracer must not be sorbable on sand, filters, of the casing and supports of the drillhole.

2) Its radiation energy must be adequate to permit recording in situ, inside the hole.

3) It must have a half-life sufficiently long to facilitate monitoring of seepage pathways at a distance of 25-30 meters.

4) The cost of the tracer must not be prohibitive.

Of the above requirements, the most important one is that relating to sorption (losses) of the radioactive tracer.

A comparison of the radioactive compounds P^{32}, Zr^{95}, I^{131} carried out to apprasie their conformity to the above requirements showed that the best tracer material for the task of monitoring filter dams is I^{131} (see the table).

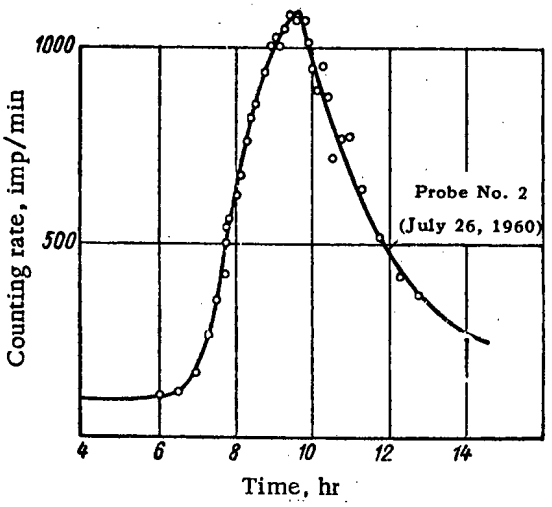

Fig. 3. Plot of passage of radiotracer past control hole No. 2.

A set of special field equipment (Fig. 1) was designed to facilitate work under field conditions. This equipment serves for monitoring soil water flow by tracer techniques and enables operators to perform all the basic operations involved in injection of the radioactive tracers into the injection hole, for sampling water extracted from the test holes, and also continuous recording of the progress of radioactive tracer past the control holes.

The following units constitute the set: accessories for introducing the radioactive tracer into the seepage flow (both mechanical and electric-fuse explosive units), a sampler, recording equipment (all-purpose control panel and automatic strip-chart recording unit with removable probes in open and sealed housings). The removable probes make it possible to carry out observations on the progress of the radioactive tracer directly, in holes 100 meters away from the observer. The set is intended for work at both injection holes and control holes (over 50 mm in diameter) and in open-channel flows.

The direction and parameters of seepage flow in a large levee were determined by use of this equipment. The tracer used was I^{131} in NaI and KI compounds. I^{131} isotope in amounts of 1.5-2 millicuries was introduced into the injection-hole filter. The mechanical device for introducing the tracer into the hole may be seen during loading in Fig.2.

The direction of flow is determined by observing tracer at the control holes. Tracer was discovered only in control holes lying in the central line of direction. This allows us to infer that seepage flow proceeds at right angles to the axis of the dam.

In order to determine the true rate of flow and seepage rate of flow, two methods are resorted to: the control-hole and the injection-hole method. To determine flow rates by the control-hole technique, the time it takes for radioactive tracer to travel a certain distance between holes is recorded. A plot of the passage of radioactive tracer past control hole No. 2 appears in Fig. 3 with corrections introduced for decay of the isotope and instrumental count errors.

The injection-hole technique is based on the reduction of tracer concentration in the injection hole with time as a function of the amount of seepage flow through the hole cross section.

Although experience in use of tracer methods in civil engineering is still meager, it can be stated at this juncture that the new method is highly promising. Featuring a number of advantages over the electrolytic and calorimetric approaches, the radioactive tracer method is opening up a steadily increasing array of possibilities.

The advantages of this technique are:

1) Use of a large number of radioactive compounds makes for a broad range of applications in any soils and waters, whereas use of the electrolytic method in highly mineralized waters or of the calorimetric method in discolored waters is beset with serious difficulties.

2) The tracer method is more accurate than its electrolytic and calorimetric competitors; this increased accuracy is achieved by releasing small aliquots of radioactive compound (0.1 mg) which more adequately reflect the nature of the flow pattern and by the use of more sensitive measuring and recording equipment.

3) The possibility of recording radioactive tracer emissions directly at the hole makes it possible to determine the place and time of appearance of tracer in fast-flowing streams to adequate precision.

When employing tracer techniques, we must bear in mind the complexity that will be encountered in the organization of the research (requirements for safety and health-physics measures, the need for specially trained personnel, etc.) and operating costs associated with tracer materials and specialized equipment. At the present state of the art, operating expenses are fully offset by the savings resulting from radiotracer work.

From investigations already concluded, we can reach the following conclusions:

1) Radioactive tracers can be employed to determine, to a high degree of accuracy, the directions and parameters of seepage flow and the filtration coefficient in levees.

2) An excellent tracer for hydraulic-levee studies is the isotope I^{131} labeling the compounds NaI and Ki.

3) Flow parameters may be determined by the injection-hole and control-hole techniques, using a honeycomb network of piezometric drillholes.

4) It is advisable to use the set of equipment described herein (accessory for loading tracer into the hole, automatic strip-chart recorder unit, set of removable probes) in tracer monitoring of seepage flow.

N. Flekser

CONFERENCE ON SEED IRRADIATION PRIOR TO SOWING

Translated from Atomnaya Énergiya, Vol. 10, No. 5
pp. 549-551, May, 1961

A conference on seed irradiation prior to sowing convened under the sponsorship of the Institute of Biophysics of the Academy of Sciences of the USSR and the Council on Uses of Atomic Energy in Agriculture of the All-Union V. I. Lenin Academy of Agricultural Sciences (VASKhNIL) in Moscow, February 20 to 23, 1961.

The conference was opened by a brief introductory speech by G. M. Frank (Institute of Biophysics of the USSR Academy of Sciences). A. M. Kuzin of the Institute of Biophysics of the USSR Academy of Sciences then took the floor with a report on the theoretical prerequisites of the method of presowing irradiation of seeds. He noted that the nature of effects of ionizing radiation on living systems is a function of irradiation dose. Under certain conditions, irradiation of seeds prior to sowing results in enhanced agricultural crop yield, acceleration of the ripening process, and improved quality of product. The required doses for plants studied to date range from 500 to 1000r. Paramagnetic resonance methods have shown that the exposure leads to the formation of free radicals which last for several days. The greater the amount of water contained in the organism, the shorter the lifetime of the radicals. Recent experiments conducted on many biological objects have demonstrated that the energy imparted by gamma radiation migrates and appears not at random sites but at certain active centers. For example, enzymes are activated preferentially, etc. Irradiation of any organism speeds up the aging process; in the case of agricultural crops in particular, this means earlier efflorescence and maturation, etc.

G. R. Rik (Agrophysical Research Institute of VASKhNIL) delivered a report of the mechanism involved in ionizing radiation effects on plants. The reporter emphasized the fact that study of the radiation-effects mechanism is absolutely necessary to lay the basis for a quantitative theory of the effects. The basic trend in this avenue of studies must be recognized as the investigation of the initial biological reaction of the organism to exposure effects. The stimulating action of ionizing radiation is the result of the protective reaction of the organism to an irritation and is realized through an excess of the protective forces of the organism.

Theoretical questions were also elucidated in other reports. N. R. Batygin (Agrophysical Research Institute of VASKhNIL) delivered a paper on the topic "Understanding radiostimulation processes," and expressed the view that a study of the causes of radiostimulation is approached best by beginning with a comparison of this phenomenon and chemostimulation and with similar phenomena observed in nature. Comparison of radiation effects and effects induced by growth activators reveals an affinity in the character of the physicological, biochemical, and physicochemical processes at work.

V. I. Savin of the Institute of Biology of the Ural Branch of the USSR Academy of Sciences devoted his report to experiments on presowing irradiation of seeds of certain plants, using a Co^{60} source, and noted acceleration of growth and development in wheat, barley, tomatoes, radishes, and other crops in response to doses ranging from 500 to 3000 r. However, these phenomena were not consistently reproduced when experiments were rerun. Moderate radiation doses are also stimulating, but only under certain plant-raising conditions. Larger doses had the effect of bringing about morphological changes in the plants, such as changes in branchiness, formation of extra ears, etc., which may become passed on as hereditary features. Improvements in plant nutrition offsets the depressing effects induced by radiations.

L. P. Breslavets (Institute of Biophysics of the USSR Academy of Sciences), in delivering her report "Significance of exposure duration in acceleration of cell fission and appearance of modifications in the nucleus and plasma," rendered an account of experiments on effects of small doses of gamma rays in prolonged exposure on plants. Low-dosage irradiation treatment of rye karyopses over a month-long interval elicited the same stimulation of growth and development (and subsequent crop increase) as did a short-term exposure with triple the dosage. Cytological investigations disclosed the fact that moderate but sufficiently protracted exposures cause acceleration of cellular fission. An increase in the radioactive background of the environmental medium makes possible an increase in the number of mutations over the previous rate, through modifications of the nucleus and chromosomes.

The report delivered by S. I. Yanushkevich of Moscow State University was devoted to a description of studies on the effect of crop-cultivation conditions on seed stability to gamma irradiation in the case of barley and wheat. Results of experiments showed that the same radiation dose brought about the same inhibition of growth in seedlings originating from different farming regions (Moscow, Odessa, Black Sea District), and revealed that variations in seed radiosensitivity are reflected in the frequency of radiation-induced chromosomal aberrations. Differences in radiosensitivity may be ascribed to physiological and biochemical modifications of the seeds brought about by crop-raising in zones differing in their agronomical and climatic characteristics.

N. M. Berezina (Institute of Biophysics of the USSR Academy of Sciences) indicated in her report that presowing irradiation processing of seeds in some cases not only stimulates growth and development of plants and speeds up the maturation process, but also alters the biochemical composition of the plants cultivated from the irradiated seeds, which frequently means an improvement in the quality of the agricultural raw material. It was found for instance that the content of ascorbic acid was increased in cabbage, potatoes, radishes, green corn meal, and other agricultural produce. Irradiation of carrot and squash seeds increases the carotene content in root vegetables, etc. This adds much to the practical significance of the method of presowing irradiation of crop seeds. The biochemical alterations brought about by presowing gamma irradiation of corn seeds, discussed in the report by V. S. Fedorova of the Central Siberian Botanical Garden of the Siberian Division of the USSR Academy of Sciences, enhance the nutritive advantages of this crop as ensilage fodder.

A. I. Khudadatov (Institute of Genetics of the Academy of Sciences of the Azerbaidzhani SSR reported that presowing gamma irradiation of corn seeds in doses of 2000-4000 r resulted in a crop increase of bulk green corn and an increased content of sugars and vitamin C in the corn. In 1960, irradiated cucumber and melon seeds were sown over a four-hectare plot on one of the collective farms in Azerbaidzhan. Papers submitted by K. K. Roze and V. T. Kietse (Institute of Biology of the Academy of Sciences of the Latvian SSR), N. G. Zhezhel' (Leningrad Agricultural Institute), and others discussed the stimulating effect of presowing irradiation processing of corn and wheat seeds, and also of barley and other cereal crops on the germinating power of the seeds, the growth and development of the plants, and increased crop yield. Z. N. Galochalova and A. M. Shkurina (Central Siberian Botanical Gardens of the Siberian Division of the USSR Academy of Sciences) revealed that the efficiency of radiation processing of wheat seeds depends in the first instance on the initial moisture of the grain, which is responsible for the particular physiological state of the embryos, and also on the type of ionizing radiations at work. Experimental findings reported by the authors may be used to select the optimum conditions under which presowing irradiation of seeds will pay off in improved biological properties and increased crop returns.

L. M. Kryukova, A. M. Kuzin, I. S. Listvin (Institute of Biophysics of the USSR Academy of Sciences and All-Union Flax Farming Research Inst.) reported on seed irradiation experiments involving gamma-ray processing of fiber-flax to increase the yield of fiber and enhance its properties. The results of irradiating seeds with a 1000-roentgen dose were 10-25% improvement in germinating power, depending on the strain of plant. Strain L-1120 showed an over-all stalk-length increase of 10 cm, or of 5 cm for technical-length increase, which pays high practical dividends.

A paper delivered by A. I. Grechushnikov and V. S. Serebrenikov (of the Potato Crops Research Institute) adduced data on the effect of radiation exposures of 150 to 500 r prior to planting on the growth and development of potato plants. When tubers and seeds were irradiated at those doses prior to planting, an increase in potato crop yield was accompanied by increased content of vitamin C and starch in the ripening tubers. The authors feel that preplanting irradiation of tubers with low gamma-ray doses holds great promise for crop yield and improvement of the quality of potato tubers.

A report presented by G. I. Shchiber' dealt with field experiments performed at the All-Union Institute for the Vitamin Industry in collaboration with the Biophysics Institute of the USSR Academy of Sciences on a comparison of the effectiveness of various methods of presowing radiation processing of carrot seeds, including gamma presowing irradiation. The radiation exposure treatment proved to be one of the most efficient, trouble-saving, and time-saving approaches to presowing treatment. Under actual farming conditions in a 26.5-hectare plot, a 30% increase in root vegetable crop was obtained along with a 9-12% increase in carotene content.

O. K. Kedrov-Zikhman and N. I. Borisov (All-Union Research Institute for Fertilizers and Agronomical Soil Science) reported on a series of 1957-1959 experiments involving presowing radiation processing of barley, wheat, corn, flax, carrot, and other crop seeds. Irradiation prior to plant sowing resulted in increased crop without adversely affecting quality (content of protein in grain, fat content in oil-producing plants, fiber in flax stalks). The authors were also concerned with irradiation of seeds which were themselves offspring of irradiated seeds. Depending upon plant species, both positive and negative results were recorded.

The conference also heard reports devoted to presowing gamma-ray treatment of perennial grass (N.I.Makarov, Institute of Biology of the Ural Branch of the USSR Academy of Sciences) and various vegetable and fruit crops. Optimized radiation doses for bringing about the stimulation of one or another plant development process were arrived at in all of the papers. Excessively large radiation doses bring the plants to grief in all cases. Irradiation of lavender seeds (a paper read by S. G. Malyarenko, State Botanical Gardens at Nikita) resulted in such high germinating power in the lavender plant that it was unmatched by any other known methods.

The Institute of Nuclear Physics of the Academy of Sciences of the Uzbek SSR presented reports on studies of the effect of presowing radiation treatment of seeds on the growth, development, and modification of properties of silk, hemp, jute, peanuts, and similar plants (by U. A. Arifov, G. A. Klein, S. A. Anastasov), and also on the effect of gammas and neutrons on growth and development of the cotton plant (A. P. Ibragimov, T. I. Ibragimov). Cotton bolls were found to ripen earlier when cotton seeds were neutron-irradiated than when the latter were gamma-irradiated. S. O. Brebinskii and V. G. Tsibukh (I. Ya. Franko L'vov State University) devoted their paper to an investigation of the effect of x-raying of seeds of the sugar beet and other vegetables on crop yield. Seeds showing evidence of sprouting are the natural choice for radiation treatment, being more homogeneous in the physiological sense than dry seeds. E. I. Preobrazhenskaya (Institute of Biology of the Ural Branch of the USSR Academy of Sciences) devoted her paper to establishing a correlation between the stimulating effect of ionizing radiations and the over-all radiation stability of plants. The stimulation phenomenon is expressed to a lesser extent in radiosensitive species than in species of average radiosensitivity or in species stable to radiation exposure. A. N. Poryadkova and N. M. Makarov (Institute of Biology of the Ural Branch of the USSR Academy of Sciences) described experiments on comparison of various approaches to radiostimulation. Seeds were soaked in solutions of uranium fission fragments of low concentration, both swelling and dry seeds were subject to x-ray and gamma-ray bombardment, radiation emitting sources were placed in soil, and some alpha particle irradiation was done. For practical purposes, the authors recommend presowing irradiation of seeds as a technique free of undesirable side effects.

After the reports were heard, an exchange of views took place between the participants at the conference, and an appropriate resolution was adopted.

The conference demonstrated that the method of presowing irradiation of seeds holds great promise from the viewpoint of its practical utilization in our nation's agriculture, and that further extensive and painstaking work is needed to undertake a careful, thorough, and versatile study and justification of the technique.

The proceedings of the conference will be published shortly.

V. M. Patskevich

BIBLIOGRAPHY

BOOKS AND SYMPOSIA

Translated from Atomnaya Énergiya, Vol. 10, No. 5,
pp. 553-560, May, 1961

D. B. Hoisington. Osnovy yadernoi tekhniki. [Russian translation of Nucleonics Fundamentals, McGraw-Hill, New York 1959]. Gosatomizdat, 1961. 398 pages, 1 ruble, 98 kopeks.

This book provides the reader with the basic information on the chemical structure of matter, the physical state of matter, the structure of the atom and nuclei. The phenomenon of radioactivity is described and artificial nuclear transmutations are discussed. Light is shed on various areas of application for radioactive isotopes. A description of high-voltage and cyclic accelerators is given. Problems of radiation shielding are illuminated, covering such topics as maximum tolerance dose and physical methods of shielding; a description of radiometric and dosimetric equipment is included. The fission reaction and the chain reaction are discussed. The operating principles of nuclear reactors are outlined and several reactor types designed for research work and some power reactors are described. The last two chapters of the book are devoted to controlled fusion and isotope separation.

Problems devised to contribute to better mastery of the material are included at the end of some chapters. The appendices include a short glossary of nucleonics terminology, a list of the most useful symbols, physical constants, atomic and nuclear data, and answers to the problems.

The book is written for all persons interested in nucleonics questions.

Biologicheskoe deistvie radiatsii i voprosy raspredeleniya radioaktivnykh izotopov[Biological effects of radiation and abundance of radioactive isotopes]. Symposium. Moscow, Gosatomizdat, 1961. 192 pages. 69 kopeks.

This symposium is made up of 20 articles devoted to problems of effects of external radiation sources and radioactive materials ingested by the organism on the organism. The problems of radiation effects on nucleic acids in tissues are discussed. Some articles are devoted to a study of the pattern of accumulation, distribution, and isolation of radioactive substances, particularly Pu^{239}. In one of the articles, an experimental justification is provided for the critical tolerance level of Sr^{90} content and uptake in the organism. Subsequent articles treat of biological and toxicological effects of such radioactive isotopes as Sr^{90}, Cs^{137}, Ce^{144}, and illuminate several problems in current radiobiology research related to the migration of artificial radioactive isotopes in the organism of farm animals. The six concluding articles in the symposium are all devoted to the biological effects of plutonium.

The book is compiled for the use of medical students and technicians and biologists interested in radiobiology problems.

Radioaktivnye izotopy i yadernye izlucheniya v narodnom khozyaistve SSSR. Vol. I. [Radioactive isotopes and nuclear radiations in the national economy of the USSR]. Proceedings of the all-union conference on the topic held April 12-16, 1960, at Riga. To appear as a four-volume set. Edited by N. A. Petrov, L. I. Petrenko, P. S. Savitskii. Moscow, Gostoptekhizdat, 1961. 340 pages. 2 rubles, 09 kopeks.

The first section of this leadoff volume deals with general problems encountered in applications for isotopes and nuclear radiations in the national economy; the present status and future perspectives for the use of isotopes are considered (P. S. Savitskii); experience in assimilating isotope and nuclear radiations techniques in enterprises under the jurisdiction of the council of the national economy of the Latvian SSR are drawn upon and generalized (G. I. Gaile, V. P. Dubovich); the economic advantages and efficiency of radiations applications in industry are analyzed (G. F. Mikheev); the perspectives for employment of devices using radioactive radiation sources for process control in particular branches of industry are studied (V. S. Sokolov); some promising applications for radiation chemistry as a tool in industrial development are discussed (V. L. Karpov); a description of new types of radiometric and dosimetric equipment is presented (V. S. Zhernov, S. V. Mamikonyan).

The second section of this volume is devoted to instruments using sources of radioactive radiations, manufactured by the Tallinn experimental plant for control and measurements instruments, the Khar'kov KIP factory, and

the Mosrentgen x-ray equipment factory. Specifications for gas-discharge counters and cold-cathode tubes are given. A description appears of radiation sources employed in process monitoring and control. Some problems in shielding and safety practice involving the use of such instruments are discussed, and experience accumulated in their use in several plants is outlined. The procedure to be followed in comparative testing of relays operating on sources of ionizing radiations is described.

The third section considers problems in radiation chemistry. Specifications for gamma-radiation sources to be used in radiation-chemical equipment are discussed, and technological characteristics and data are presented for some possible representative facilities designed for radiation polymerization of ethylene on an industrial scale and radiation vulcanization of automotive tires; a description of an irradiating facility using a Co^{60} source with an activity of 60,000 gram equivalents of radium (K = 60,000) is included. Radiation processes for chlorination of silcon-containing monomers and polymers (elastomers), sulfochlorination and sulfoxidation of polyethylene, polypropylene, polyisobutylene and paraffinic hydrocarbons, radiation-thermal cracking, localized crosslinking of teflon under neutron bombardment, etc. are described.

In the fourth section, experience in the use of instruments based on sources of ionized radiations for the monitoring and automation of process control in the chemical processing and oil refining industries is illustrated.

This work is aimed at broad circles of engineering personnel, technicians, and research workers engaged in the assimilation of nucleonic techniques into industrial practice.

V. G. Segalin. Primenenie radioaktivnykh izotopov dlya avtomatizatsii v ugol'noi promyshlennosti [Process control applications for radioactive isotopes in the coal industry]. Moscow, Gosgortekhizdat, 1960. 391 pages. 1 ruble 26 kopeks.

The fundamental requirements for automatic control, monitoring, and process control instrumentation in coal mining and coal dressing are outlined in this book. The wide promise and opportunities beckoning to process control techniques based on the use of radioactive isotopes and nuclear radiations in the coal industry are demonstrated, and experience in industrial utilization of gamma-electronic relays is generalized upon.

Devices and equipment using sources of ionizing radiations in such applications as measurement of filling level of bins and hoppers, determination of ash content of coal, automatic control of the motion of coal cleaning machines and entry-driving machines as a function of the hypsometry of the coal bed, measurements of density of heavy fluids, automatic control of the height of the jig bed in jigging machines, etc., are described.

Theoretical assessments of the accuracy of various devices, their stability, magnitude of probable errors, are given; recommendations are offered on the most feasible choice of sources and radiation detectors to meet a particular problem.

Some of the distinctive features of absorption of ionizing radiations in a multicomponent mixture are mentioned, and possibilities opened up by the exploitation of this absorption in the design of process control instrumentation are discussed.

The book is written for an audience of engineering technicians in the mining, metallurgical, coal processing, and related branches of industry engaged in work on process control, and also for scientific research workers and designers and interested students.

V. I. Postnikov, V. A. Letenko. Effektivnost' radioaktivnogo kontrolya v mashinostroenii [Efficiency of radioactive monitoring measures in machine design (with particular emphasis on gamma-ray nondestructive testing)]. Moscow, Mashgiz, 1960. 146 pages. 57 kopeks.

This book outlines the physical basics of the use of radioactive isotopes for gamma radiography. Characteristics of gamma sources utilized in quality control and nondestructive testing of metals are given, and a description appears of Soviet and foreign-manufactured gamma-radiography units. The basic criteria and indices for estimating the economic efficiency of the new technique are formulated, and fundamental information needed on the procedure for determining marginal expenses, determining the amortization time on simultaneous investments, is provided. An idea is given of the peculiar problems encountered in determining economic efficiency where radiation sources are used in gamma radiography.

Characteristics and recommendations are added in reference to the use of gamma radiation sources, in the light of such parameters as the thickness of the test specimen, radiation energy, sensitivity, and exposure. Costs for pro-

ducing a single gamma-radiography plate are discussed, and conclusions based on the discussion are drawn as to the feasibility of using one gamma radiation source or another from the vantage point of maximizing economic savings.

Problems of economic efficiency in radioactive monitoring at machine-building enterprises are discussed with an eye to the volume of production.

The book is written for a wide audience of engineering and technician personnel in machinery factories and for students in machine design courses.

N. F. Kazakov. Radioaktivnye izotopy v issledovanii iznosa rezhushchego instrumenta [Radioactive isotopes and tracer studies of wear on cutting tools]. Moscow, Mashgiz, 1960. 328 pages. 1 ruble, 35 kopeks.

An attempt is made in this book to draw general inferences from the findings of research based on the radioactive tracer method in studies of wear processes affecting cutting tools. The physical fundamentals of the tracer techniques are outlined in brief, as well as techniques for using tracers in wear studies; the results of Soviet and foreign investigations of wear processes on cutting tools are reported.

The tracer approach is accompanied by a description of simulation of the wear process in a vacuum, metal-physics techniques in studies of variation of hardness, etc.

It is shown that radioactive tracers may be used not only to speed up the research process and reduce the amount of materials and financial means expended, but also to probe experimental techniques for determining the metal-cutting programs in which wear on the cutting tool is minimized.

The book is written for scientific and engineering workers interested in materials processing and machining.

F. Laux. Radioaktivnye izotopy na sluzhbe cheloveka [Translation from the French: Radioactive isotopes in the service of mankind]. Moscow, Gosatomizdat, 1961. 112 pages. 37 kopeks.

This book makes it possible for a reader lacking any specialized training to get an idea of the nature of radioactive isotopes and the history of their development and production, their possible applications. Concrete examples are shown of how the use of radioisotopes in physics, chemistry, biology, medicine, and various branches of industry shapes up. An account is also provided of biological effects of radiation emitted by radioactive isotopes, and shielding against those radiations.

ARTICLES FROM THE PERIODICAL LITERATURE

I. NUCLEAR ENERGY PHYSICS

Neutron and Reactor Physics. Physics of Hot Plasma and Controlled Fusion. Physics of Acceleration of Charged Particles.

Voprosy filosofii, XV, No. 1 (1961)

I. A. Akchurin, 41-50. The philosophical significance of the fundamental ideas in the modern theories of "elementary" particles.

Doklady akad. nauk SSSR, 135, No. 6 (1960)

V. M. Vakhnin, G. A. Skuridin, 1354-57. On a possible mechanism of capture of charged particles in a magnetic field.

Zhur. tekhn. fiz., XXXI, No. 2 (1961)

A. N. Zaidel' et al., 129-166. Spectroscopic techniques in hot-plasma research.

Zhur. éksptl. i teoret. fiz., 40, No. 1 (1961)

M. S. Ioffe et al., 40-48. On drift of plasma from a trap with magnetic mirrors.

B. B. Kadomtsev, 328-36. On turbulence of a plasma in a trap with magnetic mirrors.

Izvestiya Tomsk. politekhn. inst., Vol. 105 (1960)

A. A. Vorob'ev, 3-4 A two-half-cycle acceleration scheme in a synchrotron.

Brit. J. Appl. Phys., 11, No. 12 (1960)

J. Kelsch et al., 555. New method for direct investigation of the fission phenomenon.

Jaderná Energie, VII, No. 1 (1961)

J. Matoušková, J. Holanova, 2-5. Measurement of fast-neutron dose using nuclear emulsions.

Nucl. Energy, 15, No. 153 (1961)

D. Carswell, J. Lawrence, 66-69. Methods and equipment for nuclear physics training courses.

Nucl. Engng., 6, No. 57 (1961)

- - -, 80-81. Exposition of the British Physical Society, 1961.

Nucl. Instrum. and Methods, 9, No. 2 (1960)

E. Kisdi-Koszó, L. Turi, 137-40. Phase and vertical particle stability in the microtron.

Nucl. Instrum. and Methods, 9, No. 3 (1960)

H. Hernandez et al., 287-302. The Livermore 230-centimeter variable-energy cyclotron.
W. Weidemann, 347-53. On the design of quadrupole focusing systems.

Nucl. Instrum. and Methods, 10, No. 1 (1961)

K. Chapman, S. Gowariker, 66-67. Convenient method of constructing accelerator tubes.
A. James, C. Jonson, 68-69. Wideband detection of small ion beam currents.

Nucl. Instrum. and Methods 11, No. 1 (1961)

P. Endt, 3-6, Resonance reactions.
L. Katz, K. Lokan 7-13. Positron generation in a thick target bombarded by fast electrons.
L. Katz, 14-18. Characteristics of linear electron accelerators required for nuclear investigations.
T. Huus, 19-28. Coulomb excitation.
G. Goldring, 29-38. Experiments using ultra-fast pulse techniques.
E. Cotton, 39. Lifetime of nuclear states.
A. Schoch, 40-46. Discussion of colliding-beam techniques.
P. Rose, 49-62. Three-cascade tandem accelerator.
H. Gove, 63-92. Tandem accelerator experiments at the Chalk River laboratory.
K. Allen, 93-111. Tandem accelerator studies of nuclear reactions at Aldermaston.
R. Fleischmann, 112-21. Sources of polarized ions (for protons and other similar particles).
R. Connor, 122-25. Generation of millimicrosecond pulses.
J. Nygard, R. Post, 126-35. Development of high-power microwave electron accelerators for physical research.
U. Gonser, K. Lücke, 139-43. Use of Van de Graaff accelerators for irradiating metals with high-intensity neutron flux.
K. Beckurts, 144-68. Applications for pulsed neutron sources in reactor-physics investigations.
F. Amman, 169-78. Use of 3-Mev Van de Graaff machine as injector for the electron synchrotron at the Frascati National Laboratory.
J. Kistemaker, 179-84. High-intensity ion sources.
J. Otvos et al., 187-95. Photoactivation and photoneutron-activation analysis.
P. Baruch, 196-209. Use of electron accelerator in solid state physics.
W. Huber, 210-26. Use of high-energy radiations in biochemistry and microbiology.
S. Pinner, W. Davison, 227-37. Development of irradiation processes.

D. Moore, 238-47. Utilization of neutron, electron, and x-ray beams from a Van de Graaff accelerator for radiation investigations.

D. Trageser, 248-53. Future accelerators – intense sources for processing.

- - - , 254-56. Tables of Van de Graaff characteristics, microwave linear electron accelerator characteristics, Cockroft-Walton accelerator characteristics, and isotope separator characteristics.

Nucl. Power, 6, No. 58 (1961)

- - - , 83-86. 1961 exposition of the British Physical Society.

Nucl. Sci. and Engng., 8, No. 6 (1960)

F. Gould et al., 453-66. Long-wavelength crystal spectrometer and the neutron absorption cross sections of gold and boron.

Nucleonics, 19, No. 1 (1961)

G. Wertheim, 52-57. The Mössbauer effect: a tool for science.

T. Eastwood, 64. Specific-activity nomogram.

Nucleonics, 19, No. 2 (1961)

D. Roberts, 53-57. A-C ion chambers are simple and reliable.

Nukleonika, 2, No. 7 (1960)

G. Wolf, 255-71. Use of the method of beta-gamma coincidences for determining the absolute number of decay events and for measuring the activation cross sections of nuclides Na^{23}, Sc^{45}, Co^{59}, and Ta^{181}.

NUCLEAR POWER ENGINEERING

Nuclear Reactor Theory and Calculations. Reactor Design. Performance of Nuclear Reactors and Nuclear Power Stations.

Kul'tura i zhizn', No. 1 (1961)

A. M. Kuzin, 15-17. Peaceful uses of atomic energy.

Trudy nauch. tekhn. obsh-va sudostroit. prom., No. 34 (1960)

B. S. Yudovin, 227-57. Features of the present stage of development of maritime nuclear facilities (based on information from the foreign press).

Atomkernenergie, 6, No. 1 (1961)

K. Illies, 1-8. Maritime propulsion nuclear reactors.

R. Dickinson, H. Polak, 9-15. Development of the graphite-moderated sodium-cooled reactor.

W. Kattwinkel, 15-18. Problems in thermal conductivity of a heat-exchanger tube-bundle board.

G. Schweizer, 18-24. Determination of frequency response of a nuclear reactor by statistical techniques.

W. Kliefoth, 37-40. 1961 perspectives for the development of nuclear power.

Atompraxis, 7, No. 1 (1961)

D. Eggen, 17-23. Critical experiments on designing an improved epithermal thorium reactor.

Atomwirtschaft, 6, No. 1 (1961)

H. Fischerhof, 2-5. Nuclear legislation in Switzerland and West Germany.

M. Higatsberger, 5-11. The Austrian reactor center at Seibersdorf.

- - - , 25-84. The experimental nuclear power station at Kahl.
P. Mandel, 25-29. Preliminary design stages for the station.
M. Ellmer, H. Kornbichler, 30-37. Design and building of the station.
R. Misenta, H. Schamle, 37-41. Core testing at zero pile power.
H. Rösch, G. Vogel, 41-46. Decision-making chain of command in construction and operation of the station.
H. Fendler, K. Knopf, 50-56. Radiation shielding.
H. Schulze et al., 56-60. Control system and station shielding.
F. Börnke, 61-65. Stages in the construction of the station.
E. Zastrow, 66-72. Structural materials.
L. Franzl et al., 73-79. High-pressure reactor vessel, hot-well condenser cooler, tubes and ducting.
H. Geismann, A. Thiel, 80-81. Steam generator.
R. Scheuten, 82-84. Problems concerning responsibility in transportation of nuclear fuel.

Jaderná Energie, VII, No. 1 (1961)

F. Voženílek, 6-9. Electrical equipment of the Czechoslovak nuclear reactor after three years of performance.
V. Zajíc, 10-12. Effect of temperature rise at the surface of a fuel element on the thermal efficiency of a nuclear power station.

J. Appl. Phys., 31, No. 12 (1960)

T. Noggle, J. Stiegler, 2199-2208. Observations of tracks of fission fragments in thin UO_2 films through the electron microscope.

J. Brit. Nucl. Energy Conf., 6, No. 1 (1961)

R. Anscomb, F. Hutber, 1-26. Control problems and equipment problems for maritime reactors.
I. Davidson, 27-35. Contribution of nuclear power to engineering: large high-pressure steel vessels and concrete biological shielding.
R. Blake, 49-61. An instrument for determining oxide content in sodium, based on measurement of electrical resistivity.
G. Smith, J. Cheetham, 62-69. Coolant leakage tests for Calder-Hall type reactors.

Kernenergie, 3, Nos. 10-11 (1960)

K. Rambusch, 932-40. Five years of development of nuclear research and nuclear engineering in the German Democratic Republic (East Germany).
A. Müller, 951-58. Boiling-water reactor criticality calculations.
B. Köhler, 959-62. Control-components calculations using modified one-group theory.
G. Lehmann, B. Kozik, 963-72. Computation of resonance absorption in uranium-containing fuel elements.
M. Balarin, O. Hauser, 973-78. Energy aspects of the formation of radiation defects.

Kerntechnik, 3, No. 1 (1961)

R. Berndt, 33-36. Survey of power reactors.

Nucl. Engng., 6, No. 57 (1961)

R. Kühnel, 56-65. The 15-Mw boiling-water reactor at Kahl.
J. Hill, 66-68. Plutonium as nuclear fuel for atomic engines.
- - -, 68. Start-up of the plutonium fuel cycle testing reactor.
- - -, 75-76. Low-frequency oscillators for tensioning control rods.
J. Pefhany, 77-79. Pneumatic gages for in-pile measurements.

Nucl. Power, 6, No. 58 (1961)

V. Emelyanov, 75-76. Reactors in the Soviet Union.
W. Havranek, T. Kierans, 77-81. Solution of reactor dynamics equations.

- - -, 81. The Juggernaut reactor.

Nucl. Sci. and Engng., 8, No. 6 (1960)

P. Haubenreich, 467-79. Two years of HRE-2 operation.

R. Jacobs, J. Merrill, 480-96. The application of statistical methods of analysis for predicting burnout heat flux.

E. Hellstrand et al., 497-506. The temperature coefficient of the resonance integral for uranium metal and oxide.

W. Hogan, 518-22. Negative-reactivity measurements.

G. Jarvis et al., 525-31. Two plutonium-metal critical assemblies.

G. Hansen, C. Maier, 532-42. Perturbation theory of reactivity coefficients for fast-neutron critical systems.

L. Engle et al., 543-69. Reactivity contributions of various materials in Topsy, Godiva, and Jezebel.

G. Hansen et al., 570-77. Critical plutonium and enriched-uranium-metal cylinders of extreme shape.

D. Wood et al., 578-87. Critical masses of cylinders of plutonium enriched with other metals.

G. Hansen et al., 588-94. Critical masses of enriched-uranium cylinders with multiple reflectors of medium-Z elements.

L. Stewart, 595-97. Leakage neutron spectrum from a bare Pu^{239} critical assembly.

C. Byers, 608-614. Cross sections of various materials in the Godiva and Jezebel critical assemblies.

E. Plassmann, D. Wood, 615-20. Critical reflector thickness for spherical U^{233} and Pu^{239} systems.

W. Roach, 621-51. Computational survey of idealized fast breeder reactors.

C. Chezem, 652-69. A uranium-metal exponential experiment.

G. Keepin, C. Cox, 670-90. General solution of the reactor kinetic equations.

T. Wimett et al., 691-708. Godiva II: an unmoderated pulse-irradiation reactor.

W. Bebbington, 720. An H_2O-D_2O moderated reactor.

Nucleonics, 19, No. 1 (1961)

G. Thornton, B. Blumberg, 45-51. Performance results from the Heat Transfer Reactor Experiment tests of aircraft nuclear propulsion.

B. Lustman et al., 58-63. Zircaloy cladding performs well in PWR.

R. Dickinson, J. Williams, 65-70. Trends in sodium equipment: design of heat exchangers, ductwork, and pumping equipment for sodium-cooled reactors.

W. Sutherland, 80, ff. Optimizing core performance.

M. Silvestri et al., 86-88. Fog-cooling: dispersion of water droplets in steam as coolant.

Nucleonics, 19, No. 2 (1961)

- - -, 5. PM-3A reactor will supply Antarctic power. (Advertisement).

- - -, 17-23. Fatal accident at the Stationary Low-power Reactor No. 1.

- - -, 47-48. Chemonuclear reactors.

- - -, 48-50. Thin unclad fuel needed for chemonuclear reactors.

J. Yevick, A. Amorosi, 64-69. Capital costs cut for fast breeders.

- - -, 82. Nitrogen and air: acceptable coolants for the ML-1 pile.

R. Casini, F. Volta, 84-85. Pressure transients following coolant loss.

- - -, 82-83. 2500°F liquid metals needed for space ion engines.

F. Tingey, 90-95. Statistical design of in-pile screening tests.

Nukleonika, V, No. 11 (1960)

L. Łabno et al., 685-88. A neutron-sensitive boron-lined thermoelectric battery.

T. Rzeszot, Z. Weiss, 689-703. Boron-filter measurements of neutron spectrum temperature.

K. Żarnowiecki, P. Szulc, 705-11. A photoneutron source for the start-up of the WWR-S reactor.

W. Byszewski et al., 727-36. Measurement of fuel-element wall temperature in the WWR-S reactor.

K. Wajs, 737-42. Estimating error introduced by linearization of reactor equations.

A. Kuszell, J. Mika, 743-54. Thermal utilization factor in lattices with water-graphite moderator.

A. Kowalew, 755-59. Some activation problems in a periodic-cycle reactor.

III. NUCLEAR FUELS AND MATERIALS

Nuclear Geology and Primary Ore Technology. Nuclear Metallurgy and Secondary Ore Technology. Chemistry of Nuclear Materials.

Zhur. neorgan. khim., 5, No. 12 (1960)

E. E. Kriss, Z. A. Sheka, 2819-23. Solvent extraction of rare earths using dibutylphosphate and tributylphosphate.

V. B. Shevchenko et al., 2832-40. Behavior of hexavalent and trivalent chromium in tributylphosphate extraction of uranyl and plutonium nitrates.

Zhur. strukturnoi khim., 1, No. 4 (1960)

L. V. Lipis et al., 417-24. Investigations of chelating of tetravalent plutonium in sulfate solutions.

Zhur. fiz. khim., 34, No. 11 (1960)

P. F. Andreev et al., 2429-30. Extraction of uranium from rock under ultrasonic irradiation.

Zavod. laboratoriya, 26, No. 12 (1960)

V. I. Kuznetsov, T. N. Kukisheva, 1344-46. Photometric determination of uranium using arsenazo reagent.

Zapisi vsesoyuz. mineralog. ob-va, 89, No. 6 (1960)

Yu. M. Dymkov, 652-62. Signs of crystallization growth in pitchblende.

N. P. Formina, 663-68. On uraniferous solid bitumens in sedimentation rocks.

Izvestiya akad. nauk UzSSR, seriya fiz.-matem. nauk, No. 5 (1960)

A. A. Abdullaev et al., 48-56. Analysis of activated rock samples by gamma-ray scintillation spectrometry.

Mirovaya ekonomika i mezhdunar. otnosheniya, No. 12 (1960) [World economy and international relations]

R. Adlivankina, 106-109. On the capitalist uranium market.

Teploénergetika, 8, No. 2 (1961)

P. A. Akol'zin, L. V. Korneeva, 55-60. Effect of chlorine ions on corrosion cracking of austenite steel 1Kh18N9T.

Uspekhi khimii, 29, No. 12 (1960)

R. Tsaletka, A. V. Lapitskii, 1487-97. Abundance of transuranium elements in nature.

Atomkernenergie, 6, No. 1 (1961)

G. Saur et al., 30-37. Possible applications for aluminum and aluminum alloys in water-cooled reactors.

Kernenergie, 3, Nos. 10-11 (1960)

A. Lehr et al., 941-50. Microscope for hot-cell work.

D. Naumann, 984-88. Synthetic inorganic ion exchange materials.

R. Münze, L. Baraniak, 989-91. Production of impurity-free $Na^{18}F$.

R. Winkler, E. Leibnitz, 992-98. Adsorption of some fission products of uranium on humic acids.

Kerntechnik, 3, No. 1 (1961)

P. Baertschi, 26-27. Nuclear energy uses of chemistry.

Nucl. Energy, 15, No. 153 (1961)

G. Hall, 59-63. Design and operation of a radiochemical laboratory.
- - -, 70. Remote control hot cells.

Nucl. Power, 6, No. 58 (1961)

E. Edmonds, 72-74. The eighth conference on hot laboratories and equipment (San Francisco, December, 1960).

Nucl. Sci. and Engng., 8, No. 6 (1960)

C. Coleman et al., 507-14. Solvent extraction recovery of technetium, neptunium, and uranium from fluorination plant residues.

Nucleonics, 19, No. 1 (1961)

C. Ziegler et al., 76-78. New x-ray technique locates core in fuel plates.
- - -, 90-91. Hot-atom chemists study nuclear-reaction effects.
R. Heemstra et al., 92 ff. Laboratory evaluations of nine water tracers.

Nucleonics, 19, No. 2 (1961)

A. Wiebe et al., 50-52. Fission fragments initiate ethylene glycol synthesis in chemonuclear reactors.
E. Roszkowski, 80. Laboratory for plutonium chemistry.

Nukleonika, V, No. 11 (1960)

T. Adamski, J. Zenkiewicz, 761-69. Investigation of feasibility of processing low-grade uranium ores by chlorination with chlorine gas in the presence of a reducing agent.

IV. NUCLEAR RADIATION SHIELDING

Radiobiology and Radiation Hygiene. Shielding Theory and Calculations. Instrumentation.

Gigiena i Sanitariya, No. 11 (1960)

Yu. V. Novikov, M. L. Godovich, 47-50. New fallout samplers.
V. P. Kasatkin, 50-54. Spectral-dosimetric studies of beta emissions aid in establishing critical tolerance levels for external beta flux.

Gigiena truda i okhrana zdorov'ya rabochikh v neft. i neftekhim. prom. 1 (1960) [Work safety in the oil refining and petrochemicals industry]

V. V. Nechaev, 55-56. Comparative safety characteristics of radiography techniques in pipeline construction work.

Zhur. Vsesoyuz. khim. ob-va im. D. I. Mendeleeva, No. 6 (1960)

A. S. Smirnov, 651-57. Decontamination of radioactive substances in water.

Izvestiya Timiryazev. sel'sko-khoz. akad., No. 6 (1960)

I. V. Gulyakin et al., 7-22. Sr^{90} accumulation in agricultural crops as a function of Sr^{90} concentration in soil.

Sel'skoye khozyaistvo Belorussii, No. 12 (1960) (Byelorussian agriculture)

S. V. Shidlovskii, 18. Labeled atoms and amelioration of meadowlands.

Trudy Tsentr. Sib. botan. sada, No. 4 (1960)

V. S. Fedorova, 123-27. Effect of ionizing radiations on storage of vitamins and monosaccharides in corn plant leaves.

L. A. Sevast'yanova, 129-38. Experimental study of the effect of ionizing radiations on storage of chlorophyll in corn plant leaves.

Tsitologiya, 2, No. 6 (1960) [Cytology]

Ya. A. Ivanov, B. N. Kulikov, 736-39. Response of wheat and barely strains and varieties to irradiation by radioactive cobalt.

Atomkernenergie, 6, No. 1 (1961)

I. Brauer, 25-29. Propagation of a radioactive fallout cloud following the February 13, 1960 test explosion of a French nuclear bomb in the Sahara.

Atompraxis, 6, No. 12 (1960)

H. Niedrig, K. Tradowsky, 480-82. A portable gamma-ray dosimeter.

H. Heinemann, K. Seidler, 483-84. Checking on observation of radiation shielding measures using the film blackening technique in laboratories where radium and isotopes are handled.

Atompraxis, 7, No. 1 (1961)

W. Schweers, 1-3. Determination of C^{14} activity in small amounts of low-boiling-point liquids.

E. Welte, et al., 3-7. Investigations of decrease in strontium uptake by plants from soil.

A. Rudloff, 11-15. Determination of shielding capacity of buildings against radioactive fallout.

Jaderná Energie, VII, No. 1 (1961)

J. Rálková, J. Slunečko, 13-15. Measurement of low radioactivity values in water. III. Counter design.

J. Brit. Nucl. Energy Conf., 6, No. 1 (1961)

E. Cooke-Yarborough, R. Barnes, 36-48. Rapid techniques for determining the activity of a low-level specimen.

Kerntechnik, 3, No. 1 (1961)

M. Oberhofer, 28-32. Centralized measurement of radiation in the operation of nuclear engineering facilities.

Nucl. Engng., 6, No. 57 (1961)

- - -, 55. Maximum tolerable radiation levels.

I. Mannah, 69-74. Thermal stresses in concrete.

Nucleonics, 19, No. 1 (1961)

G. Dearnaley, A. Whitehead, 72 ff. How Harwell makes surface-barrier detectors.

Nukleonik, 2, No. 7 (1960)

F. Pott, S. Wagner, 271-76. Selective measurement of neutron and photoneutron doses, using an ethylene dosimeter.

Nukleonika, V. No. 11 (1960)

E. Józefowicz, 714-17. Absolute measurements of beta activity of liquid scintillators.

V. RADIOACTIVE AND STABLE ISOTOPES

Labeled-Atom Techniques. Uses of Radioactive Radiations. Direct Conversion.

Azerbaidjani neft. khozyaistvo, No. 11 (1960)

M. M. Melikzade et al., 37-38. Study of cracking reaction of normal amylbenzene with tagged carbon atom in the ring over a synthetic alum silica catalyst.

Doklady akad. nauk SSSR, 136, No. 1 (1961)

L. I. Kartashova et al., 143-46. Investigation of radiation oxidation of benzene in an aqueous solution, using labeled tracer atoms.

Zemledelie, No. 1 (1961)

O. B. Andreev, 59-60. Soil humidity gage operates with gamma rays.

Metallovedenie i term. obrabotka metallov, No. 1 (1961) (Metals processing and heat treatment)

I. M. Pronman, 36-47. Variation of mechanical and physical properties of iron-carbon alloys induced by nuclear radiations.

Prikladnaya geofizika, No. 28 (1960)

V. M. Zaporozhets, V. V. Sulin, 116-29. First experiment in the use of a down-hole neutron generator in radioactive logging operations.

Sbornik nauch. trud. Ukrain. nauchno-issled. uglekhim. inst., No. 11 (1960) (Papers of the Ukrainian coal chemicals research inst.)

K. P. Medvedev, V. M. Petropol'skaya, 16-29. Tracer studies of the microstructure of anthracites, using radioisotope sorption.

Sbornik trud. TsNII chern. metallurgii, No. 21 (1960)

L. M. Efimov, 429-47. Determination of costs of beta emitters for radiography and radiometric research.

Atompraxis, 6, No. 12 (1960)

W. Huber, D. Trageser, 463-69. Cheap electrons from new powerful accelerators used in industrial radiation processing.

F. Malsch, R. Schittenhelm, 470-76. High-energy radiation sources for nondestructive testing.

Kerntechnik, 3, No. 1 (1961)

W. Rojahn, 2-4. Production and use of radioactive isotopes in Euratom nations.

H. Krauch, 4-7. Economic problems in isotope use.

N. Riehl, 8-11. Radioisotopes as energy sources.

H. Born, 12-14. The present state of the art and the range of application of activation analysis.

R. Neider, 15-19. Radioactive device for determining the properties of sheet iron in stamping operations.

H. Ramdohr, 19-21. Tracer study of wear on high-speed ball bearings.

A. Trost, 22-23. Monitoring bin filling level with beta radiation.

H. Krause, 24-26. Determination of small concentrations of radioisotopes with the aid of the filter centrifuge.

E. Pohl, 42-43. Review of papers presented to the international conference "Isotopes in Engineering and Industry" (Leipzig, November 17-19, 1960).

SIGNIFICANCE OF ABBREVIATIONS MOST FREQUENTLY ENCOUNTERED IN SOVIET PERIODICALS

FIAN	Phys. Inst. Acad. Sci. USSR
GDI	Water Power Inst.
GITI	State Sci.-Tech. Press
GITTL	State Tech. and Theor. Lit. Press
GONTI	State United Sci.-Tech. Press
Gosenergoizdat	State Power Press
Goskhimizdat	State Chem. Press
GOST	All-Union State Standard
GTTI	State Tech. and Theor. Lit. Press
IL	Foreign Lit. Press
ISN (Izd. Sov. Nauk)	Soviet Science Press
Izd. AN SSSR	Acad. Sci. USSR Press
Izd. MGU	Moscow State Univ. Press
LEIIZhT	Leningrad Power Inst. of Railroad Engineering
LET	Leningrad Elec. Engr. School
LETI	Leningrad Electrotechnical Inst.
LETIIZhT	Leningrad Electrical Engineering Research Inst. of Railroad Engr.
Mashgiz	State Sci.-Tech. Press for Machine Construction Lit.
MEP	Ministry of Electrical Industry
MES	Ministry of Electrical Power Plants
MESEP	Ministry of Electrical Power Plants and the Electrical Industry
MGU	Moscow State Univ.
MKhTI	Moscow Inst. Chem. Tech.
MOPI	Moscow Regional Pedagogical Inst.
MSP	Ministry of Industrial Construction
NII ZVUKSZAPIOI	Scientific Research Inst. of Sound Recording
NIKFI	Sci. Inst. of Modern Motion Picture Photography
ONTI	United Sci.- Tech. Press
OTI	Division of Technical Information
OTN	Div. Tech. Sci.
Stroiizdat	Construction Press
TOE	Association of Power Engineers
TsKTI	Central Research Inst. for Boilers and Turbines
TsNIEL	Central Scientific Research Elec. Engr. Lab.
TsNIEL-MES	Central Scientific Research Elec. Engr. Lab.-Ministry of Electric Power Plants
TsVTI	Central Office of Economic Information
UF	Ural Branch
VIESKh	All-Union Inst. of Rural Elec. Power Stations
VNIIM	All-Union Scientific Research Inst. of Metrology
VNIIZhDT	All-Union Scientific Research Inst. of Railroad Engineering
VTI	All-Union Thermotech. Inst.
VZEI	All-Union Power Correspondence Inst.

NOTE: Abbreviations not on this list and not explained in the translation have been transliterated, no further information about their significance being available to us. —Publisher.

Soviet Journals Available in Cover-to-Cover Translation

ABBREVIATION	RUSSIAN TITLE	TITLE OF TRANSLATION	PUBLISHER	TRANSLATION BEGAN Vol.	Issue	Year
AÉ	Atomnaya énergiya	Soviet Journal of Atomic Energy	Consultants Bureau	1	1	1956
Akust. zh.	Akusticheskii zhurnal	Soviet Physics – Acoustics	American Institute of Physics	1	1	1955
	Antibiotiki	Antibiotics	Consultants Bureau	4	1	1959
Astr(on). zh(urn).	Astronomicheskii zhurnal	Soviet Astronomy–AJ	American Institute of Physics	34	1	1957
Avto(mat). svarka	Avtomaticheskaya svarka	Automatic Welding	British Welding Research Association (London)		1	1959
	Avtomatika i Telemekhanika	Automation and Remote Control	Instrument Society of America	27	1	1956
	Biofizika	Biophysics	National Institutes of Health*		1	1957
	Biokhimiya	Biochemistry	Consultants Bureau	21	1	1956
Byull. éksp(erim). biol. i med.	Byulleten' éksperimental'noi biologii i meditsiny	Bulletin of Experimental Biology and Medicine	Consultants Bureau	41	1	1959
DAN (SSSR) / Dokl(ady) AN SSSR	Doklady Akademii Nauk SSSR	The translation of this journal is published in sections, as follows:				
		Doklady Biochemistry Section	American Institute of Biological Sciences	106	1	1956
		Doklady Biological Sciences Sections (Includes: Anatomy, biophysics, cytology, ecology, embryology, endocrinology, evolutionary morphology, genetics, histology, hydrobiology microbiology, morphology, parasitology, physiology, zoology sections)	American Institute of Biological Sciences	112	1	1957
		Doklady Botanical Sciences Sections (Includes: Botany, phytopathology, plant anatomy, plant ecology, plant embryology, plant physiology, plant morphology sections)	American Institute of Biological Sciences	112	1	1957
		Proceedings of the Academy of Sciences of the USSR, Section: Chemical Technology	Consultants Bureau	106	1	1956
		Proceedings of the Academy of Sciences of the USSR, Section: Chemistry	Consultants Bureau	106	1	1956
		Proceedings of the Academy of Sciences of the USSR, Section: Physical Chemistry	Consultants Bureau	112	1	1957
		Doklady Earth Sciences Sections (Includes: Geochemistry, geology, geophysics, hydrogeology, mineralogy, paleontology, petrography, permafrost sections)	American Geological Institute	124	1	1959
		Proceedings of the Academy of Sciences of the USSR, Section: Geochemistry	Consultants Bureau	106-123	1 6	1957- 1958
		Proceedings of the Academy of Sciences of the USSR, Sections: Geology	Consultants Bureau	106-123	1 6	1957- 1958
		Doklady Soviet Mathematics	The American Mathematics Society	131	1	1961
		Soviet Physics–Doklady (Includes: Aerodynamics, astronomy, crystallography, cybernetics and control theory, electrical engineering, energetics, fluid mechanics, heat engineering, hydraulics, mathematical physics, mechanics, physics, technical physics, theory of elasticity sections)	American Institute of Physics	106	1	1956
		Proceedings of the Academy of Sciences of the USSR, Applied Physics Sections (does not include mathematical physics or physics sections)	Consultants Bureau	106-117	1	1956- 1957
Derevoobrabat. prom-st'.	Derevoobrabatyvayushchaya promyshlennost'	Wood Processing Industry	Timber Development Association (London)		9	1959
	Élecktrosvyaz	Telecommunications	Massachusetts Institute of Technology*		1	1957
Éntom(ol). oboz(renie)	Éntomologicheskoe obozrenie	Entomological Review	American Institute of Biological Sciences	38	1	1959
Farmakol. (i) toksikol(ogiya)	Farmakologiya i toksikologiya	Pharmacology and Toxicology	Consultants Bureau	20	1	1957
FMM	Fizika metallov i metallovedenie	Physics of Metals and Metallography	Acta Metallurgica*	5	1	1957
Fiziol. zhurn. SSSR (im. Sechenova)	Fiziologicheskii zhurnal im. I. M. Sechenova	Sechenov Physiological Journal USSR	National Institutes of Health*		1	1957
Fiziol(ogiya) rast.	Fiziologiya rastenii	Plant Physiology	American Institute of Biological Sciences	4	1	1957
	Geokhimiya	Geochemistry	The Geochemical Society		1	1958
FTT	Fizika tverdogo tela	Soviet Physics–Solid State	American Institute of Physics	1	1	1959
Izmerit. tekh(nika)	Izmeritel'naya tekhnika	Measurement Techniques	Instrument Society of America		1	1959
Izv. AN SSSR, O(td). Kh(im). N(auk)	Izvestiya Akademii Nauk SSSR: Otdelenie khimicheskikh nauk	Bulletin of the Academy of Sciences of the USSR: Division of Chemical Sciences	Consultants Bureau		1	1952

Life Sciences

Chemical Sciences

Earth Sciences

Mathematics

Physics

continued

Izv. AN SSSR, O(td). T(ekhn). N(auk): Met(all). i top.	(see Met. i top.)				
Izv. AN SSSR Ser. fiz(ich).	Izvestiya Akademii Nauk SSSR: Seriya fizicheskaya	Bulletin of the Academy of Sciences of the USSR: Physical Series	Columbia Technical Translations		1 1954
Izv. AN SSSR Ser. geofiz.	Izvestiya Akademii Nauk SSSR: Seriya geofizicheskaya	Bulletin (Izvestiya) of the Academy of Sciences USSR: Geophysics Series	American Geophysical Union		1 1954
Izv. AN SSSR Ser. geol.	Izvestiya Akademii Nauk SSSR: Seriya geologicheskaya	Izvestiya of the Academy of Sciences of the USSR: Geologic Series	American Geological Institute		1 1958
Kauch. i rez.	Kauchuk i rezina	Soviet Rubber Technology	Research Association of British Rubber Manufacturers	18	1 1959
	Kinetika i kataliz	Kinetics and Catalysis	Consultants Bureau	1	3 1960
	Koks i khimiya	Coke and Chemistry USSR	Coal Tar Research Association (Leeds, England)		1 1958
Kolloidn. zh(urn).	Kolloidnyi zhurnal	Colloid Journal	Consultants Bureau	14	1 1952
	Kristallografiya	Soviet Physics – Crystallography	American Institute of Physics	2	1 1957
Metalov. i term. obrabot. metal.	Metallovedenie i termicheskaya obrabotka metallov	Metal Science and Heat Treatment of Metals	Acta Metallurgica	6	1 1958
	Metallurg	Metallurgist	Acta Metallurgica		1 1957
Met. i top.	Metallurgiya i topliva	Russian Metallurgy and Fuels	Eagle Technical Publications		1 1960
Mikrobiol.	Mikrobiologiya	Microbiology	American Institute of Biological Sciences	26	1 1957
OS	Optika i spektroskopiya	Optics and Spectroscopy	American Institute of Physics		6 1959
	Pochvovedenie	Soviet Soil Science	American Institute of Biological Sciences		1 1958
	Priborostroenie	Instrument Construction	British Scientific Instrument Research Association		1 1959
Pribory i tekhn. éks(perimenta)	Pribory i tekhnika éksperimenta	Instruments and Experimental Techniques	Instrument Society of America		1 1957
Prikl. matem. i mekh.	Prikladnaya matematika i mekhanika	Applied Mathematics and Mechanics	American Society of Mechanical Engineers		1 1958
PTÉ	(see Pribory i tekhn. éks.)				
	Problemy Severa	Problems of the North	National Research Council of Canada		
Radiotekh.	Radiotekhnika	Radio Engineering	Massachusetts Institute of Technology*	12	1 1957
Radiotekh. i élektronika	Radiotekhnika i élektronika	Radio Engineering and Electronics	Massachusetts Institute of Technology*	2	1 1957
	Stanki i instrument	Machines and Tooling	Production Engineering Research Assoc.		1 1959
	Stal'	Stal (In English)	Iron and Steel Institute		1 1959
Stek. i keram.	Steklo i keramika	Glass and Ceramics	Consultants Bureau	13	1 1956
Svaroch. proiz-vo	Svarochnoe proizvodstvo	Welding Production	British Welding Research Association		4 1959
Teor. veroyat. i prim.	Teoriya veroyatnostei i ee primenenie	Theory of Probability and Its Applications	Society for Industrial and Applied Mathematics		1 1956
Tsvet. Metally	Tsvetnye metally	Nonferrous Metals	Primary Sources		1 1960
UFN	Uspekhi fizicheskikh Nauk	Soviet Physics – Uspekhi (partial translation)	American Institute of Physics	66	1 1958
UKh	Uspekhi khimii	Russian Chemical Reviews	The Chemical Society (London)		1 1960
UMN	Uspekhi matematicheskikh nauk	Russian Mathematical Surveys	London Mathematical Society	15	1 1960
Usp. fiz. nauk	(see UFN)				
Usp. khim(ii)	(see UKh)				
Usp. matem. nauk	(see UMN)				
Usp. sovr. biol.	Uspekhi sovremennoi biologii	Russian Review of Biology	Oliver and Boyd		48 1959
Vest. mashinostroeniya	Vestnik mashinostroeniya	Russian Engineering Journal	Production Engineering Research Assoc.		4 1959
Vop. gem. i per. krovi	Voprosy gematologii i perelivaniya krovi	Problems of Hematology and Blood Transfusion	National Institutes of Health*		1 1957
Vop. onk.	Voprosy onkologii	Problems of Oncology	National Institutes of Health*		1 1957
Vop. virusol.	Voprosy virusologii	Problems of Virology	National Institutes of Health*		1 1957
Zav(odsk). lab(oratoriya)	Zavodskaya laboratoriya	Industrial Laboratory	Instrument Society of America	25	1 1959
ZhAKh Zh. anal(it). khimii	Zhurnal analiticheskoi khimii	Journal of Analytical Chemistry USSR	Consultants Bureau	7	1 1952
ZhETF Zh. éksperim. i teor. fiz.	Zhurnal éksperimental'noi i theoreticheskoi fiziki	Soviet Physics–JETP	American Institute of Physics	28	1 1955
ZhFKh Zh. fiz. khimii	Zhurnal fizicheskoi khimii	Russian Journal of Physical Chemistry	The Chemical Society (London)		7 1959
ZhMÉI Zh(urn). mikrobiol. épidemiol. i immunobiol.	Zhurnal mikrobiologii, épidemiologii i immunobiologii	Journal of Microbiology, Epidemiology and Immunobiology	National Institutes of Health*		1 1957
ZhNKh Zh(urn). neorgan(ich). khim(ii)	Zhurnal neorganicheskoi khimii	The Russian Journal of Inorganic Chemistry	The Chemical Society (London)		1 1959
ZhOKh Zh(urn). obshch(ei) khimii	Zhurnal obshchei khimii	Journal of General Chemistry USSR	Consultants Bureau	19	1 1949
ZhPKh Zh(urn). prikl. khimii	Zhurnal prikladnoi khimii	Journal of Applied Chemistry USSR	Consultants Bureau	23	1 1950
ZhSKh Zh(urn). strukt. khimii	Zhurnal strukturnoi khimii	Journal of Structural Chemistry	Consultants Bureau	1	1 1960
ZhTF Zh(urn). tekhn. fiz.	Zhurnal teknicheskoi fiziki	Soviet Physics–Technical Physics	American Institute of Physics	26	1 1956
Zh(urn). vyssh. nervn. deyat. (im. Pavlova)	Zhurnal vysshei nervnoi deyatel'nosti (im. I. P. Pavlova)	Pavlov Journal of Higher Nervous Activity	National Institutes of Health*		1 1958

*Sponsoring organization. Translation through 1960 issues is a publication of Pergamon Press.

Declassified and Approved For Release 2013/03/04 : CIA-RDP10-02196R000600060004-9

Now available . . . an insight into the Soviet problems and achievements in . . .

PRODUCTION of ISOTOPES

The eighteen papers which comprise this volume were originally read at the All-Union Scientific and Technical Conference on the Application of Radioactive Isotopes, Moscow, 1957. The reports consider the problems and achievements of Soviet scientists in the production of radioactive isotopes by irradiation of targets in Soviet reactors and cyclotrons. Not only is this work of significance to producers of isotopes, but many of the papers will prove useful to isotope users as well.

The Development of Isotope Production in the USSR.
Certain Aspects of the Production of Radioactive Isotopes in a Nuclear Reactor.
Production of Radioactive Isotopes in a 10-Mev Deuteron Cyclotron.
Determination of Product Yields in Nuclear Reactions.
Spectrochemical Methods of Analyzing High-Purity Materials Used in Reactor Construction and for the Production of Radioisotopes.
Quantitative Spectral Determination of Impurities in Radioactive Preparations.
The Production of Alpha-, Beta-, and Gamma-Sources Using Oxide Films on Aluminum and Its Alloys.
Stable Isotopes Enriched by the Electromagnetic Method.
Ultrahigh-Temperature Ion Source for Electromagnetic Separation of Isotopes of Elements in the Platinum Group.
Inhomogeneous-Field Mass-Spectrometer for Analysis of Light-Element Isotopes.
The Relative Abundance of Palladium and Germanium Isotopes.
Some Problems in the Theory of Isotope Separation.
Separation of Isotopes of Light Elements by Diffusion in Vapors.
A Diffusion Column for the Separation of Isotopes.
A Fractionating Column for Preparing BF_3 Enriched in the Isotope B^{10}.
An Investigation of the Separation of the Stable Isotopes of Light Elements.
The Separation of Carbon Isotopes.
Low-Temperature Methods for Separating Helium Isotopes ($He^3 - He^4$).

1959 durable paper covers 136 pp. $50.00

CONSULTANTS BUREAU
227 WEST 17TH STREET, NEW YORK 11, N. Y.

Declassified and Approved For Release 2013/03/04 : CIA-RDP10-02196R000600060004-9

EQUIPMENT FOR A MODERN LABORATORY... A NEW CONCEPT IN DESIGN

Apparatus Drawings Project (ADP)

Sponsored by the American Association of Physics Teachers and the American Institute of Physics under a grant from the National Science Foundation

ADP has been designed to present physics teachers and laboratory workers in the field with **complete** data and drawings concerning **over 30 unique and economical pieces of apparatus** developed in the physics laboratories of some of America's leading colleges and universities.

The equipment described in ADP was developed as up-to-date teaching apparatus for laboratory experiments and lecture demonstrations. The drawings make available to other departments designs for apparatus which would otherwise be difficult to obtain. The reports contained in this series document original equipment which can be duplicated in your shop – **economically** – often by your students.

AN INVALUABLE TEACHING AID!
USEFUL IN RESEARCH!

PLENUM PRESS will publish and distribute the entire series which will cover over 30 different pieces of apparatus. You will be sent 10 reports in the first mailing. Printed on flat sheets (11 x 17, one side) for working convenience, the sheets fit into a durable cardboard case for safe storage.

THE CASE WILL BE SENT TO YOU AT NO EXTRA CHARGE!

Approximately 10 reports will be sent to you each mailing until you have received the complete set. Then (and at no extra charge) you will receive a clothbound (8½ x 11) book which will contain all the material in the reports in handy reference form for your desk or library.

The series of over 30 reports, the attractive cardboard storage case, and the desk-size manual will be sent to you for the single subscription price of only $40.00.

The full-size drawings and the book are not sold separately.

The first ten reports will consist of	Developed at
1. Balmer Series Spectrum Tube	Massachusetts Institute of Technology
2. Magnetic Field of a Circular Coil	Rensselaer Polytechnic Institute
3. Air Suspension Gyroscope	Massachusetts Institute of Technology
4. Resolution of Forces Apparatus	Massachusetts Institute of Technology
5. Simple Mass Spectrometer	Swarthmore
6. Bragg Diffraction Apparatus	Rensselaer Polytechnic Institute
7. Versatile Mass Spectrometer	Dartmouth
8. Driven Linear Mechanical Oscillator	Bryn Mawr
9. Simple Kinetic Theory Demonstration	Princeton
10. Air Suspended Pucks for Momentum Experiments	Massachusetts Institute of Technology

Equipment designed at other leading universities and colleges will be included in future reports.

YOU MAY SEND FOR A SAMPLE PAGE.

PLENUM PRESS 227 WEST 17TH STREET, NEW YORK 11, N. Y.